
Electronic Thesis and Dissertation Repository

11-9-2016 12:00 AM

A Non-Canonical Role for Choline Acetyltransferase in Chromatin Organization and the Response to Beta-Amyloid

Warren R. Winick-Ng, *The University of Western Ontario*

Supervisor: Dr. R. Jane Rylett, *The University of Western Ontario*

A thesis submitted in partial fulfillment of the requirements for the Doctor of Philosophy degree in Physiology and Pharmacology

© Warren R. Winick-Ng 2016

Follow this and additional works at: <https://ir.lib.uwo.ca/etd>



Part of the [Neurosciences Commons](#)

Recommended Citation

Winick-Ng, Warren R., "A Non-Canonical Role for Choline Acetyltransferase in Chromatin Organization and the Response to Beta-Amyloid" (2016). *Electronic Thesis and Dissertation Repository*. 4215.
<https://ir.lib.uwo.ca/etd/4215>

This Dissertation/Thesis is brought to you for free and open access by Scholarship@Western. It has been accepted for inclusion in Electronic Thesis and Dissertation Repository by an authorized administrator of Scholarship@Western. For more information, please contact wlsadmin@uwo.ca.

Abstract

The three-dimensional structure of chromatin is essential for context-dependent regulation of gene expression in post-mitotic neurons. Chromosomal rearrangements have been observed in the aging brain, and proteins involved in chromatin organization have altered expression and/or localization in Alzheimer's disease (AD). A human- and primate-specific transcript of choline acetyltransferase produces an 82-kDa protein (82-kDa ChAT) that is localized to the nucleus of cholinergic neurons, but is found in the cytoplasm in individuals with mild cognitive impairment (MCI) and AD. The function of the 82-kDa ChAT protein is unknown, though recent evidence suggests it has a role in gene expression changes in response to cellular perturbations.

In the present study, we explore whether 82-kDa ChAT is involved in global chromatin organization and an epigenetic response to cytotoxic amyloid- β ($A\beta$) exposure. We show that 82-kDa ChAT associates with chromatin in human SH-SY5Y neural cells using chromatin immunoprecipitation with next-generation sequencing (ChIP-seq), finding that acute exposure of cells to oligomeric $A\beta_{1-42}$ increases 82-kDa ChAT associations with gene promoters and introns. Following $A\beta_{1-42}$ -exposure, 82-kDa ChAT co-localizes in nuclear aggregates with special AT-rich binding protein 1 (SATB1), which anchors DNA to scaffolding/matrix attachment regions (S/MARs). SATB1 has similar increases in genic associations following $A\beta_{1-42}$ -exposure, and both SATB1 and 82-kDa ChAT associate with synapse-related genes. The 82-kDa ChAT and SATB1 proteins have patterned genomic associations at regions enriched with S/MAR binding motifs, preventing an $A\beta_{1-42}$ -induced increase in an isoform-specific APP mRNA transcript. Finally, we show that 82-kDa ChAT expression during cholinergic differentiation of SH-SY5Y cells increases the steady-state levels of proteins related to synapse formation, resulting in increased neurite complexity.

These results demonstrate that 82-kDa ChAT and SATB1 regulate chromatin organization at S/MARs, resulting in context-dependent gene expression changes in cholinergic cells and increased expression of synapse formation-related proteins during cholinergic differentiation. Cholinergic synapse dysfunction and degeneration is observed early in AD progression and 82-kDa ChAT is mislocalized in AD, therefore the loss of both the epigenetic response to $A\beta$ and gene expression changes related to synapse formation and maintenance may have implications for the etiology or progression of MCI and AD.

Keywords

Choline acetyltransferase / Chromatin immunoprecipitation / Chromatin organization / Epigenetics / Scaffolding/matrix attachment regions / Super-resolution microscopy

Co-Authorship Statement

This thesis contains figures and data from the following first author publication:

Winick-Ng W, Caetano FA, Winick-Ng J, Morey TM, Heit B, Rylett RJ (2016) 82-kDa choline acetyltransferase and SATB1 localize to β -amyloid induced matrix attachment regions. *Sci Rep*, 6: 23914.

The co-authors of the publication contributed to the data in the following ways:

Dr. Fabiana A Caetano contributed to the design, analysis and interpretation of the SR-GSDIM experiments.

Mrs. Jennifer Winick-Ng contributed to the data analysis, statistical analysis, and interpretation of the ChIP-seq data.

Mr. Trevor Morey contributed to the data acquisition, analysis and interpretation of the western immunoblotting experiments for the SATB1 siRNA knockdown experiment.

Dr. Bryan Heit contributed to the analysis and interpretation of the SR-GSDIM experiments.

Data is attributed to each co-author on the first page of the appropriate chapter.

Acknowledgments

I wish to sincerely thank my supervisor, Dr. Jane Rylett, for her support and mentorship, and for her contributions to the design and interpretations of the studies in this thesis.

I wish to thank my advisory committee, Drs. Dan Hardy, Wei-Yang Lu and Caroline Schild-Poulter. I also wish to thank Dr. Dan Hardy for his careful review and editing of the materials presented in this thesis.

Thank you to my wife Mrs. Jennifer Winick-Ng for her expertise and advice in programming and statistics, and for her unconditional support and patience.

Thank you to Dr. Anita Woods for sharing her passion for teaching and mentorship with me.

I wish to thank Drs. Fabiana Caetano and Bryan Heit as co-authors in the presented data and for mentorship in confocal and super-resolution imaging techniques. Thank you to Dr. Mike Levy for his advice in the analysis and interpretation of the ChIP-seq data, and Dr. Melissa Mann for her help in understanding how chromatin is organized.

I wish to thank Mr. Trevor Morey for his help and expertise in several molecular techniques, and as a peer who I can always turn to for advice.

Finally, I wish to acknowledge the following members of Dr. Jane Rylett's lab (past and present) for their help in the design, interpretation and/or data collection of the present studies:

Mr. Shawn Albers

Ms. Hadir AlQot

Dr. Leah Cuddy

Dr. Katherine Fishwick

Ms. Heather Rotz

Ms. Daisy Wong

Dedication

To Kian;

As scientists, we should all aspire to the unbound curiosity and imagination of children.

Table of Contents

Abstract.....	i
Co-Authorship Statement.....	ii
Acknowledgments.....	iii
Dedication.....	iv
Table of Contents.....	v
List of Tables.....	vii
List of Figures.....	viii
List of Appendices.....	xii
Forward.....	xiii
Chapter 1.....	1
1 Introduction.....	1
1.1 Histone modifications and the regulation of transcriptional activation.....	2
1.2 Chromatin organization in post-mitotic cells.....	7
1.3 Chromatin organization and scaffolding/matrix attachment regions.....	12
1.4 Chromatin organization in aging and Alzheimer’s disease.....	14
1.5 82-kDa ChAT nuclear expression and gene regulation.....	18
1.6 Hypothesis and objectives.....	24
1.7 References.....	25
Chapter 2.....	48
2 Objective I- 82-kDa ChAT interacts with chromatin.....	48
2.1 Introduction and Rationale.....	49
2.2 Methods.....	52
2.3 Results.....	61
2.4 Discussion.....	83

2.5	References.....	88
Chapter 3..... 94		
3	Objective II- 82-kDa ChAT and SATB1 work together to regulate chromatin organization.....	94
3.1	Introduction and Rationale.....	95
3.2	Methods.....	96
3.3	Results.....	104
3.4	Discussion.....	141
3.5	References.....	149
Chapter 4..... 159		
4	Objective III- A role for nuclear 82-kDa ChAT in cholinergic synapse development	159
4.1	Introduction and Rationale.....	160
4.2	Methods.....	162
4.3	Results.....	169
4.4	Discussion.....	194
4.5	References.....	204
Chapter 5..... 216		
5	Discussion	216
5.1	Limitations of the current studies	216
5.2	Future studies that expand the presented data.....	218
5.3	New studies and hypotheses generated from the presented data	220
5.4	Future studies for 82-kDa ChAT that have not yet been explored	224
5.5	Overall conclusions and significance.....	227
5.6	References.....	229
Appendices..... 239		
Curriculum Vitae 244		

List of Tables

Table 2-1. DNA oligomer pairs used for EMSA.	60
Table 2-2. APP interacting genes with 82-kDa ChAT association by ChIP-seq.....	68
Table 3-1. ChIP-qPCR and RT-qPCR primers used in the chapter.....	103
Table 3-2. Centromere (C) and Telomere (T) enrichment for 82-kDa ChAT and SATB1 ChIP-seq. (?) indicates missing or incomplete data.....	121
Table 3-3. APP-interacting genes with 82-kDa ChAT and/or SATB1 association by ChIP-seq	124
Table 3-4. Motifs used in S/MAR analysis.....	129
Table 3-5. G-quadruplex ($G_{3+}N_{1-20}G_{3+}N_{1-20}G_{3+}N_{1-20}G_{3+}$) motifs found in ChIP-seq datasets	131
Table 4-1. RT-qPCR primers used in this chapter.....	165
Table 4-2. Antibody conditions for western immunoblotting.	166
Table 4-3. Locations for 82-kDa ChAT ChIP-seq peaks for synapse-related genes.....	174
Table 4-4. NRG1 concentrations as measured by ELISA.	193

List of Figures

Figure 1-1. Regulation of histone modifications.	4
Figure 1-2. Chromatin is organized into topology and lamina associated domains.	9
Figure 1-3. SATB1 recruitment to scaffolding/matrix attachment regions.	13
Figure 1-4. APP metabolism.	20
Figure 1-5. Possible roles for nuclear 82-kDa ChAT in gene expression changes.	23
Figure 2-1. DNA binding prediction for 82-kDa ChAT.	51
Figure 2-2. ChIP-sequencing workflow.	57
Figure 2-3. 82-kDa ChAT associates with chromatin.	62
Figure 2-4. 82-kDa ChAT has altered genome association after exposure of cells to A β	63
Figure 2-5. Examples of ChIP-seq tracks for 82-kDa ChAT.	66
Figure 2-6. 82-kDa ChAT forms nuclear aggregates after exposure to A β	69
Figure 2-7. Effect of A β ₁₋₄₂ treatment on 82-kDa ChAT nuclear distribution in SH-SY5Y cells.	71
Figure 2-8. Effect of trichostatin A treatment on 82-kDa ChAT nuclear distribution in SH-SY5Y cells.	73
Figure 2-9. Titration of Hoechst stain in cells prior to fixation reverses TSA induced Hoechst accumulation.	74
Figure 2-10. Effect of TSA on three-dimensional tau protein nuclear distribution in SH-SY5Y cells.	76
Figure 2-11. Effect of TSA on three-dimensional Matrin3 protein nuclear distribution in SH-SY5Y cells.	78

Figure 2-12. Initial EMSA testing for 82-kDa ChAT.....	81
Figure 2-13. 82-kDa ChAT DNA binding is sensitive to oxidation.	82
Figure 2-14. DREME motifs for nuclear factor of activated T-cells (NFAT).....	85
Figure 3-1. 82-kDa ChAT expression in SH-SY5Y cells increases SATB1 protein expression.	105
Figure 3-2. A β -induced 82-kDa ChAT aggregates are co-localized with SATB1.	106
Figure 3-3. Super-resolution analysis of 82-kDa ChAT co-localization with SATB1.....	108
Figure 3-4. Co-immunoprecipitations (Co-IPs) for 82-kDa ChAT and SATB1.	109
Figure 3-5. Activation of SIRT1 is required for 82-kDa ChAT/SATB1 aggregate formation.	111
Figure 3-6. SATB1 siRNA knockdown alters 82-kDa ChAT and SATB1 A β -induced nuclear aggregate formation	113
Figure 3-7. SATB1 siRNA knockdown prevents A β -induced, but not resveratrol-induced, 82- kDa ChAT aggregate formation in nuclei.....	114
Figure 3-8. SATB1 has altered genome association after exposure of cells to A β	117
Figure 3-9. Examples of ChIP-seq tracks for SATB1.	118
Figure 3-10. 82-kDa ChAT and SATB1 associate with shared cell membrane and stress related genes after A β -exposure.	122
Figure 3-11. 82-kDa ChAT and SATB1 associate with the APP gene after A β -exposure. .	126
Figure 3-12. 82-kDa ChAT and SATB1 expression prevents an increase in APP isoforms containing the Kunitz-protease inhibitor domain (KPI).	127
Figure 3-13. 82-kDa ChAT and SATB1 have significant enrichment for S/MAR motifs...	130
Figure 3-14. Analysis of the inter-peak spacing of 82-kDa ChAT and SATB1.....	133

Figure 3-15. 82-kDa ChAT has patterned protein distribution in nuclei of SH-SY5Y cells.	134
Figure 3-16. 82-kDa ChAT co-immunoprecipitation and identification of interacting proteins.	138
Figure 3-17. 82-kDa ChAT protein interactions as revealed by mass spectrometry analysis.	140
Figure 3-18. Model for 82-kDa ChAT and SATB1 chromatin association in SH-SY5Y cells.	148
Figure 4-1. 82-kDa ChAT has significant enrichment for NFAT and c-Fos motifs.....	170
Figure 4-2. NFAT binding motifs in gene ontology groups for 82-kDa ChAT and SATB1.	172
Figure 4-3. 82-kDa ChAT expression in SH-SY5Y cells alters gene expression of synapse related genes.....	176
Figure 4-4. 82-kDa ChAT expression in SH-SY5Y cells alters gene expression of synapse related genes after exposure to oligomeric A β ₁₋₄₂	177
Figure 4-5. 82-kDa ChAT expression in SH-SY5Y cells alters steady-state protein levels of neuregulin 1, neuroligin 1 and the metabotropic glutamate receptor 5.	179
Figure 4-6. 82-kDa ChAT expressing SH-SY5Y cells grow highly branched NRG1- dependent neurites.	180
Figure 4-7. Media conditioned on 82-kDa ChAT expressing SH-SY5Y cells alters neurite outgrowth of vector expressing cells.	182
Figure 4-8. Long-term NRG1 signaling promotes ERBB4 phosphorylation.	184
Figure 4-9. Acute NRG1 signaling reduces ERBB4 phosphorylation.	186
Figure 4-10. 82-kDa ChAT expressing cells have enhanced ERBB4 phosphorylation in response to growth factors.	187

Figure 4-11. 82-kDa ChAT expression increases the response to NRG1 stimulation of p-ERBB4.	189
Figure 4-12. 82-kDa ChAT expression increases NRG1 extracellular peptide release in SH-SY5Y media.	192
Figure 4-13. ERBB4 signaling promotes cholinergic synapse maintenance and new synapse formation.	196
Figure 4-14. Proposed model for the role of 82-kDa ChAT in neurite outgrowth and complexity.	200

List of Appendices

Appendix 1- DNA fragment optimization for ChIP.	239
Appendix 2- 82-kDa ChAT vehicle gene ontology.	240
Appendix 3- 82-kDa ChAT A β gene ontology.	240
Appendix 4- 82-kDa ChAT vehicle and A β gene ontology.	240
Appendix 5- EMSA optimization experiments.	241
Appendix 6- Representative PCR gel for primers used in RT-qPCR experiments.	242
Appendix 7- SATB1 vehicle gene ontology.	243
Appendix 8- SATB1 A β gene ontology.	243
Appendix 9- SATB1 vehicle and A β gene ontology.	243
Appendix 10- 82-kDa ChAT and SATB1 A β gene ontology.	243
Appendix 11- 82-kDa ChAT and SATB1 vehicle and A β gene ontology.	243

Forward

Non-dividing post-mitotic cells present a unique challenge in biology – how can cells survive, in some cases for the entire lifespan of an organism, while dealing with environmental challenges such as oxidative or endoplasmic reticulum stress, DNA damage, or changes in metabolic state? Many cellular homeostatic changes require a DNA response to either activate or repress transcription of response genes, which implies state-dependent dynamic regulation of gene access. It is thus critical for the cell to have tools dedicated to facilitating these responses.

This concept has led the idea of the “epigenome”, a set of specific DNA modifications that can dynamically alter transcriptional access to DNA depending on cell state. These modifications can be to the DNA itself, or to the core histones which together with the DNA make up the chromatin fiber (together called the nucleosome). Examples of well-known histone modifications include methylation and acetylation, but can also include phosphorylation, ubiquitination and sumoylation. Non-histone changes to chromatin are also possible; directly modifying nucleosome position can change what portion of DNA is accessible between nucleosomes, and methylation of DNA can restrict access of transcriptional activators.

Together, chromatin modifications represent an incredible amount of dynamic regulation of chromatin access - but this system does not confer much specificity. Global changes to chromatin access with one or more modifications is likely counter-productive; state-dependent cellular responses often need varying levels of both chromatin access and restriction. Thus, it is advantageous for cells to be able to target specific genes for specific modifications in specific contexts. This is partially accomplished by transcription factors (TFs), which usually recruit transcriptional activators such as RNA Polymerase II, and can recruit chromatin modifiers as part of a TF complex. However, this does not account for all of the possible context-dependent chromatin modifications, nor does it account for transcriptional repression. Importantly, this also does not account for single gene changes – in fact, in order to target a single gene in each scenario the cell would need a TF for each modification, which would require an exponential number of proteins above the ~25,000

known human protein-coding genes. Thus, another level of chromatin regulation must be present in the cell. Cells organize genes into functional regions that can be accessed when needed, and there must exist context-dependent cell signaling events and/or chaperones to bring the correct modifications to genes. It is now becoming evident that gene expression depends on the three-dimensional folding of chromatin, where active and inactive segments of the genome tend to segregate in the same co-regulated space.

This reasoning led me to explore how post-mitotic cells (i.e. neurons) respond to contextual environmental challenges through the regulation of chromatin organization. I placed emphasis on the special case of human cholinergic neurons, which are critical for cognition, memory, attention and sleep, but are lost early in dementia-related neurological disorders such as mild cognitive impairment and Alzheimer's disease (AD). This case is especially interesting from a chromatin organization perspective; genetic background only accounts for ~1-5% of AD cases, while environment and lifestyle have been shown to be of etiological significance. There is now mounting evidence that there are epigenetic and chromatin organization related changes in both aging and AD. Therefore, elucidating how chromatin is organized in these cells, and how this is altered in stress and disease, is critical for understanding the pathogenesis of AD.

The following story explores how a human and primate specific protein variant interacts with chromatin and is critical for chromatin organization in cholinergic neurons. 82-kDa choline acetyltransferase (ChAT) is stably expressed in cholinergic nuclei but is reduced in aging individuals and redistributed to the cytoplasm in AD patients. The work presented here will show a novel role for 82-kDa ChAT in gene expression changes and chromatin organization during cholinergic differentiation and following cellular stress. These gene expression changes promote the healthy function of synaptic connections, an important point given that synaptic destabilization and degeneration are seen early in AD. Thus the work presented here is important for understanding healthy neuron function and disease etiology, and may help identify targets for AD prevention or treatment.

Chapter 1

1 Introduction

Proper chromatin organization is imperative for promoting accurate context-dependent epigenetic modifications - changes in gene expression due to alterations directly to DNA or to the core histones that DNA wraps around in the nucleosome complex. Chromatin organization is essential for neuronal development and function, and defects in chromatin-associated processes has been implicated in many neurological disorders such as schizophrenia, intellectual disorder and autism spectrum disorder (Gong *et al.* 2008; Gregor *et al.* 2013; McCarthy *et al.* 2014). More recently, chromatin organization changes have been observed in neurodegenerative diseases such as Alzheimer's disease (AD) and Parkinson's disease (reviewed in Marques and Outeiro 2013; Walker *et al.* 2013). Therefore, understanding how chromatin is organized in neurons and can become disrupted in disease is essential for identifying biomarkers for early disease detection, and for the development of novel therapeutics.

This review will address how epigenetic modifications regulate gene expression, the relationship between these modifications and chromatin organization, and the disruptions in chromatin organization observed in aging and neurodegenerative disease. Several proteins related to epigenetic processes and chromatin organization are mislocalized to the cytoplasm in aging and AD, including DNA methyltransferase (DNMT) and repressor element 1-silencing transcription (REST) (Mastroeni *et al.* 2013; Lu *et al.* 2014). A human and primate-specific 82-kDa variant of choline acetyltransferase (ChAT) also has altered localization in AD and may be related to changes in gene expression (Gill *et al.* 2007; Albers *et al.* 2014); therefore this review will also explore the known literature for 82-kDa ChAT. It is beyond the scope of this review to present all the known literature on epigenetic processes and chromatin organization comprehensively, though there are several excellent reviews (Politz *et al.* 2013; Alexander and Lomvardas 2014; Luperchio *et al.* 2014) that address these topics have had influence on the authors' research.

1.1 Histone modifications and the regulation of transcriptional activation

Epigenetic changes can result in the formation of euchromatin - DNA that is available for transcription and loosely packed; or heterochromatin - highly compacted DNA that is often transcriptionally repressed (Croft *et al.* 1999; Zink *et al.* 2004; Harnicarová *et al.* 2006). Heterochromatin can be further divided into facultative repression - DNA that is transiently repressed and easily reversed; and constitutive repression - a more permanent repressive state (Li and Zhou 2013; Saksouk *et al.* 2015; Stunnenberg *et al.* 2015; Jamieson *et al.* 2016). The sum of epigenetic alterations to both the DNA and 4 core histones (H3, H4, H2A and H2B) will determine this state, but in the case of activation still require recruitment of transcription factors (TFs) and transcriptional activators for transcription to occur. Together these alterations are known as the “histone code” and are a result of post-translational histone modifications, direct methylation of DNA, nucleosome positioning or microRNA (miRNA)-mediated gene repression.

The most widely studied epigenetic alterations are to the core histones that make up the nucleosome complex. A well-known example of post-translational histone modifications is acetylation, where an acetyl group is reversibly added to lysine, removing its positive charge (Reviewed in Sterner and Berger 2000; Bannister and Kouzarides 2011). Histone acetylation by histone acetyltransferases (HATs) mainly occurs on histone H3 or H4, with the net negative charge causing the histones to repel each other, increasing access to the DNA strand between nucleosomes and allowing TFs and RNA polymerase II (Pol II) to bind DNA (Zhang *et al.* 2012; Vamos and Boros 2012; Henry *et al.* 2013; Zhu *et al.* 2014). Deacetylation is accomplished by histone deacetylases (HDACs) which remove the acetyl groups and increases the positive charge on the histone that restricts DNA access by positioning nucleosomes closer together (Nagl *et al.* 2007; Choe *et al.* 2009; Reviewed in Li and Kumar 2010; Bannister and Kouzarides 2011).

While histone acetylation can directly alter access to DNA, histone methylation results in recruitment of transcriptional modifiers and either HATs or HDACs to DNA. Histones are methylated on lysine or arginine residues by replacing 1, 2 or 3 hydrogens in the NH₃ (amino) group, resulting in mono-, di- or tri-methylation, respectively (Reviewed in Lachner *et al.* 2003; Sharma *et al.* 2010). Similar to acetylation, histones are methylated on lysine by histone methyltransferases (HMTs) and demethylated by histone demethylases (HMDs) (Lachner *et al.* 2003). Arginine methylation is accomplished by protein arginine methyltransferases (PRMTs) (Pal *et al.* 2004). Some examples of methylation that leads to transcriptional activation include histone H3 lysine 4 (H3K4) tri-methylation (H3K4me₃) and histone H3 lysine 79 tri-methylation (H3K79me₃) (Liang *et al.* 2004; Kim *et al.* 2012). H3K4me₃ is enriched at gene promoter regions that have active markers of transcription such as acetyl groups added by HATs and Pol II recruitment (Liang *et al.* 2004). In addition, H3K4me₃ can lead to Histone 2A (H2A) replacement by the variant H2A.Z at transcription initiation sites, important for destabilizing the histone complex and allowing access to the nucleosome-related DNA (**Fig. 1-1A**) (Bártfai *et al.* 2010; Brunelle *et al.* 2015).

Histone methylation by polycomb repressive complexes (PRCs) leads to the transient, facultative repression of transcription often found at the borders of heterochromatic regions (**Fig. 1-1B**) (Cheutin and Cavalli 2012; Dixon *et al.* 2012; Abraham and Kulesza 2013; Boros *et al.* 2014). Histone H3 lysine 27 tri-methylation (H3K27me₃) is methylated by PRC2, recruited by HDACs and other chromatin organizers (Cheutin and Cavalli 2012; Abraham and Kulesza 2013; Kim *et al.* 2015). Importantly, PRC1 is also recruited to this region, which then adds the small molecule ubiquitin to H2A.Z (Cao *et al.* 2005; Sarcinella *et al.* 2007). Both the recruitment of HDACs and ubiquitination of H2A.Z facilitate the attenuation of transcription in these regions, but do not cause chromatin compaction (Sarcinella *et al.* 2007). Therefore, these regions are still accessible for chromatin modifiers and can be transcriptionally activated if needed.

Finally, heterochromatin that is constitutively repressed is often enriched with histone H3 lysine 9 tri-methylation (H3K9me₃), methylated by K9-HMT (**Fig. 1-1C**)

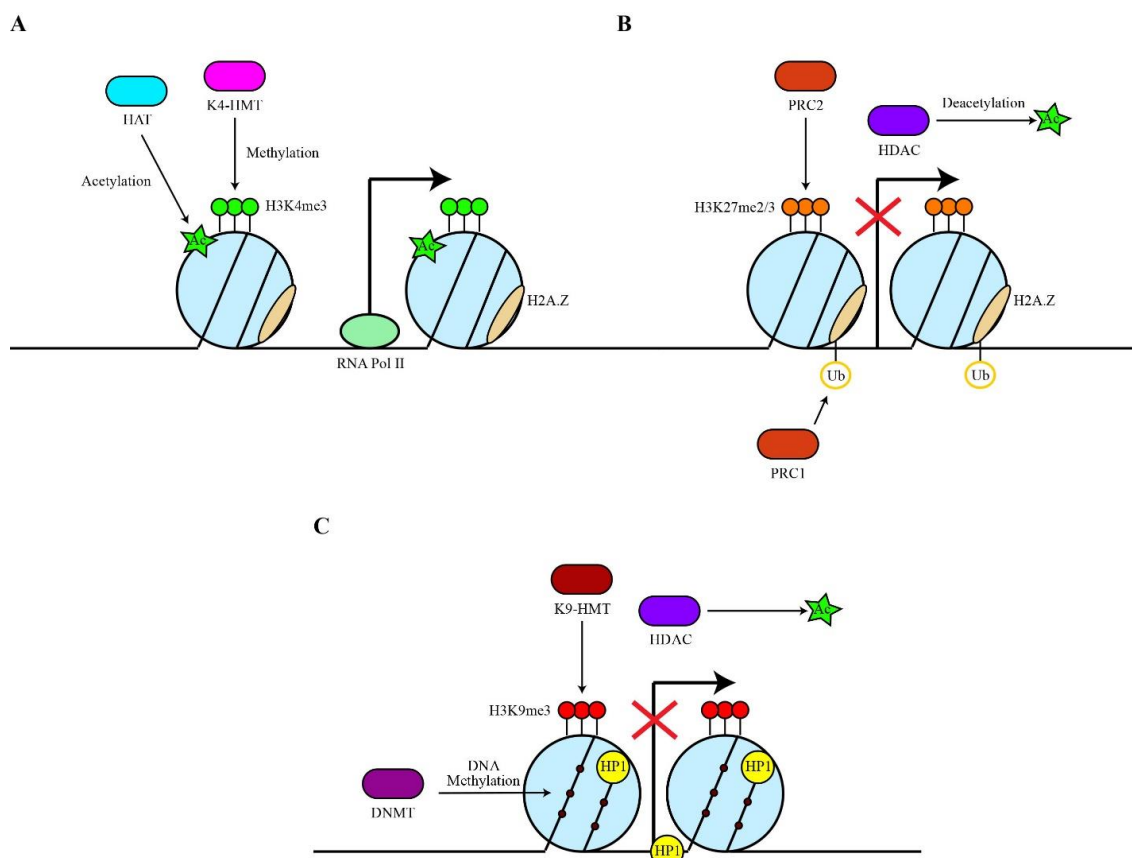


Figure 1-1. Regulation of histone modifications.

(A) Histone acetyltransferases (HATs) acetylate histones, histone 3 lysine 4 (H3K4) methyltransferase (K4-HMT) tri-methylates histone H3K4 and histone H2A is replaced by H2A.Z. These modifications produce an ‘open’ histone state that allows RNA polymerase II (RNA Pol II) to bind to promoter regions and initiate transcription. (B) To promote facultative repression, polycomb repressive complex 1 (PRC1) ubiquitinates H2A.Z while PRC2 di-/tri-methylates H3K27. Histone deacetylases (HDACs) are responsible for the removal of acetyl groups resulting in a ‘closed’, but reversible, repressive state. (C) In the constitutively repressed state, H3K9 HMTs (K9-HMT) tri-methylates H3K9, DNMTs methylate DNA and HDACs remove acetyl groups from the histones. In addition, heterochromatin protein 1 (HP1) is recruited to promoters to repress transcription further. Adapted from Sharma *et al.* 2010.

(Nakayama *et al.* 2001; Barski *et al.* 2007; Vaquero *et al.* 2007). As with facultative repression, HDACs are also recruited to H3K9me3 regions to reduce histone acetylation (Nakayama *et al.* 2001). In addition, H2A.Z is replaced by H2A, and DNMTs are recruited to promoter regions to methylate the DNA which, in most cases, prevents the binding of TFs and Pol II (Nakayama *et al.* 2001; Barski *et al.* 2007). H3K9me3 rich regions are often bound with heterochromatin protein 1 (HP1) at gene promoters, which further promotes gene silencing and chromatin compaction (Nakayama *et al.* 2001). These modifications together lead to a repressive model of DNA compaction that is difficult, but not impossible to access. Constitutively repressed regions rich in H3K9me3 tend to be found within heterochromatin regions, flanked by facultative repressive regions or activated regions (Barski *et al.* 2007). H3K9me3 is also enriched in the inactivated X chromosome (Brinkman *et al.* 2006).

Both telomeres and centromeres are often enriched with H3K9me3 (Schotta *et al.* 2002; Guenatri *et al.* 2004; Mikkelsen *et al.* 2007; Nakano *et al.* 2008). Telomeres have tandem repeats which are important for mitosis in dividing cells and often shorten with age, increasing the risk of cancer and an impaired DNA damage response (Allsopp *et al.* 1992; Jurk *et al.* 2002; Zhang *et al.* 2007). Telomeric length is important for post-mitotic cells, as neurons respond to DNA damage through proteins that stabilize telomeres (Zhang *et al.* 2007; Jurk *et al.* 2012). Changes to telomeric length in post-mitotic neurons has been linked to neurological disorders such as Alzheimer's disease (AD) and amyotrophic lateral sclerosis (Jurk *et al.* 2012; Linkus *et al.* 2016). Centromere silencing is especially important for post-mitotic neurons, as centromeres are key mediators of cell division (reviewed in Herrup and Yang 2007; Frade and Ovejero-Benito 2015). Neurons in AD can re-enter the cell cycle, with recent evidence showing that these cells may undergo abnormal centromere division on the X chromosome (Spremo-Potporević *et al.* 2008), though it is unclear if this precedes or is a consequence of cell cycle re-entry.

Interestingly, the resulting changes to transcriptional activation can depend on how many methyl groups are added to a specific lysine. For example, H3K9 can be mono- di- or tri- methylated (H3K9me/me2/me3) by the K9-HMT, which results in increased transcription, facultative repression, and constitutive repression, respectively

(Peters *et al.* 2003; Rougeulle *et al.* 2004; Barski *et al.* 2007). Another example is H3K20 methylation; H3K20me is associated with constitutive repression (Oda *et al.* 2007), H3K20me₂ is involved in recruitment of DNA damage repair proteins (Fradet-Turcotte *et al.* 2013), and H3K20me₃ has been found in heterochromatic regions and thus hypothesized to play a role in repression as well (Wongtawan *et al.* 2011). Arginine methylation is associated with both transcriptional activation and repression depending on the residues methylated (Reviewed by Di Lorenzo and Bedford 2011). The mechanisms that lead to arginine methylation related changes in gene expression are largely unknown, though there is evidence to suggest that these modifications may promote or prevent docking of transcriptional modifiers (Di Lorenzo and Bedford 2011).

Other histone modifiers have been studied to a lesser extent, but are also essential for chromatin regulation. These include the aforementioned H2A.Z ubiquitination – important for transient facultative repression, as well as phosphorylation and sumoylation. Histone phosphorylation is essential for demarcation of regions with DNA damage and recruitment of acetyltransferases essential to begin the repair process (Burma *et al.* 2009). In addition, phosphorylation of H3 serine 10 (H3S10ph), threonine 11 (H3T11ph) or H3S28ph has been shown to increase H3 acetylation and transcriptional activation (Duan *et al.* 2008; Metzger *et al.* 2008; Sawicka *et al.* 2014), and phosphorylation of histone H2B serine 14 (H2BS14ph) is critical for the initiation of chromatin condensation during apoptosis (Cheung *et al.* 2003; Fernandez-Capetillo *et al.* 2004). Finally, the addition of small ubiquitin-related modifier (SUMO) by sumoylation to histone H4 (H4-SUMO) is important for the attenuation of histone acetylation, and an important intermediary for the transition from transcriptional activation to constitutive repression (Yang *et al.* 2002; Girdwood *et al.* 2003; Shiio and Eisenmann 2003).

Though not explored in this review, it is important to note that post-translational histone modifications work together with other epigenetic related changes to dynamically regulate access to DNA. Other epigenetic mechanisms which are important for the short and long-term regulation of transcription include DNA methylation by DNMTs, gene repression by miRNAs and the regulation of nucleosome positioning. All of these mechanisms work together to support the normal regulation of transcription, but are also

important for the response to environmental challenges, such as changes in metabolic state, DNA damage, oxidative and nitrosative stress, or cell-cell communication events (*e.g.* neurotransmission) (see Zawia *et al.* 2009; Shahani and Sawa 2011; Brochier and Langley 2013; Vogel-Ciernia and Wood 2014 for reviews). In order to respond with specificity, chromatin must be organized in a manner that allows access to the correct genomic sequences at the correct time. How cells organize chromatin, with emphasis on neurons, will be explored in the following section.

1.2 Chromatin organization in post-mitotic cells

During interphase and in non-dividing cells, chromatin is generally organized into both heterochromatic and euchromatic compartments. Heterochromatin is found largely at the nuclear periphery, associated with nuclear lamina proteins, lamin A or B, or in perinucleolar regions (Peric-Hupkes *et al.* 2010; Shah *et al.* 2013; Reviewed in Luperchio *et al.* 2014). Euchromatic regions of activated chromatin are mainly found in the nuclear interior, with very little nuclear membrane or lamina association (see Kalverda *et al.* 2008; Luperchio *et al.* 2014 for reviews). In the absence of outside input, post-mitotic cells must maintain this organization for their entire lifespan. In contrast, a mitotic cell does change its chromatin organization during cell division, as chromosomes must become compacted during prophase and remain in this state until cell division is complete (Hinde *et al.* 2012).

One advantage to having this type of localization-dependent organization is that cells can change the state of gene activation and response time to environmental input by altering the localization of individual genes. One example of this function in neurons is the *BDNF* gene. *BDNF* encodes brain-derived neurotrophic factor (BDNF), a protein important for neuron development, survival and synaptic development (Bamji *et al.* 2006; Chen *et al.* 2013). BDNF also has an important role in synaptic plasticity; changes in synapse number and strength based on repeated stimulation (Montalbano *et al.* 2013). In adult non-dividing neurons, *BDNF* is localized to the nuclear periphery. However, after

repeated activation of hippocampal neurons by kainate-induced seizures, the gene is rapidly internalized and activated (Walczak *et al.* 2013). *BDNF* mRNA levels peak by 2 h after stimulation, with this fully attenuated by 7 d. Though the mRNA levels are no longer elevated, an interesting observation is that the gene remains localized in the nuclear interior for at least 28 d following stimulation (Walczak *et al.* 2013). This localization change is important for sensitivity to the next stimulation. When Walczak *et al.* (2013) stimulated these cells 28 d following the initial stimulation, Pol II recruitment to the *BDNF* gene was significantly increased compared to naïve animals, suggesting that gene localization is important for magnitude of response.

Recently, mounting evidence has shown that chromatin organization is more complex than simple heterochromatin/euchromatin regions. Active and inactive segments of the genome tend to segregate in space, while co-regulated regions group within the same Topologically Associating Domain (TAD) which are thought to contribute to their coordinated expression or silencing (Dixon *et al.* 2012; Heidari *et al.* 2014; reviewed in Luperchio *et al.* 2014) (**Fig. 1-2**). Centrally localized TADs tend to be rich in H3K27me3 and are flanked by boundary elements (BoEs); DNA/protein complexes (also termed insulators) that can organize chromatin into looped structures (Lin *et al.* 2011; Dixon *et al.* 2012; Heidari *et al.* 2014). BoEs allow DNA to be accessed by chromatin remodeling proteins, TFs, and Pol II, and are enriched with H3K27me3 or H3K4me3 depending on the state of transcriptional activation (Dixon *et al.* 2012; Narendra *et al.* 2015). TAD architecture has been described as a domain within domain system: Inter-TAD contact results in coordinated regulation of inter-TAD regions into megabase pair (Mb) large ‘meta-TADs’ (Heidari *et al.* 2014; Fraser *et al.* 2015), and BoEs can also be found within 50-100 kb ‘sub-TAD’ regions (Dixon *et al.* 2012; Heidari *et al.* 2014). Meta-TAD and sub-TAD interacting regions are often sites of transcriptional activation (Heidari *et al.* 2014; Fraser *et al.* 2015; Smith *et al.* 2016). TADs can also interact with and bind to the nuclear lamina at 0.1-10 Mb wide lamina-associated domains (LADs; Guelen *et al.* 2008). This correlates well with the finding of heterochromatin at the nuclear periphery, as LADs are mainly enriched with H3K9me3 and highly compacted (Guelen *et al.* 2008; Meuleman *et al.* 2013). LADs are also flanked by BoEs that interact with chromatin that is enriched with H3K27me2/3 and accessible to chromatin organizers (Guelen *et al.*

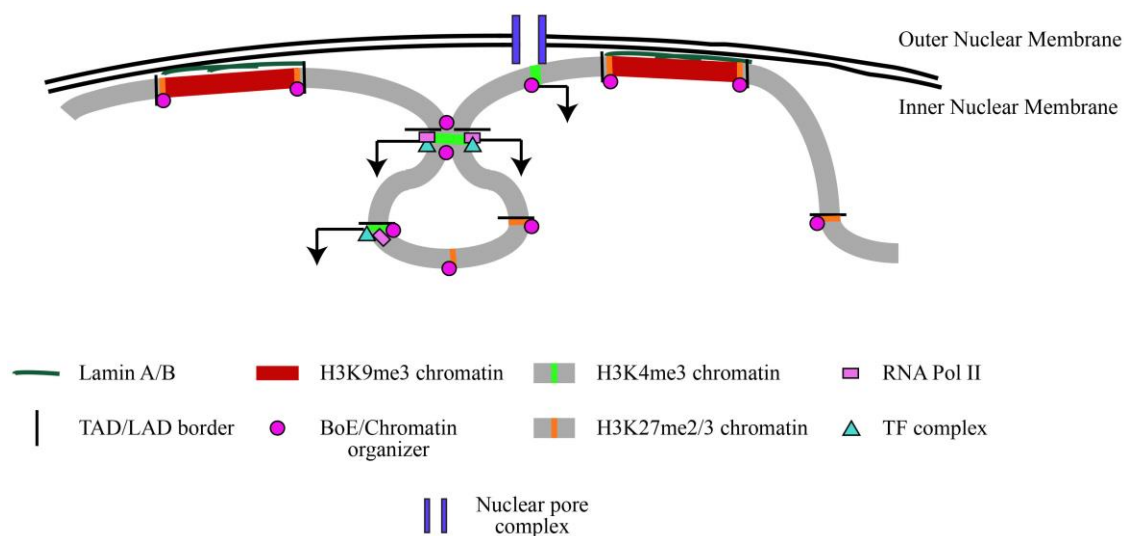


Figure 1-2. Chromatin is organized into topology and lamina associated domains.

Chromatin is organized into large 0.1-1 megabase pair wide topology-associated domains (TADs), flanked by boundary elements (BoEs) that organize chromatin and allow access for chromatin modifying proteins. BoEs are found at chromatin enriched with H3K27me2/3 or H3K4me3. In H3K4me3 boundary regions, transcription factors (TFs) and RNA Pol II are recruited for activation of transcription. TADs found at the nuclear periphery are associated with lamin A/B and termed lamina-associated domains (LADs). LADs are often constitutively repressed, enriched with H3K9me3 and flanked by BoEs and H3K27me2/3 regions. A notable exception is where euchromatic regions of LADs interact with nuclear pore complexes. Adapted from Luperchio *et al.* 2014.

2008). This type of organization is critical to maintain transcriptional repression, but still allow access to genes when environmental state-dependent changes occur. As an exception, genes within LADs that are localized near nuclear pores are often euchromatic to facilitate transcriptional activation and rapid mRNA transport out of the nucleus (Brickner *et al.* 2012).

Chromatin looping by BoEs can help to regulate gene expression of differentially expressed alleles. One well-known example of this type of regulation is the imprinted *H19/Igf2* locus. Chromatin organizers bring an enhancer close to the promoter of the *H19* gene on the maternal allele, while segregating it from the *Igf2* promoter (Engel *et al.* 2008). On the paternal allele the region that binds these organizers is hypermethylated, inhibiting *H19* expression and allowing the enhancer to activate *Igf2* transcription (Engel *et al.* 2008). *H19* encodes H19, which is involved in the attenuation of cell proliferation (Gabory *et al.* 2009), while *Igf2* encodes the insulin-like growth factor 2 (IGF-2), a critical protein for cell growth (reviewed in Pollak 2012). In this case, proper imprinting is critical for homeostatic balance of cell growth, and dysregulation of proper *H19* repression on the paternal allele has been shown to lead to tumor development and proliferation in cancer cells (Cui *et al.* 2002; Ulaner *et al.* 2003).

There are a few exceptions to the peri-nucleolar and lamina-associated heterochromatin seen in neurons. Olfactory neurons, which each have a uniquely expressed olfactory receptor, have a large amount of heterochromatin in the center of the nucleus (Clowney *et al.* 2012). This heterochromatin ‘core’ contains the approximately ~2800 olfactory receptor genes, which are enriched with H3K9me3 histone markers and tightly compacted, leading to constitutive repression (Clowney *et al.* 2011; Clowney *et al.* 2012). However, during development one of these genes is looped out of the core, associated with a distal transcription enhancer leading to gene activation (Lomvardas *et al.* 2006; Clowney *et al.* 2012). Only one gene is activated in a single olfactory sensory neuron, and each neuron has a unique gene that is activated (Clowney *et al.* 2012). Thus, chromatin organization is critical in olfactory sensory neurons for receptor specificity.

Another exception where heterochromatin is not associated with the nuclear lamina is in retinal rod cells of nocturnal animals. At birth, these animals display a normal pattern of chromatin organization, with heterochromatin associated with the lamina at the nuclear periphery (Solovei *et al.* 2013; Reviewed in Alexander and Lomvardas 2014). However, by post-natal day 14 (P14) nuclear lamina proteins are downregulated leading to the internalization of the heterochromatin (Solovei *et al.* 2013). By adulthood, and throughout the entire lifespan of these animals, the heterochromatin is found exclusively in the center of the nucleus with the euchromatin surrounding it (Solovei *et al.* 2009; Solovei *et al.* 2013). This inside out configuration allows for the rod cells to diffract light more efficiently at night, when these cells are more active (Solovei *et al.* 2009).

As these examples highlight, chromatin organization is important for neuron specialization and normal function. Chromatin organization in post-mitotic cells is also critical for neuronal development and synaptic plasticity. For example, *Ctcf* encodes CTCF (CCCTC-binding factor), a BoE critical for chromatin topology and organization (Dixon *et al.* 2012). Children born with mutations in *Ctcf* display intellectual disability, microcephaly and often show autistic features (Gregor *et al.* 2013). *Ctcf* was also identified recently as a schizophrenia susceptibility gene (Juraeva *et al.* 2014). Dysregulation of Alpha Thalassemia/Mental Retardation Syndrome X-Linked (ATRX), a protein involved in chromatin remodeling and downregulation of gene expression, has also been linked to intellectual disorder and autism-spectrum disorder (Gong *et al.* 2008; Martínez *et al.* 2014).

In terms of normal neural development and synaptic plasticity, Vogel-Ciernia *et al.* (2013) showed that the Brg1-associated factor subunit BAF53b (part of the SWI/SNF chromatin remodeling complex) is important for long-term memory consolidation, dendritic arborization and hippocampal synaptic plasticity. Mutations in BAF53b leads to impairments in synaptic plasticity, driven by abnormal gene expression of postsynaptic genes (Vogel-Ciernia *et al.* 2013). Thus, chromatin organization is important for proper neuron function and development, but may also be important for environmental and context-based gene regulation.

1.3 Chromatin organization and scaffolding/matrix attachment regions

A large advantage of having a high level of organization of chromatin is the ability to have state-dependent dynamic regulation of chromatin access. This is accomplished by accessing the chromatin loops created by chromatin organizers and results in locus-specific regulation. One method to produce this type of looping involves anchoring either local or distant genes to nuclear matrix proteins at scaffolding/matrix attachment regions (S/MARs) (Heng *et al.* 2004; Reviewed in Politz *et al.* 2013). DNA is anchored to S/MARs by organizers such as special AT-rich binding protein 1 (SATB1; Cai *et al.* 2003; reviewed by Kohwi-Shigematsu *et al.* 2013) and S/MAR-binding protein 1 (SMAR1; Sinha *et al.* 2010). These organizers recruit chromatin modifying enzymes to the region to either activate or repress transcription, depending on what is recruited (**Fig. 1.3**). For example, SATB1 can recruit HDAC1 to repressed regions and the HAT p300 to activated regions (reviewed by Kohwi-Shigematsu *et al.* 2013). SATB1 has previously been shown to be important for anchoring chromatin loops on the beta-globin locus, in order to bring the gene encoding the activated beta-globin subunit close to hypersensitive sites but segregate other genes away from this region (Wen *et al.* 2005; Wang *et al.* 2009). SATB1-mediated chromatin looping is also involved in cytokine activation through the TH2-cytokine (IL4/5/13) locus in T-cells (Cai *et al.* 2006), regulation of the switch from the pro-apoptotic BCL2 gene to the anti-apoptotic NOXA gene (Yang *et al.* 2015), X-chromosome inactivation (Agrelo *et al.* 2009), as well as in regulating gene expression of the major histocompatibility complex (MHC) class I locus (Kumar *et al.* 2007).

There is now emerging evidence that S/MARs may also be involved in context-dependent regulatory events. In HCT116 p53^{+/+} cells exposed to UV radiation to induce DNA double strand breaks, SMAR1 recruits HDAC1 to the *BAX* and *PUMA* promoters (Sinha *et al.* 2010). This results in deacetylation and repression of these pro-apoptotic genes. However, if DNA damage is extensive, SMAR1 releases HDAC1, allowing acetylation of the *BAX* and *PUMA* promoters and the initiation of apoptosis (Sinha *et al.*

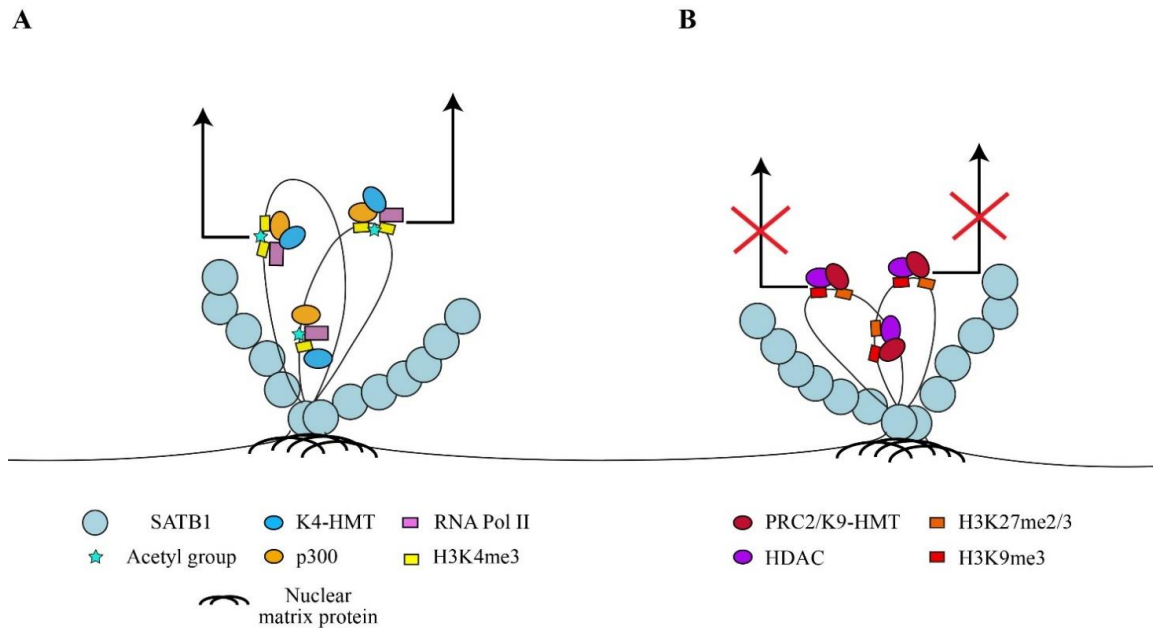


Figure 1-3. SATB1 recruitment to scaffolding/matrix attachment regions.

SATB1 binds to DNA at regions that interact with the nuclear matrix, known as scaffolding/matrix attachment regions (S/MARs). This results in locus specific chromatin looping of local or distant genes that can be accessed by chromatin organizers. **(A)** SATB1-mediated looping at S/MARs can recruit histone H3K4 methyltransferase (K4-HMT) for H3K4 tri-methylation (H3K4me3) and histone acetyltransferases such as p300 for acetylation, resulting in RNA Pol II recruitment and transcriptional activation. **(B)** SATB1 can also recruit histone deacetylases (HDACs) and either polycomb repressive complex 2 (PRC2) or K9-HMT for H3K27me2/3 or H3K9me3, respectively. Recruitment of these chromatin modifiers results in facultative or constitutive repression. Adapted from Kohwi-Shigematsu *et al.* 2013.

2010). While this is a good example of how cells can respond to environmental challenges, we are just beginning to unravel how these mechanisms work and under which conditions cells utilize these processes. There are only a few studies assessing how organizers such as SATB1 or SMAR1 function in neural cells, and these studies only focus on neural development (Balamotis *et al.* 2012; Close *et al.* 2012; Wang *et al.* 2015). Understanding how these processes may contribute to cell-state changes is critical, as chromatin organization is disrupted in aging cells and in neurodegenerative diseases such as AD.

1.4 Chromatin organization in aging and Alzheimer's disease

There is now an immense amount of data showing that there are large scale epigenetic and organizational changes in disease conditions. For example, there is a large amount of evidence showing that dysregulation of chromatin organization may be an etiological factor in many types of cancer (reviewed in Sharma *et al.* 2010). Recently, researchers have become interested in chromatin organization related changes during aging and senescence. Shah *et al.* (2013) showed that LADs predominantly enriched with H3K9me3 start to lose this histone marker during aging, replaced by H3K27me2/3 'canyons' and H3K4me3 'mesas' in senescent human IMR90 cells. Along with decreased lamin A and B, the increase in H3K4me3 results in abnormal activation of genes and destabilization of peripheral-associated heterochromatin leading to internalization of these genes (Shah *et al.* 2013). It has been proposed that this may be a model for the increases in inappropriate gene activation seen in many cell types during both aging and senescence (reviewed in Luperchio *et al.* 2014), and we can speculate that regions enriched with H3K27me2/3 would be more easily activated compared to H3K9me3 enrichment.

In post-mitotic neurons, aging related changes in epigenetic regulation are less clearly defined. Studies have reported increases in H3K27me2/3, H3K9me3 and DNA methylation, leading to inappropriate repression of gene expression (Wang *et al.* 2010;

Hernandez *et al.* 2011; Walker *et al.* 2013). In addition, Cheung *et al.* (2010) found that in aging human prefrontal cortex neurons there are approximately 100 genes abnormally enriched in H3K4me3, all related to cell cycle regulation. In a separate study from Tang *et al.* (2011), neurons from human prefrontal cortex of older subjects had reductions in histone acetylation of H3K9/K14 on genes related to inhibitory neurotransmission and mitochondrial function.

There is also increasing evidence that neurons in aging-related diseases, such as AD and related dementias, have complex changes in epigenetic related regulation. AD is characterized by the progressive dysfunction and loss of cholinergic neurons, resulting in impairments in memory, cognition, attention, mood and motor control (see Sheridan and Hausdorff 2007; McCade *et al.* 2011; Arshavsky 2014; Stella *et al.* 2014 for reviews). While AD is the most common form of dementia worldwide, only ~1-5% of cases can be explained completely by genetic origin (reviewed in Piaceri *et al.* 2013); this is most commonly related to mutations in amyloid precursor protein (APP) or presenilin 1/2 (PS1/PS2) that result in the overproduction of toxic β -amyloid ($A\beta$) and an early-onset of disease symptoms (see Tanzi 2012; Wu *et al.* 2012 for reviews). Accumulation of $A\beta$ together with hyperphosphorylation of the microtubule-associated protein tau are thought to underlie cholinergic dysfunction and neurodegeneration in AD (Alonso *et al.* 1996; reviewed in Hardy and Selkoe 2002; Zussy *et al.* 2013), though the etiology of the ~95% of 'sporadic' late-onset cases is not well understood. Recently, Miller *et al.* (2008) provided evidence that individuals with moderate to severe AD have large changes in transcription for functional groups of genes related to ion transport, synaptic transmission and RNA processing among others. Despite these transcriptional changes, efforts to identify susceptibility genes have been largely unsuccessful; only a few genes have been identified that have single-nucleotide polymorphisms or alleles related to AD susceptibility (Bertram 2011; Piaceri *et al.* 2013). These data suggest that both genetic and environmental factors may underlie the observed transcriptional changes in AD, providing rationale for a recent focus on identifying whether epigenetic changes also occur in AD and related dementias.

Initial studies exploring epigenetic changes in AD have shown complex and mixed results. For example, in CK-p25 AD model mice which have increased A β -peptide production and severe cognitive impairment, there is abnormal enrichment of H3K4me3 and H3K27 acetylation (H3K27ac) on promoters of immune response genes (Gjoneska *et al.* 2015), whereas in the same mice neuroplasticity-related genes show hypoacetylation (Gräff *et al.* 2012). Primary cortical cultures treated with A β also have increased H3K4me3 on somatostatin and cortistatin genes (Rubio *et al.* 2012), and in 3xTg AD model mice H3 and H4 acetylation is elevated (Walker *et al.* 2013). 3xTg AD mice have APP, PS1 and tau transgenes, resulting in a severe AD phenotype (Sterniczuk *et al.* 2010a; 2010b). However, aged AD model mice and human AD patients have increased HDAC2-related deacetylation of synaptic plasticity related genes (Guan *et al.* 2009; Gräff *et al.* 2012), and inhibition of HDACs in AD mouse models improves learning and memory deficits (Guan *et al.* 2009). Findings from human post-mortem brain samples are also variable, with some studies reporting increases and others decreases in global acetylation levels (Gräff *et al.* 2012; Zhang *et al.* 2012b; Narayan *et al.* 2015). Finally, 3xTg AD model mice show increases in H3K9me2 levels and related chromatin compaction (Walker *et al.* 2013), further adding to the complexity of the epigenetic changes seen in AD pathology. It is clear that more studies are needed to help define the complex epigenetic landscape in aging and AD, but evidence suggests that these changes are gene specific and therefore are likely due to changes in chromatin organization.

In support of this hypothesis, shRNA depletion of chromodomain helicase DNA binding protein 5 (CDH5, a paralog to the mi-2/Nurd remodeling complex) in primary rat cortical cultures causes both activation and repression of aging and AD-related genes (Potts *et al.* 2011). Aging-related downregulation of lamin B in neurons results in centrally located senescence-associated heterochromatic foci (Jurk *et al.* 2012). Interestingly, Zhang *et al.* (2009) showed that inhibiting SATB1 orthologs in *C. elegans* reduces lifespan. Zhang *et al.* (2009) further showed that changes in SATB1 expression levels and activation may also be related to AD pathology; knockdown of CREB-binding protein, a binding partner for SATB1, accelerates A β -induced paralysis in a transgenic *C. elegans* AD model. In PS19 AD model mice, there are observed reductions in sirtuin 1 (SIRT1), a histone and protein deacetylase that activates SATB1 (Xue *et al.* 2012; Cho *et*

al. 2015). SIRT1 expression increases activation of a disintegrin and metalloproteinase domain-containing protein 10 (ADAM10) in human glioma cells and N2a cells (Theendakara *et al.* 2013; Lee *et al.* 2014). A β is produced by cleavage of APP; ADAM10 promotes non-amyloidogenic processing APP and is thought to be neuroprotective (APP processing will be discussed in further detail in the next section) (Reviewed by Endres and Fahrenholz 2012). Given that SIRT1 can deacetylate and activate SATB1 (Xue *et al.* 2012), reductions in SIRT1 could further affect global chromatin organization, but this remains to be elucidated. It is evident that, while there is some evidence that chromatin organization may be altered in AD, more studies are needed to clarify these changes and elucidate how this may relate to disease etiology and progression.

An interesting observation in AD neurons is that proteins involved in epigenetic regulation and gene expression are mislocalized in AD patients. Recently, Mastroeni *et al.* (2013) showed that DNMT1 and Pol II were abnormally sequestered in the cytoplasm of CA1 hippocampal neurons from AD patients. They were able to recapitulate this effect after 36 h of exposure to toxic A β -oligomers in human SK-N-Be(2) neuroblastoma cells. As another example, REST, a neuronal gene repressor that is activated in aging and is involved in the cell stress response, is abnormally localized to autophagosomes in prefrontal cortex neurons of AD patients (Lu *et al.* 2014). In addition, there is observed cytoplasmic accumulation of H3K4me3 in early stage AD patients (Mastroeni *et al.* 2015).

Mastroeni *et al.* (2013) showed that the cytosolic sequestering of DNMT and Pol II was due to reduced nuclear import caused by decreased Ran-GTP mRNA and protein expression in both AD patients and in SK-N-Be(2) cells. In addition, Lee *et al.* (2006) have shown that importin- α is abnormally localized to Hirano bodies (intracellular aggregates of actin) in hippocampal neurons from AD patients. Both of these proteins are part of critical nuclear import/export mechanisms that regulate the import a large number of nuclear proteins (Reviewed in Chook and Blobel 2001).

Recently, a human and primate specific 82-kDa variant of choline acetyltransferase (82-kDa ChAT) was also found to have altered localization in cholinergic neurons of AD and frontotemporal dementia patients. 82-kDa ChAT is localized to the nucleus of cholinergic neurons of healthy adults, but is mislocalized to the cytoplasm in patients with AD and MCI (Gill *et al.*, 2007). Though the function of 82-kDa ChAT is currently unknown, there are a few clues that this protein may also be involved in gene expression changes.

1.5 82-kDa ChAT nuclear expression and gene regulation

Cholinergic neurons are critical for functions such as motor control, cognition, attention, sleep, learning and memory (see Hasselmo 2006; Woolf and Butcher 2011; Brown *et al.* 2012 for reviews). Understanding cholinergic neuron function and communication is important as AD and MCI are characterized by changes in the function of cholinergic neurons. Following a period of enhanced activity that may be due to changes in synaptic plasticity, cholinergic neuron function is eventually lost due to the effects of A β (Walsh *et al.* 2002; Townsend *et al.* 2006; Shankar *et al.* 2008). A β can oligomerize and form aggregates, which can lead to cellular toxicity, synapse degeneration, inhibition of synaptic plasticity, oxidative stress and apoptosis (Lambert *et al.* 1998; Nunomura *et al.* 2001; Shankar *et al.* 2008; Dewachter *et al.* 2009; Zussy *et al.* 2013). A β toxicity in basal forebrain cholinergic neurons results in reduced choline uptake and ChAT activity, leading to reduced acetylcholine (ACh) release (Bao *et al.* 2012; Nunes-Tavares *et al.* 2012).

Canonical ChAT enzyme function includes the production of the neurotransmitter ACh, catalyzed from choline and acetyl Coenzyme A (Traiffort *et al.* 2005). ChAT is encoded at the cholinergic gene locus, which also encodes the vesicular acetylcholine transporter (Misawa *et al.* 1997; Traiffort *et al.* 2005). There are at least 8 known splice variants of ChAT mRNA, all of which produce a 69-kDa protein (Misawa *et al.* 1997; Traiffort *et al.* 2005). In humans and non-human primates, the M-transcript is transcribed

by an additional in-frame transcription initiation site that results in the production of 82-kDa ChAT (Misawa *et al.* 1997; Traiffort *et al.* 2005). While both 69 and 82-kDa-ChAT can enter the cell nucleus, in healthy cells 82-kDa ChAT is localized predominantly in the nucleus, while 69-kDa ChAT is a nucleo-cytoplasmic shuttling protein that is primarily localized within the cytoplasm (Resendes *et al.*, 1999).

The 82-kDa ChAT protein has a unique nuclear import signal (Gill *et al.*, 2003) which may be responsible for an absence of nuclear export in healthy cells. 82-kDa ChAT is not the only nuclear localized neurotransmitter synthesizing enzyme; Olalla *et al.* (2002) reported that glutaminase, which synthesizes the excitatory neurotransmitter glutamate, is found in both the mitochondria and nuclei of glutamatergic neurons. Interestingly, in human brain tissue obtained from the basal forebrain of aged patients with MCI or AD, the nuclear localization of 82-kDa ChAT is redistributed mainly to the cytoplasm (Gill *et al.*, 2007). The regulation of nuclear import/export mechanisms for these enzymes is currently unknown. Additionally, the mechanisms that contribute to the redistribution of 82-kDa ChAT, and the consequences of this altered localization have yet to be elucidated.

Recently, our lab has published data providing evidence for a role of 82-kDa ChAT in gene expression changes. Primary neuronal cultures prepared from brain of APP/presenilin 1 (PS1) double transgenic mice that transiently express 82-kDa ChAT have increased gene expression of *GGA3*, which encodes golgi-associated, gamma-adaptin ear-containing, ARF binding protein 3 (GGA3) (Albers *et al.* 2014). GGA3 is involved in endosomal vesicle trafficking of β -secretase 1 (BACE1) for lysosomal degradation and recycling (Tesco *et al.* 2007; Kang *et al.* 2010), and in this model 82-kDa ChAT expression resulted in reductions in the protein expression and activity of BACE1 (Albers *et al.* 2014). APP can be cleaved by either α - (*e.g.* ADAM10) or β -secretases prior to cleavage by γ -secretase (**Fig. 1.4**) (reviewed in Chow *et al.* 2010). If APP is cleaved by an α -secretase, it results in the generation of a soluble APP- α fragment (sAPP α) and a membrane bound fragment that when cleaved by γ -secretase produces β -amyloid peptide A $\beta_{17-40/42}$ (p3) and the APP intracellular C-terminal domain (AICD) (Chow *et al.* 2010). Conversely, if cleaved by β -secretase, APP produces a soluble APP- β

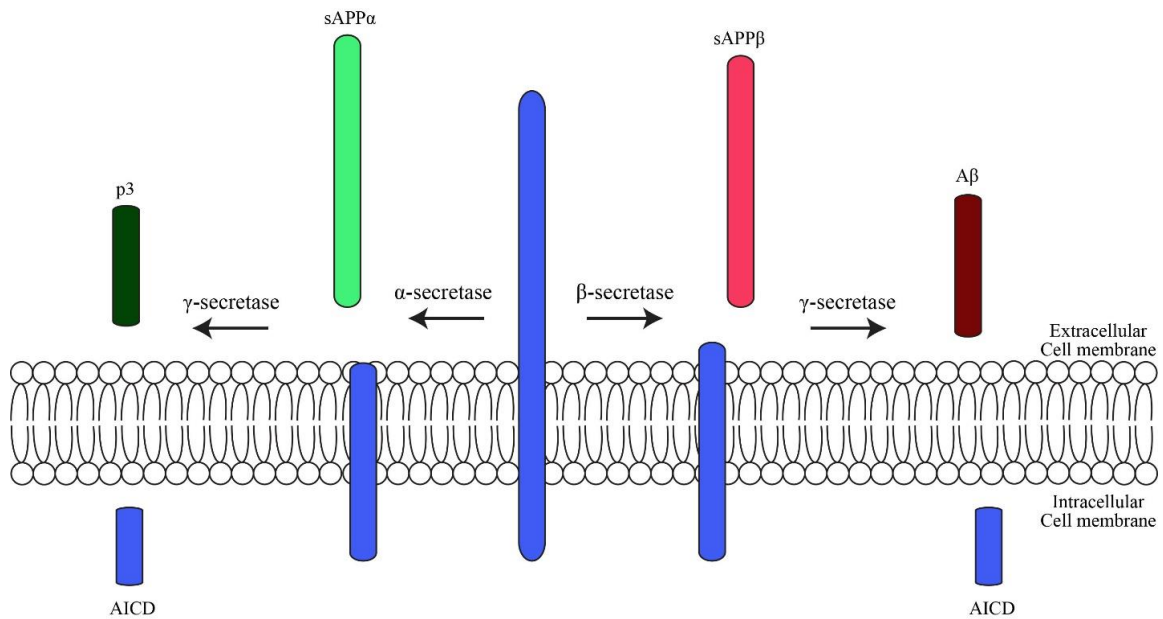


Figure 1-4. APP metabolism.

APP is a membrane bound protein that can be cleaved by either α - or β -secretases. Cleavage by α -secretases produces a soluble APP α fragment (sAPP α) and a membrane-bound fragment that is cleaved by γ -secretase to produce amyloid β - peptide A $\beta_{17-40/42}$ (p3) and the APP intracellular c-terminal domain (AICD). The p3 peptide promotes synapse formation and maintenance. Cleavage of APP by β -secretases produces a shorter sAPP β fragment and longer membrane-bound fragment. When this fragment is cleaved by γ -secretase it produces AICD and A $\beta_{1-40/42}$. The production of A β_{1-42} has been linked to cellular toxicity, protein misfolding, synapse degeneration, inhibition of synaptic plasticity, oxidative stress, and apoptosis. Adapted from Chow *et al.* 2010.

fragment (sAPP β) and a membrane bound fragment that produces a longer A $\beta_{1-40/42}$ peptide and AICD when cleaved by γ -secretase (Chow *et al.* 2010). Though it is likely that cholinergic neurons require a balance between both α - and β -secretase mediated cleavage, the production of p3 is thought to be neuroprotective and promote synapse formation and maintenance (Furukawa *et al.* 1996; Furukawa *et al.* 1996b; Kojro *et al.* 2001; Stein *et al.* 2004). Oligomeric A β_{1-42} is thought to be the more toxic form of the peptide (Shankar *et al.* 2008; Zussy *et al.* 2013; Jin and Selkoe 2015). It is unclear how exposure of cells to A β may mediate this toxicity, though it is known that A β binds to cell surface receptors that mediate cell-signaling events (Young *et al.* 2009; Beraldo *et al.* 2016). It is also possible that A β may enter the cell through endocytosis, and promote toxicity through oxidative or nitrosative stress (reviewed by Rowan *et al.* 2007; Lana *et al.* 2016; Singh *et al.* 2016). Therefore, limiting A β_{1-42} production in cholinergic neurons is likely a protective mechanism. Consequently, as a result of the observed reduction in BACE1 levels in 82-kDa ChAT-expressing APP/PS1 neurons, Albers *et al.* (2014) showed that these cells also decreased production and secretion of A β_{1-42} .

In addition to the indirect protein expression changes of BACE1, 82-kDa ChAT may have a direct role in changing gene expression related to APP processing. In human IMR32 neuroblastoma cells expressing 82-kDa ChAT, there are several genes altered related to APP metabolism and binding, as measured by microarray (Albers *et al.* 2014). One of these genes included *ADAM10*, which encodes ADAM10. Other genes included the α -secretase *ADAM17*, and genes that encode proteins related to APP binding, such as *APBA2* (which encodes X11-like [X11L]), *APPBP2* (which encodes protein interacting with APP tail 1 [PAT1]), and *RTN1* (which encodes reticulon 1 [RTN1]) (He *et al.* 2004; Sakuma *et al.* 2009; Dilsizoglu Senol *et al.* 2015). Finally, related to cholinergic neuron function, Matsuo *et al.* (2011) reported that 82-kDa ChAT expression in SH-SY5Y cells enhances transcription of the cholinergic-specific sodium-coupled choline transporter (CHT).

In the same microarray evaluating gene expression changes in IMR32 cells expressing 82-kDa ChAT, we also observed gene expression changes related to histone acetylation and chromatin organization. Some of these genes included upregulation of

CBFA2T1, which can bind to and facilitate the activity of HDACs (Baby *et al.* 2014); *KPNB1*, which can control nuclear import of the PER/CRY repressor complex (Lee *et al.* 2005); *CHD3*, a component of the Mi-2/NuRD histone remodeling complex (reviewed by Kunert and Brehm 2009); *ACTL6*, which is part of a neuron-specific chromatin remodeling complex (Yoo *et al.*, 2009); and *SATB1*, involved in chromatin organization as discussed above. There were also changes in genes related to the cell stress response, cell cycle, and inflammation/immune response. Taken together, these results clearly indicate that 82-kDa ChAT has a role in gene expression changes for multiple pathways. Elucidating how 82-kDa ChAT expression leads to these changes is essential to understanding the gene expression changes that may occur when 82-kDa ChAT expression is reduced in aging individuals, or when the localization is altered in AD and MCI patients (Gill *et al.* 2007).

Based on the above observations, one hypothesis is that 82-kDa ChAT changes gene expression, either by direct interactions with DNA or by recruiting chromatin modifying proteins or transcription factors (**Fig. 1.5**). Another possible role for 82-kDa ChAT may be recruiting or acting as a non-canonical HAT. We previously solved the crystal structure of 69-kDa ChAT, an O-acetyltransferase that has the small molecule choline as its normal substrate (Kim *et al.* 2005). There is no evidence to indicate that ChAT is able to mediate the N-acetylation required for histone acetylation (Grant and Berger 1999; Sterner and Berger 2000), and the structural features of its catalytic domain may not be accessible to accommodate a protein-based amino acid residue such as lysine (Kim *et al.* 2005). Interestingly, Britton *et al.* (2013) showed that histone H3 can be acetylated by O-acetylation at several serine and threonine residues. This recent finding provides an intriguing hypothesis for the recruitment of 82-kDa ChAT to DNA for the O-acetylation of histones. Finally, 82-kDa ChAT could be modulating the available acetyl-CoA pool via its canonical production of ACh to “fine-tune” the local amount of histone acetylation. Our laboratory demonstrated previously that 82-kDa ChAT in isolated nuclei is catalytically active and can mediate ACh synthesis (Gill *et al.* 2003). The work presented in this thesis will test the first hypothesis; that 82-kDa ChAT interacts directly with DNA to modulate context-dependent gene expression.

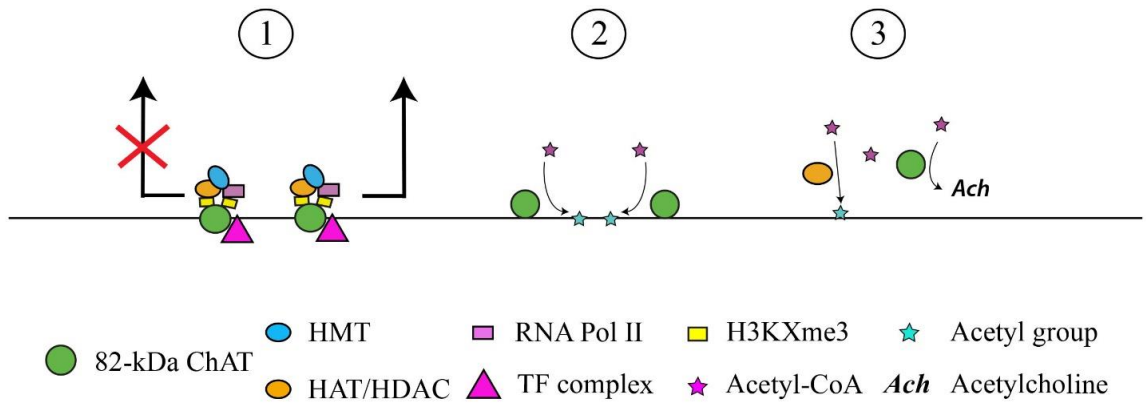


Figure 1-5. Possible roles for nuclear 82-kDa ChAT in gene expression changes.

82-kDa ChAT expression in neural cells has previously been shown to alter gene expression. These changes could be mediated through (1) recruitment of chromatin modifying enzymes such as histone methyltransferases (HMTs), histone acetyltransferases (HATs) or deacetylases (HDACs), transcription factor (TF) complexes and/or RNA polymerase II (RNA Pol II). Whether this results in transcriptional activation or repression depends on the state of histone acetylation and methylation (H3KXme3). (2) As an acetyltransferase, 82-kDa ChAT may be acting as a HAT and directly altering histone acetylation; or (3) could be modifying the available local pool of acetyl-CoA by canonical acetylcholine production.

1.6 Hypothesis and objectives

The following work was designed to test the specific hypothesis that:

The nuclear localization of 82-kDa ChAT mediates gene expression and chromatin organizational changes.

To test this hypothesis, we will:

- (1) Explore the relationship between 82-kDa ChAT and chromatin, and determine whether this relationship changes following cellular perturbations, such as exposure to oligomeric A β .
- (2) Explore the relationship between 82-kDa ChAT and SATB1 at chromatin, and show that the interaction with chromatin is dependent on both proteins. We will also explore whether 82-kDa ChAT and SATB1 may be involved in S/MAR formation and chromatin organization, and show a functional result of this interaction on the *APP* gene.
- (3) Show that 82-kDa ChAT regulates the gene expression of synapse formation and maintenance-related genes, leading to developmental changes in synapse formation.

1.7 References

- Abraham CG, Kulesza CA (2013) Polycomb repressive complex 2 silences human cytomegalovirus transcription in quiescent infection models. *J Virol*, 87: 13193-13205.
- Agrelo R, Souabni A, Novatchkova M, Haslinger C, Leeb M, Komnenovic V, Kishimoto H, Gresh L, Kohwi-Shigematsu T, Kenner L, Wutz A (2009) SATB1 defines the developmental context for gene silencing by Xist in lymphoma and embryonic cells. *Dev Cell*, 16: 507-516.
- Albers S, Inthathirath F, Gill SK, Winick-Ng W, Jaworski E, Wong DY, Gros R, Rylett RJ (2014) Nuclear 82-kDa choline acetyltransferase decreases amyloidogenic APP metabolism in neurons from APP/PS1 transgenic mice. *Neurobiol Dis*, 69: 32-42.
- Alexander JM, Lomvardas S (2014) Nuclear architecture as an epigenetic regulator of neural development and function. *Neuroscience*, 264: 39-50.
- Allsopp RC, Vaziri H, Patterson C, Goldstein S, Younglai EV, Futcher AB, Greider CW, Harley CB (1992) Telomere length predicts replicative capacity of human fibroblasts. *Proc Natl Acad Sci U S A*, 89: 10114-10118.
- Alonso AC, Grundke-Iqbal I, Iqbal K (1996) Alzheimer's disease hyperphosphorylated tau sequesters normal tau into tangles of filaments and disassembles microtubules. *Nat Med*, 2: 783-787.
- Arshavsky YI (2014) Alzheimer disease and cellular mechanisms of memory storage. *J Neuropathol Exp Neurol*, 73: 192-205.
- Baby N, Li Y, Ling EA, Lu J, Dheen ST (2014) Runx1t1 (Runt-related transcription factor 1; translocated to, 1) epigenetically regulates the proliferation and nitric oxide production of microglia. *PLoS One*, 9: e89326.

- Balamotis MA, Tamberg N, Woo YJ, Li J, Davy B, Kohwi-Shigematsu T, Kohwi Y (2012) *Satb1* ablation alters temporal expression of immediate early genes and reduces dendritic spine density during postnatal brain development. *Mol Cell Biol*, 32: 333-347.
- Bamji SX, Rico B, Kimes N, Reichardt LF (2006) BDNF mobilizes synaptic vesicles and enhances synapse formation by disrupting cadherin-beta-catenin interactions. *J Cell Biol*, 174: 289-299.
- Bannister AJ, Kouzarides T (2011) Regulation of chromatin by histone modifications. *Cell Res*, 21: 381-395.
- Bao F, Wicklund L, Lacor PN, Klein WL, Nordberg A, Marutle A (2012) Different β -amyloid oligomer assemblies in Alzheimer brains correlate with age of disease onset and impaired cholinergic activity. *Neurobiol Aging*, 33: 825.e1-13.
- Barski A, Cuddapah S, Cui K, Roh TY, Schones DE, Wang Z, Wei G, Chepelev I, Zhao K (2007) High-resolution profiling of histone methylations in the human genome. *Cell*, 129: 823-837.
- Bártfai R, Hoeijmakers WA, Salcedo-Amaya AM, Smits AH, Janssen-Megens E, Kaan A, Treeck M, Gilberger TW, François KJ, Stunnenberg HG (2010) H2A.Z demarcates intergenic regions of the *Plasmodium falciparum* epigenome that are dynamically marked by H3K9ac and H3K4me3. *PLoS Pathog*, 6: e1001223.
- Beraldo FH, Ostapchenko VG, Caetano FA, Guimaraes AL, Ferretti GD, Daude N, Bertram L, Nogueira KO, Silva JL, Westaway D, Cashman NR, Martins VR, Prado VF, Prado MA (2016) Regulation of Amyloid β Oligomer Binding to Neurons and Neurotoxicity by the Prion Protein-mGluR5 Complex. *J Biol Chem*, 291: 21945-21955.
- Bertram L (2011) Alzheimer's genetics in the GWAS era: a continuing story of 'replications and refutations'. *Curr Neurol Neurosci Rep*, 11: 246-253.

- Boros J, Arnoult N, Stroobant V, Collet JF, Decottignies A (2014) Polycomb repressive complex 2 and H3K27me3 cooperate with H3K9 methylation to maintain heterochromatin protein 1 α at chromatin. *Mol Cell Biol*, 34: 3662-3674.
- Brickner DG, Ahmed S, Meldi L, Thompson A, Light W, Young M, Hickman TL, Chu F, Fabre E, Brickner JH (2012) Transcription factor binding to a DNA zip code controls interchromosomal clustering at the nuclear periphery. *Dev Cell*, 22: 1234-1246.
- Britton LM, Newhart A, Bhanu NV, Sridharan R, Gonzales-Cope M, Plath K, Janicki SM, Garcia BA (2013) Initial characterization of histone H3 serine 10 O-acetylation. *Epigenetics*, 8: 1101-1113.
- Brinkman AB, Roelofsen T, Pennings SW, Martens JH, Jenuwein T, Stunnenberg HG (2006) Histone modification patterns associated with the human X chromosome. *EMBO Rep*, 7: 628-634.
- Brochier C, Langley B (2013) Chromatin modifications associated with DNA double-strand breaks repair as potential targets for neurological diseases. *Neurotherapeutics*, 10: 817-830.
- Brown RE, Basheer R, McKenna JT, Strecker RE, McCarley RW (2012) Control of sleep and wakefulness. *Physiol Rev*, 92: 1087-1187.
- Brunelle M, Nordell Markovits A, Rodrigue S, Lupien M, Jacques PÉ, Gévry N (2015) The histone variant H2A.Z is an important regulator of enhancer activity. *Nucleic Acids Res*, 43: 9742-9756.
- Burma S, Chen BP, Murphy M, Kurimasa A, Chen DJ (2001) ATM phosphorylates histone H2AX in response to DNA double-strand breaks. *J Biol Chem*, 276: 42462-42467.
- Cai S, Han HJ, Kohwi-Shigematsu T (2003) Tissue-specific nuclear architecture and gene expression regulated by SATB1. *Nat Genet*, 34: 42-51.

- Cai S, Lee CC, Kohwi-Shigematsu T (2006) SATB1 packages densely looped, transcriptionally active chromatin for coordinated expression of cytokine genes. *Nat Genet*, 38: 1278-1288.
- Cao R, Tsukada Y, Zhang Y (2005) Role of Bmi-1 and Ring1A in H2A ubiquitylation and Hox gene silencing. *Mol Cell*, 20: 845-854.
- Chen BY, Wang X, Wang ZY, Wang YZ, Chen LW, Luo ZJ (2013) Brain-derived neurotrophic factor stimulates proliferation and differentiation of neural stem cells, possibly by triggering the Wnt/ β -catenin signaling pathway. *J Neurosci Res*, 91: 30-41.
- Cheung I, Shulha HP, Jiang Y, Matevossian A, Wang J, Weng Z, Akbarian S (2010) Developmental regulation and individual differences of neuronal H3K4me3 epigenomes in the prefrontal cortex. *Proc Natl Acad Sci U S A*, 107: 8824-8829.
- Cheung WL, Ajiro K, Samejima K, Kloc M, Cheung P, Mizzen CA, Beeser A, Etkin LD, Chernoff J, Earnshaw WC, Allis CD (2003) Apoptotic phosphorylation of histone H2B is mediated by mammalian sterile twenty kinase. *Cell*, 113: 507-517.
- Cheutin T, Cavalli G (2012) Progressive polycomb assembly on H3K27me3 compartments generates polycomb bodies with developmentally regulated motion. *PLoS Genet*, 8: e1002465.
- Cho SH, Chen JA, Sayed F, Ward ME, Gao F, Nguyen TA, Krabbe G, Sohn PD, Lo I, Minami S, et al. (2015) SIRT1 deficiency in microglia contributes to cognitive decline in aging and neurodegeneration via epigenetic regulation of IL-1 β . *J Neurosci*, 35: 807-818.
- Choe SK, Lu P, Nakamura M, Lee J, Sagerström CG (2009) Meis cofactors control HDAC and CBP accessibility at Hox-regulated promoters during zebrafish embryogenesis. *Dev Cell*, 17: 561-570.
- Chook YM, Blobel G (2001) Karyopherins and nuclear import. *Curr Opin Struct Biol*, 11: 703-715.

- Chow VW, Mattson MP, Wong PC, Gleichmann M (2010) An overview of APP processing enzymes and products. *Neuromolecular Med*, 12: 1-12.
- Close J, Xu H, De Marco García N, Batista-Brito R, Rossignol E, Rudy B, Fishell G (2012) *Satb1* is an activity-modulated transcription factor required for the terminal differentiation and connectivity of medial ganglionic eminence-derived cortical interneurons. *J Neurosci*, 32: 17690-17705.
- Clowney EJ, LeGros MA, Mosley CP, Clowney FG, Markenskoff-Papadimitriou EC, Myllys M, Barnea G, Larabell CA, Lomvardas S (2012) Nuclear aggregation of olfactory receptor genes governs their monogenic expression. *Cell*, 151: 724-737.
- Clowney EJ, Magklara A, Colquitt BM, Pathak N, Lane RP, Lomvardas S (2011) High-throughput mapping of the promoters of the mouse olfactory receptor genes reveals a new type of mammalian promoter and provides insight into olfactory receptor gene regulation. *Genome Res*, 21: 1249-1259.
- Croft JA, Bridger JM, Boyle S, Perry P, Teague P, Bickmore WA (1999) Differences in the localization and morphology of chromosomes in the human nucleus. *J Cell Biol*, 145: 1119-1131.
- Cui H, Onyango P, Brandenburg S, Wu Y, Hsieh CL, Feinberg AP (2002) Loss of imprinting in colorectal cancer linked to hypomethylation of H19 and IGF2. *Cancer Res*, 62: 6442-6446.
- Dewachter I, Filipkowski RK, Priller C, Ris L, Neyton J, Croes S, Terwel D, Gysemans M, Devijver H, Borghgraef P, et al. (2009) Deregulation of NMDA-receptor function and down-stream signaling in APP[V717I] transgenic mice. *Neurobiol Aging*, 30: 241-256.
- Di Lorenzo A, Bedford MT (2011) Histone arginine methylation. *FEBS Lett*, 585: 2024-2031.

- Dilsizoglu Senol A, Tagliafierro L, Huguet L, Gorisse-Hussonnois L, Chasseigneaux S, Allinquant B (2015) PAT1 inversely regulates the surface Amyloid Precursor Protein level in mouse primary neurons. *BMC Neurosci*, 16: 10.
- Dixon JR, Selvaraj S, Yue F, Kim A, Li Y, Shen Y, Hu M, Liu JS, Ren B (2012) Topological domains in mammalian genomes identified by analysis of chromatin interactions. *Nature*, 485: 376-380.
- Duan Q, Chen H, Costa M, Dai W (2008) Phosphorylation of H3S10 blocks the access of H3K9 by specific antibodies and histone methyltransferase. Implication in regulating chromatin dynamics and epigenetic inheritance during mitosis. *J Biol Chem*, 283: 33585-33590.
- Endres K, Fahrenholz F (2012) The Role of the anti-amyloidogenic secretase ADAM10 in shedding the APP-like proteins. *Curr Alzheimer Res*, 9: 157-164.
- Engel N, Raval AK, Thorvaldsen JL, Bartolomei SM (2008) Three-dimensional conformation at the H19/Igf2 locus supports a model of enhancer tracking. *Hum Mol Genet*, 17: 3021-3029.
- Fernandez-Capetillo O, Allis CD, Nussenzweig A (2004) Phosphorylation of histone H2B at DNA double-strand breaks. *J Exp Med*, 199: 1671-1677.
- Frade JM, Ovejero-Benito MC (2015) Neuronal cell cycle: the neuron itself and its circumstances. *Cell Cycle*, 14: 712-720.
- Fradet-Turcotte A, Canny MD, Escribano-Díaz C, Orthwein A, Leung CC, Huang H, Landry MC, Kitevski-LeBlanc J, Noordermeer SM, Sicheri F, Durocher D (2013) 53BP1 is a reader of the DNA-damage-induced H2A Lys 15 ubiquitin mark. *Nature*, 499: 50-54.
- Fraser J, Ferrai C, Chiariello AM, Schueler M, Rito T, Laudanno G, Barbieri M, Moore BL, Kraemer DC, Aitken S, et al. (2015) Hierarchical folding and reorganization of chromosomes are linked to transcriptional changes in cellular differentiation. *Mol Syst Biol*, 11: 852.

- Furukawa K, Barger SW, Blalock EM, Mattson MP (1996) Activation of K⁺ channels and suppression of neuronal activity by secreted beta-amyloid-precursor protein. *Nature*, 379: 74-78.
- Furukawa K, Sopher BL, Rydel RE, Begley JG, Pham DG, Martin GM, Fox M, Mattson MP (1996b) Increased activity-regulating and neuroprotective efficacy of alpha-secretase-derived secreted amyloid precursor protein conferred by a C-terminal heparin-binding domain. *J Neurochem*, 67: 1882-1896.
- Gabory A, Ripoche MA, Le Digarcher A, Watrin F, Ziyat A, Forné T, Jammes H, Ainscough JF, Surani MA, Journot L, Dandolo L (2009) H19 acts as a trans regulator of the imprinted gene network controlling growth in mice. *Development*, 136: 3413-3421.
- Gill SK, Bhattacharya M, Ferguson SS, Rylett RJ (2003) Identification of a novel nuclear localization signal common to 69- and 82-kDa human choline acetyltransferase. *J Biol Chem*, 278: 20217-20224.
- Gill SK, Ishak M, Dobransky T, Haroutunian V, Davis KL, Rylett RJ (2007) 82-kDa choline acetyltransferase is in nuclei of cholinergic neurons in human CNS and altered in aging and Alzheimer disease. *Neurobiol Aging*, 28: 1028-1040.
- Girdwood D, Bumpass D, Vaughan OA, Thain A, Anderson LA, Snowden AW, Garcia-Wilson E, Perkins ND, Hay RT (2003) P300 transcriptional repression is mediated by SUMO modification. *Mol Cell*, 11: 1043-1054.
- Gjoneska E, Pfenning AR, Mathys H, Quon G, Kundaje A, Tsai LH, Kellis M (2015) Conserved epigenomic signals in mice and humans reveal immune basis of Alzheimer's disease. *Nature*, 518: 365-369.
- Gong X, Bacchelli E, Blasi F, Toma C, Betancur C, Chaste P, Delorme R, Durand CM, Fauchereau F et al. (2008) Analysis of X chromosome inactivation in autism spectrum disorders. *Am J Med Genet B Neuropsychiatr Genet*, 147B: 830-835.

- Gräff J, Rei D, Guan JS, Wang WY, Seo J, Hennig KM, Nieland TJ, Fass DM, Kao PF, Kahn M, et al. (2012) An epigenetic blockade of cognitive functions in the neurodegenerating brain. *Nature*, 483: 222-226.
- Grant PA, Berger SL (1999) Histone acetyltransferase complexes. *Semin Cell Dev Biol*, 10: 167-177.
- Gregor A, Oti M, Kouwenhoven EN, Hoyer J, Sticht H, Ekici AB, Kjaergaard S, Rauch A, Stunnenberg HG, Uebe S, et al. (2013) De novo mutations in the genome organizer CTCF cause intellectual disability. *Am J Hum Genet*, 93: 124-131.
- Guan JS, Haggarty SJ, Giacometti E, Dannenberg JH, Joseph N, Gao J, Nieland TJ, Zhou Y, Wang X, Mazitschek R, et al. (2009) HDAC2 negatively regulates memory formation and synaptic plasticity. *Nature*, 459: 55-60.
- Guelen L, Pagie L, Brasset E, Meuleman W, Faza MB, Talhout W, Eussen BH, de Klein A, Wessels L, de Laat W, van Steensel B (2008) Domain organization of human chromosomes revealed by mapping of nuclear lamina interactions. *Nature*, 453: 948-951.
- Guenatri M, Bailly D, Maison C, Almouzni G (2004) Mouse centric and pericentric satellite repeats form distinct functional heterochromatin. *J Cell Biol*, 166: 493-505.
- Hardy J, Selkoe DJ (2002) The amyloid hypothesis of Alzheimer's disease: progress and problems on the road to therapeutics. *Science*, 297: 353-356.
- Harnicarová A, Kozubek S, Pacherník J, Krejci J, Bártová E (2006) Distinct nuclear arrangement of active and inactive c-myc genes in control and differentiated colon carcinoma cells. *Exp Cell Res*, 312: 4019-4035.
- Hasselmo ME (2006) The role of acetylcholine in learning and memory. *Curr Opin Neurobiol*, 16: 710-715.

- He W, Lu Y, Qahwash I, Hu XY, Chang A, Yan R (2004) Reticulon family members modulate BACE1 activity and amyloid-beta peptide generation. *Nat Med*, 10: 959-965.
- Heidari N, Phanstiel DH, He C, Grubert F, Jahanbani F, Kasowski M, Zhang MQ, Snyder MP (2014) Genome-wide map of regulatory interactions in the human genome. *Genome Res*, 24: 1905-1917.
- Heng HH, Goetze S, Ye CJ, Liu G, Stevens JB, Bremer SW, Wykes SM, Bode J, Krawetz SA (2004) Chromatin loops are selectively anchored using scaffold/matrix-attachment regions. *J Cell Sci*, 117: 999-1008.
- Henry RA, Kuo YM, Andrews AJ (2013) Differences in specificity and selectivity between CBP and p300 acetylation of histone H3 and H3/H4. *Biochemistry*, 52: 5746-5759.
- Hernandez DG, Nalls MA, Gibbs JR, Arepalli S, van der Brug M, Chong S, Moore M, Longo DL, Cookson MR, Traynor BJ, Singleton AB (2011) Distinct DNA methylation changes highly correlated with chronological age in the human brain. *Hum Mol Genet*, 20: 1164-1172.
- Herrup K, Yang Y (2007) Cell cycle regulation in the postmitotic neuron: oxymoron or new biology? *Nat Rev Neurosci*, 8: 368-378.
- Hinde E, Cardarelli F, Digman MA, Gratton E (2012) Changes in chromatin compaction during the cell cycle revealed by micrometer-scale measurement of molecular flow in the nucleus. *Biophys J*, 102: 691-697.
- Jamieson K, Wiles ET, McNaught KJ, Sidoli S, Leggett N, Shao Y, Garcia BA, Selker EU (2016) Loss of HP1 causes depletion of H3K27me3 from facultative heterochromatin and gain of H3K27me2 at constitutive heterochromatin. *Genome Res*, 26: 97-107.

- Jin M, Selkoe DJ (2015) Systematic analysis of time-dependent neural effects of soluble amyloid β oligomers in culture and in vivo: Prevention by scyllo-inositol. *Neurobiol Dis*, 82: 152-163.
- Juraeva D, Haenisch B, Zapatka M, Frank J; GROUP Investigators; PSYCH-GEMS SCZ Working Group, Witt SH, Mühleisen TW, Treutlein J, Strohmaier J, et al. (2014) Integrated pathway-based approach identifies association between genomic regions at CTCF and CACNB2 and schizophrenia. *PLoS Genet*, 10: e1004345.
- Jurk D, Wang C, Miwa S, Maddick M, Korolchuk V, Tsolou A, Gonos ES, Thrasivoulou C, Saffrey MJ, Cameron K, von Zglinicki T (2012) Postmitotic neurons develop a p21-dependent senescence-like phenotype driven by a DNA damage response. *Aging Cell*, 11: 996-1004.
- Kalverda B, Röling MD, Fornerod M (2008) Chromatin organization in relation to the nuclear periphery. *FEBS Lett*, 582: 2017-2022.
- Kang EL, Cameron AN, Piazza F, Walker KR, Tesco G (2010) Ubiquitin regulates GGA3-mediated degradation of BACE1. *J Biol Chem*, 285: 24108-24119.
- Kim AR, Dobransky T, Rylett RJ, Shilton BH (2005) Surface-entropy reduction used in the crystallization of human choline acetyltransferase. *Acta Crystallogr D Biol Crystallogr*, 61: 1306-1310.
- Kim SK, Jung I, Lee H, Kang K, Kim M, Jeong K, Kwon CS, Han YM, Kim YS, Kim D, Lee D (2012) Human histone H3K79 methyltransferase DOT1L protein [corrected] binds actively transcribing RNA polymerase II to regulate gene expression. *J Biol Chem*, 287: 39698-39709.
- Kim TW, Kang BH, Jang H, Kwak S, Shin J, Kim H, Lee SE, Lee SM, Lee JH, Kim JH, et al. (2015) Ctbp2 Modulates NuRD-Mediated Deacetylation of H3K27 and Facilitates PRC2-Mediated H3K27me3 in Active Embryonic Stem Cell Genes During Exit from Pluripotency. *Stem Cells*, 33: 2442-2455.

- Kohwi-Shigematsu T, Poterlowicz K, Ordinario E, Han HJ, Botchkarev VA, Kohwi Y (2013) Genome organizing function of SATB1 in tumor progression. *Semin Cancer Biol*, 23: 72-79.
- Kojro E, Gimpl G, Lammich S, Marz W, Fahrenholz F (2001) Low cholesterol stimulates the nonamyloidogenic pathway by its effect on the alpha -secretase ADAM 10. *Proc Natl Acad Sci U S A*, 98: 5815-5820.
- Kumar PP, Bischof O, Purbey PK, Notani D, Urlaub H, Dejean A, Galande S (2007) Functional interaction between PML and SATB1 regulates chromatin-loop architecture and transcription of the MHC class I locus. *Nat Cell Biol*, 9: 45-56.
- Kunert N, Brehm A (2009) Novel Mi-2 related ATP-dependent chromatin remodelers. *Epigenetics*, 4: 209-211.
- Lachner M, O'Sullivan RJ, Jenuwein T (2003) An epigenetic road map for histone lysine methylation. *J Cell Sci*, 116: 2117-2124.
- Lambert MP, Barlow AK, Chromy BA, Edwards C, Freed R, Liosatos M, Morgan TE, Rozovsky I, Trommer B, Viola KL, et al. (1998) Diffusible, nonfibrillar ligands derived from Abeta1-42 are potent central nervous system neurotoxins. *Proc Natl Acad Sci U S A*, 95: 6448-6453.
- Lana E, Khanbolouki M, Degavre C, Samuelsson EB, Åkesson E, Winblad B, Alici E, Lithner CU, Behbahani H (2016) Perforin Promotes Amyloid Beta Internalisation in Neurons. *Mol Neurobiol*, Epub ahead of print, DOI: 10.1007/s12035-016-9685-9.
- Lee HG, Ueda M, Miyamoto Y, Yoneda Y, Perry G, Smith MA, Zhu X (2006) Aberrant localization of importin alpha1 in hippocampal neurons in Alzheimer disease. *Brain Res*, 1124: 1-4.
- Lee HR, Shin HK, Park SY, Kim HY, Lee WS, Rhim BY, Hong KW, Kim CD (2014) Cilostazol suppresses β -amyloid production by activating a disintegrin and

metalloproteinase 10 via the upregulation of SIRT1-coupled retinoic acid receptor- β . *J Neurosci Res*, 92: 1581-1590.

Lee Y, Jang AR, Francey LJ, Sehgal A, Hogenesch JB (2015) KPNB1 mediates PER/CRY nuclear translocation and circadian clock function. *Elife*, 4.

Li DQ, Kumar R (2010) Mi-2/NuRD complex making inroads into DNA-damage response pathway. *Cell Cycle*, 9: 2071-2079.

Li G, Zhou L (2013) Genome-wide identification of chromatin transitional regions reveals diverse mechanisms defining the boundary of facultative heterochromatin. *PLoS One*, 8:e67156.

Liang G, Lin JC, Wei V, Yoo C, Cheng JC, Nguyen CT, Weisenberger DJ, Egger G, Takai D, Gonzales FA, Jones PA (2004) Distinct localization of histone H3 acetylation and H3-K4 methylation to the transcription start sites in the human genome. *Proc Natl Acad Sci U S A*, 101: 7357-7362.

Lin N, Li X, Cui K, Chepelev I, Tie F, Liu B, Li G, Harte P, Zhao K, Huang S, Zhou L (2011) A barrier-only boundary element delimits the formation of facultative heterochromatin in *D. melanogaster* and vertebrates. *Mol Cell Biol*, 31: 2729-2741.

Linkus B, Wiesner D, Meßner M, Karabatsiakakis A, Scheffold A, Rudolph KL, Thal DR, Weishaupt JH, Ludolph AC, Danzer KM (2016) Telomere shortening leads to earlier age of onset in ALS mice. *Aging (Albany NY)*, 8: 382-393.

Lomvardas S, Barnea G, Pisapia DJ, Mendelsohn M, Kirkland J, Axel R (2006) Interchromosomal interactions and olfactory receptor choice. *Cell*, 126: 403-413.

Lu T, Aron L, Zullo J, Pan Y, Kim H, Chen Y, Yang TH, Kim HM, Drake D, Liu XS, et al. (2014) REST and stress resistance in ageing and Alzheimer's disease. *Nature*, 507: 448-454.

- Luperchio TR, Wong X, Reddy KL (2014) Genome regulation at the peripheral zone: lamina associated domains in development and disease. *Curr Opin Genet Dev*, 25: 50-61.
- Marques S, Outeiro TF (2013) Epigenetics in Parkinson's and Alzheimer's diseases. *Subcell Biochem*, 61: 507-525.
- Martínez F, Roselló M, Mayo S, Monfort S, Oltra S, Orellana C (2014) Duplication at Xq13.3-q21.1 with syndromic intellectual disability, a probable role for the ATRX gene. *Am J Med Genet A*, 164A: 918-923.
- Mastroeni D, Chouliaras L, Grover A, Liang WS, Hauns K, Rogers J, Coleman PD (2013) Reduced RAN expression and disrupted transport between cytoplasm and nucleus; a key event in Alzheimer's disease pathophysiology. *PLoS One*, 8: e53349.
- Mastroeni D, Delvaux E, Nolz J, Tan Y, Grover A, Oddo S, Coleman PD (2015) Aberrant intracellular localization of H3k4me3 demonstrates an early epigenetic phenomenon in Alzheimer's disease. *Neurobiol Aging*, 36: 3121-3129.
- Matsuo A, Bellier JP, Nishimura M, Yasuhara O, Saito N, Kimura H (2011) Nuclear choline acetyltransferase activates transcription of a high-affinity choline transporter. *J Biol Chem*, 286: 5836-5845.
- McCade D, Savage G, Naismith SL (2011) Review of emotion recognition in mild cognitive impairment. *Dement Geriatr Cogn Disord*, 32: 257-266.
- McCarthy SE, Gillis J, Kramer M, Lihm J, Yoon S, Berstein Y, Mistry M, Pavlidis P, Solomon R, Ghiban E, et al. (2014) De novo mutations in schizophrenia implicate chromatin remodeling and support a genetic overlap with autism and intellectual disability. *Mol Psychiatry*, 19: 652-658.
- Metzger E, Yin N, Wissmann M, Kunowska N, Fischer K, Friedrichs N, Patnaik D, Higgins JM, Potier N, Scheidtmann KH, et al. (2008) Phosphorylation of histone

H3 at threonine 11 establishes a novel chromatin mark for transcriptional regulation. *Nat Cell Biol*, 10: 53-60.

Meuleman W, Peric-Hupkes D, Kind J, Beaudry JB, Pagie L, Kellis M, Reinders M, Wessels L, van Steensel B (2013) Constitutive nuclear lamina-genome interactions are highly conserved and associated with A/T-rich sequence. *Genome Res*, 23: 270-280.

Mikkelsen TS, Ku M, Jaffe DB, Issac B, Lieberman E, Giannoukos G, Alvarez P, Brockman W, Kim TK, Koche RP, et al. (2007) Genome-wide maps of chromatin state in pluripotent and lineage-committed cells. *Nature*, 448: 553-560.

Miller JA, Oldham MC, Geschwind DH (2008) A systems level analysis of transcriptional changes in Alzheimer's disease and normal aging. *J Neurosci*, 28: 1410-1420.

Misawa H, Matsuura J, Oda Y, Takahashi R, Deguchi T (1997) Human choline acetyltransferase mRNAs with different 5'-region produce a 69-kDa major translation product. *Brain Res Mol Brain Res*, 44: 323-333.

Montalbano A, Baj G, Papadia D, Tongiorgi E, Sciancalepore M (2013) Blockade of BDNF signaling turns chemically-induced long-term potentiation into long-term depression. *Hippocampus*, 23: 879-889.

Nagl NG Jr, Wang X, Patsialou A, Van Scoy M, Moran E (2007) Distinct mammalian SWI/SNF chromatin remodeling complexes with opposing roles in cell-cycle control. *EMBO J*, 26: 752-763.

Nakano M, Cardinale S, Noskov VN, Gassmann R, Vagnarelli P, Kandels-Lewis S, Larionov V, Earnshaw WC, Masumoto H (2008) Inactivation of a human kinetochore by specific targeting of chromatin modifiers. *Dev Cell*, 14: 507-522.

Nakayama J, Rice JC, Strahl BD, Allis CD, Grewal SI (2001) Role of histone H3 lysine 9 methylation in epigenetic control of heterochromatin assembly. *Science*, 292: 110-113.

- Narayan PJ, Lill C, Faull R, Curtis MA, Dragunow M (2015) Increased acetyl and total histone levels in post-mortem Alzheimer's disease brain. *Neurobiol Dis*, 74: 281-294.
- Narendra V, Rocha PP, An D, Raviram R, Skok JA, Mazzoni EO, Reinberg D (2015) CTCF establishes discrete functional chromatin domains at the Hox clusters during differentiation. *Science*, 347: 1017-1021.
- Nunes-Tavares N, Santos LE, Stutz B, Brito-Moreira J, Klein WL, Ferreira ST, de Mello FG (2012) Inhibition of choline acetyltransferase as a mechanism for cholinergic dysfunction induced by amyloid- β peptide oligomers. *J Biol Chem*, 287: 19377-19385.
- Nunomura A, Perry G, Aliev G, Hirai K, Takeda A, Balraj EK, Jones PK, Ghanbari H, Wataya T, Shimohama S, et al. (2001) Oxidative damage is the earliest event in Alzheimer disease. *J Neuropathol Exp Neurol*, 60: 759-767.
- Oda H, Okamoto I, Murphy N, Chu J, Price SM, Shen MM, Torres-Padilla ME, Heard E, Reinberg D (2009) Monomethylation of histone H4-lysine 20 is involved in chromosome structure and stability and is essential for mouse development. *Mol Cell Biol*, 29: 2278-2295.
- Pal S, Vishwanath SN, Erdjument-Bromage H, Tempst P, Sif S (2004) Human SWI/SNF-associated PRMT5 methylates histone H3 arginine 8 and negatively regulates expression of ST7 and NM23 tumor suppressor genes. *Mol Cell Biol*, 24: 9630-9645.
- Peric-Hupkes D, Meuleman W, Pagie L, Bruggeman SW, Solovei I, Brugman W, Gräf S, Flicek P, Kerkhoven RM, van Lohuizen M, et al. (2010) Molecular maps of the reorganization of genome-nuclear lamina interactions during differentiation. *Mol Cell*, 38: 603-613.
- Peters AH, Kubicek S, Mechtler K, O'Sullivan RJ, Derijck AA, Perez-Burgos L, Kohlmaier A, Opravil S, Tachibana M, Shinkai Y, et al. (2003) Partitioning and

plasticity of repressive histone methylation states in mammalian chromatin. *Mol Cell*, 12: 1577-1589.

Piaceri I, Nacmias B, Sorbi S (2013) Genetics of familial and sporadic Alzheimer's disease. *Front Biosci (Elite Ed)*, 5:167-177.

Politz JC, Scalzo D, Groudine M (2013) Something silent this way forms: the functional organization of the repressive nuclear compartment. *Annu Rev Cell Dev Biol*, 29: 241-270.

Pollak M (2012) The insulin and insulin-like growth factor receptor family in neoplasia: an update. *Nat Rev Cancer*, 12: 159-169.

Potts RC, Zhang P, Wurster AL, Precht P, Mughal MR, Wood WH 3rd, Zhang Y, Becker KG, Mattson MP, Pazin MJ (2011) CHD5, a brain-specific paralog of Mi2 chromatin remodeling enzymes, regulates expression of neuronal genes. *PLoS One*, 6: e24515.

Resendes MC, Dobransky T, Ferguson SS, Rylett RJ (1999) Nuclear localization of the 82-kDa form of human choline acetyltransferase. *J Biol Chem*, 274: 19417-19421.

Rougeulle C, Chaumeil J, Sarma K, Allis CD, Reinberg D, Avner P, Heard E (2004) Differential histone H3 Lys-9 and Lys-27 methylation profiles on the X chromosome. *Mol Cell Biol*, 24: 5475-5484.

Rowan MJ, Klyubin I, Wang Q, Hu NW, Anwyl R (2009) Synaptic memory mechanisms: Alzheimer's disease amyloid beta-peptide-induced dysfunction. *Biochem Soc Trans*, 35: 1219-1223.

Rubio A, Sánchez-Mut JV, García E, Velasquez ZD, Oliver J, Esteller M, Avila J (2012) Epigenetic control of somatostatin and cortistatin expression by β amyloid peptide. *J Neurosci*, 90: 13-20.

- Saksouk N, Simboeck E, Déjardin J (2015) Constitutive heterochromatin formation and transcription in mammals. *Epigenetics Chromatin*, 8: 3.
- Sakuma M, Tanaka E, Taru H, Tomita S, Gandy S, Nairn AC, Nakaya T, Yamamoto T, Suzuki T (2009) Phosphorylation of the amino-terminal region of X11L regulates its interaction with APP. *J Neurochem*, 109: 465-475.
- Sarcinella E, Zuzarte PC, Lau PN, Draker R, Cheung P (2007) Monoubiquitylation of H2A.Z distinguishes its association with euchromatin or facultative heterochromatin. *Mol Cell Biol*, 27: 6457-6468.
- Sawicka A, Hartl D, Goiser M, Pusch O, Stocsits RR, Tamir IM, Mechtler K, Seiser C (2014) H3S28 phosphorylation is a hallmark of the transcriptional response to cellular stress. *Genome Res*, 24: 1808-1820.
- Schotta G, Ebert A, Krauss V, Fischer A, Hoffmann J, Rea S, Jenuwein T, Dorn R, Reuter G (2002) Central role of *Drosophila* SU(VAR)3-9 in histone H3-K9 methylation and heterochromatic gene silencing. *EMBO J*, 21: 1121-1131.
- Shah PP, Donahue G, Otte GL, Capell BC, Nelson DM, Cao K, Aggarwala V, Cruickshanks HA, Rai TS, McBryan T, et al. (2013) Lamin B1 depletion in senescent cells triggers large-scale changes in gene expression and the chromatin landscape. *Genes Dev*, 27: 1787-1799.
- Shahani N, Sawa A (2011) Nitric oxide signaling and nitrosative stress in neurons: role for S-nitrosylation. *Antioxid Redox Signal*, 14: 1493-1504.
- Sharma S, Kelly TK, Jones PA (2010) Epigenetics in cancer. *Carcinogenesis*, 31: 27-36.
- Shankar GM, Li S, Mehta TH, Garcia-Munoz A, Shepardson NE, Smith I, Brett FM, Farrell MA, Rowan MJ, Lemere CA, et al. (2008) Amyloid-beta protein dimers isolated directly from Alzheimer's brains impair synaptic plasticity and memory. *Nat Med*, 14: 837-842.

- Sheridan PL, Hausdorff JM (2007) The role of higher-level cognitive function in gait: executive dysfunction contributes to fall risk in Alzheimer's disease. *Dement Geriatr Cogn Disord*, 24: 125-137.
- Shiio Y, Eisenman RN (2003) Histone sumoylation is associated with transcriptional repression. *Proc Natl Acad Sci U S A*, 100: 13225-13230.
- Singh AK, Kashyap MP, Tripathi VK, Singh S, Garg G, Rizvi SI (2016) Neuroprotection Through Rapamycin-Induced Activation of Autophagy and PI3K/Akt1/mTOR/CREB Signaling Against Amyloid- β -Induced Oxidative Stress, Synaptic/Neurotransmission Dysfunction, and Neurodegeneration in Adult Rats. *Mol Neurobiol*, Epub ahead of print, DOI: 10.1007/s12035-016-0129-3.
- Sinha S, Malonia SK, Mittal SP, Singh K, Kadreppa S, Kamat R, Mukhopadhyaya R, Pal JK, Chattopadhyay S (2010) Coordinated regulation of p53 apoptotic targets BAX and PUMA by SMAR1 through an identical MAR element. *EMBO J*, 29: 830-842.
- Smith EM, Lajoie BR, Jain G, Dekker J (2016) Invariant TAD Boundaries Constrain Cell-Type-Specific Looping Interactions between Promoters and Distal Elements around the CFTR Locus. *Am J Hum Genet*, 98: 185-201.
- Solovei I, Kreysing M, Lanctôt C, Kösem S, Peichl L, Cremer T, Guck J, Joffe B (2009) Nuclear architecture of rod photoreceptor cells adapts to vision in mammalian evolution. *Cell*, 137: 356-368.
- Solovei I, Wang AS, Thanisch K, Schmidt CS, Krebs S, Zwerger M, Cohen TV, Devys D, Foisner R, Peichl L, et al. (2013) LBR and lamin A/C sequentially tether peripheral heterochromatin and inversely regulate differentiation. *Cell*, 152: 584-598.
- Spremo-Potparević B, Zivković L, Djelić N, Plečas-Solarović B, Smith MA, Bajić V (2008) Premature centromere division of the X chromosome in neurons in Alzheimer's disease. *J Neurochem*, 106: 2218-2223.

- Stein TD, Anders NJ, DeCarli C, Chan SL, Mattson MP, Johnson JA (2004) Neutralization of transthyretin reverses the neuroprotective effects of secreted amyloid precursor protein (APP) in APPSW mice resulting in tau phosphorylation and loss of hippocampal neurons: support for the amyloid hypothesis. *J Neurosci*, 24: 7707-7717.
- Stella F, Radanovic M, Aprahamian I, Canineu PR, de Andrade LP, Forlenza OV (2008) Neurobiological correlates of apathy in Alzheimer's disease and mild cognitive impairment: a critical review. *J Alzheimers Dis*, 39: 633-648.
- Sterner DE, Berger SL (2000) Acetylation of histones and transcription-related factors. *Microbiol Mol Biol Rev*, 64: 435-459.
- Sterniczuk R, Antle MC, Laferla FM, Dyck RH (2010a) Characterization of the 3xTg-AD mouse model of Alzheimer's disease: part 2. Behavioral and cognitive changes. *Brain Res*, 1348: 149-155.
- Sterniczuk R, Dyck RH, Laferla FM, Antle MC (2010b) Characterization of the 3xTg-AD mouse model of Alzheimer's disease: part 1. Circadian changes. *Brain Res*, 1348: 139-148.
- Stunnenberg R, Kulasegaran-Shylini R, Keller C, Kirschmann MA, Gelman L, Bühler M (2015) H3K9 methylation extends across natural boundaries of heterochromatin in the absence of an HP1 protein. *EMBO J*, 34: 2789-2803.
- Tang B, Dean B, Thomas EA (2011) Disease- and age-related changes in histone acetylation at gene promoters in psychiatric disorders. *Transl Psychiatry*, 1: e64.
- Tanzi RE (2012) The genetics of Alzheimer disease. *Cold Spring Harb Perspect Med*, 2: a006296.
- Tesco G, Koh YH, Kang EL, Cameron AN, Das S, Sena-Esteves M, Hiltunen M, Yang SH, Zhong Z, Shen Y, et al. (2007) Depletion of GGA3 stabilizes BACE and enhances beta-secretase activity. *Neuron*, 54: 721-737.

- Theendakara V, Patent A, Peters Libeu CA, Philpot BD, Flores S, Descamps O, Poksay KS, Zhang Q, Cailing G, Hart M, et al. (2013) Neuroprotective Sirtuin ratio reversed by ApoE4. *Proc Natl Acad Sci U S A*, 110: 18303-18308.
- Townsend M, Shankar GM, Mehta T, Walsh DM, Selkoe DJ (2006) Effects of secreted oligomers of amyloid beta-protein on hippocampal synaptic plasticity: a potent role for trimers. *J Physiol*, 572: 477-492.
- Traiffort E, Ruat M, O'Regan S, Meunier FM (2005) Molecular characterization of the family of choline transporter-like proteins and their splice variants. *J Neurochem*, 92: 1116-1125.
- Ulaner GA, Vu TH, Li T, Hu JF, Yao XM, Yang Y, Gorlick R, Meyers P, Healey J, Ladanyi M, Hoffman AR (2003) Loss of imprinting of IGF2 and H19 in osteosarcoma is accompanied by reciprocal methylation changes of a CTCF-binding site. *Hum Mol Genet*, 12: 535-549.
- Vaquero A, Scher M, Erdjument-Bromage H, Tempst P, Serrano L, Reinberg D (2007) SIRT1 regulates the histone methyl-transferase SUV39H1 during heterochromatin formation. *Nature*, 450: 440-444.
- Vamos EE, Boros IM (2012) The C-terminal domains of ADA2 proteins determine selective incorporation into GCN5-containing complexes that target histone H3 or H4 for acetylation. *FEBS Lett*, 586: 3279-3286.
- Vogel-Ciernia A, Matheos DP, Barrett RM, Kramár EA, Azzawi S, Chen Y, Magnan CN, Zeller M, Sylvain A, Haettig J, et al. (2013) The neuron-specific chromatin regulatory subunit BAF53b is necessary for synaptic plasticity and memory. *Nat Neurosci*, 16: 552-561.
- Vogel-Ciernia A, Wood MA (2014) Neuron-specific chromatin remodeling: a missing link in epigenetic mechanisms underlying synaptic plasticity, memory, and intellectual disability disorders. *Neuropharmacology*, 80: 18-27.

- Walczak A, Szczepankiewicz AA, Ruszczycki B, Magalska A, Zamlynska K, Dzwonek J, Wilczek E, Zybura-Broda K, Rylski M, Malinowska M, et al. (2013) Novel higher-order epigenetic regulation of the Bdnf gene upon seizures. *J Neurosci*, 33: 2507-2511.
- Walker MP, LaFerla FM, Oddo SS, Brewer GJ (2013) Reversible epigenetic histone modifications and Bdnf expression in neurons with aging and from a mouse model of Alzheimer's disease. *Age (Dordr)*, 35: 519-531.
- Walsh DM, Klyubin I, Fadeeva JV, Cullen WK, Anwyl R, Wolfe MS, Rowan MJ, Selkoe DJ (2002) Naturally secreted oligomers of amyloid beta protein potently inhibit hippocampal long-term potentiation in vivo. *Nature*, 416: 535-539.
- Wang CM, Tsai SN, Yew TW, Kwan YW, Ngai SM (2010) Identification of histone methylation multiplicities patterns in the brain of senescence-accelerated prone mouse 8. *Biogerontology*, 11: 87-102.
- Wang F, Tidei JJ, Polich ED, Gao Y, Zhao H, Perrone-Bizzozero NI, Guo W, Zhao X (2015) Positive feedback between RNA-binding protein HuD and transcription factor SATB1 promotes neurogenesis. *Proc Natl Acad Sci U S A*, 112: E4995-5004.
- Wang L, Di LJ, Lv X, Zheng W, Xue Z, Guo ZC, Liu DP, Liang CC (2009) Inter-MAR association contributes to transcriptionally active looping events in human beta-globin gene cluster. *PLoS One*, 4: e4629.
- Wen J, Huang S, Rogers H, Dickinson LA, Kohwi-Shigematsu T, Noguchi CT (2005) SATB1 family protein expressed during early erythroid differentiation modifies globin gene expression. *Blood*, 105: 3330-3339.
- Wongtawan T, Taylor JE, Lawson KA, Wilmut I, Pennings S (2011) Histone H4K20me3 and HP1 α are late heterochromatin markers in development, but present in undifferentiated embryonic stem cells. *J Cell Sci*, 124: 1878-1890.

- Woolf NJ, Butcher LL (2011) Cholinergic systems mediate action from movement to higher consciousness. *Behav Brain Res*, 221: 488-498.
- Wu L, Rosa-Neto P, Hsiung GY, Sadovnick AD, Masellis M, Black SE, Jia J, Gauthier S (2012) Early-onset familial Alzheimer's disease (EOFAD). *Can J Neurol Sci*, 39: 436-445.
- Xue Z, Lv X, Song W, Wang X, Zhao GN, Wang WT, Xiong J, Mao BB, Yu W, Yang B, et al. (2012) SIRT1 deacetylates SATB1 to facilitate MAR HS2-MAR ϵ interaction and promote ϵ -globin expression. *Nucleic Acids Res*, 40: 4804-4815.
- Yang SH, Bumpass DC, Perkins ND, Sharrocks AD (2002) The ETS domain transcription factor Elk-1 contains a novel class of repression domain. *Mol Cell Biol*, 22: 5036-5046.
- Yang Y, Wang Z, Sun L, Shao L, Yang N, Yu D, Zhang X, Han X, Sun Y (2015) SATB1 Mediates Long-Range Chromatin Interactions: A Dual Regulator of Anti-Apoptotic BCL2 and Pro-Apoptotic NOXA Genes. *PLoS One*, 10: e0139170.
- Yoo AS, Staahl BT, Chen L, Crabtree GR (2009) MicroRNA-mediated switching of chromatin-remodelling complexes in neural development. *Nature*, 460: 642-646.
- Young KF, Pasternak SH, Rylett RJ (2009) Oligomeric aggregates of amyloid beta peptide 1-42 activate ERK/MAPK in SH-SY5Y cells via the alpha7 nicotinic receptor. *Neurochem Int*, 55: 796-801.
- Zawia NH, Lahiri DK, Cardozo-Pelaez F (2009) Epigenetics, oxidative stress, and Alzheimer disease. *Free Radic Biol Med*, 46: 1241-1249.
- Zhang H, Han J, Kang B, Burgess R, Zhang Z (2012) Human histone acetyltransferase 1 protein preferentially acetylates H4 histone molecules in H3.1-H4 over H3.3-H4. *J Biol Chem*, 287: 6573-6581.

- Zhang K, Schrag M, Crofton A, Trivedi R, Vinters H, Kirsch W (2012b) Targeted proteomics for quantification of histone acetylation in Alzheimer's disease. *Proteomics*, 12: 1261-1268.
- Zhang M, Poplawski M, Yen K, Cheng H, Bloss E, Zhu X, Patel H, Mobbs CV (2009) Role of CBP and SATB-1 in aging, dietary restriction, and insulin-like signaling. *PLoS Biol*, 7: e1000245.
- Zhu X, Li Q, Chang R, Yang D, Song Z, Guo Q, Huang C (2014) Curcumin alleviates neuropathic pain by inhibiting p300/CBP histone acetyltransferase activity-regulated expression of BDNF and cox-2 in a rat model. *PLoS One*, 6: e91303.
- Zink D, Amaral MD, Englmann A, Lang S, Clarke LA, Rudolph C, Alt F, Luther K, Braz C, Sadoni N, et al. (2004) Transcription-dependent spatial arrangements of CFTR and adjacent genes in human cell nuclei. *J Cell Biol*, 166: 815-825.
- Zussy C, Brureau A, Keller E, Marchal S, Blayo C, Delair B, Ixart G, Maurice T, Givalois L (2013) Alzheimer's disease related markers, cellular toxicity and behavioral deficits induced six weeks after oligomeric amyloid- β peptide injection in rats. *PLoS One*, 8: e53117.

Chapter 2

2 Objective I- 82-kDa ChAT interacts with chromatin

Portions of this chapter have been reproduced with permission from:

Winick-Ng W, Caetano FA, Winick-Ng J, Morey TM, Heit B, Rylett RJ (2016) 82-kDa choline acetyltransferase and SATB1 localize to β -amyloid induced matrix attachment regions. *Sci Rep*, 6: 23914.

Figure 2-4 (A) was produced in collaboration with Mrs. Jennifer Winick-Ng, using the statistical programming software SAS.

Figures 2-12 and 2-13 were produced in collaboration with Mr. Trevor Morey, who made the recombinant 82-kDa choline acetyltransferase protein.

2.1 Introduction and Rationale

We have shown previously that 82-kDa choline acetyltransferase (82-kDa ChAT) expression in neural cells alters the expression of genes related to amyloid precursor protein (APP) processing (Albers *et al.* 2014). In addition, the expression of 82-kDa ChAT in cortical neurons cultured from brains of transgenic mice expressing mutant APP/Presenilin-1 leads to changes in the amount of β -amyloid ($A\beta$) produced and secreted, as well as the expression and activity of the β -secretase BACE1 which cleaves APP in the amyloidogenic pathway (Albers *et al.* 2014). These changes were mediated by gene expression increases in the golgi-lysosome trafficking protein GGA3, which resulted in lysosomal degradation of BACE1 (Albers *et al.* 2014). Collectively, these data demonstrate that the expression of 82-kDa ChAT in neural cells can lead to gene expression changes, therefore we predict that 82-kDa ChAT could interact with chromatin, either directly or in combination with other DNA-interacting proteins.

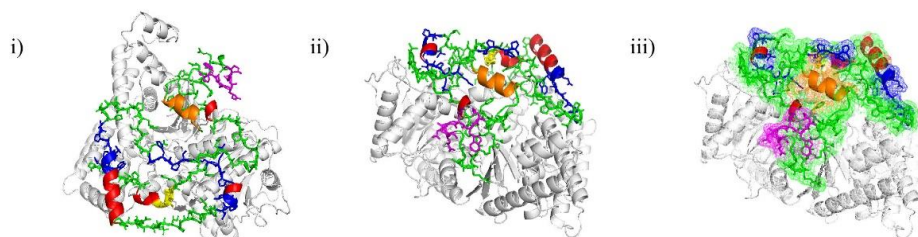
When modelled using the DNA-binding prediction software BindN+ (Wang and Brown 2006) and DNABindR (Yan *et al.* 2006), the 118 amino acid N-terminal extension found on 82-kDa ChAT contains several potential DNA-binding motifs (**Fig. 2-1A**). These included a basic residue region with high DNA-binding prediction and several tandem (S/T)PXX or XPRK motifs. These latter motifs bind AT-rich DNA at the minor groove and each have a 50% probability to bind DNA based upon both surface accessibility and orientation (Suzuki 1989, Yang *et al.* 2003). It is noteworthy that the crystal structure of 69-kDa ChAT has been solved by our lab previously and shows several surface-accessible regions of basic residues that could facilitate the association with DNA (Kim *et al.* 2005). To test whether these 82-kDa ChAT N-terminal DNA-binding motifs were surface exposed, we used the Iterative Threading ASSEmbly Refinement (I-TASSER) server to perform predictive modelling of 82-kDa ChAT using the 69-kDa ChAT crystal structure as a backbone (Zhang 2008; Roy *et al.* 2010; Roy *et al.* 2012) (**Fig. 2-1B**). These models show that the N-terminal region of 82-kDa ChAT is

also predicted to be surface exposed and could interact with DNA. Thus we hypothesized that 82-kDa ChAT interacts with chromatin. The data presented in this chapter demonstrates that 82-kDa ChAT interacts with chromatin, and that this interaction is altered by cellular perturbations such as oligomeric A β ₁₋₄₂, Hoechst dye (a DNA-binding competitor), or the histone deacetylase inhibitor trichostatin A (TSA).

A

1 MGLRTAKKRG LGGGGKWKREE GGGTRGRREVRPACFLQSGGRGDPGDVGGPAGNPGC SPHPR 62
 63 AATRPPLPAH TPAHTPEW CGAASAEAAEPRRAGPHLCIPAPGLTK TPILEK VPRKMAAK TPSS EE 128
 129 SGLPKLPVPPLQQTLATYLQCMRHLVSEEQFRKSQAIVQQFGAPGGLGETLQQKLLERQEKA... 190

Start codon
 Nuclear localization signal (NLS)
 Basic residue region
 S(T)PXX or XPRK motif, 82-kDa region
 S(T)PXX or XPRK motif, 69-kDa region

B

82-kDa ChAT N-terminus
 NLS
 Predicted α -helix
 Basic residue region
 S(T)PXX or XPRK motif, 82-kDa region
 S(T)PXX or XPRK motif, 69-kDa region
 69-kDa ChAT region

Figure 2-1. DNA binding prediction for 82-kDa ChAT.

(A) The 118 amino acid residue amino-terminus of 82-kDa ChAT is flanked by two in-frame methionine initiation sites, and contains a unique nuclear localization sequence. Several DNA binding prediction software databases predicted high DNA binding probability at 2 basic residue regions, as well as 5 SPXX/XPRK DNA binding motifs. There was an additional SPXX motif in the 69-kDa ChAT region near the amino terminus with high DNA binding prediction. (B) (i) and (ii) show protein prediction modelling for 82-kDa ChAT with surface exposed DNA-binding motifs and NLS. (iii) is the same view as (ii), but with a surface mesh to visualize the surface-exposed amino acid residues.

2.2 Methods

Cell Culture and transfection

SH-SY5Y cells obtained from American Type Culture Collection (Manassus, VA) were grown on 35 mm glass-bottom plates (0.14 mm thick; MatTek Corp., Ashland, MD, USA) for live cell imaging. In other experiments, SH-SY5Y cells stably expressing heterologous 82-kDa ChAT (Albers *et al.* 2014) were plated on coverslips for immunostaining. Cells were differentiated using 10 μ M all-trans-retinoic acid for 3 days, which produces substantial morphological and biochemical cholinergic differentiation of cells (Hashemi *et al.* 2003). Experiments from stably transfected cells were derived from a single clone. This clone was selected from multiple clones that were screened for low levels of expression. For live imaging, cells were transfected with a plasmid encoding an 82-kDa ChAT-eGFP fusion protein or the peGFP vector (Clontech Laboratories Inc., Mountain View, CA, USA) using Lipofectamine 2000 (Invitrogen, Burlington, ON, Canada). A β oligomers were prepared as described (Stine *et al.* 2003) from lyophilized A β ₁₋₄₂ or the reverse peptide purchased from rPeptide (Bogart, GA, USA). Cells were treated with 100 nM oligomeric A β ₁₋₄₂, 10 nM trichostatin a (TSA), or F12 media (vehicle) for the indicated times.

Antibodies

The 82-kDa ChAT protein was detected with a custom rabbit polyclonal antibody CTab (Dobrinsky *et al.* 2000). Other antibodies used were: anti- β -tubulin (2146S; Cell Signaling, Danvers, MA, USA); anti-Matrin3 (BL2526; Bethyl Laboratories Inc., Montgomery, Tx, USA); and anti-histone H2A (H2A) (PA1-41004; Thermo Fisher Scientific, Waltham, MA, USA). The pan-anti-Tau antibody was a generous gift from the laboratory of Dr. Michael Strong. AlexaFluor 647-conjugated secondary antibody (Invitrogen) was used for immunostaining visualization.

Nuclear sub-fractionation and immunoblotting

Total, cytosolic and nuclear subcellular fractions were isolated from cells treated with either vehicle or A β ₁₋₄₂ as described previously (Ye and de Lange 2004). SH-SY5Y cells were plated on 60 mm dishes at a density of 1×10^6 cells/plate, then treated for 4 h with either vehicle or A β ₁₋₄₂. Cells were then lysed in Buffer A (containing 10 mM HEPES pH 7.9, 10% glycerol, 0.5% (v/v) Triton X-100, 5 mM MgCl₂, 1 mM dithiothreitol (DTT), 10 mM KCl, protease inhibitor cocktail [Sigma Aldrich; final concentration: 1.04 mM 4-(2-Aminoethyl) benzenesulfonyl fluoride hydrochloride (AEBSF), 0.8 μ M aprotinin, 40 μ M bestatin, 14 μ M N-[N-(L-3-trans-carboxyirane-2-carbonyl)-L-leucyl]-agmatine; 1-[N-[(L-3-trans-carboxyoxirane-2-carbonyl)-L-leucyl]amino]-4-guanidinobutane (E-64), 20 μ M leupeptin and 15 μ M pepstatin], and phosphatase inhibitors [final concentration: 10 mM sodium fluoride, 1 mM sodium vanadate, 20 mM sodium phosphate, 3 mM β -glycerolphosphate, 5 mM sodium pyrophosphate]). After incubation for 15 min on ice, lysates were viewed under a light microscope to confirm that cells had been lysed and nuclei were intact. Lysates were then spun at 0.3 x g for 10 min at 4°C. The supernatant containing soluble cytosolic proteins was transferred to a new tube and the pellet was washed with cold PBS (containing inhibitors, as above). The pellet was then lysed in Buffer B (20 mM HEPES pH 7.9, 25% Glycerol, 0.2% Nonidet P-40, 5 mM MgCl₂, 1 mM DTT, 150 mM KCl and inhibitors as described above) to lyse the nuclei and release soluble proteins. After incubation on ice for 15 min, lysates were spun at 0.9 x g for 5 min at 4°C. The supernatant was transferred to a new tube, and the pellet was washed in PBS. The pellet was then lysed in Buffer C (same as Buffer B, but containing 420 mM KCl and 700 U/mL DNase I) to release euchromatic chromatin associated proteins. After incubation for 15 min on ice, the lysate was spun at 18,800 x g for 15 min at 4°C and the supernatant was transferred to a new tube. The resulting pellet containing insoluble and nuclear matrix associated proteins was lysed using 2x Laemmli buffer (2% (w/v) sodium dodecyl sulfate (SDS), 10% glycerol, 62.5 mM Tris-HCl, pH 6.8, 2.5% β -mercaptoethanol, and 0.001% bromophenol blue), then incubated at 100°C for 10 min with intermittent vortex mixing. Cells were also

lysed in duplicate with radioimmunoprecipitation (RIPA) buffer (50 mM Tris-HCl, pH 8.0, 150 mM NaCl, 1% (v/v) Triton-X 100), 0.5% (w/v) sodium deoxycholate, 0.1% (w/v) SDS, 700 U/mL DNase I, and inhibitors as described above), sonicated for 3 x 10s, and spun at 18,800 x g for 15 min at 4°C to obtain whole cell extract.

Ten µg of protein from each of the whole cell extract, cytosolic (10 mM KCl) and soluble nuclear fractions, and half of the chromatin and insoluble protein fractions were separated on SDS–polyacrylamide gel electrophoresis (SDS-PAGE) gels. The density of protein bands was visualized using Image Lab (Version 5.0, BioRad).

Live cell imaging and immunostaining

For live imaging, cells were exposed to 625 ng/mL Hoechst 33342 DNA stain (Sigma-Aldrich) for 20 min prior to imaging in growth medium containing phenol-red free FluroBrite DMEM (Invitrogen) and 20 mM 4-(2-hydroxyethyl)-1-piperazineethanesulfonic acid (HEPES). For immunostaining, cells were stained with primary antibody CTab (1:1,000) followed by AlexaFluor 647 (for 82-kDa ChAT) secondary antibodies. Cells were either treated with 625 ng/mL Hoechst prior to fixation or counterstained with 2.5 µg/mL Hoechst after immunostaining.

For confocal microscopy, digital images were acquired with a Zeiss LSM510-Meta laser-scanning confocal microscope (Carl Zeiss Canada Ltd., Toronto, ON, Canada) using a 63X oil-immersion objective (NA = 1.4). For live cell imaging, images were acquired using 405 nm excitation and 420–480 emission for Hoechst; and 488-nm excitation and 505-nm emission using a long-pass filter for 82-kDa ChAT-EGFP at 1024 × 1024 resolution. For immunostaining, images were acquired for Hoechst as above; and 647-nm excitation and 650-nm long-pass emission filter for 82-kDa ChAT. In some experiments, 1 µm slices through the z-plane were taken in series. Images were processed in ImageJ (Schneider *et al.* 2012) where manipulations included filtering, thresholding, digital magnification, and deconvolution, then formatted in Adobe Illustrator (Adobe Systems Inc, San Jose, CA, USA). For z-stack images, the images were rendered in 3D

by Imaris (version 7.0.0; Bitplane Scientific Software, Connecticut, USA) before creating a 3D surface for 82-kDa ChAT and Hoechst.

Chromatin immunoprecipitation with next-generation sequencing (ChIP-seq)

ChIP samples were obtained from 82-kDa ChAT-expressing cells treated for 4 h with vehicle (F-12 media) or 100 nM A β ₁₋₄₂. SH-SY5Y cells were plated on 10 cm dishes at a density of 4.0x10⁶ cells per plate (10x10⁶ cells final), with 3 plates per treatment. Following differentiation and treatment, cells were exposed to 0.5% methanol-free ultra-pure paraformaldehyde for 20 min at room temperature to cross-link proteins and DNA. Cross-linking was halted with 5 min of 125 mM glycine added to the media, and then cells were lysed in 1% SDS (containing 50 mM Tris-HCl, 10 mM EDTA with the addition of protease and phosphatase inhibitors). Lysates were then sonicated in a cold room for 10 s followed by 1 min on ice, repeated 5 times. Lysates were centrifuged and then diluted in buffer containing Tris-HCl and EDTA (Tris-EDTA) to 0.1% SDS. Each sample was divided into 4 equal parts, and 3 of these aliquots were incubated in 2.5 μ g of anti-ChAT antibody overnight at 4°C on a rocker. For each sample, one aliquot did not have anti-ChAT antibody added prior to the incubation to serve as a negative control; this also allowed us to determine if the sonication step was successful (**Appendix 1**). Following incubation with antibody, lysates were added to 25 μ l magnetic Dynabeads (Invitrogen, Ontario, Canada) and incubated for 2 h at 4°C on a rocker. Dynabeads with antibody-protein-DNA complexes were recovered then washed in a cold room once in a 0.1% SDS low-salt buffer (150mM NaCl), once in a high-salt buffer (500mM NaCl), then in a 0.5 M LiCl buffer before two final washes in Tris-EDTA buffer at room temperature. Protein-DNA complexes were then eluted from the beads by a Tris-EDTA buffer containing 1% SDS for 2 h at 55°C with 20 μ g Proteinase K to digest proteins. Samples were then incubated overnight at 65°C to reverse the cross-linking. DNA was extracted by phenol:chloroform, then precipitated by adding 100% ethanol containing 150 mM sodium acetate overnight at -20°C. DNA pellets were washed twice in 70% ethanol, and then the pellets was resuspended in ultrapure water.

A single ChIP sample for 82-kDa ChAT and input after cell exposure to either 4 h of vehicle (F-12 media) or 100 nM A β ₁₋₄₂ was analyzed at the Donnelly Sequencing Centre (Toronto, ON). ChIP-seq samples were individually barcoded with Illumina TruSeq® adapter sequences (Illumina, San Diego, CA, USA) for library construction, then run on 2 single read 1:51bp lanes using a HiSeq2500.

ChIP-seq samples generated ten to twenty million 50 base pair, paired-end reads for each sample. Each ChIP-seq FASTQ file was loaded onto the Galaxy server (<http://usegalaxy.org>) (Giardine *et al.* 2005) for analysis. The general ChIP-seq analysis workflow can be found in **Figure 2-2**. First, each sample was tested for quality control (QC) statistics, including quality scores, GC content and over-represented sequences. All the sequences were of sufficient quality, the GC content approximated the GC content of the human genome (~41%) (Antonarakis 2010) and the only overrepresented sequences that were found corresponded to the adapter sequences used in the library construction and were at ~1% of the total reads. Reads were then mapped to the human genome (hg38, updated December 2013) using the Burrows-Wheeler Aligner (Li and Durbin 2009), with repeat-masking and default parameters. Unique peaks were identified for each sample using the model-based analysis of ChIP-seq (MACS) (Zhang *et al.* 2008) tool with p-value < 0.00001, and filtered out significant peaks found in the corresponding input sample.

Peaks found by the MACS procedure were compared to genomic features obtained from the UCSC genome table browser (Kent *et al.* 2002) using in-house SAS programs (version 9.4, Cary, NC, USA). SAS was used to compute average peak lengths for each sample and to annotate peaks found within a known gene. ChIP-seq tracks were visualized using the Integrative Genomics Viewer (Broad Institute, Cambridge, MA, USA; version 2.3.59) (Robinson *et al.* 2011). These gene lists were uploaded to the Database for Annotation, Visualization and Integrated Discovery (DAVID) server (<http://david.abcc.ncifcrf.gov/>) (Huang da *et al.* 2009; 2009a) for GO analysis. Finally, FASTA formatted peaks were uploaded to the discriminative DNA motif discovery (DREME) tool (<http://meme.nbcr.net/meme/cgi-bin/dreme.cgi>) (Bailey 2011) for motif

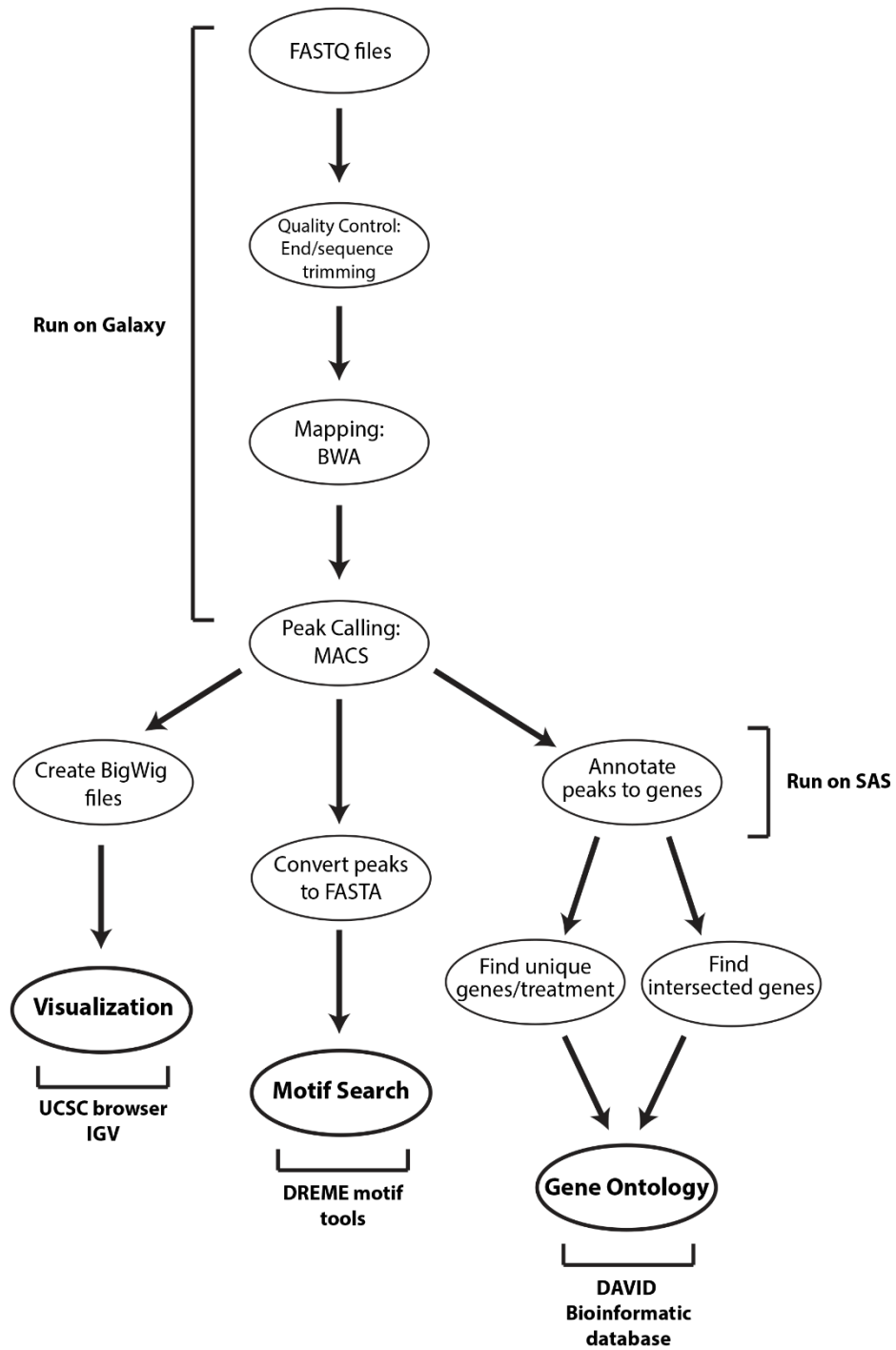


Figure 2-2. ChIP-seq workflow.

discovery. SAS was also used in several downstream analyses to compute additional features of the ChIP-seq data.

Data deposition

The ChIP-seq data were deposited in the NCBI Geo Database, accession number: GSE73576.

Recombinant 82-kDa ChAT preparation

Recombinant 82-kDa ChAT protein was prepared as described previously for 69-kDa ChAT protein (Kim *et al.* 2005a). Briefly, cDNA encoding for wild-type 82-kDa ChAT was inserted into a pProEX HTa plasmid containing a 6X His6 tag and a TEV cleavage site and transformed and expressed in competent BL-21 cells. Recombinant 82-kDa ChAT protein was purified and verified for antibody specificity (using both a C- and N-terminal anti-ChAT antibodies) and enzymatic activity using a radioenzymatic assay (unpublished data).

Electrophoretic mobility shift assay

Purified recombinant 82-kDa ChAT protein was used for an electrophoretic mobility shift assay (EMSA) using biotinylated DNA oligomers annealed to their reverse complement (Table 2.1). Samples were prepared using the LightShift Chemiluminescent EMSA kit (Thermo Scientific) according to manufacturer's instructions. Recombinant protein (0-500 ng) was combined with reaction buffer (final concentration: 1X Binding Buffer, 1-2 μ g Poly (dI•dC), 2.5% glycerol, 5mM MgCl₂, 0-100 mM KCl, 0-20 mM EDTA, 0.05% NP-40, and 0-3 μ g BSA) prior to incubation with 20 - 200 fmol biotin-labelled DNA. In some experiments, a 200-fold molar excess of non-biotinylated DNA was added as a competitor. As a positive control reaction, Epstein-Barr nuclear antigen

(EBNA) extract was incubated with reaction buffer and biotin-labelled DNA (**Table 2-1**). Samples were incubated for 20-60 min at room temperature prior to the addition of 1X Loading Buffer. Some samples had 2.5 μg anti-ChAT antibody added to the reaction at 15 min prior to completion. Samples were then separated on a 6% Tris-Borate EDTA electrophoresis gel and transferred to an Amersham Hybond-XL nylon membrane (GE Healthcare, Mississauga, ON). Membranes were then cross-linked for 10 min at 254 nm prior to incubation in stabilized streptavidin-horseradish peroxidase conjugate and detection by chemiluminescence.

Data Analysis

The data are presented as mean \pm SEM, with n values indicating the number of independent experiments performed with separate cell populations. Each n value represented the average of multiple sample replicates for each experiment. GraphPad Prism 5 (GraphPad Software, San Diego, CA, USA) was used for data analysis. Data were assessed for normality using Bartlett's test and statistically significant differences were tested by unpaired Student's t-test, or between groups using one or two-way ANOVA with Dunnett's, Tukey's or Bonferroni's post hoc multiple comparison test as appropriate, with statistical significance defined as $p \leq 0.05$. For cell counting, an independent and blinded observer determined the number of cells with nuclear aggregations on 63x magnification images. Each image had at least 20 cells, and 5 images were counted for each replicate of each treatment. The total number of cells in all 5 images was pooled to determine the percentage of cells with nuclear aggregations.

Table 2-1. DNA oligomer pairs used for EMSA.

Name	Details	Oligomer 5' - 3'	Reverse Compliment 3' - 5'
EBNA target	Provided in EMSA kit	...TAGCATATGCTA...	...TAGCATATGCTA...
DREME	TCCAT (from DREME analysis in ChIP-seq)	GCAGTCCATCGTCCATG CTCCATCTCCATCTCCAT TCCATTCCATTAGAC	GTCTAATGGAATGGAATGG AGATGGAGATGGAGCATG GACGATGGACTGC
AT-Rich	Random A/T	GCAGAAAAAAAAAAAAA AAAAAAAAAAAAAAAAA AAAAAAAAAAAAAAAAAGG AC	GTCCTTTTTTTTTTTTTTTT TTTTTTTTTTTTTTTTTTTT TTTTCTGC
ATC-Rich 1	(A/T) _{3-n} C(A/T) ₃₋₆	GCGCATTCTTACTTTACT ATGGATTCTATATATCTT TGATACTATTTTTCATTG GAC	GTCCAATGAAAAATAGTAT CAAAGATATATAGAATCCA TAGTAAAGTAAGAATGCGC
ATC-Rich 2	ATACATA	GCAGATACATAGATACA TAATACATAGATACATA ATACATAATACATAGGA C	GTCCTATGTATTATGTATTA TGTATCTATGTATTATGTAT CTATGTATCTGC
<i>APP</i> peak	Found from ChIP-Seq	GCAGTATTTTGGTATTTT GTTATGGCAGCCCTAGC AGACTAATGCATTTAGG AC	GTCCTAAATGCATTAGTCT GCTAGGGCTGCCATAACAA AATACCAAATACTGC
Random motif	ATGC random order (50% GC)	GCAGACCGCAGAGTGCG CAATACGAGGTAAAGCC AGTCACCCAGTGAGAC	GTCTCACTGGGTGACTGGC TTTACCTCGTATTGCGCACT CTGCGGTCTGC

2.3 Results

82-kDa ChAT associates with chromatin at synapse and cell stress genes

The 82-kDa ChAT protein structure contains predicted DNA-binding motifs, and has been demonstrated to alter gene expression in neural cells. Therefore, we inquired if 82-kDa ChAT could be associated with chromatin. An additional objective was to determine the impact of A β -exposure on the ability of 82-kDa ChAT to interact with chromatin. We chose 100 nM A β ₁₋₄₂, as this treatment has previously been shown to be rapidly internalized in SH-SY5Y cells (Lana *et al.* 2016), and to activate the ERK/MAPK signaling pathway in SH-SY5Y cells within 10 min of treatment (Young *et al.* 2009). Further, signaling events leading to immediate early gene activation alter gene expression of target genes several hours after stimulation (Li *et al.* 1996; Yaniv *et al.* 2010). Thus, we used cell fractionation analysis in retinoic acid-differentiated SH-SY5Y cells that stably express heterologous 82-kDa ChAT, to identify subcellular compartments whereby 82-kDa ChAT was localized after 4 h of cell treatment with either vehicle (F-12 media) or 100 nM A β ₁₋₄₂. (**Fig. 2-3**). A large proportion of the 82-kDa ChAT protein was found in the fraction containing soluble nuclear proteins (150 mM KCl). In control cells, a small immuno-positive band for 82-kDa ChAT protein was found in the euchromatic chromatin (420 mM KCl) fraction, but no immuno-positive band was observed in the insoluble pellet fraction containing heterochromatic associated, nuclear matrix associated and insoluble proteins. Interestingly, after 4 h exposure of cells to 100 nM A β ₁₋₄₂, there was a strong 82-kDa ChAT protein immuno-positive band in the 420 mM KCl fraction and a small band detected in the insoluble pellet fraction. As a control, β -tubulin was found mainly in the 10 mM KCl (cytosolic) fraction, while histone H2A was found only in the insoluble pellet fraction.

Given that the 82-kDa ChAT protein was found in sub-cellular fractions containing euchromatic- and heterochromatic-associated proteins after exposure to A β ₁₋₄₂, we next employed chromatin immunoprecipitation followed by next-generation sequencing (ChIP-seq) for 82-kDa ChAT in cells treated for 4 h with either vehicle or 100 nM A β ₁₋₄₂ (**Fig. 2-4**). We found 7460 peaks for 82-kDa ChAT after vehicle

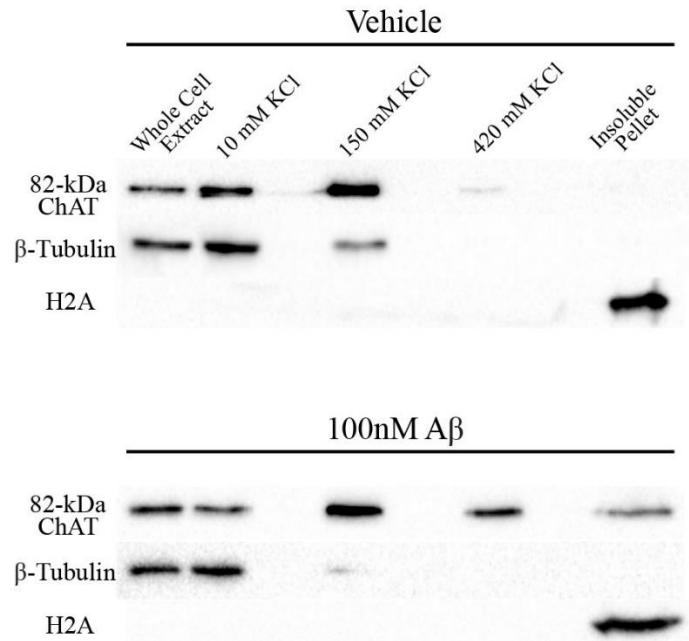


Figure 2-3. 82-kDa ChAT associates with chromatin.

Immunoblot showing cell fractionation of SH-SY5Y cells stably expressing 82-kDa ChAT treated with either vehicle or 100 nM oligomeric A β_{1-42} for 4 h. A β -treated cells showed an increase in 82-kDa ChAT protein levels present in the 420 mM KCl fraction, with a small amount of protein detected in the insoluble protein fraction. β -tubulin and histone H2A were used as controls for the 10 mM KCl and insoluble protein fractions, respectively, n = 8.

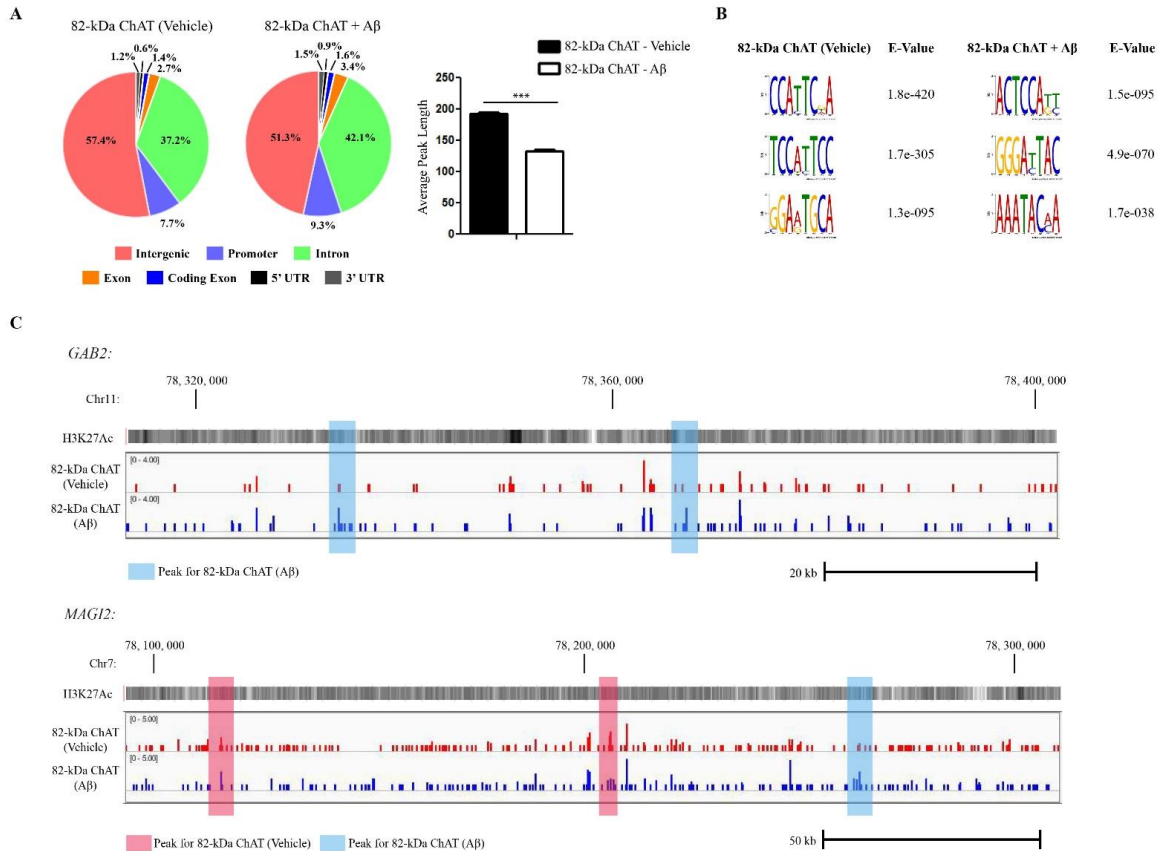


Figure 2-4. 82-kDa ChAT has altered genome association after exposure of cells to A β .

(A) ChIP-seq was performed for SH-SY5Y cells stably expressing 82-kDa ChAT treated with either vehicle or 100 nM oligomeric A β_{1-42} for 4 h. Genomic features identified for 82-kDa ChAT. Both treatment groups had over 50% of the peaks at intergenic regions, but A β_{1-42} treatment increased association with introns, promoters and exons. Average peak length for 82-kDa ChAT after either vehicle or A β_{1-42} -exposure was also tested. Treatment with A β_{1-42} significantly decreased the 82-kDa ChAT peak length. ***p < 0.001 (Student's t-test). (B) Top DREME motif hits for 82-kDa ChAT after vehicle or A β_{1-42} -exposure of cells. The top motifs for both treatments revealed a TC₂₋₃AT motif. (C) Example ChIP-seq tracks for 82-kDa ChAT after vehicle or A β_{1-42} -exposure of cells for regions of *GAB2* and *MAGI2* genes. Peaks are highlighted in blue for A β_{1-42} peaks and red for vehicle peaks. H3K27Ac is overlaid to show active transcription initiation sites.

treatment, and 6345 peaks after A β_{1-42} treatment, with 250 peaks overlapped and an additional 414 peaks within 200 nt of one another. We further observed that 57.4% of peaks were found in intergenic regions after vehicle-treatment, compared to 51.3% after A β_{1-42} -exposure (**Fig. 2-4A**). The decrease in intergenic regions after exposure to A β_{1-42} was explained by an increase in the percentage of the peaks found in introns (42.1%) compared to vehicle treatment (37.2%). In addition, the percentage of peaks found in promoters and exons was also increased after A β_{1-42} -exposure (9.3% and 3.4%, respectively) compared to vehicle treatment (7.7% and 2.7%, respectively). We also observed that the average peak length was significantly reduced after A β_{1-42} treatment for 82-kDa ChAT (132.6 ± 2.2 nucleotides (nt)) compared to vehicle treatment (192.6 ± 3.2 nt). Smaller peak sizes suggest targeted genomic associations with sequence-specific DNA targets (Pepke *et al.* 2009). Next, we used the DREME tool for motif discovery (**Fig. 2-4B**) and observed that the top DREME motifs contained the motif TC₂₋₃AT in both conditions. DREME also revealed an additional ATC-rich motif only after exposure to A β_{1-42} . This sequence was identical to a known binding motif ((A/T)₃₋₆C(A/T)_{3-n}; Yasui *et al.* 2002) for special AT-rich sequence binding protein 1 (SATB1), an organizing component of the nuclear matrix (Yasui *et al.* 2002; Cai *et al.* 2003; Galande *et al.* 2007). Examples of ChIP-seq tracks from random genomic targets for 82-kDa ChAT, treated with vehicle or A β_{1-42} , are shown in **Fig. 2-4C** for *GAB2* and *MAGI2* genes, with H3K27 acetylation (H3K27ac) overlaid to show one example of active transcription initiation sites. We identified no relationship between the peaks for 82-kDa ChAT and H3K27ac. Additional tracks can be found in **Figure 2-5** for chromosomes 1, 7 and 10, the full *GAB2* and *MAGI2* genes, as well as a region of the *APP* gene. Chromosomes 7 and 10 showed large peaks for 82-kDa ChAT flanking the centromeres (**Fig. 2-5A**).

Next, we annotated 82-kDa ChAT ChIP-seq peaks found in intergenic regions for cells treated with either vehicle or 100 nM A β_{1-42} . In agreement with the genomic features, we found 3700 non-duplicate genes that contained peaks for 82-kDa ChAT, with this increasing to 4507 genes after A β_{1-42} -exposure. Of these genes, there were 820 genes in common for both treatments. Using these annotations, we evaluated whether there were significant functional groups for annotated genes using the DAVID server

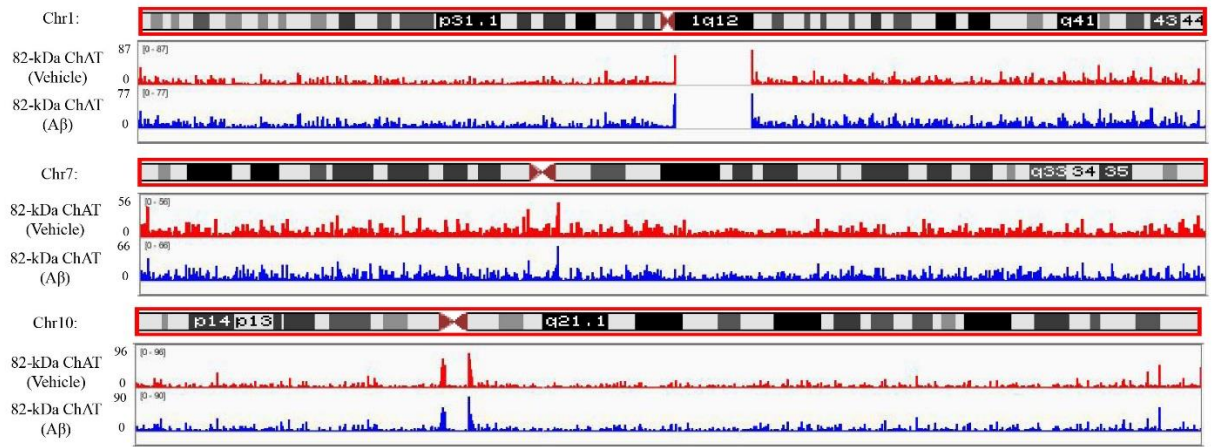
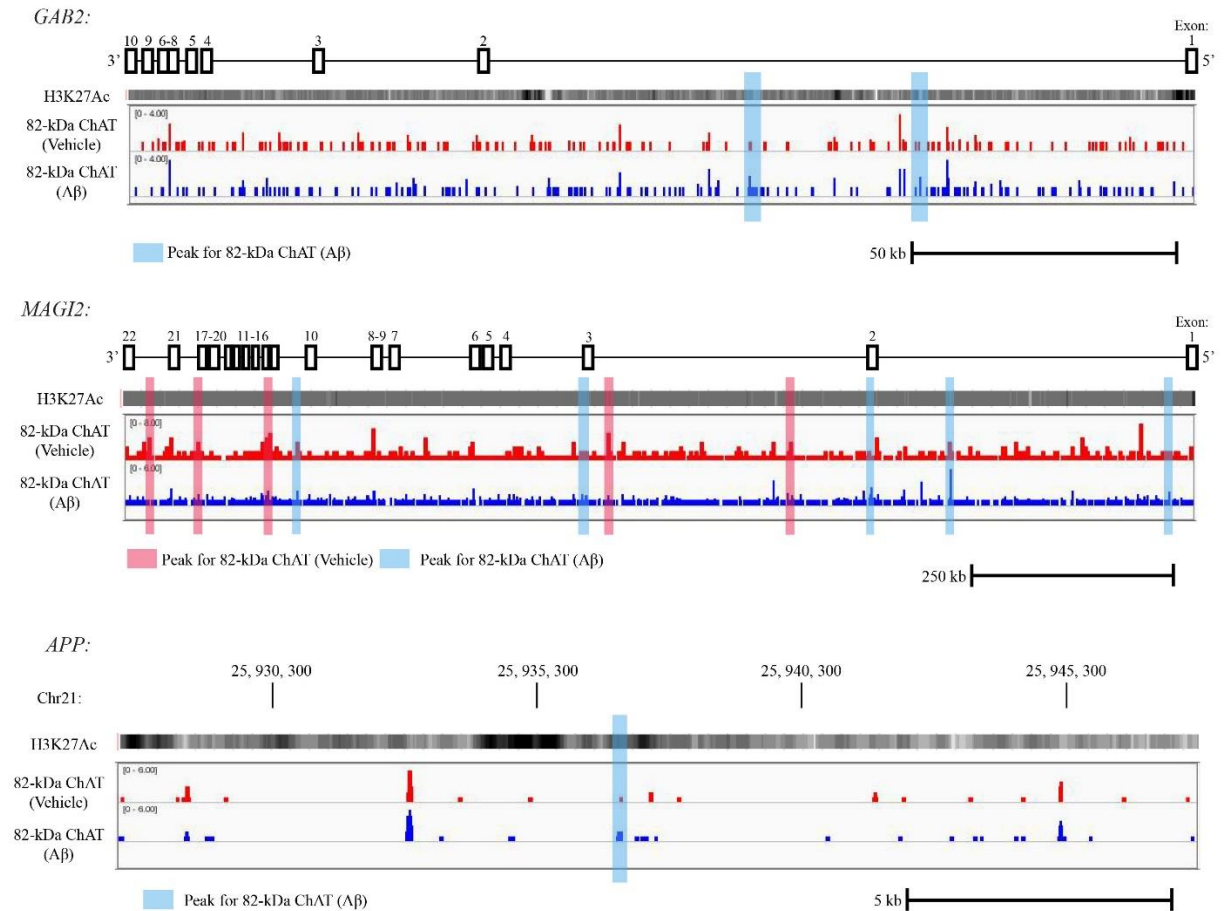
A**B**

Figure 2-5. Examples of ChIP-seq tracks for 82-kDa ChAT.

(A) ChIP-seq tracks for chromosomes 1, 7 and 10 for 82-kDa ChAT in cells treated with either vehicle or $A\beta_{1-42}$. For chromosome 1, there was a portion of data not covered at the start of the q-arm. No other chromosome had a gap in data coverage. For chromosomes 7 and 10, there was a large peak of coverage flanking the centromeres. (B) ChIP-seq tracks for GAB2 and MAGI2 whole genes, as well as for a region of APP, for 82-kDa ChAT in cells treated with either vehicle or $A\beta_{1-42}$. Peaks are highlighted in blue for 82-kDa ChAT $A\beta_{1-42}$ peaks and red for 82-kDa ChAT vehicle peaks. H3K27Ac is overlaid to show active transcription initiation sites.

(**Appendices 2-4**). DAVID is an integrated bioinformatics approach to gene ontology (GO) that combines multiple computational and statistical methods and has been cited in over 21,000 publications (Huang da *et al.* 2009; 2009a). For genes associated with 82-kDa ChAT after vehicle or A β_{1-42} -exposure, we found no significant GO terms (defined as $p < 1.0E-05$ and $-\log(\text{FDR}) > 1.5$). However, for genes associated with 82-kDa ChAT in both treatment conditions, we found significant GO terms for cell adhesion ($p = 1.2E-08$, $-\log(\text{FDR}) = 4.7$), synapse ($p = 1.3E-08$, $-\log(\text{FDR}) = 4.8$), membrane ($p = 7.1E-08$, $-\log(\text{FDR}) = 4.0$), and glycoprotein ($p = 3.2E-06$, $-\log(\text{FDR}) = 2.3$). In addition to these GO terms we also identified several genes previously identified by a meta-analysis of genome wide association studies assessing AD risk, including *BIN1*, *CRI*, *EFNA5*, *GAB2*, *MAGI2*, *MTHFD1L* and *PRUNE2* (Bertram 2011). We also found several APP binding and metabolism related genes in several conditions (**Table 2-2**). It is of interest that *ADAM10*, *ADAM17*, *APBA2*, *APPBP2*, and *RTN1* were previously identified as upregulated by 82-kDa ChAT in a gene expression microarray. We also identified several additional APP related genes, such as *ADAM12*, *APBB1*, *APBB2* and *NAE1*, as well as *APP* itself.

82-kDa ChAT sub-nuclear distribution is altered after cell exposure to oligomeric A β_{1-42} or trichostatin A

As previously stated, we found that 82-kDa ChAT associated with chromatin after both vehicle and A β_{1-42} -exposure, with increases in genic associations at introns, promoters and exons after 4 h of 100 nM A β_{1-42} -exposure. Therefore, we imaged changes to the sub-nuclear localization of 82-kDa ChAT after 4 h of vehicle or A β_{1-42} -exposure by confocal microscopy. We observed diffuse, slightly punctate staining for 82-kDa ChAT in the nuclei of vehicle-treated cells, with a small amount of cytoplasmic staining (**Fig. 2-6A[a-c]**). After exposure of cells to 100 nM oligomeric A β_{1-42} for 4 h, immunofluorescence staining of cells for 82-kDa ChAT reveals highly-fluorescent aggregates of the protein within the nuclei of many cells (**Fig. 2-6A[d-f]**). We

Table 2-2. Selected APP interacting genes with 82-kDa ChAT association by CHIP-seq.

Gene	Function	82-kDa ChAT (Vehicle)	82-kDa ChAT (A β)	Microarray fold change
ADAM10	Alpha secretase proteolytic cleavage of APP	Intron 1	Intron 14	2.4
ADAM12	matrix metalloproteinase, multiple catalytic targets	Intron 3	Intron 2	n/a
ADAM17	MAP-kinase signalling, APP cleavage	Intron 1	--	1.2
APBA2 (x11 β)	signal transduction, APP binding	--	Promoter	2.2
APBB1	APP binding, involved in APP signaling	Promoter	--	n/a
APBB2	APP binding, involved in signaling	Intron 1	Intron 6	n/a
APP	β -amyloid precursor, synapse maintenance	--	Intron 13	n/a
APPBP2	Binds to APP intracellular domain	Intron 4	--	1.4
NAE1	APP binding, can drive APP-mediated apoptosis	--	Intron 7	n/a
RTN1	Modulates β -secretase activity, APP binding near cleavage site	--	Intron 1, 3	14.8

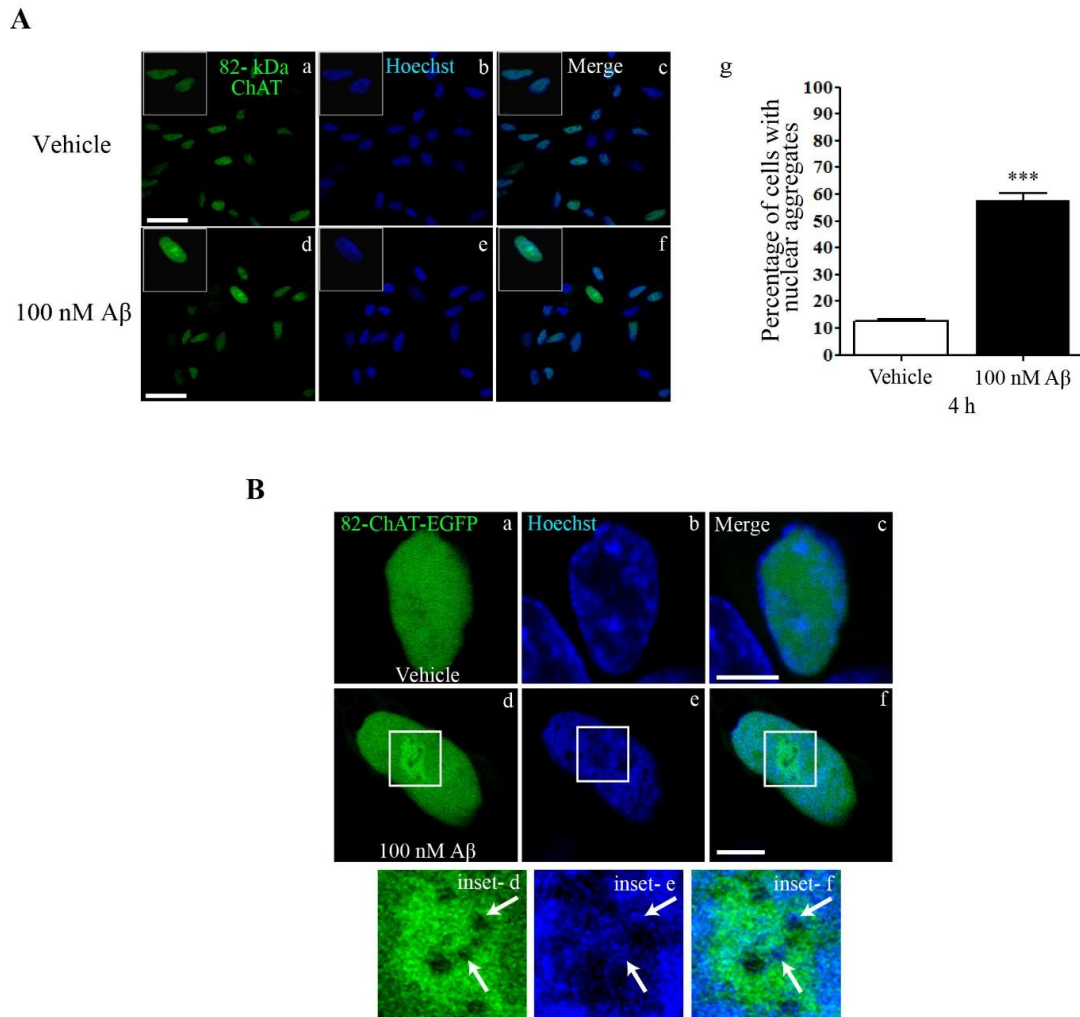


Figure 2-6. 82-kDa ChAT forms nuclear aggregates after exposure to A β .

(A) SH-SY5Y cells stably expressing 82-kDa ChAT were exposed to either vehicle (F12 media; a–c) or 100 nM oligomeric A β_{1-42} for 4 h (d–f). A β -treated cells had nuclear aggregates of 82-kDa ChAT protein. The left panel shows 82-kDa ChAT staining, center panel shows staining with Hoechst dye to label DNA, and right panel is the overlay; $n = 5$, with at least 6 cells imaged per treatment; scale bar 20 μm . (g) Quantification of the number of cells with nuclear aggregates of 82-kDa ChAT, $n = 8$ with at least 100 cells counted per treatment. *** $p < 0.001$ (Student's t -test). (B) SH-SY5Y cells were transiently transfected with 82-kDa ChAT-eGFP and treated with either vehicle (a–c) or 100 nM oligomeric A β_{1-42} (d–f) for 4 h, then live cells were exposure to Hoechst dye for 20 min prior to imaging. A β -exposed cells had aggregates of 82-kDa ChAT-eGFP (inset on d) surrounding areas with little ChAT-eGFP and aggregates of Hoechst dye (inset on e,f). Scale bar 5 μm ; $n = 5$.

determined that $58 \pm 2\%$ of A β -treated cells had at least 1 nuclear aggregate of 82-kDa ChAT, compared to $13 \pm 1\%$ of vehicle-treated cells (**Fig. 2-6A[g]**).

Next, we determined whether these A β -induced aggregates are also formed in live cells that express 82-kDa ChAT as a fusion protein with enhanced green fluorescent protein (82-kDa ChAT-eGFP; **Fig. 2-6B**). Consistent with findings in the previous experiment, vehicle-treated cells had a diffuse distribution of 82-kDa ChAT-eGFP in nucleus (a–c), whereas cells treated for 4 h with 100 nM A β_{1-42} had nuclear aggregates of 82-kDa ChAT-eGFP (**Fig. 2-6B[d–f]**). As a DNA marker, we treated live cells with 625 ng/mL Hoechst 33342 for 20 min prior to imaging. When the A β -induced aggregates of 82-kDa ChAT-eGFP were imaged at higher magnification, it is apparent that there were areas within the aggregates that have lower levels of 82-kDa ChAT staining (**Fig. 2-6B[inset d]**) and that these were enriched with Hoechst dye (**Fig. 2-6B[inset e–f]**).

The competitive minor groove binding compound Hoechst 33342 stains DNA at the minor groove in live cells or in cells that have been fixed with paraformaldehyde. When added to live cells or *in vitro* to purified protein-DNA complexes, Hoechst can compete with and displace proteins that bind DNA using S(T)PXX or XPRK motifs (Amirand et al. 1998; Deka et al. 1999). However, if protein-DNA complexes are crosslinked with paraformaldehyde then the DNA can no longer be accessed by Hoechst and binding at that specific region will not occur. Given that 82-kDa ChAT has S(T)PXX and XPRK motifs which can bind to AT-rich DNA motifs, we next determined whether treatment with Hoechst in SH-SY5Y cells stably expressing heterologous 82-kDa ChAT prior to fixation could alter the sub-nuclear distribution of 82-kDa ChAT by confocal microscopy. Cells were treated for 4 h with either vehicle or 100 nM A β_{1-42} followed by exposure to Hoechst stain, either following fixation (2500 ng/mL for 5 min) or prior to fixation (625 ng/mL for 20 min). As observed in previous experiments, vehicle-treated cells had a diffuse distribution of 82-kDa ChAT in the nucleus, both in cells treated with Hoechst following fixation (**Fig. 2-7[A-C]**) or prior to fixation [**D-F**]. After exposure to A β_{1-42} , cells that were treated with Hoechst dye following fixation (**Fig. 2-7[G-I]**) had aggregates of 82-kDa ChAT that did not appear to have any relationship with the Hoechst

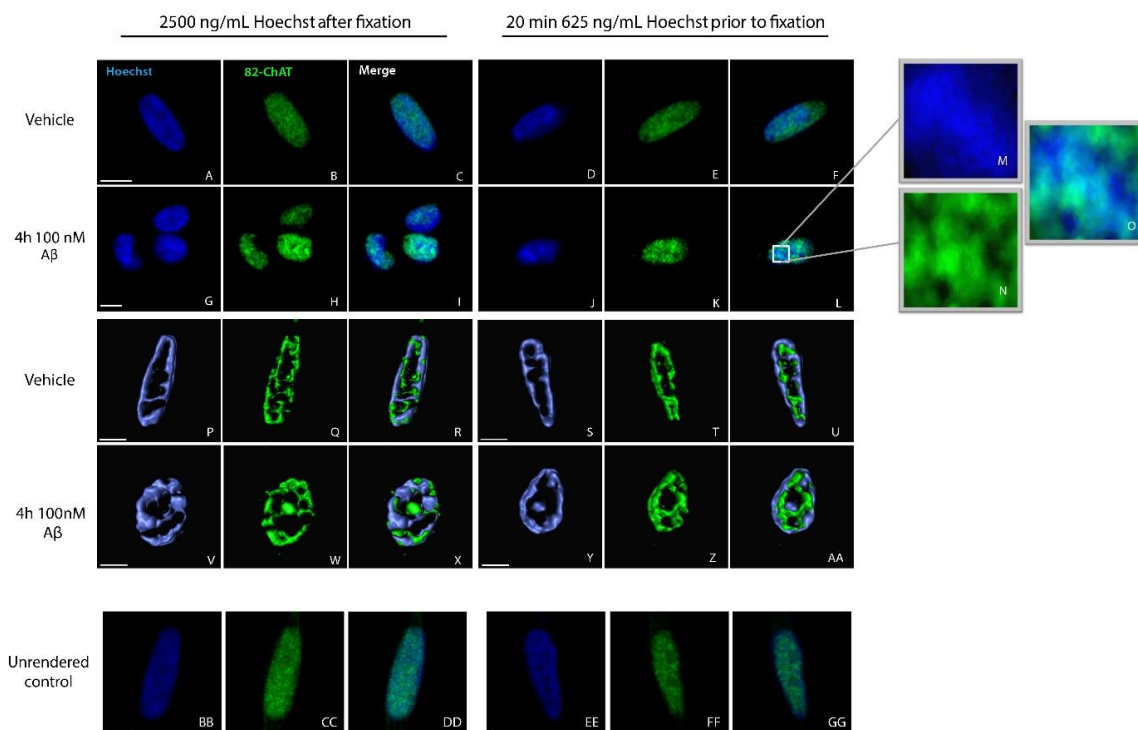


Figure 2-7. Effect of $A\beta_{1-42}$ treatment on 82-kDa ChAT nuclear distribution in SH-SY5Y cells.

Retinoic acid differentiated SH-SY5Y cells stably expressing 82-kDa ChAT were treated for 4 h with either vehicle (**A-F, P-U**) or 100 nM $A\beta_{1-42}$ (**G-L, V-AA**). For each treatment, cells were either treated with Hoechst stain following fixation or prior to fixation, and immunostained for 82-kDa ChAT prior to being imaged. For vehicle treated cells, 82-kDa ChAT appeared to be diffusely localized with a punctate-like appearance, and overlapped with the Hoechst stain when applied following (**A-C**) and prior to (**D-F**) imaging. For cells treated with $A\beta_{1-42}$ and Hoechst stain following fixation (**G-I**), there were aggregations of 82-kDa ChAT in the nuclei. However for $A\beta_{1-42}$ treated cells that had Hoechst applied prior to fixation (**J-L**), there were accumulations of 82-kDa ChAT surrounding regions with lower ChAT expression. For some cells, 3D images were acquired by taking 1 μm sections through the entire nucleus, and then compiled and rendered in Imaris before creating a 3D surface for each fluorophore. For vehicle treated cells, 82-kDa ChAT appeared to be localized mainly to the periphery of the nucleus, and overlapped with the Hoechst stain when applied following (**P-R**) and prior to (**S-U**) imaging. For cells treated with $A\beta_{1-42}$ and Hoechst stain following fixation (**V-X**), there were regions of ChAT aggregation surrounded by regions of Hoechst accumulation. This pattern was reversed for $A\beta_{1-42}$ treated cells that had Hoechst applied prior to fixation (**Y-AA**). Un-rendered 3D vehicle samples are shown for Hoechst stain following (**AA-CC**) and prior to (**DD-FF**) fixation. The left panel shows Hoechst staining, the center panel shows 82-kDa ChAT and the right panel is the overlay of the first two panels. Scale bar 8 μm ; $n = 4$ with at least 3 cells images per treatment.

dye. However, in A β ₁₋₄₂-treated cells exposed to Hoechst dye prior to fixation, there were areas within the aggregates that have lower levels of 82-kDa ChAT staining (**Fig. 2-7[J-L, N,O]**) and these areas were enriched with Hoechst dye (**Fig. 2-7[J-L, M,O]**). These latter results are similar to observations made in the previous experiment using live cells. In order to better visualize and identify patterns in the 3-dimensional structure of the nucleus, we next captured images at 1 μ m intervals through the entire nucleus in the z-plane. For vehicle-treated cells, 82-kDa ChAT appeared to be localized mainly to the periphery of the nucleus, and there appeared to be no difference in localization when the Hoechst stain was applied either following or prior to imaging (**Fig. 2-7[P-U]**). After exposure to A β ₁₋₄₂, cells that were treated with Hoechst dye following fixation had aggregates of 82-kDa ChAT that were surrounded by regions where Hoechst dye accumulated (**Fig. 2-7[V-X]**). This pattern was reversed for A β treated cells where Hoechst dye was applied prior to fixation (**[Y-AA]**). The vehicle-treated cell images prior to rendering are also shown as a comparison to the 3D images (**Fig. 2-7[BB-GG]**).

In some experiments, we chose to pre-treat cells with trichostatin A (TSA), a histone deacetylase (HDAC) inhibitor (Hu and Colburn 2005), prior to exposure of the cells to either vehicle or 100 nM A β , because of evidence previously linking 82-kDa ChAT to changes in histone acetylation (Gill 2005) and linking increases in oxidative stress with increases in histone acetylation (Duclot *et al.* 2010; Gu *et al.* 2013). We chose a concentration of 10 nM TSA based on a previous study that showed TSA-induced increases in histone acetylation in SH-SY5Y cells with this concentration (De los Santos *et al.* 2007). In cells treated for 6 h with either TSA or 2 h with TSA followed by the addition of A β ₁₋₄₂ for an additional 4 h, when Hoechst dye was applied following fixation there was nearly complete separation of 82-kDa ChAT and Hoechst (**Fig. 2-8[A-F]**). However, when Hoechst dye was added to the live cells prior to fixation there appeared to be regions of Hoechst accumulation surrounded by 82-kDa ChAT (**Fig. 2-8[G-L]**). We next evaluated the effect of decreasing the Hoechst dye concentration when applied prior to fixation on the localization of 82-kDa ChAT in TSA-treated cells (**Fig. 2-9**). Compared to 625 ng/mL Hoechst-treatment prior to fixation (**Fig. 2-8[J-L]**, **Fig. 2-9[A-C]**) cells treated with 125 ng/mL Hoechst prior to fixation had less Hoechst staining, but still had

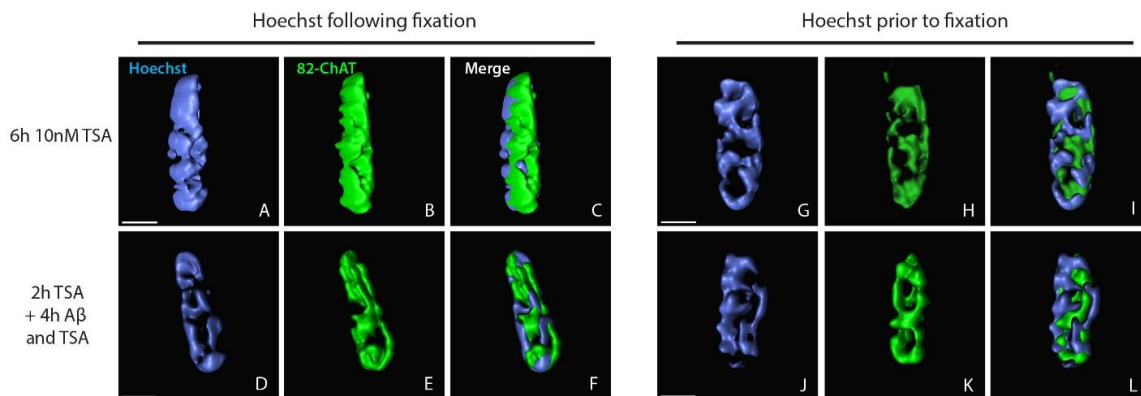


Figure 2-8. Effect of trichostatin A treatment on 82-kDa ChAT nuclear distribution in SH-SY5Y cells.

Retinoic acid differentiated SH-SY5Y cells stably expressing 82-kDa ChAT were treated for 6 h with either 10 nM trichostatin A (TSA) alone (**A-C, G-I**) or TSA and 4 h 100 nM $A\beta_{1-42}$ (**D-F, J-L**). 3D images were produced by capturing 1 μm sections through the entire nucleus, with these then compiled and rendered in Imaris before creating a 3D surface for each fluorophore. In cells treated with either TSA or TSA plus $A\beta_{1-42}$, when Hoechst dye was applied following fixation (**A-C, D-F**, respectively) there was nearly complete separation of 82-kDa ChAT and Hoechst. However, when Hoechst dye was applied to these cells prior to their fixation (**G-I, J-L**) there appeared to be regions of Hoechst stain accumulation surrounded by 82-kDa ChAT. The left panel shows Hoechst staining, the center panel shows 82-kDa ChAT and the right panel is the overlay of the first two panels. Scale bar 3 μm ; $n = 3$ with at least 3 cells images per treatment.

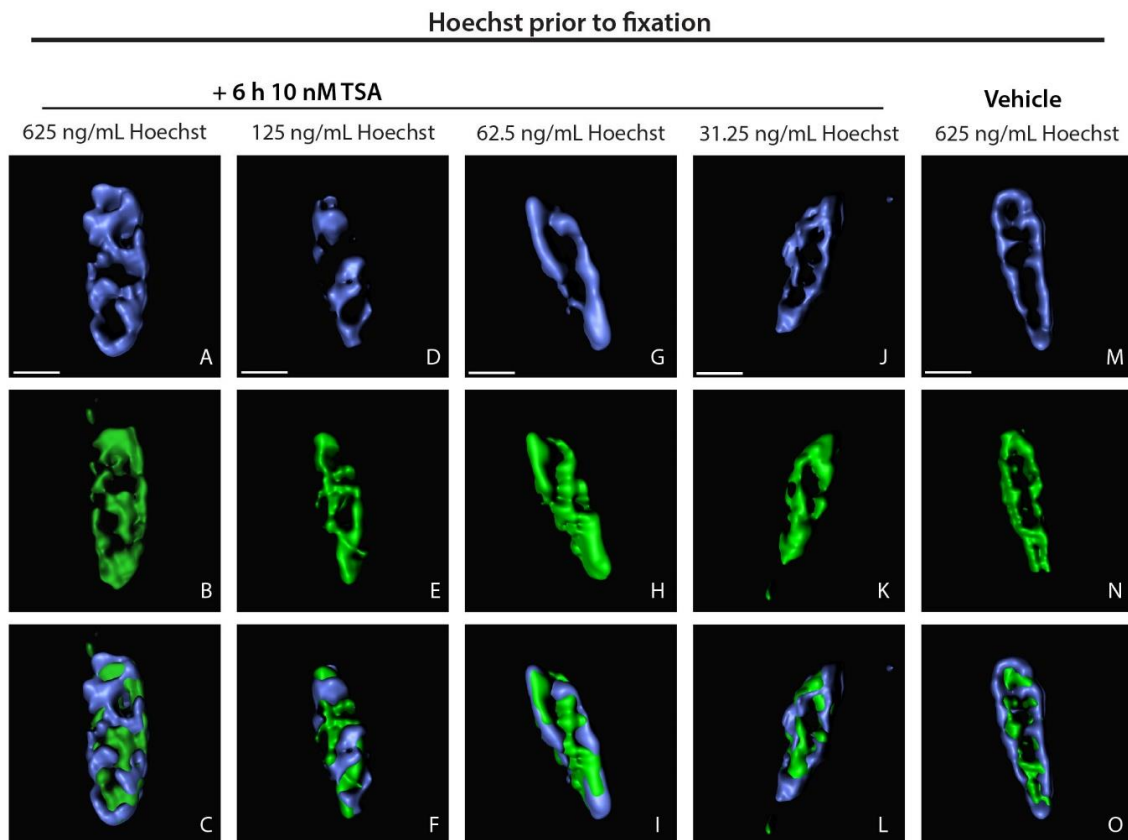


Figure 2-9. Titration of Hoechst stain in cells prior to fixation reverses TSA induced Hoechst accumulation.

Retinoic acid differentiated SH-SY5Y cells stably expressing 82-ChAT were treated for 6 h with 10 nM TSA and a range of concentrations of Hoechst dye prior to fixation, then fixed and immunostained for 82-kDa ChAT. Cells were imaged by taking 1 μ m sections through the entire nucleus, and 3D images were compiled and rendered in Imaris before creating a 3D surface for each fluorophore. In cells treated with TSA, when Hoechst was applied prior to fixation at 625 ng/ml (**A-C**) or 125 ng/ml (**D-F**), there appeared to be regions of Hoechst stain accumulation surrounded by 82-kDa ChAT. For Hoechst dye at 62.5 ng/ml (**G-I**), there appeared to be less accumulations of Hoechst, and at 32.5 ng/ml Hoechst dye (**J-L**) both ChAT and Hoechst appeared to overlap completely similar to vehicle treated cells (**M-O**). The top panels show Hoechst staining, the middle panels show 82-kDa ChAT and the bottom panels is the overlay of the first two panels. Scale bar 3 μ m; n = 2 with at least 3 cells images per treatment.

regions of Hoechst surrounded by 82-kDa ChAT (**Fig. 2-9[D-F]**). However, when cells were treated prior to fixation with 62.5 ng/mL (**Fig. 2-9[G-I]**) or 31.25 ng/mL (**Fig. 2-9[J-L]**) Hoechst dye, there appeared to be no relationship between 82-kDa ChAT and the Hoechst, similar to observations made in vehicle-treated cells (**Fig. 2-7[S-U]**, **Fig. 2-9[M-O]**). These data suggest that treatment with TSA facilitates changes in 82-kDa ChAT localization in live unfixed cells incubated with Hoechst dye, dependent on the Hoechst dye concentration.

To further provide evidence that 82-kDa ChAT may display Hoechst displacement, we repeated the 3D z-stack imaging experiments with endogenous tau, a protein that binds to DNA at the minor groove via S(T)PXX motifs (**Fig. 2-10**; Wei *et al.* 2008). Although tau has not been shown previously to be displaced by Hoechst stain, it is displaced by the minor groove binder distamycin A in gel shift assays (Krylova *et al.* 2005; Wei *et al.* 2008; Majumder and Dasgupta 2011). For our experiments, wild-type SH-SY5Y cells were differentiated for 3 days with retinoic acid, then treated for 6 h either with or without 10 nM TSA followed by exposure to Hoechst stain either prior to or after being fixed with paraformaldehyde. Cells were then immunostained for total tau protein, and imaged as described above. In vehicle-treated cells exposed to Hoechst dye following fixation, tau protein appeared to be localized mainly to the periphery of the nucleus, and overlapped with the Hoechst stain (**Fig. 2-10[A-C]**). However, when treated with Hoechst dye prior to fixation, there appeared to be accumulations of Hoechst dye surrounded by tau protein in the nuclei (**Fig. 2-10[G-I]**). Compared to vehicle treatment, we observed the same pattern in cells that were treated with TSA and Hoechst dye either following or prior to fixation (**Fig. 2-10[D-F, J-L]**). Single slice images were taken from the same 3D images for TSA treated cells with Hoechst dye following or prior to fixation (**Fig. 2-10[M-W]**). These images indicate that for cells treated with Hoechst dye prior to fixation, there appears to be the same pattern of expression as 82-kDa ChAT, with accumulations of tau surrounding accumulations of Hoechst dye. We also decided to perform 3D z-stack imaging for the endogenous expression of Matrin3, a major groove DNA binding protein that contains very few S(T)PXX regions, but does have two zinc finger domains that bind to the major groove of DNA (**Fig. 2-11[A]**; Salton *et al.* 2011). Therefore, we treated retinoic acid differentiated wild-type SH-SY5Y cells either with or

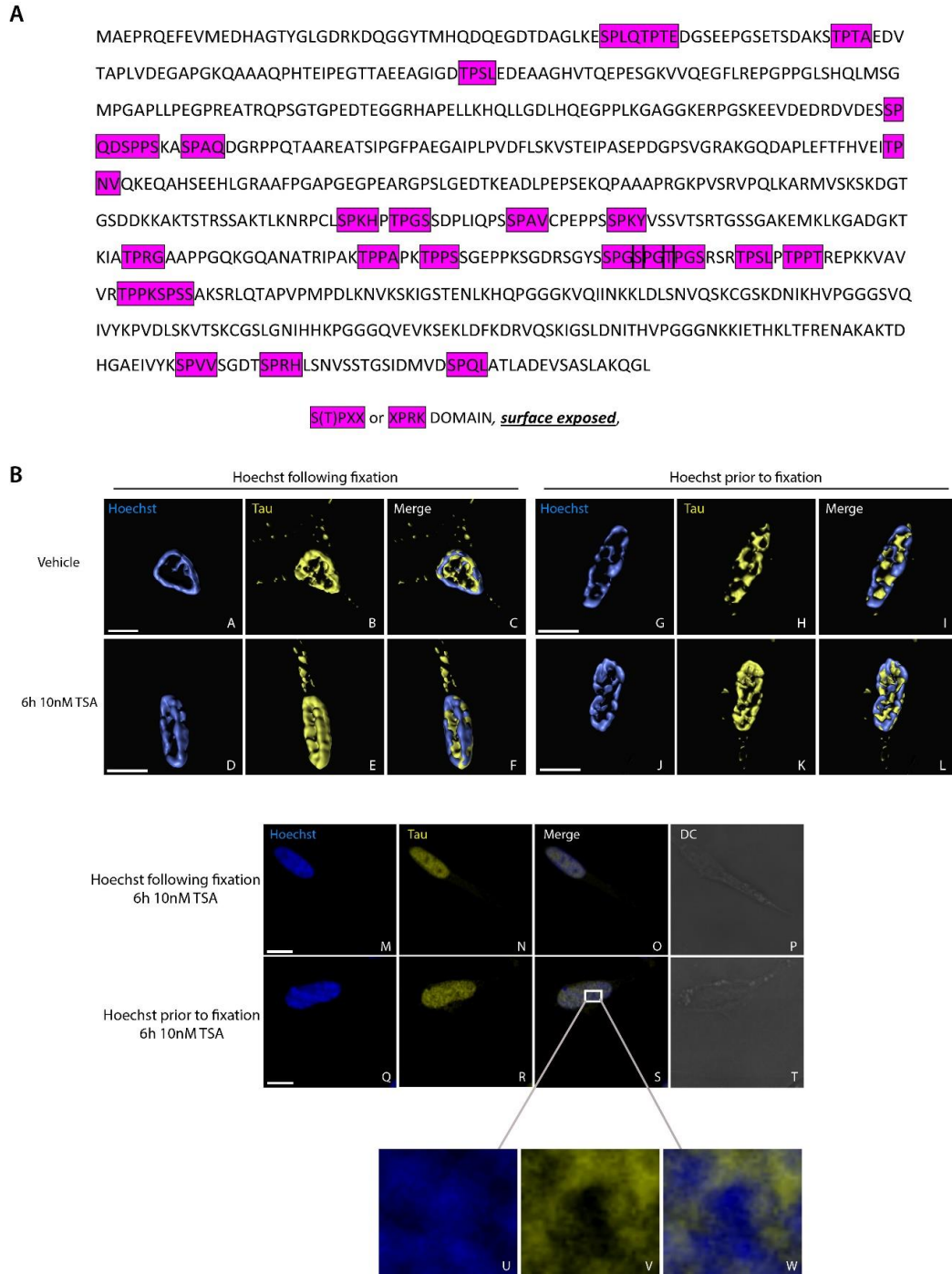


Figure 2-10. Effect of TSA on three-dimensional tau protein nuclear distribution in SH-SY5Y cells.

- (A) S(T)PXX DNA binding domains located in human tau isoform 1. There are several groupings of DNA binding regions found throughout the primary sequence of the protein.
 (B) Retinoic acid differentiated SH-SY5Y cells were treated with either vehicle or 10 nM

TSA for 6 h. For each treatment, cells were treated with Hoechst stain either following fixation (**A-F**) or prior to fixation (**G-L**), then immunostained for endogenous tau prior to being imaged. Cells were imaged by taking 1 μm sections through the entire nucleus, and 3D images were compiled and rendered in Imaris before creating a 3D surface for each fluorophore. For control cells, tau appeared to be localized mainly to the periphery of the nucleus, and overlapped with the Hoechst stain when it was applied following fixation (**A-C**). For control cells treated with Hoechst prior to fixation (**G-I**), there appeared to be accumulations of Hoechst dye surrounded by tau. The same pattern as control was observed in cells treated with TSA and Hoechst dye either following (**D-E**) or prior to (**J-L**) fixation. Single slice images were taken from the same 3D images for TSA treated cells treated with Hoechst dye either following (**M-P**) or prior to (**Q-T**) fixation. The inset on (**S**) shows a region of Hoechst dye accumulation (**U**) surrounded by tau (**V**), and the overlay of the two (**W**). In the top image (**A-L**), the left panel shows Hoechst staining, the center panel shows tau protein and the right panel is the overlay of the first two panels. In the bottom image (**M-T**), an additional right panel shows the differential contrast image for each slice. Scale bar 3 μm ; $n = 2$ with at least 5 cells images per treatment.

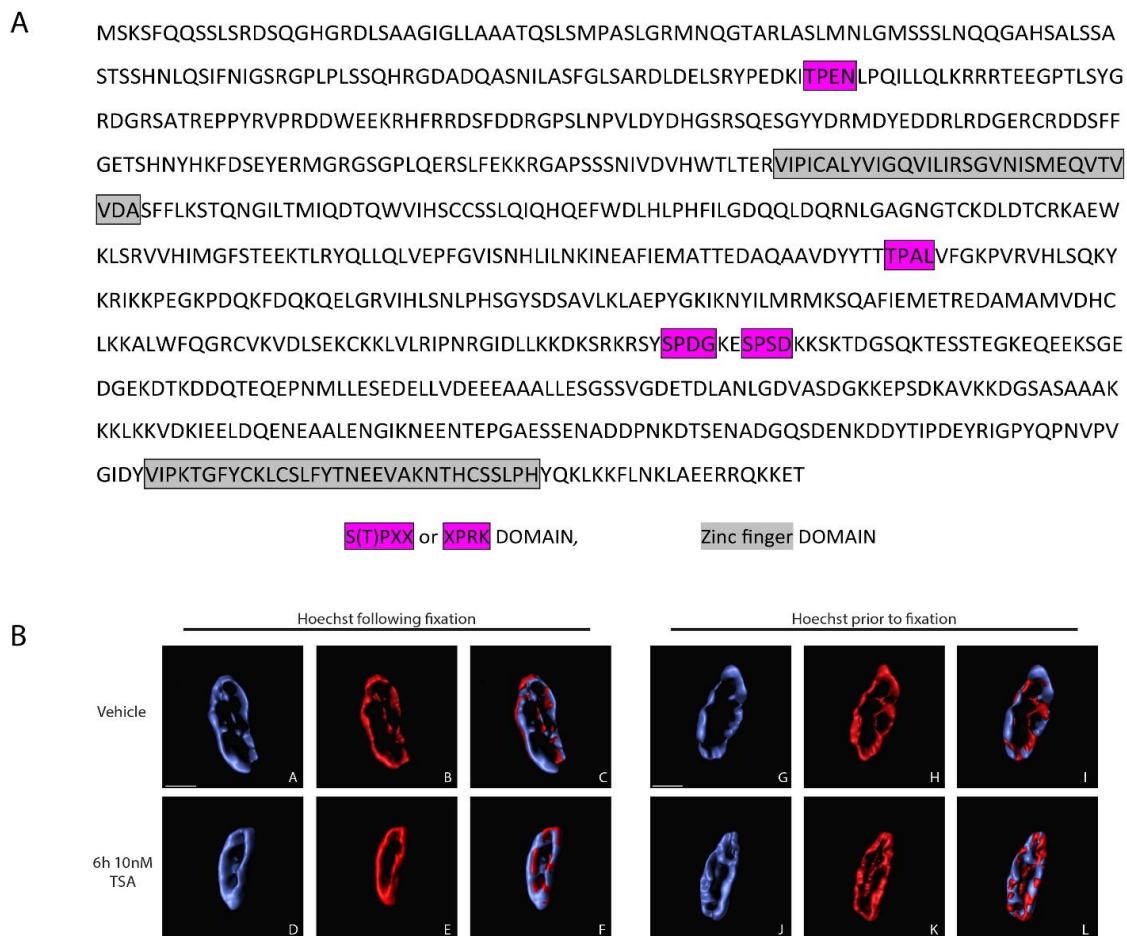


Figure 2-11. Effect of TSA on three-dimensional Matrin3 protein nuclear distribution in SH-SY5Y cells.

(A) DNA binding domains located in human Matrin3. There are two zinc finger domains located within the protein, but only a few S(T)PXX domains which are not grouped together. (B) Retinoic acid differentiated SH-SY5Y cells were treated with either vehicle or 10 nM TSA for 6 h. For each treatment, cells were treated with Hoechst stain either following fixation (A-F) or prior to fixation (G-L), then immunostained for endogenous matrin 3 prior to being imaged. Cells were imaged by taking 1 μ m sections through the entire nucleus, and 3D images were compiled and rendered in Imaris before creating a 3D surface for each fluorophore. For control and TSA treated cells, Matrin3 appeared to be localized mainly to the periphery of the nucleus, and overlapped with the Hoechst stain when applied following fixation (A-C, D-F; respectively). For control and TSA treated cells with Hoechst dye applied prior to fixation (G-I, J-L; respectively), both Hoechst and Matrin3 expression appeared similar to Hoechst following fixation. Scale bar 3 μ m; n = 2 with at least 5 cells images per treatment.

without TSA for 6 h, then stained with Hoechst dye either following or prior to fixation and immunostained for endogenous Matrin3 protein (**Fig. 2-11[B]**). In each treatment condition, Matrin3 was completely overlapped with Hoechst, and there did not appear to be any aggregates of Hoechst or Matrin3.

Assessment of the in vitro DNA-binding potential for 82-kDa ChAT protein

Based on the observations that 82-kDa ChAT protein associates with chromatin and has altered localization following live exposure to Hoechst dye, we assessed whether purified recombinant 82-kDa ChAT could bind directly to oligomeric DNA (**Table 2-1**). In our initial study, we performed EMSA experiments according to the manufacturer's recommendations for the EBNA extract with the objective of detecting the positive EBNA control and testing several of the DNA oligomers (at 200 fmol) for 82-kDa ChAT (**Fig. 2-12**). These results suggest that the EBNA positive control worked as intended. Moreover, both the AT-rich and SATB1 motif DNA oligomers potentially show DNA binding of 82-kDa ChAT, though a non-specific band appeared at the same height in samples that contained no protein. Therefore, we used these two sequences for further testing. **Appendix 5** shows the results in the EMSA optimization using the ATC-rich motif $(A/T)_{3-n}C(A/T)_{3-6}$. Increasing the incubation time to either 45 or 60 min increased the intensity of the shifted band, but this did not differ from that of the non-specific band. Both mixing the samples by rotation during the incubation period and increasing the incubation temperature to 37°C increased the intensity of the bands for reaction samples either containing and not containing 82-kDa ChAT protein (125 fmol DNA oligomer concentration). Addition of an antibody recognizing 82-kDa ChAT to the samples for 15 min prior to the end of the incubation period appeared to produce a small reduction in signal (100 fmol DNA oligomer concentration). Importantly, when we added the reducing agent tris(2-carboxyethyl)phosphine (TCEP) to block reactive cysteine residues and prevent oxidation of ChAT protein (Kim *et al.* 2005a), we were observed a stronger intensity band compared to samples incubated in the absence of TCEP (**Fig. 2-13**). These

data suggest that 82-kDa ChAT is sensitive to oxidation, which may interfere with its ability to bind DNA.

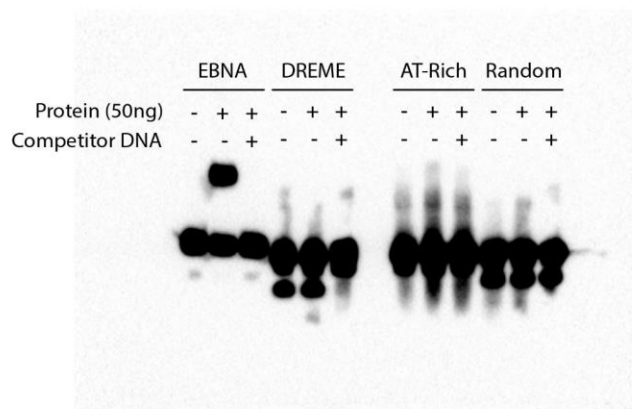
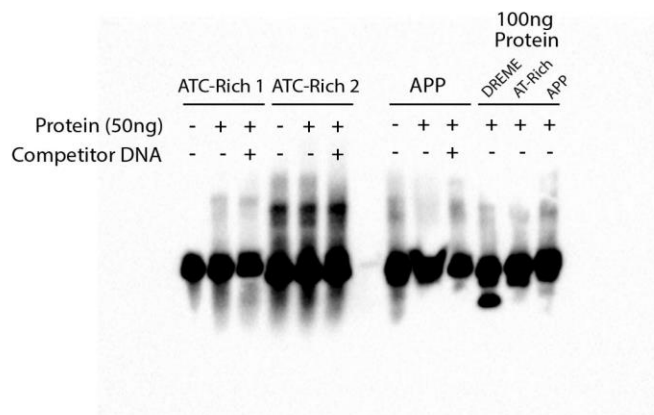
A**B**

Figure 2-12. Initial EMSA testing for 82-kDa ChAT.

Purified recombinant 82-kDa ChAT (50 ng) or control EBNA extract was incubated with annealed biotinylated DNA oligomers from Table 2.1 and then separated on TBE electrophoresis gels. DNA and proteins were transferred to nylon membranes and exposed to stabilized streptavidin-horseradish peroxidase conjugate. (**A**) The control EBNA extract shows a strong shift when incubated with its target DNA sequence (20 fmol), with this shift not observed for samples containing 200-molar excess non-biotinylated competitor DNA. The AT-Rich and (**B**) ATC-Rich 1 motif sequences (200 fmol) showed a shifted band of stronger intensity after incubation with 82-kDa ChAT, though a non-specific background band at the same height was observed in samples that did not contain 82-kDa ChAT. Competition appeared to attenuate the AT-Rich shifted band, but not the ATC-Rich 1 shifted band. The ATC-Rich 2 sequence resulted in a strong non-specific shifted band that was present in all conditions, while the random, APP and DREME oligomers did not produce a shifted band. Increasing the 82-kDa ChAT protein incubated to 100 ng did not produce a shift for the DREME, AT-Rich or APP sequences.

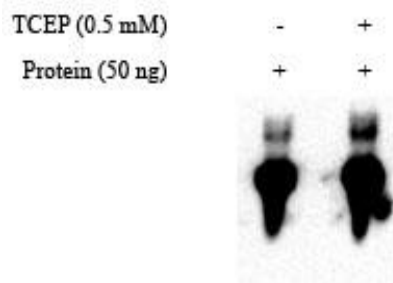


Figure 2-13. 82-kDa ChAT DNA binding is sensitive to oxidation.

Purified recombinant 82-kDa ChAT was incubated with annealed biotinylated DNA oligomers from Table 2.1 (only the ATC-Rich 1 motif was used for these experiments at 100 fmol). Addition of the reducing agent TCEP to prevent oxidation of 82-kDa ChAT resulted in an increase in the intensity of shifted immunoreactive band. N = 2.

2.4 Discussion

This chapter explored the novel finding that 82-kDa ChAT can associate with chromatin, and that this association is altered in neural cells treated with A β ₁₋₄₂. Specifically, we found that (1) 82-kDa ChAT associates with chromatin; (2) 82-kDa ChAT increases its association with gene introns and promoters at synapse and membrane associated genes after cells have been exposed to A β ₁₋₄₂; and (3) nuclear localized 82-kDa ChAT forms aggregates in A β ₁₋₄₂-treated cells. These aggregates were enriched with DNA, and are dependent on whether Hoechst stain was applied prior to fixation of the cells and upon the concentration of Hoechst dye. Finally, while we observed DNA-protein shifts by EMSA when we incubated 82-kDa ChAT with DNA oligomers, more data and optimizations are required to determine whether 82-kDa ChAT is directly binding to DNA.

When we assessed the cellular distribution of 82-kDa ChAT by nuclear subfractionation, we observed that there was an 82-kDa ChAT immuno-reactive band in the fraction containing proteins associated with euchromatic chromatin (150 mM KCl) in both vehicle and A β ₁₋₄₂-treated cells, though the A β ₁₋₄₂ treated cells had higher 82-kDa ChAT levels in this fraction compared to vehicle treated cells. It was interesting that we observed a stronger band in the A β ₁₋₄₂-exposed samples, as we found a similar number of ChIP-seq associations regardless of treatment. This could be explained partially by the increased genic associations observed after A β ₁₋₄₂ treatment, as regions such as exons and promoters are naturally more likely targets for transcriptional activation. In addition, the 82-kDa ChAT ChIP associations had smaller peak sizes in cells treated with A β ₁₋₄₂, indicative of more targeted gene associations at regulatory sites that could alter gene transcriptional states (Pepke *et al.* 2009). An important limitation for the cellular fractionation experiments is that while we observed a positive immuno-reactive band for the insoluble fraction after A β ₁₋₄₂ treatment, we could not distinguish whether the proteins in this fraction were associated with heterochromatin or the nuclear matrix, or whether these were insoluble proteins. For example, previous unpublished work from our laboratory has found by co-immunoprecipitation that 82-kDa ChAT may interact with

Matrin3, a nuclear matrix protein. Therefore, it will be important for future studies to explore whether or not 82-kDa ChAT has insoluble components or changes its interaction with the nuclear matrix after exposure to A β ₁₋₄₂.

In addition to the A β ₁₋₄₂-induced increases in 82-kDa ChAT genic associations, we also observed multiple significant DREME motifs for both vehicle and A β ₁₋₄₂-exposed cells. Multiple DREME motifs often indicate that proteins may be in a complex with other proteins or transcription factors (Bailey 2011), and small, targeted ChIP peaks usually indicate transcription factor binding (Pepke *et al.* 2009). It is interesting to note that the DREME motif sequences may support both these observations. For example, the TC₂₋₃AT motif observed after both vehicle and A β ₁₋₄₂-treatment has partial sequence homology to the nuclear factor of activated T-cells (NFAT) transcription factor (Kheradpour and Kellis 2014; **Fig. 2-14**). NFAT is dephosphorylated by calcineurin after neuronal activation and cell exposure to oligomeric A β ₁₋₄₂, leading to transcriptional activation of calcium homeostasis, synapse maintenance and neuro-inflammation related genes (Schwartz *et al.* 2009; Abdul *et al.* 2010). Interestingly, we observed that 82-kDa ChAT associated with synapse and membrane related genes regardless of treatment, and a previous microarray in human neural cells expressing 82-kDa ChAT found gene expression changes in many membrane-associated genes related to APP processing (Albers *et al.* 2014). These data suggest that NFAT could be part of a complex with 82-kDa ChAT, a relationship that is explored further in Chapter 4. In addition to the partial NFAT motifs, we also observed a DNA-binding motif for SATB1, which anchors chromatin loops to the nuclear matrix as part of scaffolding/matrix attachment regions (S/MARs), and can recruit HDACs or histone acetyltransferases (HATs) specifically to these regions (Yasui *et al.* 2002; Cai *et al.* 2003; Galande *et al.* 2007). S/MARs are anchored to the nuclear matrix by SATB1 binding to local and distant ATC-rich DNA sequences, forming chromatin loops that are accessible for chromatin modifying factors to repress or activate transcription (Yasui *et al.* 2002; Galande *et al.* 2007). The role of SATB1 in the association of 82-kDa ChAT with chromatin is explored further in Chapter 3.

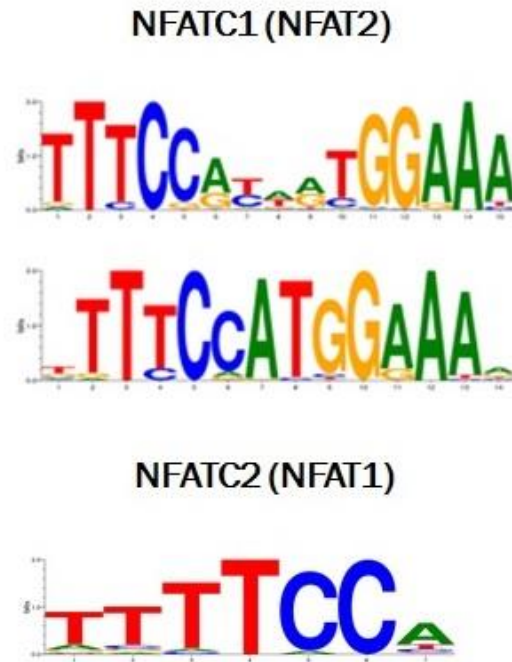


Figure 2-14. DREME motifs for nuclear factor of activated T-cells (NFAT).

NFAT DNA-binding motifs with partial sequence homology to the TC₂₋₃AT motif found by ChIP-seq for 82-kDa ChAT.

An important result from the ChIP-seq data is that 82-kDa ChAT is highly associated with centromeric regions of chromatin, a feature known to be important for heterochromatin organization and cell cycle regulation (DeBeauchamp *et al.* 2008; Fernius *et al.* 2013). As previously discussed in the Introduction, constitutive repression and chromatin compaction in the centromere is essential for proper regulation of cell cycle division (Spremo-Potparević *et al.* 2008); in the case of neurons, cells are maintained in G₀. It is of interest that neurons in the brains of AD patients show evidence of cell cycle re-entry attempts and abnormal centromere division (Spremo-Potparević *et al.* 2008). This is especially interesting given that the nuclear localization of 82-kDa ChAT is lost in AD (Gill *et al.* 2007). Future studies will be important to determine if there is a role for 82-kDa ChAT in cell cycle regulation.

Finally, an observation from the ChIP-seq data was that there was very little overlap in the genomic associations for 82-kDa ChAT after vehicle and A β ₁₋₄₂-exposure, with only 250 peaks in common out of a total of 13,805 peaks (1.8%). This observation, combined with the observed increases in intron, promoter and exon associations after A β ₁₋₄₂-exposure, led us to explore how 82-kDa ChAT was expressed in nuclei and whether there were any observable A β ₁₋₄₂-induced changes in 82-kDa ChAT sub-nuclear localization. When visualized by confocal microscopy, we observed that exposure to A β ₁₋₄₂ induced the formation of 82-kDa ChAT aggregates in the nuclei of SH-SY5Y cells. Importantly, when live cells were treated with Hoechst dye, we observed DNA staining within the aggregates. Hoechst binds to AT-rich DNA sequences and can displace other proteins that bind to DNA at AT-rich regions of the minor groove (Amirand *et al.* 1998; Deka *et al.* 1999). The 82-kDa ChAT protein is predicted to bind to DNA through S(T)PXX and XPRK motifs that bind AT-rich DNA (Suzuki 1989, Yang *et al.* 2003), therefore we determined whether Hoechst treatment in live cells could alter 82-kDa ChAT nuclear localization. We noted that 82-kDa ChAT sub-nuclear localization was altered when Hoechst dye was added to cells prior to fixation with paraformaldehyde, but not after fixation in A β ₁₋₄₂-treated cells. We did not observe this effect in vehicle treated cells. When taken in combination with the data suggesting that there is increased association of 82-kDa ChAT DNA with euchromatic DNA after cells are exposed to A β ₁₋₄₂, these findings suggest that the A β ₁₋₄₂-induced 82-kDa ChAT

aggregates are associated with euchromatic AT-rich DNA. To test this possibility further, we also treated cells with the HDAC inhibitor TSA, which increases histone acetylation and availability of chromatin for transcription (Hu and Colburn 2005), observing that this treatment also facilitated the changes in 82-kDa ChAT localization in live unfixed cells incubated with Hoechst dye. These data support the hypothesis that 82-kDa ChAT may be binding to DNA at AT-rich sequences, however it is important to consider a few limitations of this study. While TSA is a class I and II HDAC inhibitor and increases histone acetylation, these changes may not be global as there are also class III and IV HDACs which would not be affected. Thus, it is possible that some regions may remain heterochromatic, and local chromatin regions will have non-uniform acetylation levels. Though we showed that the sub-nuclear distribution of Hoechst in 82-kDa ChAT expressing cells is altered by cellular perturbations, confirmation of Hoechst displacement should be confirmed by EMSA methods (Amirand et al. 1998; Deka et al. 1999). Our preliminary EMSA results suggest that 82-kDa ChAT could bind to AT- and ATC-rich DNA sequences, however there were non-specific bands in the non-82-kDa ChAT containing samples, indicating that this assay requires further optimization. Despite these limitations, the ChIP-seq data also showed that 82-kDa ChAT associates with DNA at AT and ATC-rich sequences. Thus, the notion that 82-kDa ChAT associates with euchromatic chromatin at AT-rich sequences is promising and warrants further investigation.

The data presented in this chapter shows that 82-kDa ChAT associates with chromatin, with increased genic associations after cells are exposed to oligomeric A β ₁₋₄₂. The results suggest that the chromatin associations of 82-kDa ChAT may be dynamically regulated after environmental challenges and cellular perturbations, with possible implications for genes related to synapse and membrane maintenance, AD risk, and APP processing. Given that the nuclear levels of 82-kDa ChAT decline with increasing age and the onset of cognitive impairment (Gill *et al.* 2007), and that synaptic dysfunction is seen early in the pathogenesis of AD, the loss of this epigenetic response may have implications for the onset or progression of MCI and AD.

2.5 References

- Abdul HM, Furman JL, Sama MA, Mathis DM, Norris CM (2010) NFATs and Alzheimer's Disease. *Mol Cell Pharmacol*, 2: 7-14.
- Albers S, Inthathirath F, Gill SK, Winick-Ng W, Jaworski E, Wong DY, Gros R, Rylett RJ (2014) Nuclear 82-kDa choline acetyltransferase decreases amyloidogenic APP metabolism in neurons from APP/PS1 transgenic mice. *Neurobiol Dis*, 69: 32-42.
- Amirand C, Viari A, Ballini JP, Rezaei H, Beaujean N, Jullien D, Käs E, Debey P (1998) Three distinct sub-nuclear populations of HMG-I protein of different properties revealed by co-localization image analysis. *J Cell Sci*, 23: 3551-3561.
- Antonarakis, SE (2010) Human genome sequence and variation in *Vogel and Motulsky's Human Genetics Problems and Approaches* (eds: Speicher M. *et al.*) 31–53 (Springer-VerlagPublishing).
- Bailey TL (2011) DREME: motif discovery in transcription factor ChIP-seq data. *Bioinformatics*, 27: 1653-1659.
- Bertram L (2011) Alzheimer's genetics in the GWAS era: a continuing story of 'replications and refutations'. *Curr Neurol Neurosci Rep*, 11: 246-253.
- Cai S, Han HJ, Kohwi-Shigematsu T (2003) Tissue-specific nuclear architecture and gene expression regulated by SATB1. *Nat Genet*, 34: 42-51.
- De los Santos M, Zambrano A, Aranda A (2007) Combined effects of retinoic acid and histone deacetylase inhibitors on human neuroblastoma SH-SY5Y cells. *Mol Cancer Ther*, 6: 1425-1437.

- Debeauchamp JL, Moses A, Noffsinger VJ, Ulrich DL, Job G, Kosinski AM, Partridge JF (2008) Chp1-Tas3 interaction is required to recruit RITS to fission yeast centromeres and for maintenance of centromeric heterochromatin. *Mol Cell Biol*, 28: 2154-2166.
- Deka J, Herter P, Sprenger-Haussels M, Koosch S, Franz D, Müller KM, Kuhnen C, Hoffmann I, Müller O (1999) The APC protein binds to A/T rich DNA sequences. *Oncogene*, 18: 5654-5661.
- Dobransky T, Davis WL, Xiao GH, Rylett RJ (2000) Expression, purification and characterization of recombinant human choline acetyltransferase: phosphorylation of the enzyme regulates catalytic activity. *Biochem J*, 349: 141-151.
- Duclot F, Meffre J, Jacquet C, Gongora C, Maurice T (2010) Mice knock out for the histone acetyltransferase p300/CREB binding protein-associated factor develop a resistance to amyloid toxicity. *Neuroscience* 167: 850-863.
- Fernius J, Nerusheva OO, Galander S, Alves Fde L, Rappsilber J, Marston AL (2013) Cohesin-dependent association of scc2/4 with the centromere initiates pericentromeric cohesion establishment. *Curr Biol*, 23: 599-606.
- Galande S, Purbey PK, Notani D, Kumar PP (2007) The third dimension of gene regulation: organization of dynamic chromatin loopscape by SATB1. *Curr Opin Genet Dev*, 17: 408-414.
- Giardine B, Riemer C, Hardison RC, Burhans R, Elnitski L, Shah P, Zhang Y, Blankenberg D, Albert I, Taylor J, Miller W, Kent WJ, Nekrutenko A (2005) Galaxy: a platform for interactive large-scale genome analysis. *Genome Res* 15: 1451-1455.
- Gill SK (2005) Characterization of Human and 69-kDa and 82-kDa Choline Acetyltransferase Proteins. PhD Thesis, Western University, London Ontario Canada.

- Gill SK, Ishak M, Dobransky T, Haroutunian V, Davis KL, Rylett RJ (2007) 82-kDa choline acetyltransferase is in nuclei of cholinergic neurons in human CNS and altered in aging and Alzheimer disease. *Neurobiol Aging*, 28: 1028-1040.
- Gu X, Sun J, Li S, Wu X, Li L (2013) Oxidative stress induces DNA demethylation and histone acetylation in SH-SY5Y cells: potential epigenetic mechanisms in gene transcription in A β production. *Neurobiol Aging*, 34: 1069-1079.
- Hashemi SH, Li JY, Ahlman H, Dahlström A (2003) SSR2(a) receptor expression and adrenergic/cholinergic characteristics in differentiated SH-SY5Y cells. *Neurochem Res*, 28: 449-460.
- Hu J, Colburn NH (2005) Histone Deacetylase Inhibition Down-Regulates Cyclin D1 Transcription by Inhibiting Nuclear Factor- κ B/p65 DNA Binding. *Mol Cancer Res*, 3: 100-109.
- Huang da W, Sherman BT, Lempicki RA (2009) Systematic and integrative analysis of large gene lists using DAVID bioinformatics resources. *Nat Protoc*, 4: 44-57.
- Huang da W, Sherman BT, Lempicki RA (2009a) Bioinformatics enrichment tools: paths toward the comprehensive functional analysis of large gene lists. *Nucleic Acids Res*, 37: 1-13.
- Kent WJ, Sugnet CW, Furey TS, Roskin KM, Pringle TH, Zahler AM, Haussler D (2002) The human genome browser at UCSC. *Genome Res*, 12: 996-1006.
- Kheradpour P, Kellis M (2014) Systematic discovery and characterization of regulatory motifs in ENCODE TF binding experiments. *Nucleic Acids Res*, 42: 2976-2987.
- Kim AR, Dobransky T, Rylett RJ, Shilton BH (2005) Surface-entropy reduction used in the crystallization of human choline acetyltransferase. *Acta Crystallogr D Biol Crystallogr*, 61: 1306-1310.

- Kim AR, Doherty-Kirby, A., Lajoie, G., Rylett, R.J., and Shilton, B.H. (2005a) Two methods for large-scale purification of recombinant human choline acetyltransferase. *Protein Expr. Purif.*, **40**, 107-117.
- Krylova SM, Musheev M, Nutiu R, Li Y, Lee G, Krylov SN (2005) Tau protein binds single-stranded DNA sequence specifically--the proof obtained in vitro with non-equilibrium capillary electrophoresis of equilibrium mixtures. *FEBS Lett*, **579**: 1371-1375.
- Lana E, Khanbolouki M, Degavre C, Samuelsson EB, Åkesson E, Winblad B, Alici E, Lithner CU, Behbahani H (2016) Perforin Promotes Amyloid Beta Internalisation in Neurons. *Mol Neurobiol*, Epub ahead of print, DOI: 10.1007/s12035-016-9685-9.
- Li H, Durbin R (2009) Fast and accurate short read alignment with Burrows-Wheeler transform. *Bioinformatics* **25**: 1754-1760.
- Li X, Song L, Jope RS (1996) Cholinergic stimulation of AP-1 and NF kappa B transcription factors is differentially sensitive to oxidative stress in SH-SY5Y neuroblastoma: relationship to phosphoinositide hydrolysis. *J Neurosci*, **16**: 5914-5922.
- Majumder P, Dasgupta D (2011) Effect of DNA groove binder distamycin A upon chromatin structure. *PLoS One*, **6**: e26486.
- Pepke S, Wold B, Mortazavi A (2009) Computation for ChIP-seq and RNA-seq studies. *Nat Methods*, **6**: S22-32.
- Robinson JT, Thorvaldsdóttir H, Winckler W, Guttman M, Lander ES, Getz G, Mesirov JP (2011) Integrative genomics viewer. *Nat Biotechnol*, **29**: 24-26.
- Roy A, Kucukural A, Zhang Y (2010) I-TASSER: a unified platform for automated protein structure and function prediction. *Nature Protoc*, **5**: 725-738.

- Roy A, Yang J, Zhang Y (2012) COFACTOR: an accurate comparative algorithm for structure-based protein function annotation. *Nucleic Acids Res*, 40: W471-W477.
- Salton M, Elkon R, Borodina T, Davydov A, Yaspo ML, Halperin E, Shiloh Y (2011) Matrin 3 binds and stabilizes mRNA. *PLoS One*, 6: e23882.
- Schneider CA, Rasband WS, Eliceiri KW (2012) NIH Image to ImageJ: 25 years of image analysis. *Nat Methods*, 9: 671-675.
- Schwartz N, Schohl A, Ruthazer ES (2009) Neural activity regulates synaptic properties and dendritic structure in vivo through calcineurin/NFAT signaling. *Neuron*, 62: 655-669.
- Spremo-Potparević B, Zivković L, Djelić N, Plečas-Solarović B, Smith MA, Bajić V (2008) Premature centromere division of the X chromosome in neurons in Alzheimer's disease. *J Neurochem*, 106: 2218-2223.
- Stine WB Jr, Dahlgren KN, Krafft GA, LaDu MJ (2003) In vitro characterization of conditions for amyloid-beta peptide oligomerization and fibrillogenesis. *J Biol Chem*, 278: 11612-11622.
- Suzuki M (1989) SPXX, a frequent sequence motif in gene regulatory proteins. *J Mol Biol*, 207: 61-84.
- Wang L, Brown SJ (2006) BindN: a web-based tool for efficient prediction of DNA and RNA binding sites in amino acid sequences. *Nucleic Acids Res*, 34: W243-248.
- Wei Y, Qu MH, Wang XS, Chen L, Wang DL, Liu Y, Hua Q, He RQ (2008) Binding to the minor groove of the double-strand, tau protein prevents DNA from damage by peroxidation. *PLoS One*, 3: e2600.
- Yan C, Terribilini M, Wu F, Jernigan RL, Dobbs D, Honavar V (2006) Predicting DNA-binding sites of proteins from amino acid sequence. *BMC Bioinformatics*, 7: 262.

- Yaniv SP, Lucki A, Klein E, Ben-Shachar D (2010) Dexamethasone enhances the norepinephrine-induced ERK/MAPK intracellular pathway possibly via dysregulation of the alpha2-adrenergic receptor: implications for antidepressant drug mechanism of action. *Eur J Cell Biol*, 89: 712-722.
- Yang CH, Chou PJ, Luo ZL, Chou IC, Chang JC, Cheng CC, Martin CR, Waring MJ, Sheh L (2003) Preferential binding to DNA sequences of peptides related to a novel XPRK motif. *Bioorg Med Chem*, 11: 3279-3288.
- Yasui D, Miyano M, Cai S, Varga-Weisz P, Kohwi-Shigematsu T (2002) SATB1 targets chromatin remodelling to regulate genes over long distances. *Nature*, 419: 641-645.
- Ye JZ, de Lange T (2004) TIN2 is a tankyrase 1 PARP modulator in the TRF1 telomere length control complex. *Nat Genet*, 36: 618-623.
- Young KF, Pasternak SH, Rylett RJ (2009) Oligomeric aggregates of amyloid beta peptide 1-42 activate ERK/MAPK in SH-SY5Y cells via the alpha7 nicotinic receptor. *Neurochem Int*, 55: 796-801.
- Zhang Y (2008) I-TASSER server for protein 3D structure prediction. *BMC Bioinform*, 9: 40.
- Zhang Y, Liu T, Meyer CA, Eeckhoutte J, Johnson DS, Bernstein BE, Nusbaum C, Myers RM, Brown M, Li W, Liu XS (2008) Model-based analysis of ChIP-Seq (MACS). *Genome Biol*, 9: R137.

Chapter 3

3 Objective II- 82-kDa ChAT and SATB1 work together to regulate chromatin organization

Portions of this chapter have been reproduced with permission from:

Winick-Ng W, Caetano FA, Winick-Ng J, Morey TM, Heit B, Rylett RJ (2016) 82-kDa choline acetyltransferase and SATB1 localize to β -amyloid induced matrix attachment regions. *Sci Rep*, 6: 23914.

Figure 3-6 (A) - data collection was done by Mr. Trevor Morey.

Figures 3-8, 3-10, 3-13 and 3-14 and Tables 3-4 and 3-5 were produced in collaboration with Mrs. Jennifer Winick-Ng, using the statistical programming software SAS.

Figures 3-3 and 3-15 were produced in collaboration with Dr. Fabiana A Caetano.

Figure 3-15 [h] and [i] – analysis was performed by Dr. Bryan Heit.

3.1 Introduction and Rationale

The 82-kDa choline acetyltransferase (82-kDa ChAT) protein interacts with chromatin, with increased genic association at promoters and introns after SH-SY5Y cells are exposed to oligomeric A β ₁₋₄₂. An important observation from these data included the identification of an A β -specific motif that had sequence similarity with special AT-rich sequence binding protein 1 (SATB1). SATB1 anchors chromatin loops to the nuclear matrix as part of scaffolding/matrix attachment regions (S/MARs), and can recruit histone deacetylases (HDACs) or histone acetyltransferases (HATs) specifically to these regions (Yasui *et al.* 2002; Cai *et al.* 2003; Galande *et al.* 2007). S/MARs are anchored to the nuclear matrix by SATB1 binding to local and distant AT-rich DNA sequences, forming chromatin loops that are accessible for chromatin modifying factors to repress or activate transcription (Yasui *et al.* 2002; Galande *et al.* 2007).

In the previous chapter, we demonstrated that A β ₁₋₄₂-exposure increases 82-kDa ChAT protein levels in heterochromatic/nuclear matrix associated nuclear fractions, suggesting that 82-kDa ChAT could interact with the nuclear matrix. Interestingly, co-immunoprecipitation experiments performed in our laboratory suggest that 82-kDa ChAT could interact with the nuclear matrix protein matrin-3 (unpublished data). Moreover, from microarray data previously published by our laboratory (Albers *et al.* 2014), *SATB1* mRNA levels are increased 5.5 fold in IMR32 cells transiently expressing 82-kDa ChAT. Together, these data indicate that SATB1 could be a target for complex formation with 82-kDa ChAT. In this chapter, we explore the relationship between 82-kDa ChAT and SATB1 in human SH-SY5Y neuroblastoma cells. We test how SATB1 interacts with chromatin, and compare this interaction to the genomic distribution of 82-kDa ChAT after exposure to oligomeric A β ₁₋₄₂. Finally, we ask whether both 82-kDa ChAT and SATB1 are involved in chromatin organization, and whether this results in changes to gene expression.

3.2 Methods

Cell Culture and transfection

SH-SY5Y cells stably expressing heterologous 82-kDa ChAT (Albers *et al.* 2014) were differentiated as described in Chapter 2. Cells were treated with either 100 nM oligomeric A β ₁₋₄₂ (as described in Chapter 2), F12 media (vehicle), NAD⁺ (Sigma-Aldrich, Oakville, ON, Canada) or resveratrol (Sigma-Aldrich) with or without pre-treatment with EX527 (Sigma-Aldrich) at the times and concentrations indicated. Cells in some experiments were transfected with either scrambled control siRNA or specific siRNA duplexes targeted against human SATB1 (Santa-Cruz Biotechnology, Dallas, TX, USA) for 24 h with Lipofectamine RNAiMAX (Invitrogen) prior to treatment with A β or resveratrol. As an additional negative control, cells were mock transfected with Lipofectamine containing no siRNA.

Antibodies

The 82-kDa ChAT protein was detected as described in Chapter 2. Goat anti-SATB1 (sc-5989) was from Santa Cruz Biotechnology; AlexaFluor 546 or 647-conjugated secondary antibody (Invitrogen) was used for immunostaining visualization as appropriate.

Nuclear isolation and Co-Immunoprecipitations

To assess protein-protein interactions, we recovered proteins from cell lysates by Co-IP, then identified proteins by immunoblot and mass spectrometry. For nuclear isolation and subsequent immunoprecipitation, samples were prepared using the Universal Magnetic Co-IP kit (Active Motif, California, U.S.A.) according to the manufacturer's directions. Briefly, cells were lysed in hypotonic buffer (provided by the Universal Magnetic Co-IP kit and containing deacetylase, protease and phosphatase

inhibitors), and centrifuged at 14,400 x g for 30 s at 4°C. The pellet containing cell nuclei was lysed in complete digestion buffer (provided by the Universal Magnetic Co-IP kit and containing deacetylase, protease and phosphatase inhibitors) and DNA was digested with DNase I (800 units/mL) for 10 min at 37°C, followed by the addition of 10 mM EDTA to stop the reaction. Protein lysates were quantified using the Bradford method (Bradford 1976), and an aliquot containing 500 µg of lysate was diluted to a final volume of 500 µl in Co-IP/wash buffer (provided by the Universal Magnetic Co-IP kit and containing 50 mM NaCl and 0.1% NP-40) and incubated with 4 µg CTab for 4 h at 4°C, followed by immunocapture onto 25 µL protein G magnetic beads (provided by the Universal Magnetic Co-IP kit) for 1 h at 4°C. Samples were washed 4 times with Co-IP/wash buffer and immune complexes were eluted into 20 µL 2x Reducing Loading Buffer (130 mM Tris; pH 6.8, 20% (v/v) glycerol, 4% (w/v) SDS, 0.02% (w/v) bromophenol blue, and 100 mM DTT) then heated for 5 min at 95°C prior to separation of proteins on SDS–polyacrylamide gel electrophoresis (SDS-PAGE) gels. Five µg of total nuclear lysate for each sample was also loaded onto each gel prior to separation on SDS-PAGE gels. Gels were stained with Imperial Protein Stain (Thermo Fisher Scientific, Waltham, MA, USA) for 20 min, then washed in water for 16 h at RT prior to mass spectrometry preparation (see below).

For 82-kDa ChAT-SATB1 co-immunoprecipitations (Co-IPs), cells were lysed in Triton X-100 buffer (10 mM HEPES, pH 7.4, 5 mM MgCl₂, 1 mM ethylene glycol tetraacetic acid, 5% glycerol (v/v), 0.5% Triton X-100 (v/v), protease inhibitor cocktail [Sigma Aldrich; final concentration: 1.04 mM 4-(2-aminoethyl) benzenesulfonyl fluoride hydrochloride (AEBSF), 0.8 µM Aprotinin, 40 µM Bestatin, 14 µM N-[N-(L-3-trans-carboxyirane-2-carbonyl)-L-leucyl]-agmatine; 1-[N-[(L-3-trans-carboxyoxirane-2-carbonyl)-L-leucyl]amino]-4-guanidinobutane (E-64), 20 µM Leupeptin and 15 µM Pepstatin], and phosphatase inhibitors [final concentration: 10 mM sodium fluoride, 1 mM sodium vanadate, 20 mM sodium phosphate, 3 mM β-glycerolphosphate, 5 mM sodium pyrophosphate]) containing either 150 mM or 450 mM NaCl. Aliquots of cell lysate containing 4 mg of protein were diluted to a final volume of 1 ml in Triton X-100 buffer. To immunoprecipitate 82-kDa ChAT and associated proteins (ChAT Co-IP), diluted lysates were incubated with 2.5 µg/mg lysate of anti-ChAT antibody (CTab) at

4°C for 24 h, followed by immunocapture onto 50 µL of protein-G Dynabeads (Invitrogen, Life Technologies, Burlington, ON, Canada) for 1 h at 4°C. Immunocaptured samples were washed 6x with Triton X-100 buffer, then immune complexes were eluted into 50 µL of 2x Laemmli sample buffer (126 mM Tris-HCl; pH 6.8, 20% (v/v) glycerol, 4% (w/v) SDS, 0.01% (w/v) bromophenol blue, and 5% (v/v) 2-mercaptoethanol) by heating samples at 75°C for 15 min before separation of proteins on SDS-PAGE gels. Immunoreactive bands were analyzed by immunoblotting.

To analyze SATB1 protein expression, cells were lysed in radioimmunoprecipitation (RIPA) buffer as described in Chapter 2. Cell lysates were centrifuged at 21,100 \times g for 15 min at 4°C, then heated at 95°C for 5 min in 1x Laemmli sample buffer (63 mM Tris-HCl; pH 6.8, 10% (v/v) glycerol, 2% (w/v) SDS, 0.01% (w/v) bromophenol blue, and 2.5% (v/v) 2-mercaptoethanol). Aliquots of cell lysate containing 50 µg of protein were separated on SDS-PAGE gels, followed by transfer onto polyvinylidene difluoride (PVDF) membranes. Non-specific proteins were blocked in 5% horse serum in PBS containing 0.1% Triton-X 100 (PBS-T) for 1 h at room temperature, followed by incubation in 1:100 anti-SATB1 antibody in 3% bovine serum albumin in PBS-T overnight at 4°C. Following 1 h in 1:5000 HRP-conjugated anti-goat antibody, the density of immunoreactive bands were visualized using Image Lab (Version 5.0, BioRad). Immunoreactive band density for SATB1 was normalized to total density levels for each band, followed by normalization to β -actin.

Mass Spectrometry

Individual protein bands from Imperial Protein stained SDS-PAGE gels were isolated by an Ettan Spot Picker (GE Healthcare, Mississauga, Ontario, Canada) at the MALDI Mass Spectrometry Facility (London, Ontario, Canada). In-gel digestion was performed using a MassPREP automated digester station (PerkinElmer). Gel pieces were Coomassie destained using 50mM ammonium bicarbonate and 50% acetonitrile which was followed by protein reduction using 10 mM dithiotreitol (DTT), alkylation using 55 mM iodoacetamide (IAA), and tryptic digestion. Peptides were extracted using a solution

of 1% formic acid and 2% acetonitrile and lyophilized. Prior to mass spectrometric analysis, dried peptide samples were re-dissolved in a 10% acetonitrile and 0.1 % TFA (trifluoroacetic acid) solution. MALDI matrix, α -cyano-4-hydroxycinnamic acid (CHCA), was prepared as 5 mg/mL in 6mM ammonium phosphate monobasic, 50% acetonitrile, 0.1 % trifluoroacetic acid and mixed with the sample at 1:1 ratio (v/v). 0.75 μ L of the samples/matrix mixture was deposited on the MALDI target and allowed to air dry.

Mass Spectrometry data were obtained using a 4700 Proteomics Analyzer, MALDI TOF TOF (Applied Biosystems, Foster City, CA, USA). Data acquisition and data processing were respectively done using 4000 Series Explorer and Data Explorer (both from Applied Biosystems). The instrument is equipped with a 355 nm Nd:YAG laser; the laser rate is 200 Hz. Reflectron and linear positive ion modes were used. Reflectron mode was calibrated at 50 ppm mass tolerance. Each mass spectrum was collected as a sum of 1000 shots. MALDI-TOF results were entered into the Mascot server (<http://www.matrixscience.com/>; Matrix Science, Massachusetts, USA) to determine significant sequence similarity with known proteins. Mascot searches were performed with the following parameters: NCBI database, trypsin digest with 1 missed cleavage allowed, carbamidomethyl fixed modification, oxidation (M) variable modification, 50 ppm peptide mass tolerance.

Immunofluorescence staining of cells and confocal imaging

For immunofluorescence staining, cells were incubated with primary rabbit anti-human CTab antibody (1:1000), either with or without goat anti-SATB1 antibody (1:100), followed by AlexaFluor 647 (for 82-kDa ChAT) or AlexaFluor 542 (for SATB1) secondary antibodies. Cells were then counterstained with 2.5 μ g/mL Hoechst dye. Images were acquired and processed as described in Chapter 2, with 543-nm excitation and 560- to 615-nm band-pass emission filter for SATB1, and 647-nm excitation and 650-nm long-pass emission filter for 82-kDa ChAT. In some experiments, cells were

imaged with an Olympus Fluoview 1000 (Olympus Canada Inc., Richmond Hill, ON, Canada) using a 60X oil-immersion objective (NA = 1.35).

Super-resolution ground-state depletion imaging

For super-resolution ground-state depletion imaging (SR-GSDIM), digital images of fixed cells were acquired with a Leica super resolution ground-state depletion microscope (SR-GSD; Leica Microsystems Inc., Concord, ON, Canada) using a 160X oil-immersion objective, NA 1.47. Images were captured using the reversible saturable optical fluorescence transitions principle, as described (Heintzmann *et al.* 2002; Fölling *et al.* 2008). Images were captured using the Leica Application Suite Advanced Fluorescence software, then processed on Imaris (version 7.5.0, Bitplane USA, Concord, MA, USA). Identification of 82-kDa ChAT clusters and quantification of cluster size and spacing was performed in Matlab (Mathworks, Natick, MA, USA) using a custom-written implementation of the Ordering Points To Identify Clusters algorithm (Ankerst *et al.* 1999; Caetano *et al.* 2015). Regular spacing of ChAT molecular clusters was detected by measuring the inter-cluster distance between each cluster and all other clusters in an image, and then performing a normalized Fast Fourier Transform to detect any regular cluster spacing.

To quantify co-localization on SR-GSDIM images, Imaris was used to create surface dots representing each protein, based on the estimated size for each protein and resolution of the image. We defined the protein size with the addition of both primary and secondary antibodies as 60 nm. Using the XT co-localize spots module, we set the threshold distance for co-localized dots to be 2/3rds the size of the smallest protein and computed the distance between each pair of dots, and thus the threshold for co-localization was set to 40 nm.

Chromatin immunoprecipitation with next-generation sequencing (ChIP-seq)

ChIP and subsequent next-generation sequencing (ChIP-seq) was performed as described in Chapter 2, with the exception that the concentration of anti-SATB1 primary antibody used in these experiments was 5 μ g. To visualize non-normal distribution of the distance between ChIP peaks, kernel density estimation was used, with a smoothing parameter of 0.5. We also included a published (Law *et al.* 2010) human ATRX dataset (NCBI accession: GSE22162) that was mapped to hg19 using Bowtie2.

Data deposition

ChIP-seq data was deposited in the NCBI Geo Database, accession number: GSE73576.

Reverse transcription (RT) real-time PCR (qPCR) and ChIP-qPCR

For ChIP-qPCR, primers (**Table 3-1**) were incubated with DNA from either the primary antibody sample or corresponding input sample. Duplicate samples were incubated without primary antibody (IgG control). For reverse transcription-qPCR (RT-qPCR), total RNA was isolated from SH-SY5Y cells and reverse transcribed as described previously (Albers *et al.* 2014). 1x iQ SYBR Green Supermix (Bio-Rad) was added prior to PCR amplification and real-time detection using a Bio-Rad C1000™ Thermal Cycler and CFX95 Real-Time system. After each cycle, fluorescent activity was determined, and a final crossing point (threshold cycle, C_t) was calculated. Primer efficiency and amplifications of a single PCR product was confirmed, and a representative gel for RT-PCR amplification can be found in **Appendix 6**. For ChIP-qPCR, the average C_t in each treatment and control was analyzed using the $\Delta\Delta C_t$ method given by the formula: $\Delta\Delta C_t$ (ChIP – IgG) = (Mean C_t (ChIP) – Mean C_t (Input)) – (Mean C_t (IgG) – Mean C_t (Input)). After determining the $\Delta\Delta C_t$, we used this to calculate a fold-change compared to the IgG control, given by the formula: Fold Change = $2^{(-\Delta\Delta C_t \text{ (ChIP– IgG)})}$. For RT-qPCR, the average C_t in each treatment was analyzed by the $2^{-\Delta\Delta C_t}$ method,

normalized to glyceraldehyde 3-phosphate dehydrogenase (GAPDH) and vehicle-treated samples.

Data Analysis

The data are presented as mean \pm SEM, with n values indicating the number of independent experiments performed with separate cell populations. Each n value represents the average of multiple sample replicates for each experiment. GraphPad Prism 5 (GraphPad Software, San Diego, CA, USA) was used for data analysis. Data were assessed for normality using Bartlett's test and statistically significant differences were tested by unpaired Student's t-test, or between groups using one or two-way ANOVA with Dunnett's, Tukey's or Bonferroni's post hoc multiple comparison test as appropriate, with statistical significance defined as $p \leq 0.05$. For cell counting, an independent and blinded observer determined the number of cells with nuclear aggregations on 63x magnification images. Each image had at least 20 cells, and 5 images were counted for each replicate of each treatment. The total number of cells in all 5 images was pooled to determine the percentage of cells with nuclear aggregations.

Table 3-1. ChIP-qPCR and RT-qPCR primers used in the chapter.

Gene	Direction	Primer, 5'-3'
<i>ChIP-qPCR</i>		
Human APP	Forward	GCCAGACCACAACCTCGTTT
	Reverse	TTGGGAACTTGCGTGGCAAA
<i>RT-qPCR</i>		
Human SATB1	Forward	GTAGAGCTAGCGAGGGAGAGA
	Reverse	TTGTTGTTGTGACGAGGCCG
Human Total APP	Forward	AACCAGTGACCATCCAGAAC
	Reverse	ACTTGTGAGGAACGAGAAGG
Human APP-KPI	Forward	GTCTGTGGAAGAGGTGGTTC
	Reverse	GTCAAAGTTGTTCCGGTTG
Human GAPDH	Forward	TGTTGCCATCAATGACCCCTT
	Reverse	CTCCACGACGTACTCAGCG

3.3 Results

A β -induced 82-kDa ChAT aggregates co-localize with special AT-rich binding protein 1

To assess the distribution of SATB1 in SH-SY5Y cells that stably express heterologous 82-kDa ChAT, we first confirmed SATB1 mRNA and protein levels in these cells. When measured by qPCR, we found a significant 1.47 ± 0.15 -fold ($p < 0.05$, $n = 3$) increase in *SATB1* mRNA levels in SH-SY5Y cells stably expressing 82-kDa ChAT compared to empty vector. When measured by immunoblotting, we observed increased band density for SATB1 in SH-SY5Y cells stably expressing 82-kDa ChAT compared to empty vector (**Fig. 3-1**). Quantification of the steady-state levels of SATB1 compared to actin revealed a significant increase in steady-state SATB1 protein levels in 82-kDa ChAT expressing cells (1.16 ± 0.1) compared to vector expressing cells (0.81 ± 0.1).

We targeted SATB1 as potentially having a role in A β -induced 82-kDa ChAT aggregation. First, the expression of 82-kDa ChAT in cells influences the subcellular localization of SATB1 protein in response to acute A β treatment (**Fig. 3-2**). When assessed by confocal microscopy, SATB1 protein is distributed in cells between the cytoplasm and nucleus, with the protein level in the nucleus being higher at the nuclear periphery. This subcellular distribution of SATB1 did not differ between vehicle-treated cells that do not express 82-kDa ChAT (**Fig. 3-2A[a-c]**) and cells that do express the ChAT protein (**Fig. 3-2B[c]**), and is not altered by A β_{1-42} -treatment for vector-expressing cells (**Fig. 3-2A[d-f]**). Importantly however, in A β -treated cells that express 82-kDa ChAT, the SATB1 protein in the nucleus forms aggregates (**Fig. 3-2B[j]**). 82-kDa ChAT protein distribution is diffuse and slightly punctate in nuclei of vehicle-treated cells (**Fig. 3-2B[a-g]**), but in cells treated with A β_{1-42} aggregates of 82-kDa ChAT (**Fig. 3-2B[h-n]**) and SATB1 co-localize in the nucleus (**Fig. 3-2B[l]**).

To further evaluate the interaction between 82-kDa ChAT and SATB1 after cellular exposure to A β_{1-42} , we used super-resolution ground-state depletion microscopy

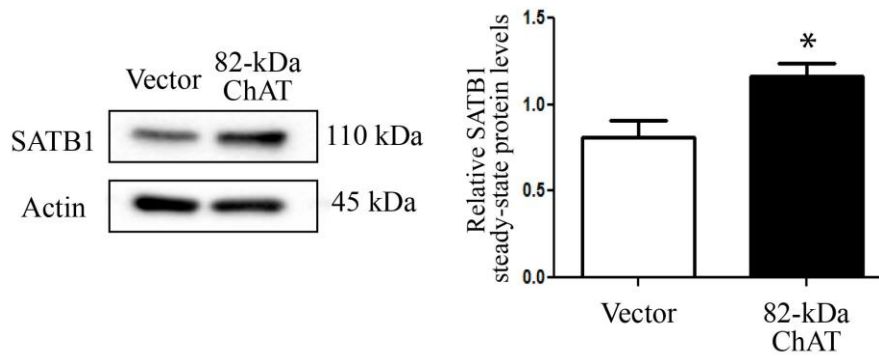


Figure 3-1. 82-kDa ChAT expression in SH-SY5Y cells increases SATB1 protein expression.

Representative immunoblot showing SATB1 steady-state protein levels in SH-SY5Y cells that either stably express 82-kDa ChAT or an empty vector. Densitometric quantification of band intensity revealed significantly greater SATB1 steady-state levels in cells expressing 82-kDa ChAT compared to cells expressing empty vector. * $p < 0.05$, $n = 4$.

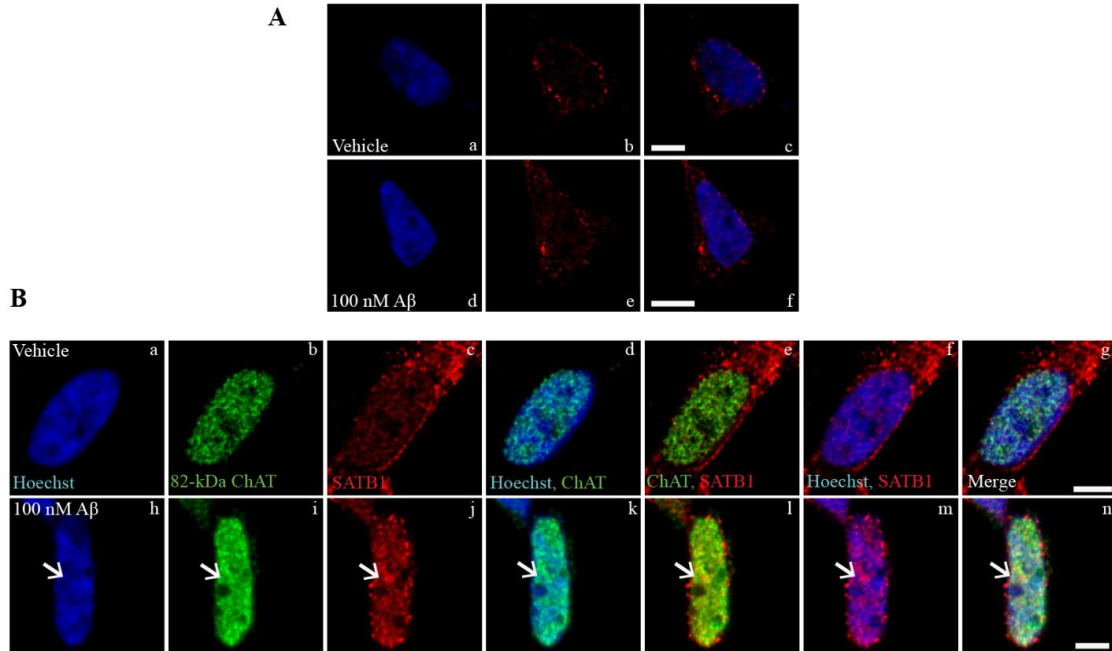


Figure 3-2. A β -induced 82-kDa ChAT aggregates are co-localized with SATB1.

(A) SH-SY5Y cells expressing empty vector were treated with either vehicle (a–c) or 100 nM oligomeric A β 1–42 (d–f) for 4 h. SATB1 was localized to nucleus and cytoplasm, with diffuse expression in nucleus in both vehicle and A β -treated cells. The left panel shows Hoechst staining, center panel shows SATB1 immunostaining, and right panel is the overlay. (B) SH-SY5Y cells stably expressing 82-kDa ChAT treated with vehicle (a–g) or 100 nM oligomeric A β 1–42 (h–n) for 4 h. After treatment with A β , 82-kDa ChAT (i) formed nuclear aggregates (arrows). SATB1 nuclear expression was greater than in control cells and showed aggregate formation (j) in the same region as the 82-kDa ChAT aggregates (l). Scale bar 5 μ m; n = 5, with at least 6 cells imaged per treatment.

followed by individual molecule return (SR-GSDIM) (**Fig. 3-3**). First, we analysed the SR-GSDIM images for co-localization of 82-kDa ChAT and SATB1, indicated by the pixels in **Fig. 3-3A[b,d]** and defined as a distance between the two proteins of less than 2/3rd protein size. In control cells, there is a small amount of co-localization of the two proteins (**Fig. 3-3A[a,b]**) that is increased significantly after exposure to A β ₁₋₄₂ (**Fig. 3-3A[c,d]**). Quantification revealed $4.6 \pm 0.14\%$ of co-localized pixels in control images, with this increased significantly by 50% ($6.9 \pm 0.51\%$) in A β -treated cells (**Fig. 3-3A[e]**). While this method allowed co-localization analysis between the two proteins, it was difficult to observe the nuclear aggregates under these conditions. Therefore, we digitally magnified the SR-GSDIM images to a 500 nm scale, in order to evaluate the relationship between the nuclear aggregates of 82-kDa ChAT protein (**Fig. 3-3B[a]**) and SATB1 protein (**Fig. 3-3B[b]**). When SATB1 aggregate localization was overlaid with that of 82-kDa ChAT, there was a close association between the two proteins, compared to regions outside of the aggregate (**Fig. 3-3B[c]**).

Based on the observed interaction between 82-kDa ChAT and SATB1 by confocal and SR-GSDIM imaging, we next used co-immunoprecipitation to determine whether we could observe a direct interaction between these proteins (**Fig. 3-4**). We used several different buffer and salt conditions in the Co-IP, but were not able to detect a protein-protein interaction between SATB1 and ChAT. The conditions tested included a Triton X-100 buffer containing 150 mM NaCl, a concentration of salt that is needed to lyse the SH-SY5Y nuclei (**Fig. 3-4A**; n = 2). We also tested buffer containing 450 mM NaCl to release proteins associated with heterochromatic chromatin, but also did not detect SATB1 in the co-IP (**Fig. 3-4B**; n = 2). We were also unable to detect total levels of SATB1 following lysis with buffer containing 450 mM NaCl.

Though we could not confirm whether 82-kDa ChAT and SATB1 proteins were interacting directly, we next explored whether modulators of the NAD-dependent deacetylase sirtuin 1 (SIRT1) could alter 82-kDa ChAT or SATB1 subcellular localization. SIRT1 can deacetylate histones and other proteins, and has been shown previously to deacetylate SATB1 leading to the formation of S/MARs (Xue *et al.* 2012). We used three pharmacological approaches to accomplish this, by exposing cells to the

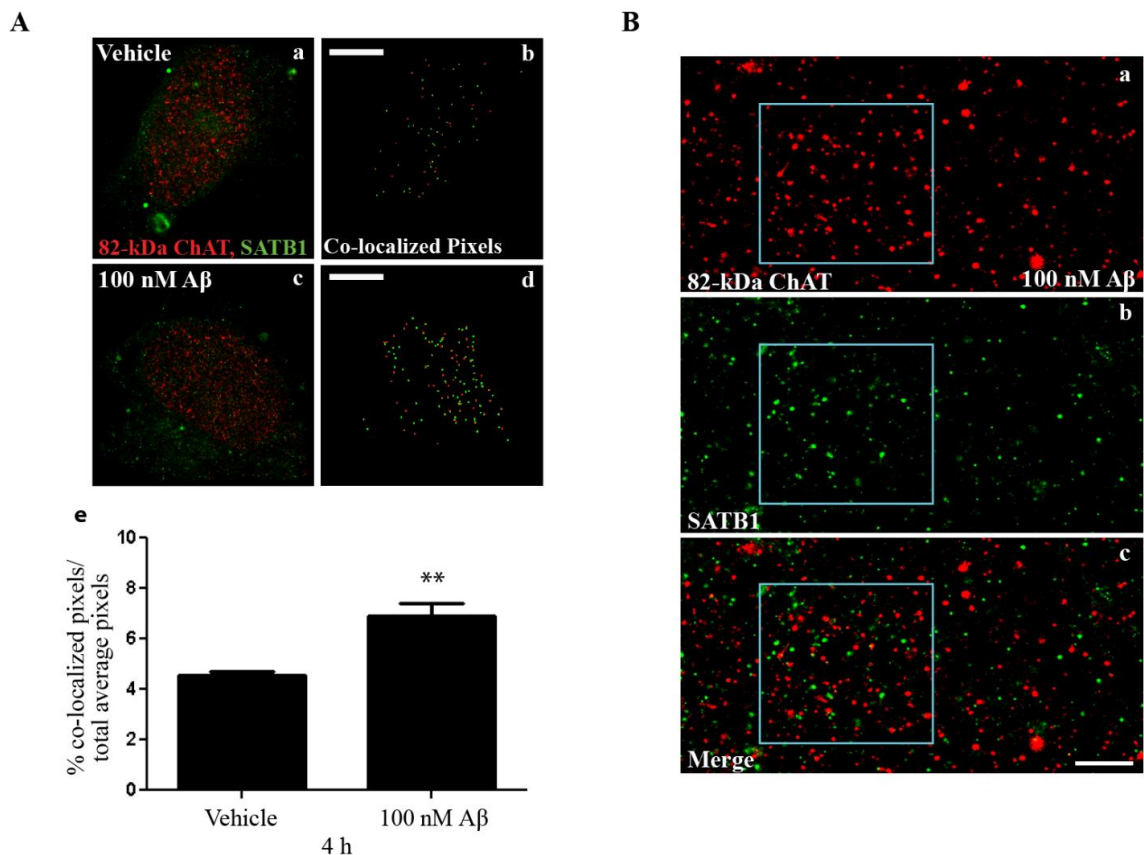


Figure 3-3. Super-resolution analysis of 82-kDa ChAT co-localization with SATB1.

(A) Co-localization analysis for SR-GSDIM images of 82-kDa ChAT and SATB1. (b) and (d) are the co-localization results for the respective SR-GSDIM image of vehicle (a) and 100 nM A β 1–42 (c) treatments. (e) The percentage of co-localized pixels was increased significantly in A β -treated cells. ** $p < 0.01$ (Student's t-test, $n = 5$). (B) Digitally magnified SR-GSDIM images for 82-kDa ChAT (a) and SATB1 (b) levels after 100 nM oligomeric A β 1–42 for 4 h. The boxed region shows an A β -induced aggregate of 82-kDa ChAT and SATB1. The overlay (c) revealed SATB1 protein within the 82-kDa ChAT accumulation. Scale bar 500 nm; $n = 6$, with at least 4 cells imaged per treatment.

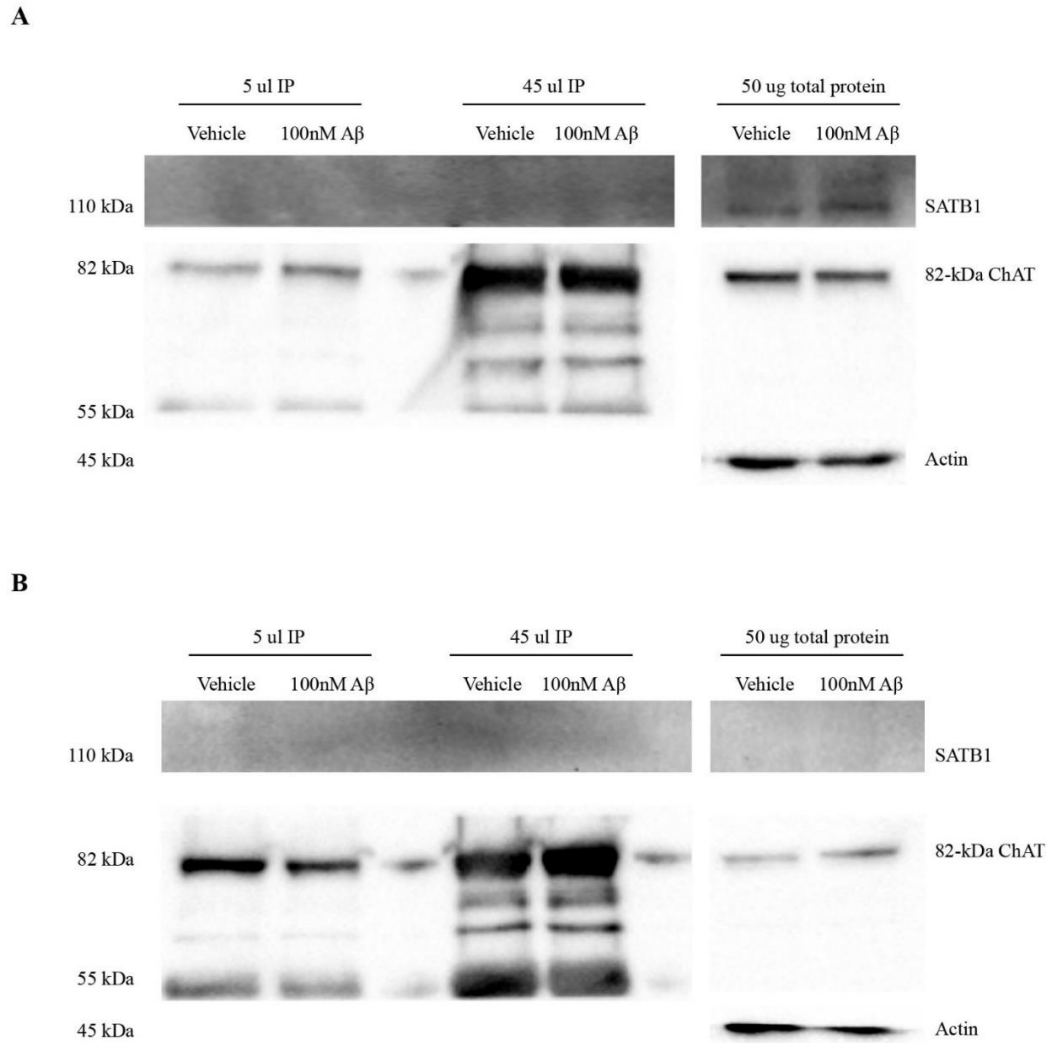


Figure 3-4. Co-immunoprecipitations (Co-IPs) for 82-kDa ChAT and SATB1.

SH-SY5Y cells stably expressing 82-kDa ChAT were treated for 4 h with vehicle or 100 nM A β_{1-42} . Co-IPs for 82-kDa ChAT were carried out with anti-C τ ab antibody in buffer containing 0.1% Triton X-100 and 150 mM (A) or 450 mM (B) NaCl. No SATB1 was detected in for 150 mM or 450 mM NaCl Co-IPs, regardless of whether 5 μ l or 45 μ l of the immunocaptured proteins eluted from Dynabeads (50 μ l total in 2x Laemmli sample buffer) were loaded on SDS-PAGE gels. 82-kDa ChAT was detected in both the Co-IP samples and the total lysate (50 μ g). Total SATB1 is present in the total lysate for the 150 mM NaCl buffer, but was not detected in the 450 mM NaCl buffer. Actin is shown as a loading control for total lysate samples.

SIRT1 activator resveratrol (Ye *et al.* 2013), the SIRT1 co-factor NAD⁺ (Davenport *et al.* 2014), or the specific SIRT1 inhibitor 6-chloro-2,3,4,9-tetrahydro-1H-carbazole-1-carboxamide (EX527) (Peck *et al.* 2010).

We treated cells with resveratrol to activate SIRT1 in the absence of A β ₁₋₄₂ (**Fig. 3-5A**). We chose doses of resveratrol that were previously demonstrated to have effects on SIRT1 activity in SH-SY5Y cells (Chong and Maiese 2008; Wu *et al.* 2011). No aggregates of either of the two proteins are observed in the nuclei of cells treated for 5 h with 25 μ M resveratrol (**Fig. 3-5A[a-g]**). However, when the concentration of resveratrol is increased to 50 μ M, numerous aggregates of both 82-kDa ChAT and SATB1 are observed in cell nuclei (**Fig. 3-5A[h-n]**).

Next we treated cells with the SIRT1 co-factor NAD⁺ for 3 h prior to the addition of either vehicle or 100 nM A β ₁₋₄₂ for 4 h. Following the addition of 2.5 mM NAD⁺ and 100 nM A β ₁₋₄₂, we observed multiple nuclear aggregates of both 82-kDa ChAT and SATB1 in cell nuclei (**Fig. 3-5B[a-g]**). When the concentration of NAD⁺ was increased to 5 mM, the aggregates of both SATB1 and 82-kDa ChAT increased in size, but became less compact (**Fig. 3-5B[h-n]**).

In other experiments, we pre-treated cells with the SIRT1-specific inhibitor EX527 for 1 h prior to exposure to A β ₁₋₄₂ (**Fig. 3-5C**). Importantly, aggregates of 82-kDa ChAT are not observed in cells that were pre-treated with 1 μ M EX527 for 1 h prior to the addition of either vehicle (**Fig. 3-5C[a-e]**) or 100 nM A β ₁₋₄₂ for 4 h (**Fig. 3-5C[f-j]**). We found that $10 \pm 2\%$ of cells contain aggregates after pre-treatment with EX527 alone. Compared to A β ₁₋₄₂ alone ($40 \pm 2\%$), the number of aggregates is significantly reduced in cells pre-treated with EX527 prior to exposure to A β ₁₋₄₂ ($10\% \pm 2\%$) (**Fig. 3-5C[k]**). As an additional control we included treatment of cells with a reverse A β ₁₋₄₂ peptide, which did not result in the production of significant 82-kDa ChAT aggregates compared to control.

We assessed whether SATB1 was necessary for the formation of the A β -induced aggregates of 82-kDa ChAT using small-interfering RNA (siRNA) targeted to SATB1 (**Fig. 3-6**). Compared to non-transfected (1.08 ± 0.03), mock transfected (1.05 ± 0.08),

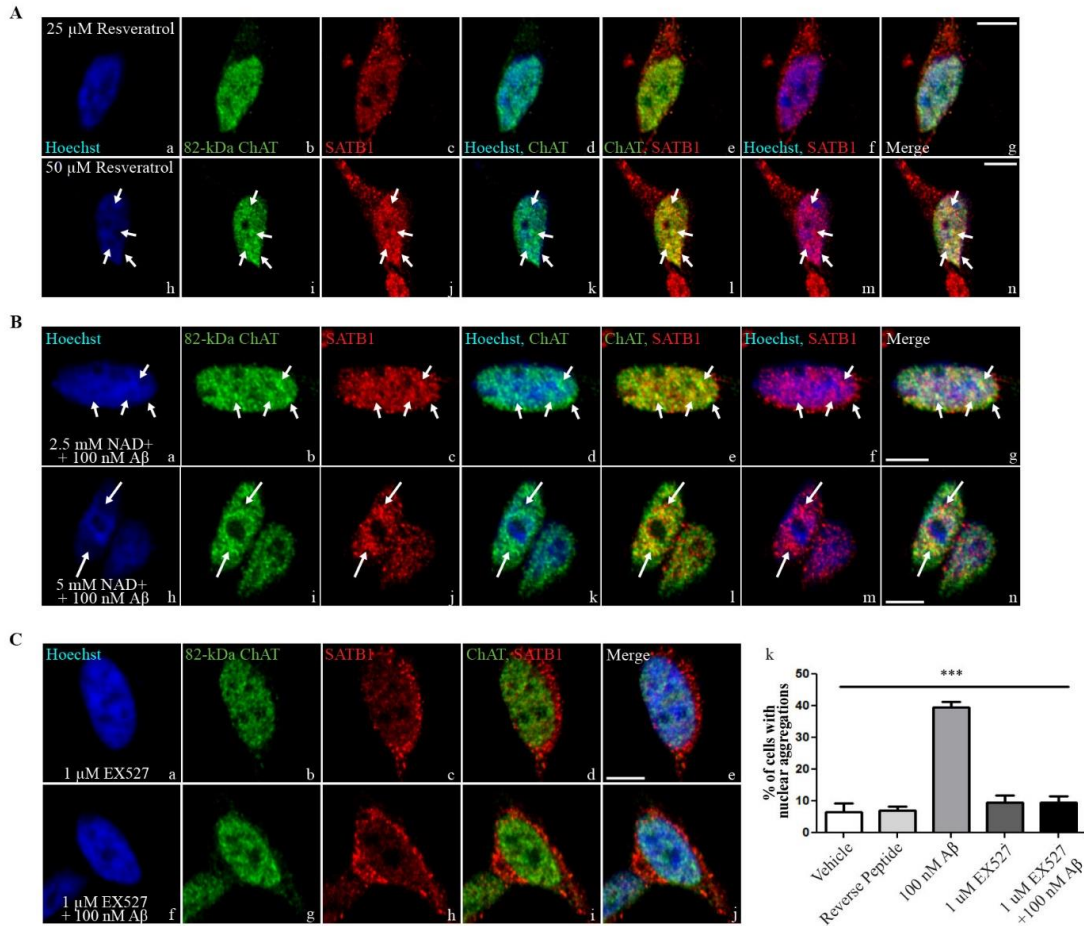


Figure 3-5. Activation of SIRT1 is required for 82-kDa ChAT/SATB1 aggregate formation.

(A) SH-SY5Y cells stably expressing 82-kDa ChAT and treated with the SIRT1 activator resveratrol at 25 μ M for 5 h (a–g) did not result in formation of aggregates of either 82-kDa ChAT or SATB1 proteins. Treatment with 50 μ M resveratrol promoted aggregate formation (arrows on h–n) of both 82-kDa ChAT (i) and SATB1 (j) proteins that were co-localized (l,n). Scale bar 5 μ m; n = 5 with at least 5 cells imaged for each treatment. (B) Cells were pretreated for 3 h with the SIRT1 co-factor NAD⁺ prior to 4 h treatment with 100 nM A β _{1–42}. Cells treated with 2.5 mM NAD⁺ had multiple nuclear aggregates of both 82-kDa ChAT and SATB1 (a–g). Cells treated with 5 mM NAD⁺ had larger, more diffuse aggregates of 82-kDa ChAT and SATB1. n = 3 with at least 5 cells imaged for each treatment. (C) Cells were pretreated with the SIRT1 inhibitor EX527 for 1 h prior to 4 h treatment with vehicle (a–e) or 100 nM oligomeric A β _{1–42} (f–j). Pretreatment of cells with EX527 prior to A β -exposure prevented the formation of 82-kDa ChAT aggregates (k). n = 5, ***p < 0.001 (one-way ANOVA).

and non-targeted control siRNA (1.13 ± 0.07), we observed a 29% reduction in SATB1 protein levels after transfection of cells with SATB1 siRNA for 24 h (0.76 ± 0.06) (**Fig. 3-6A**). This resulted in a significant reduction in SATB1 steady-state protein levels compared to untransfected, mock transfected and control siRNA cells. We next counted the percentage of cells that had at least one nuclear aggregate in cells that were treated with either vehicle for 4 h, 100 nM A β_{1-42} for 4 h or 50 μ M resveratrol for 5 h (**Fig. 3-6B**). We found no significant differences for non-transfected cells ($26 \pm 2\%$), cells transfected with control siRNA ($26 \pm 4\%$), or transfection with SATB1 siRNA ($26 \pm 3\%$) in vehicle-treated cells. For cells that were treated with A β_{1-42} , transfection with SATB1 siRNA significantly reduced the number of 82-kDa ChAT aggregates observed to $37 \pm 3\%$ compared to cells that were non-transfected ($60 \pm 7\%$) or cells transfected with control siRNA ($60 \pm 2\%$). Surprisingly, after resveratrol treatment we observed no significant differences for SATB1 siRNA transfected cells ($50 \pm 8\%$) compared to control siRNA ($57 \pm 4\%$) or non-transfected ($55\% \pm 3\%$) cells.

Representative images can be found in **Figure 3-7** for cells treated for 4 h with 100 nM A β_{1-42} (A) or for 5 h with 50 μ M resveratrol (B) after SATB1 siRNA transfection. Treatment with A β_{1-42} resulted in aggregates of both 82-kDa ChAT and SATB1 (**Fig. 3-7A[a-e]**, white arrows) or 82-kDa ChAT only (orange arrows). These aggregates were also observed when cells were transfected with non-specific control siRNA (**Fig. 3-7A[f-j]**). In agreement with the data from cell counting experiments, when cells were transfected with SATB1 siRNA and then treated with A β_{1-42} we observed only a few cells that contained aggregates (**Fig. 3-7A[k-o]**). Interestingly, these were aggregates of 82-kDa ChAT only (orange arrows). Similar to **Figure 3-5**, when we treated cells with 50 μ M resveratrol we observed multiple nuclear aggregates of both 82-kDa ChAT and SATB1 (**Fig. 3-7B[a-e]**, white arrows), or 82-kDa ChAT only (orange arrows). We also observed these aggregates when cells were transfected with control siRNA (**Fig. 3-7B[f-j]**). Finally, when we treated cells with SATB1 siRNA followed by resveratrol treatment, we observed multiple aggregates of 82-kDa ChAT alone (**Fig. 3-7B[k-o]**, orange arrows), with very few aggregates of both 82-kDa ChAT and SATB1 (white arrows). Together with the cell counting data, these data indicate that SATB1 is

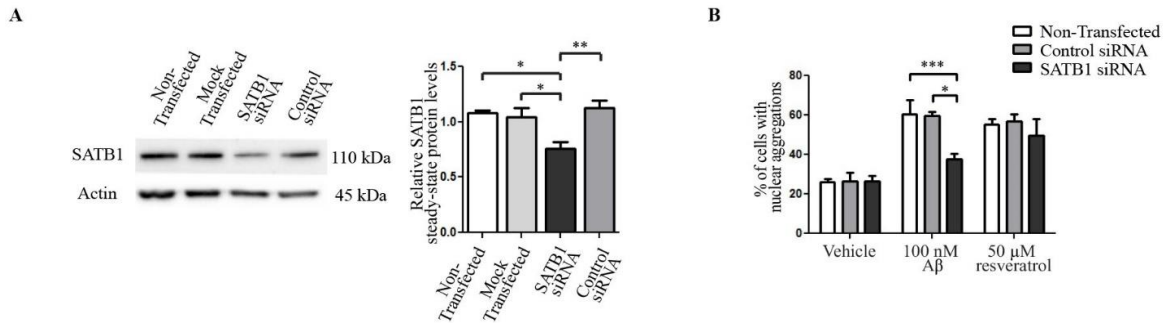
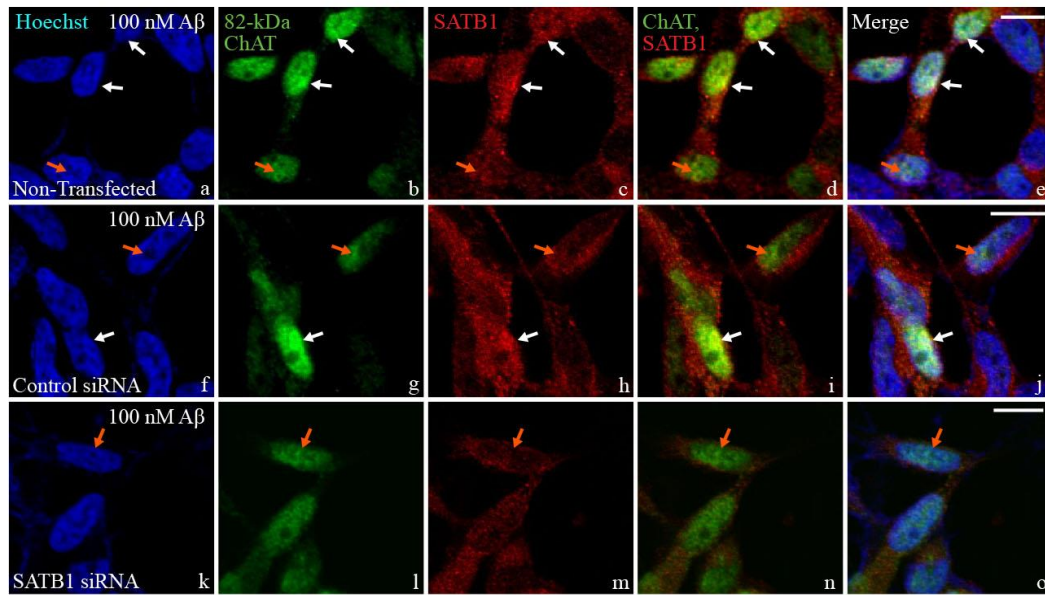


Figure 3-6. SATB1 siRNA knockdown alters 82-kDa ChAT and SATB1 A β -induced nuclear aggregate formation

(A) Representative immunoblot showing SATB1 steady-state protein levels in SH-SY5Y cells stably expressing 82-kDa ChAT and either non-transfected, mock transfected with no siRNA, transfected with untargeted control siRNA, or transfected with siRNA targeted to SATB1 for 24 h. Quantification revealed a 29% reduction in SATB1 protein expression compared to controls. $n = 5$, $**p < 0.01$, $*p < 0.05$ (one-way ANOVA with Tukey's post hoc test). (B) SH-SY5Y cells stably expressing 82-kDa ChAT were either non-transfected, transfected with untargeted control siRNA, or transfected with siRNA targeted to SATB1 for 24 h, followed by either 100 nM oligomeric A β_{1-42} for 4 h or 50 μ M resveratrol for 5 h. The number of cells positive for nuclear aggregates of 82-kDa ChAT were quantified by a blinded observer as a percentage of the total number of cells counted. After A β_{1-42} exposure, the percentage of 82-kDa ChAT aggregates were significantly reduced after SATB1 siRNA knockdown compared to non-transfected or control siRNA transfected cells. We observed no significant differences for resveratrol or vehicle treatment. $n = 3$ independent experiments with at least 100 cells counted per treatment group, $***p < 0.001$, $*p < 0.05$ (two-way ANOVA with Bonferroni's post hoc test).

A



B

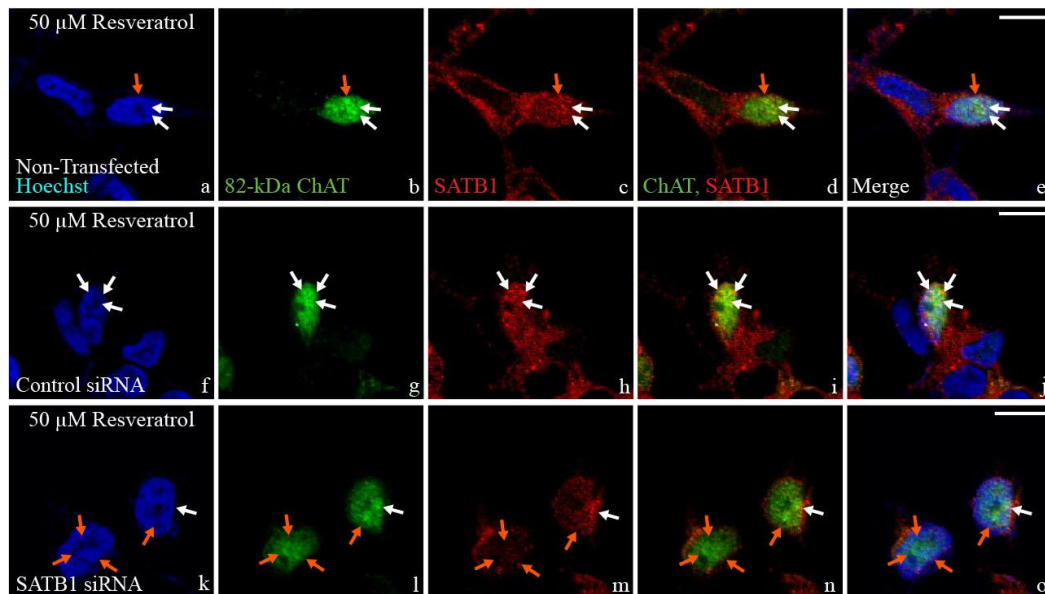


Figure 3-7. SATB1 siRNA knockdown prevents A β -induced, but not resveratrol-induced, 82-kDa ChAT aggregate formation in nuclei.

(A) SH-SY5Y cells stably expressing 82-kDa ChAT were either non-transfected, transfected with untargeted control siRNA, or transfected with siRNA targeted to SATB1 for 24 h, followed by treatment with 100 nM A β_{1-42} for 4 h. Cells that were not transfected with siRNA (a-e) or that were transfected with control siRNA (f-j) had aggregates of 82-kDa ChAT that were induced by A β_{1-42} treatment that overlapped with SATB1 aggregates (white arrows; orange arrows indicate 82-kDa ChAT aggregate only). For cultures that were transfected with SATB1 siRNA, there were few cells with

aggregates of 82-kDa ChAT protein and no SATB1 aggregates (k-o). For these experiments, $n = 3$ with at least 100 cells imaged per treatment. **(B)** SH-SY5Y cells stably expressing 82-kDa ChAT were either non-transfected, transfected with untargeted control siRNA, or transfected with siRNA targeted to SATB1 for 24 h, followed by 50 μ M resveratrol for 5 h. Cells that were not transfected with siRNA (a-e) or that were transfected with control siRNA (f-j) contained $A\beta_{1-42}$ -induced aggregates of 82-kDa ChAT that overlapped with SATB1 aggregates (white arrows; orange arrows indicate 82-kDa ChAT aggregate only). Cells that were transfected with SATB1 siRNA contained a similar number of aggregates of 82-kDa ChAT, but these aggregates did not overlap with SATB1 (k-o). For these experiments, $n = 3$ with at least 100 cells imaged per treatment, scale bar = 10 μ m.

required for the A β ₁₋₄₂-induced aggregates. In addition, SIRT1 activation can produce aggregates of 82-kDa ChAT, but this is not dependent on SATB1 expression.

82-kDa ChAT and SATB1 associate with chromatin at synapse and cell stress genes

82-kDa ChAT and SATB1 proteins are co-localized after cells are exposed to A β , therefore we performed ChIP-seq for SATB1 as a comparison to 82-kDa ChAT (**Fig. 3-8**). We found 2884 peaks for SATB1 after vehicle treatment, and 5857 peaks for SATB1 after A β ₁₋₄₂ treatment, with 36 peaks overlapped and 35 additional peaks within 200 nt of one another. Similar to 82-kDa ChAT, we observed that 57.1% of peaks were found in intergenic regions after vehicle treatment for SATB1, compared to 44.4% after A β ₁₋₄₂-exposure. Moreover, the decrease in intergenic regions after exposure of cells to A β ₁₋₄₂ was explained by an increase in peaks found in introns (47.3%) and promoters (12.6%) compared to vehicle (37.9% and 7.6%, respectively). We again observed that the average peak length was significantly reduced after A β ₁₋₄₂ treatment for SATB1 (146.6 ± 2.2 nt) compared to vehicle treatment (173.9 ± 4.9 nt) (**Fig. 3-8A**). Using the DREME tool, we observed that both vehicle and A β ₁₋₄₂ treatment of cells resulted in the same TC₂₋₃AT motif seen in the 82-kDa ChAT samples (**Fig. 3-8B**). In addition, peaks for SATB1 from cells treated with either vehicle or A β ₁₋₄₂ contained the SATB1 motif (A/T)_{3-n}C(A/T)₃₋₆ seen in the A β -exposed 82-kDa ChAT sample. Examples of ChIP-seq tracks from random genomic targets for SATB1 at *GAB2* and *MAGI2* genes and treated with either vehicle or A β are shown in **Fig. 3-8C**. We identified no relationship between the peaks for SATB1 and H3K27ac. Additional tracks can be found in **Figure 3-9** for chromosomes 1, 7 and 10, the full *GAB2* and *MAGI2* genes, as well as a region of the *APP* gene for SATB1 (see **Fig 2-5** for 82-kDa ChAT). Chromosomes 7 and 10 showed large peaks for SATB1 flanking the centromeres that overlapped the 82-kDa ChAT peaks (**Fig. 3-9A**).

Based on the observed relationship for both 82-kDa ChAT and SATB1 at the centromeres, we extended the analysis to determine if there was enrichment of 82-kDa ChAT and SATB1 at either centromeres or telomeres. Enrichment was defined as a peak

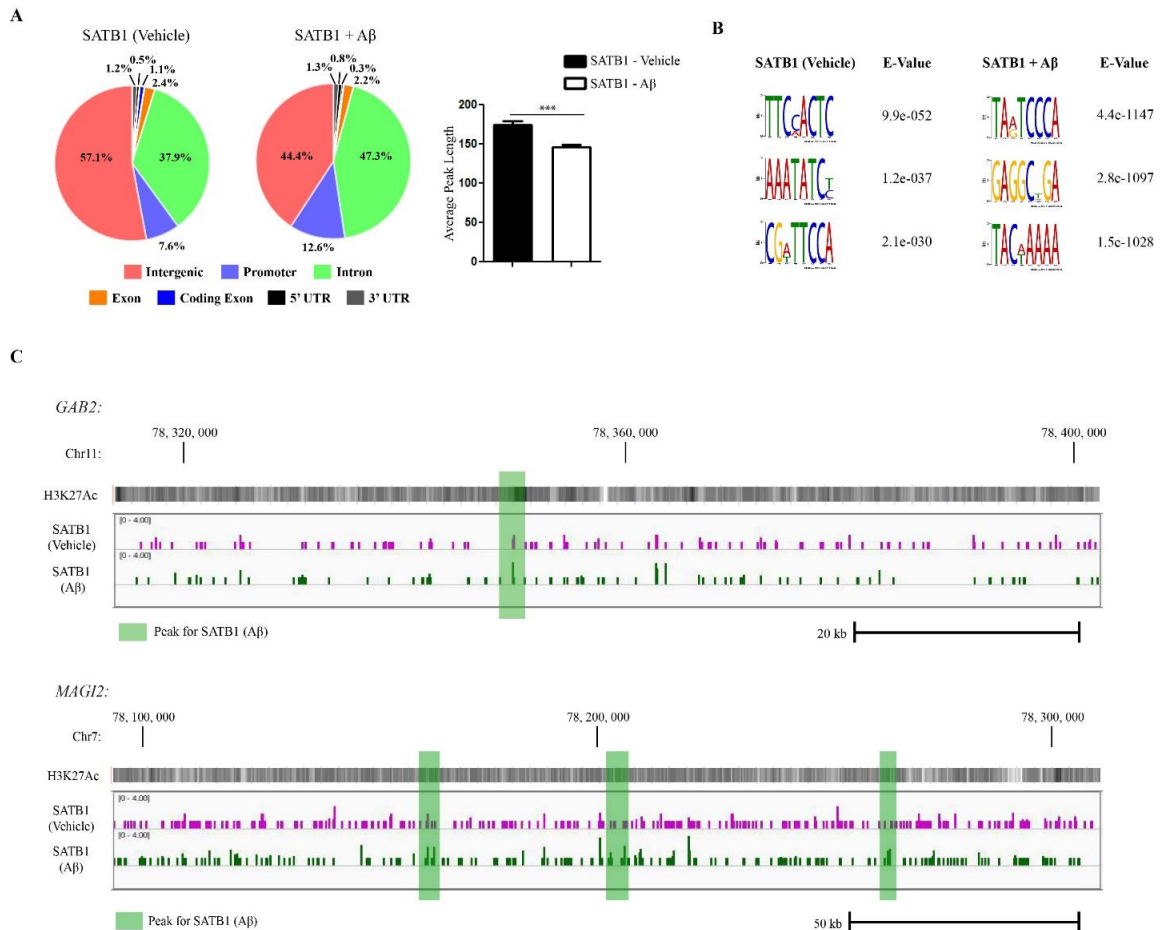


Figure 3-8. SATB1 has altered genome association after exposure of cells to A β .

(A) ChIP-seq analysis was performed for SATB1 using SH-SY5Y cells stably expressing 82-kDa ChAT and exposed to either vehicle or 100 nM oligomeric A β ₁₋₄₂. Genomic features identified for SATB1. A β treatment increases SATB1 association with introns and promoters. Treatment with A β ₁₋₄₂, significantly decreased average peak length for SATB1. *** $p < 0.001$ (Student's *t*-test). (B) The top DREME motif hits for SATB1 after vehicle or A β ₁₋₄₂-exposure revealed a TC₂₋₃AT motif, and a known SATB1 binding motif. (C) Example ChIP-seq tracks for SATB1 after vehicle or A β ₁₋₄₂-exposure of cells for regions of *GAB2* and *MAGI2* genes corresponding to the same regions in Fig. 2C. Peaks are highlighted in green for A β ₁₋₄₂ peaks. There were no vehicle related peaks in these regions. H3K27Ac is overlaid to show active transcription initiation sites.

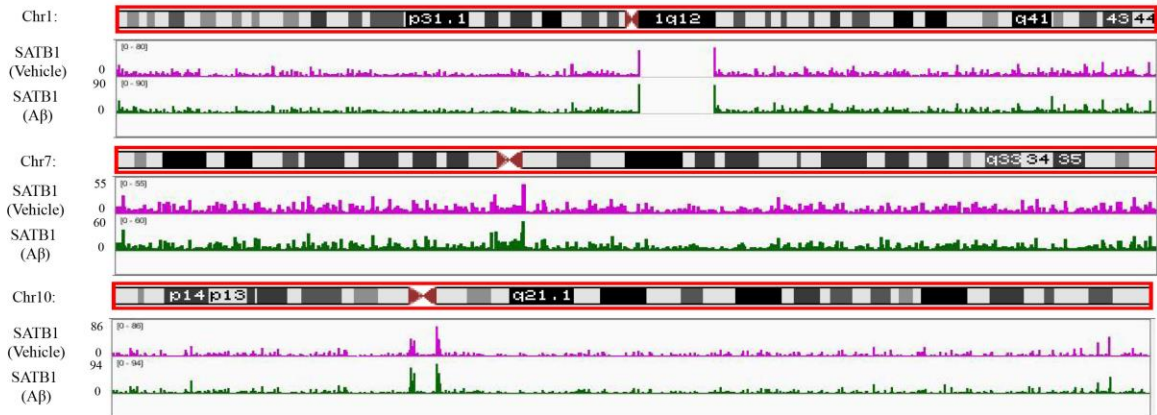
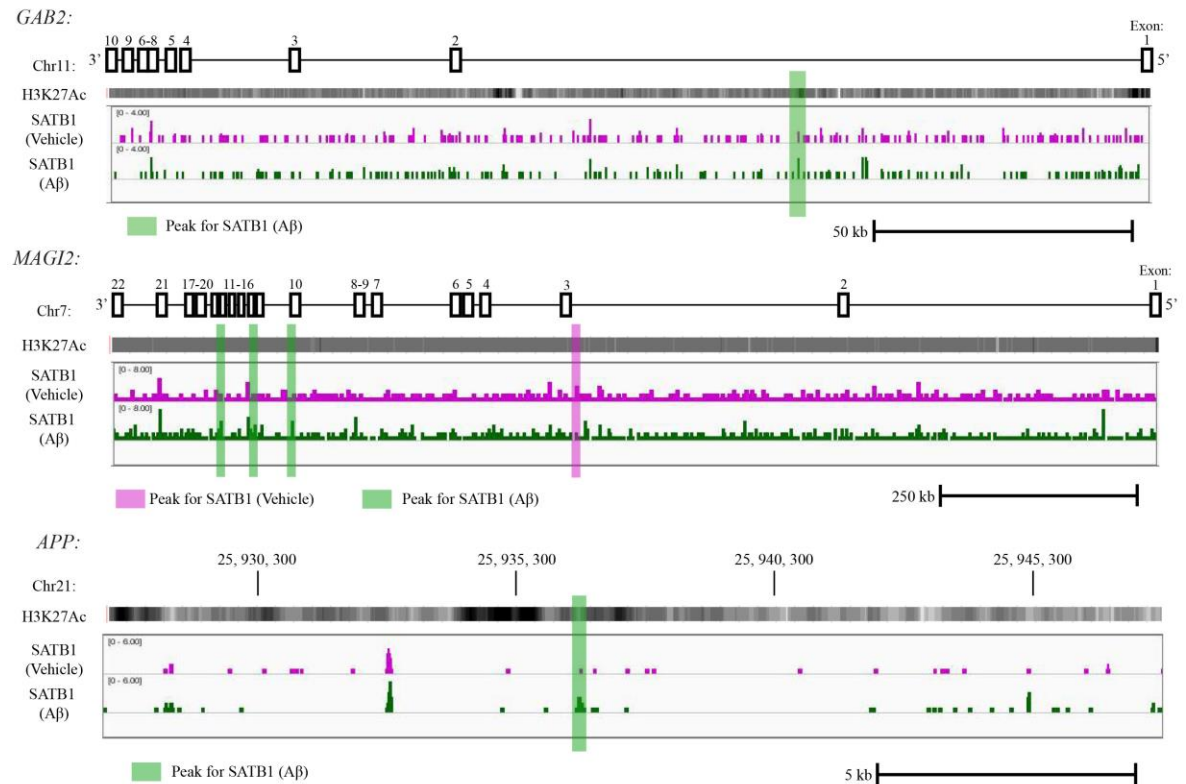
A**B**

Figure 3-9. Examples of ChIP-seq tracks for SATB1.

(A) ChIP-seq tracks for chromosomes 1, 7 and 10 for SATB1 in cells treated with either vehicle or A β_{1-42} . For chromosome 1, there was a portion of data not covered at the start of the q-arm. No other chromosome had a gap in data coverage. For chromosomes 7 and 10, there was a large peak of coverage flanking the centromeres. (B) ChIP-seq tracks for

GAB2 and MAGI2 whole genes, as well as for a region of APP, for SATB1 in cells treated with either vehicle or A β ₁₋₄₂. Peaks are highlighted in green for SATB1 A β ₁₋₄₂ peaks and purple for SATB1 vehicle peaks. H3K27Ac is overlaid to show active transcription initiation sites.

region with at least 20% of the maximum peak intensity normalized to input values and with a false discovery rate (FDR) < 0.05, as described (Zhao *et al.* 2015). Given that chromatin organizers, such as CCCTC-binding insulator protein (CTCF) and SATB1, have been shown to organize chromatin loops into large megabase pair (Mb) wide regions (Kumar *et al.* 2007; Junier *et al.* 2012), we defined flanking regions of centromeres or telomeric association as 1 Mb from the centromere start site or the end of the chromosome, respectively. Based on these criteria, we observed that 13 chromosomes had p arm centromere association, 10 chromosomes that had q arm association, and 9 chromosomes had peaks within the centromere (**Table 3-2**). Only chromosomes 6, 11 and X had no centromeric association for either 82-kDa ChAT or SATB1. By contrast, only 8 chromosomes had telomeric association for either protein. In most cases, the peaks overlapped for both proteins and were not affected by treatment with either vehicle or A β ₁₋₄₂. There were a few exceptions to this; on chromosome 7, there was enrichment within the centromere for all treatments except for SATB1 after cells were treated with vehicle. On chromosome 13, associations within the centromeres was observed for 82-kDa ChAT after vehicle or A β ₁₋₄₂-exposure, but not for SATB1. Finally, on chromosome 17 there was enrichment within the centromere for all treatments except for 82-kDa ChAT after cells were treated with A β ₁₋₄₂. Taken together, these data suggest that both 82-kDa ChAT and are enriched at centromeres, with some telomeric associations.

We next annotated peaks contained in intergenic components for SATB1 and compared these to the gene annotations for 82-kDa ChAT. We found that, similar to the gene annotations for 82-kDa ChAT, there was a higher number of associated genes after exposure of cells to A β ₁₋₄₂ for SATB1 (4672) compared to vehicle treatment (3700 and 2615, respectively) (**Fig. 3-10A**). An important finding was that there were more genes in common between 82-kDa ChAT and SATB1 after exposure of cells to A β ₁₋₄₂ (885) than there were for common genes for either 82-kDa ChAT (820) or SATB1 (617) in either of the conditions. We found 138 genes associated with all treatments. We next evaluated what functional groups the genes were associated with using the DAVID server. For SATB1, there were no significant gene ontology (GO) terms (defined as $p < 1.0E-05$ and $-\log(\text{FDR}) > 1.5$) for vehicle treated cells (**Appendix 7**), but for A β (**Appendix 8**), we found significant GO enrichment for nucleotide ($p = 8.45E-08$, $-\log(\text{FDR}) = 3.9$) and

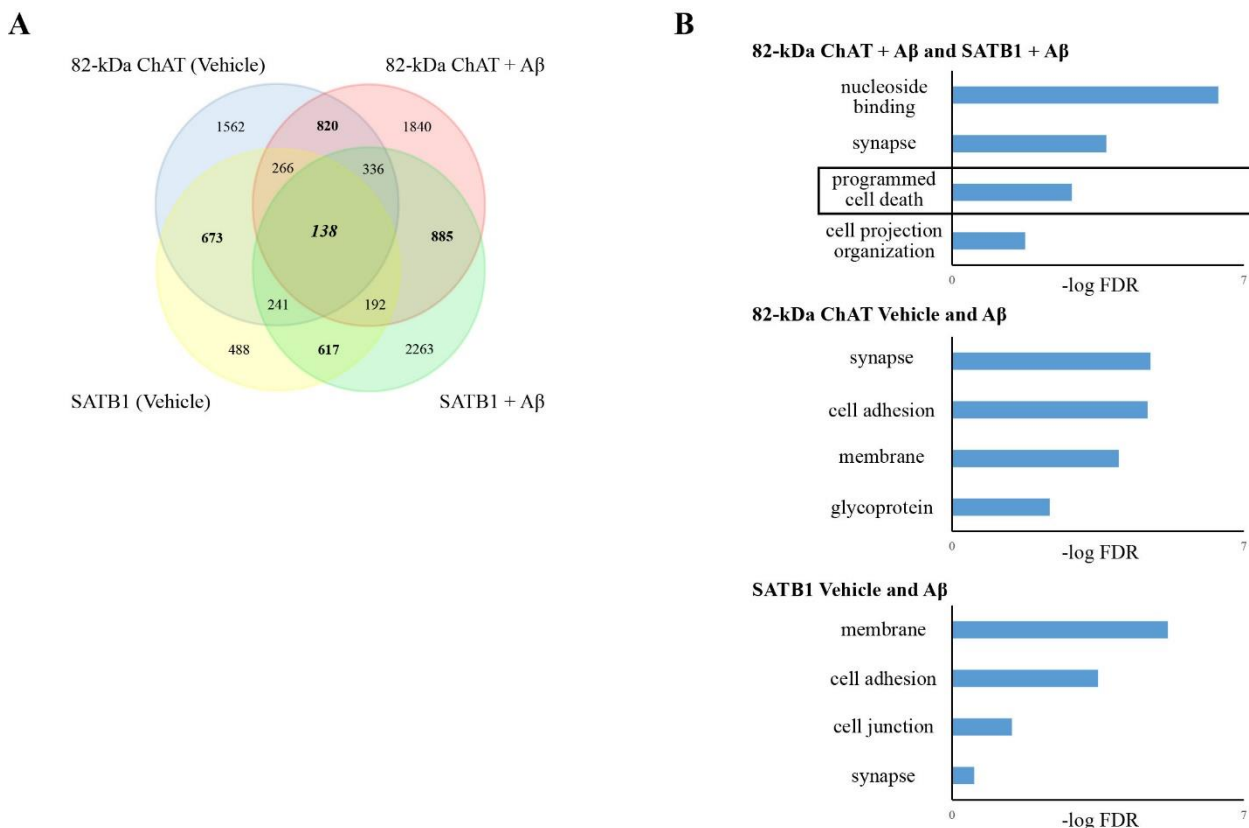


Figure 3-10. 82-kDa ChAT and SATB1 associate with shared cell membrane and stress related genes after A β -exposure.

(A) Number of genes associated with ChIP-seq peaks for 82-kDa ChAT and/or SATB1 after treatment of cells with vehicle or 100 nM oligomeric A β_{1-42} . There was increased gene association between the proteins after exposure of cells to A β . (B) Gene ontology analysis for groups of gene associations found by ChIP-seq. 82-kDa ChAT and SATB1 had significant associations with genes encoding proteins involved in synapse function, cell adhesion and cell membrane function with both treatments. For genes associated with both 82-kDa ChAT and SATB1 after exposure to A β_{1-42} , there were significant gene associations for nucleoside binding and programmed cell death (box). Gene ontology terms are presented with the $-\log$ value of the FDR.

ATP-binding ($p = 1.01E-07$, $-\log(\text{FDR}) = 3.8$), zinc ($p = 3.88E-06$, $-\log(\text{FDR}) = 2.2$) and zinc-finger ($p = 1.16E-05$, $-\log(\text{FDR}) = 1.8$), nucleus ($p = 8.11E-07$, $-\log(\text{FDR}) = 2.9$), and homophilic cell adhesion ($p = 6.93E-07$, $-\log(\text{FDR}) = 2.9$). We also explored GO enrichment for genes that were found in more than one condition (**Fig. 3-10B**, **Appendices 9-11**). After exposure of cells to $A\beta_{1-42}$, we found significant GO terms related to nucleoside binding ($p = 3.63E-12$, $-\log(\text{FDR}) = 8.3$), synapse ($p = 1.42E-07$, $-\log(\text{FDR}) = 3.7$), and cell projection ($p = 1.00E-05$, $-\log(\text{FDR}) = 1.8$) for both 82-kDa ChAT and SATB1 (see **Appendices 9,10** for additional significant GO terms). Similarly, we found synapse, membrane and cell adhesion GO terms for SATB1 and 82-kDa ChAT regardless of treatment with either vehicle or $A\beta_{1-42}$ (**Appendix 11**). We also found the GO term regulation of programmed cell death ($p = 6.15E-05$, $-\log(\text{FDR}) = 2.9$) for both 82-kDa ChAT and SATB1 after $A\beta$ -exposure. Similar to 82-kDa ChAT, we also found peaks for SATB1 in several APP binding and metabolism related genes (**Table 3-3**). Of interest, *APP* had peaks for both 82-kDa ChAT and SATB1 only after exposure of cells to $A\beta_{1-42}$.

82-kDa ChAT and SATB1 are associated with APP, leading to altered gene expression

To validate peaks found within the ChIP-seq dataset, we chose to examine a peak found after exposure of cells to $A\beta_{1-42}$ for both SATB1 and 82-kDa ChAT on the *APP* gene at intron 13 (**Table 3-3**), that were within 160 nt of one another. *APP* has previously been found to have altered transcription in AD patients following transcriptome analysis (Karim *et al.* 2014), and after MAPK activation by anisomycin in SH-SY5Y cells (Guo *et al.* 2011). Combined with recent evidence demonstrating that 82-kDa ChAT is implicated in alterations in APP processing (Albers *et al.* 2014), we identified *APP* as a potential target for an 82-kDa ChAT/SATB1 S/MAR. Using the in silico MAR-Wiz S/MAR prediction tool (Singh *et al.* 1997), we identified a predicted S/MAR ~55 kb upstream of the 3' end of *APP* that was ~2 kb upstream of the ChIP-seq peaks (**Fig. 3-11A**). Pathak *et al.* (2014) identified DNA associated with nuclear matrix S/MARs from *D. melanogaster*

Table 3-3. APP-interacting genes with 82-kDa ChAT and/or SATB1 association by ChIP-seq

Gene	Function	82-kDa ChAT (Vehicle)	SATB1 (Vehicle)	82-kDa ChAT (A β)	SATB1 (A β)	Microarray fold change
ADAM10	Alpha secretase proteolytic cleavage of APP	Intron 1	--	Intron 14	--	2.4
ADAM12	matrix metalloproteinase, multiple catalytic targets	Intron 3	--	Intron 2	--	n/a
ADAM17	MAP-kinase signalling, APP cleavage	Intron 1	--	--	--	1.2
APBA2 (x11 β)	signal transduction, APP binding	--	Intron 3	Promoter	--	2.2
APBB1	APP binding, involved in APP signaling	Promoter	--	--	Intron 1	n/a
APBB2	APP binding, involved in signaling	Intron 1	--	Intron 6	Intron 10	n/a
APP	β -amyloid precursor, synapse maintenance	--	--	Intron 13	Intron 13	n/a
APPBP2	Binds to APP intracellular domain	Intron 4	--	--	--	1.4
NAE1	APP binding, can drive APP-mediated apoptosis	--	--	Intron 7	--	n/a
RTN1	Modulates β -secretase activity, APP binding near cleavage site	--	Intron 1	Intron 1, 3	--	14.8

embryos using next generation sequencing (NCBI Sequence Read Archive accession number: SRX443533). We identified 3 peaks in the APP homolog *App1* associated with potential S/MARs, with one peak found in the same region as the ChIP-seq peaks (**Fig. 3-11A**). In addition, the region containing the ChIP-seq peaks had several sequence similarities with known SATB1 binding motifs (Yasui *et al.* 2012). We tested for enrichment of both SATB1 and 82-kDa ChAT using ChIP followed by quantitative PCR (ChIP-qPCR) (**Fig. 3-11B**). For 82-kDa ChAT, we observed a 1.6 ± 0.5 -fold enrichment after vehicle treatment, which was significantly higher after $A\beta_{1-42}$ -exposure (9.8 ± 2.9 -fold). We found a 4.9 ± 0.9 -fold enrichment for SATB1 after vehicle treatment, compared to 2.4 ± 0.5 -fold after exposure of cells to $A\beta_{1-42}$, though there was no statistical difference between the treatments.

Next, we used RT-qPCR to assess any potential changes to *APP* steady-state mRNA levels (**Fig. 3-12A**). Using SH-SY5Y cells stably expressing either 82-kDa ChAT or empty vector, we found no significant changes in total *APP* steady-state mRNA levels after exposure for 4 h 100 nM $A\beta_{1-42}$ (0.96 ± 0.02 -fold, 1.00 ± 0.05 -fold respectively). Several groups have reported that *APP* mRNA isoforms (including APP751 and 770) containing the Kunitz-type serine protease inhibitor domain (APP-KPI) are increased in AD patients, which correlates to increases in $A\beta_{1-42}$ (Moir *et al.* 1998; Preece *et al.* 2004). Therefore we tested whether there were any $A\beta$ -induced changes in APP-KPI mRNA steady-state levels, and observed that there is significantly increased expression of APP-KPI mRNA steady-state levels in vector-expressing cells (1.18 ± 0.09 -fold) compared to cells expressing 82-kDa ChAT (0.86 ± 0.03 -fold).

Finally, we assessed whether siRNA knockdown targeted to SATB1 could alter steady-state levels of total *APP* mRNA or the $A\beta$ -induced change in APP-KPI mRNA observed in 82-kDa ChAT-expressing cells (**Fig. 3-12B**). After exposure for 4 h with 100 nM $A\beta_{1-42}$, we observed no significant changes in total *APP* steady-state mRNA levels for SH-SY5Y cells stably expressing 82-kDa ChAT after a mock transfection, control siRNA or siRNA targeted to SATB1 compared to cells that were not transfected. When we measured APP-KPI steady-state mRNA levels, we observed significantly

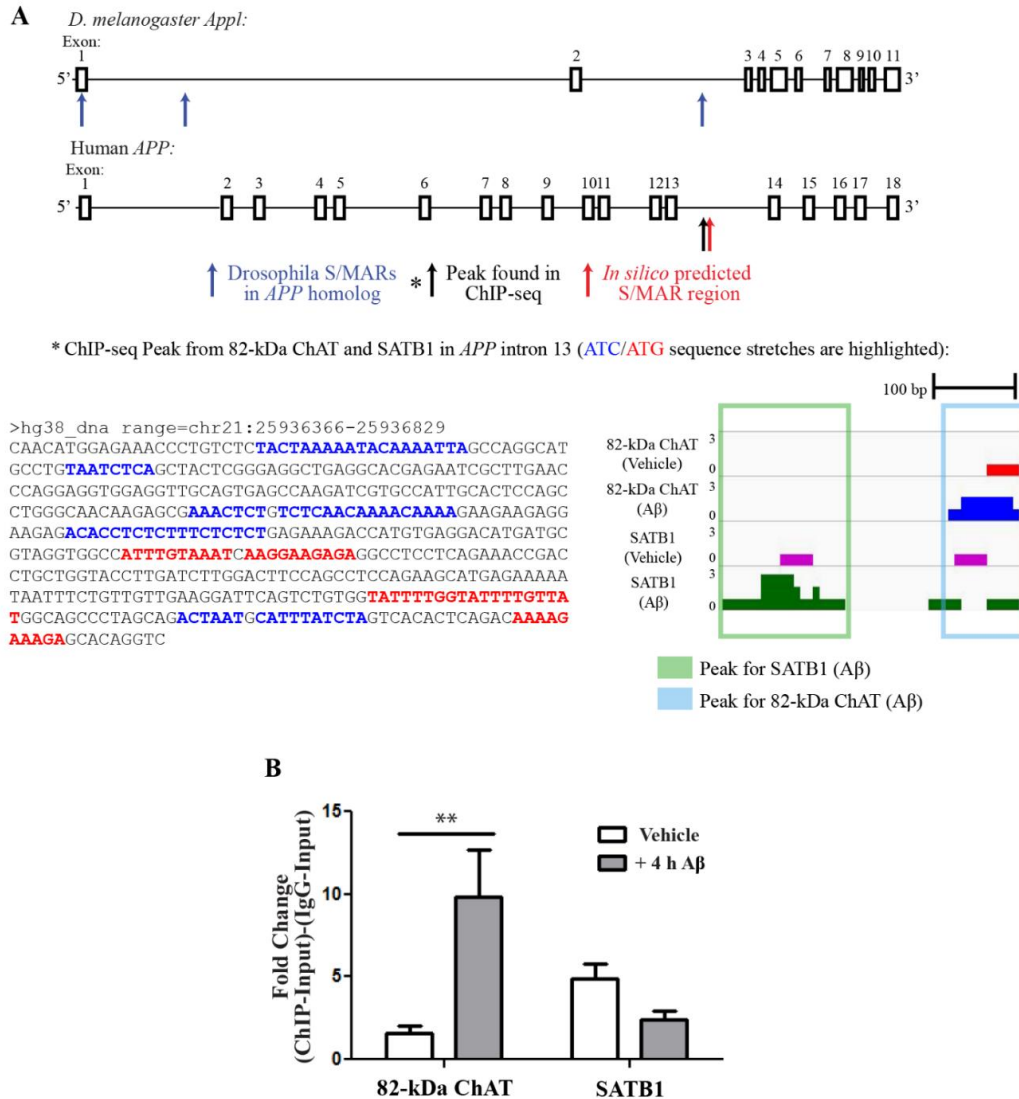


Figure 3-11. 82-kDa ChAT and SATB1 associate with the APP gene after A β -exposure.

(A) Schematic showing exons (boxes) and introns (horizontal lines) for the *D. melanogaster Appl* and human *APP* genes. Blue arrows indicate S/MARs regions on *Appl* identified by Pathak *et al.* (2014), the red arrow a predicted S/MAR in *APP* by *in silico* analysis, and the black arrow a ChIP-seq peak found for 82-kDa ChAT and SATB1 after A β ₁₋₄₂-exposure. ATC/ATG rich sequences are highlighted in this region. ChIP-seq tracks for 82-kDa ChAT and SATB1 are also shown for this region. (B) Verification of 82-kDa ChAT and SATB1 ChIP-seq peaks on *APP*. 82-kDa ChAT showed significantly increased fold-enrichment after exposure of cells to 100 nM oligomeric A β ₁₋₄₂ for 4 h, while SATB1 did not significantly change its association with the region after either vehicle or A β ₁₋₄₂ treatment. $n = 6$, ** $p < 0.01$ (two-way ANOVA with Bonferroni's post-hoc test).

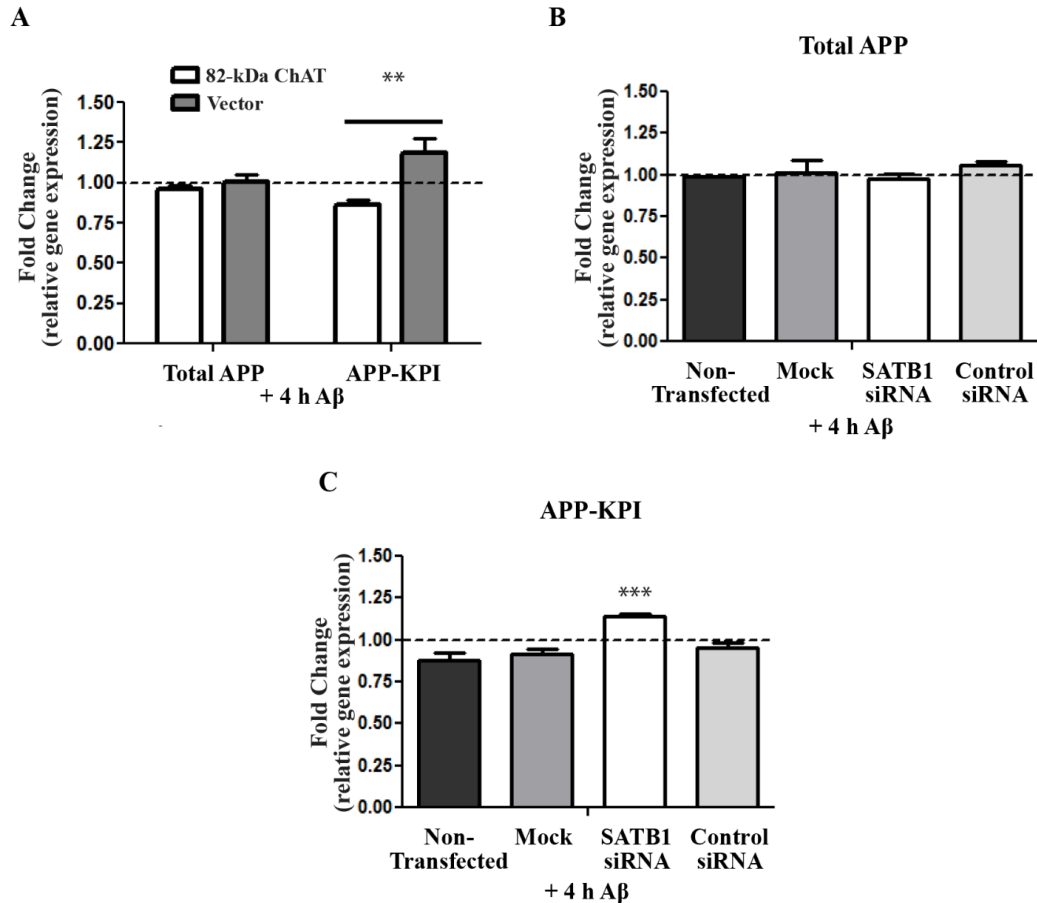


Figure 3-12. 82-kDa ChAT and SATB1 expression prevents an increase in APP isoforms containing the Kunitz-protease inhibitor domain (KPI).

(A) APP steady-state mRNA expression in 82-kDa ChAT or vector-expressing cells after exposure to 100 nM oligomeric A β ₁₋₄₂. Data are presented as fold-enrichment compared to reference (GAPDH) mRNA levels and vehicle-treated cells (dashed-line). Vector-expressing cells showed higher steady-state mRNA levels of isoforms containing KPI compared to 82-kDa ChAT-expressing cells. $n = 4$, $**p < 0.01$ (two-way ANOVA with Bonferroni's post-hoc test). (B) APP steady-state mRNA expression in 82-kDa ChAT-expressing cells after exposure to 100 nM oligomeric A β ₁₋₄₂ after either no transfection, a mock transfection, transfection with untargeted control siRNA, or transfection with siRNA targeted to SATB1. Data are presented as fold-enrichment compared to reference (GAPDH) mRNA levels and vehicle-treated cells (dashed-line). There were no significant changes in total APP mRNA levels for any of the treatments. (C) Cells transfected with SATB1 siRNA showed higher steady-state mRNA levels of APP isoforms containing KPI compared to non-transfected 82-kDa ChAT-expressing cells. $n = 5$, $***p < 0.001$ (one-way ANOVA with Dunnett's post-hoc test).

increased expression of APP-KPI levels in cells expressing 82-kDa ChAT and transfected with SATB1-targeted siRNA (1.14 ± 0.01 -fold) compared to non-transfected cells (0.88 ± 0.05 -fold) (**Fig. 3-12C**). There were no significant differences for mock transfected cells (0.91 ± 0.03 -fold) or control siRNA transfected cells (0.95 ± 0.03 -fold) compared to non-transfected cells.

82-kDa ChAT and SATB1 associate with chromatin at S/MARs

Because SATB1 is involved in the anchoring of S/MARs to the nuclear matrix, and we showed that both SATB1 and 82-kDa ChAT associated with a predicted S/MAR on *APP*, we asked whether 82-kDa ChAT may also be localized at S/MARs. We used motifs used by the *in silico* MAR-Wiz tool (Singh *et al.* 1997), along with known SATB1 motifs (Yasui *et al.* 2002) and select motifs discovered in the *D. melanogaster* S/MAR dataset (Pathak *et al.* 2014; **Table 3-4**). In addition to the analysis of 82-kDa ChAT and SATB1, we also included a ChIP-seq dataset for Alpha Thalassemia/Mental Retardation Syndrome X-Linked (ATR_X) (NCBI GEO database accession number: GSE22162; Law *et al.* 2010), as this protein is involved in chromatin reorganization, but has not previously been associated with S/MARs (Law *et al.* 2010; Kernohan *et al.* 2014; Levy *et al.* 2015). ATR_X had a total of 6368 peaks, with an average peak length of 483.4 ± 2.4 nt. Due to the large differences in peak lengths, we examined the number of motifs found in each peak weighted by the inverse of the peak length divided by a scaling factor of 100 (**Fig. 3-13**). Overall, we found that ATR_X ($0.9 \pm 0.002\%$) had significantly fewer weighted motifs/peak compared to both 82-kDa ChAT and SATB1 after both vehicle and A β_{1-42} -exposure. Surprisingly, after A β_{1-42} treatment of cells, SATB1 ($1.4 \pm 0.007\%$) was also significantly reduced compared to all treatments other than ATR_X. We also tested the weighted motifs/peak for the 5 motifs that had the highest number of associated peaks. For motifs 1 (an origin of replication motif) and 20–21 (SATB1 motifs), we saw a similar pattern as the overall data, indicating that 82-kDa ChAT and SATB1 peaks significantly associated with genomic regions containing S/MAR binding sites.

Table 3-4. Motifs used in S/MAR analysis

Motifs 1-18 were used previously to determine S/MAR association (Singh *et al.* 1997), motifs 19-21 are SATB1 binding motifs (Yasui *et al.* 2002) and motifs 22-26 were identified in a *D. melanogaster* S/MAR study (Pathak *et al.* 2014).

Number	Name	Motif
1	Origin of Replication Signal 1	ATTA
2	Origin of Replication Signal 2	ATTTA
3	Origin of Replication Signal 3	ATTTTA
4	TG-Rich Signal 1	TGTTTTG
5	TG-Rich Signal 2	TGTTTTTTG
6	TG-Rich Signal 3	TTTTGGGG
7	Curved DNA Signal 1	AAAA(N ₇)AAAA(N ₇)AAAA
8	Curved DNA Signal 2	TTTT(N ₇)TTTT(N ₇)TTTT
9	Curved DNA Signal 3	TTTAAA
10	Kinked DNA Signal 1	TA(N ₃)TG(N ₃)CA
11	Kinked DNA Signal 2	TA(N ₃)CA(N ₃)TG
12	Kinked DNA Signal 3	TG(N ₃)TA(N ₃)CA
13	Kinked DNA Signal 4	TG(N ₃)CA(N ₃)TA
14	Kinked DNA Signal 5	CA(N ₃)TA(N ₃)TG
15	Kinked DNA Signal 6	CA(N ₃)TG(N ₃)TA
16	mtopo-II Signal	(A/G)N(T/C)NNCNNG(T/C)NG(G/T)TN(T/C)n(T/C)
17	dtopo-II Signal	GTN(A/T)A(T/C)ATTNATNN(A/G)
18	AT-Rich Signal	(A/T) ₆
19	SATB1 Motif 1	(A/T) _{3-n} (C/G)(A/T) ₃₋₆
20	SATB1 Motif 2	(A/T/[C OR G]) ₂₀₊
21	SATB1 Motif 3	(A/T) ₂₊ (C)(A/T) ₂₊ ; <i>palindrome</i>
22	Drosophila MAR Motif 1	A ₁₂₊
23	Drosophila MAR Motif 2	(AG) ₈ or (AC) ₈
24	Drosophila MAR Motif 3	(AGC) ₅
25	Drosophila MAR Motif 4	(AACAGC) ₂
26	Drosophila MAR Motif 5	(AAAAA[C/G/T]) ₂

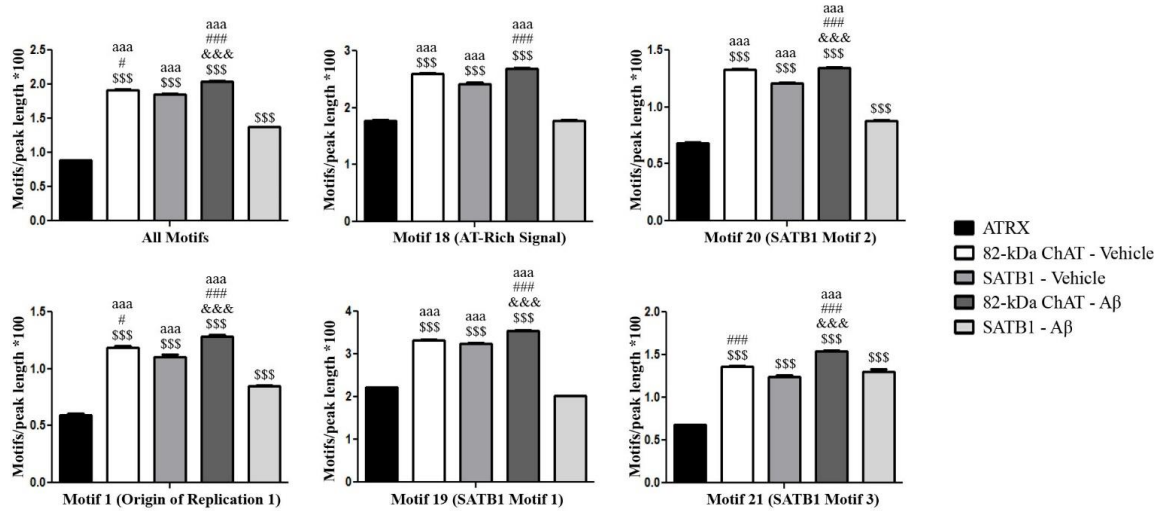


Figure 3-13. 82-kDa ChAT and SATB1 have significant enrichment for S/MAR motifs.

Mean weighted S/MAR motifs (**Table 3-4**)/ChIP-seq peak computed as the number of motifs/peak length*100. Both vehicle and Aβ₁₋₄₂-treated cells for 82-kDa ChAT and SATB1 had a higher number of weighted motifs/peak compared to ATRX for all motifs. A similar pattern was found for the 5 highest represented motifs. \$\$\$ p < 0.001 compared to ATRX, aaa p < 0.001 compared to Aβ₁₋₄₂-treated SATB1, &&& p < 0.001 compared to vehicle-treated 82-kDa ChAT, and ### p < 0.001 and # p < 0.05 compared to vehicle-treated SATB1.

Table 3-5. G-quadruplex ($G_3+N_{1-20}G_3+N_{1-20}G_3+N_{1-20}G_3+$) motifs found in ChIP-seq datasets

Sample	Peaks with G-Quadruplex motifs	Total G-Quadruplex motifs
ATRX	732	1327
82-kDa ChAT (Vehicle)	113	204
SATB1 (Vehicle)	60	109
82-kDa ChAT (A β)	89	121
SATB1 (A β)	30	41

As a control, we also determined the number of motifs in each peak of the ATRX-binding G-quadruplex motif: $G_{3+N_{1-20}}G_{3+N_{1-20}}G_{3+N_{1-20}}G_{3+N_{1-20}}$ (**Table 3-5**; Law *et al.* 2010). For ATRX we found 732 peaks with at least one G-quadruplex motif and 1327 motifs total. By comparison, for 82-kDa ChAT we found only 113 peaks and 204 motifs after vehicle treatment, and 89 peaks with 121 motifs after $A\beta_{1-42}$ -exposure. For SATB1, we found 60 peaks and 109 motifs after vehicle treatment, and 30 peaks with only 41 motifs after $A\beta_{1-42}$ -exposure. These data indicate that G-quadruplex motifs are enriched in ATRX, but not for 82-kDa ChAT or SATB1.

Pathak *et al.* (2014) found that the inter-MAR distance in the *D. melanogaster* genome ranged from <1 kb to 150 kb, with an average distance of 16 kb and a peak of inter-MAR distances at approximately 5 kb. Due to the potential association with S/MARs, we also assessed whether there was any pattern to the spacing between successive peaks across each chromosome (**Fig. 3-14**). We found that the distance between peaks for each treatment ranged from <1 kb to 28 Mb, except for ATRX which had an upper range of 56 Mb. For 82-kDa ChAT, 75% of peaks were less than 1.4 Mb apart after either vehicle or $A\beta_{1-42}$ treatment of cells. For SATB1, 75% of peaks were less than 1.1 Mb apart following $A\beta_{1-42}$ -exposure, with this number increasing to 3.8 Mb after vehicle treatment. For ATRX, 75% of peaks were less than 0.5 Mb apart. Through kernel density estimation with an upper bound of 4.0 Mb, we found that there were peaks in the distributions of the distance between successive peaks, indicative that regular patterned spacing was present. For 82-kDa ChAT, the peak occurred at a spacing of 125.0 kb after vehicle treatment, and 123.9 kb after $A\beta_{1-42}$ -exposure. We also found regular spacing for SATB1 after exposure to $A\beta_{1-42}$ (92.5 kb) and for ATRX (31.2 kb). Interestingly, we did not observe any pattern to the inter-peak distances for SATB1 after vehicle exposure. These data show that, after $A\beta$ exposure, both SATB1 and 82-kDa ChAT have regular patterned spacing on the genome similar to S/MAR genome spacing.

As a comparison to the genomic patterned spacing observed for 82-kDa ChAT, we tested whether there was patterning to the nuclear protein localization using SR-GSDIM. Images of 82-kDa ChAT immunostaining in nuclei of vehicle-treated cells by either epi-fluorescence or SR-GSDIM microscopy are shown in **Figure 3-15[a,b]**

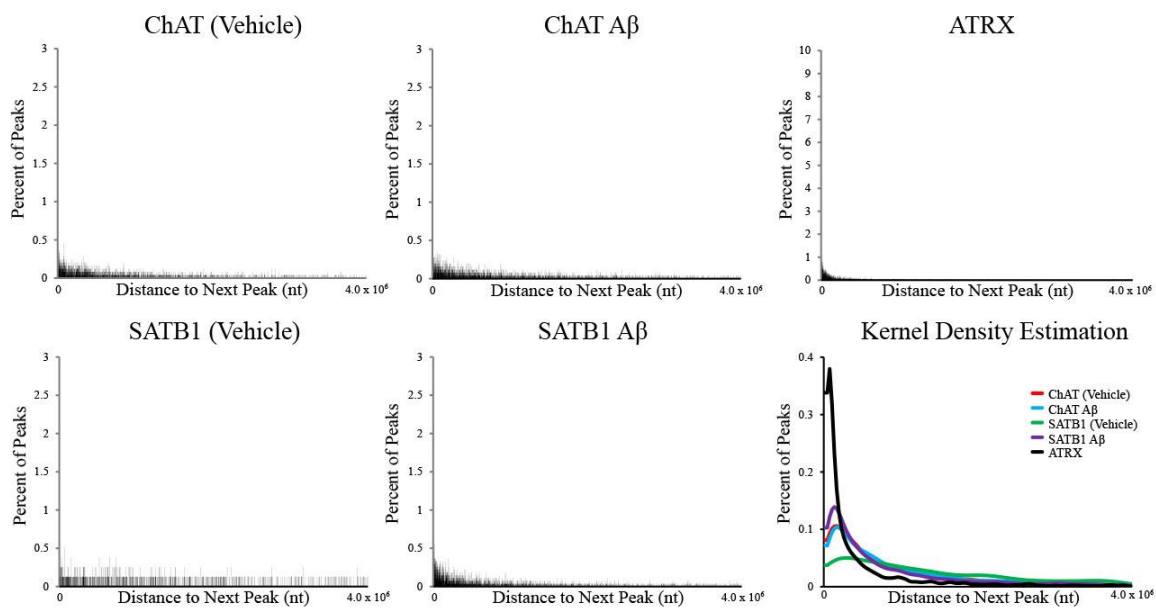


Figure 3-14. Analysis of the inter-peak spacing of 82-kDa ChAT and SATB1.

Distribution of inter-peak distances for ChIP-seq peaks. For each graph, the shape of the graph was estimated using a kernel density estimation. Indicated by a single curve, the kernel density estimation revealed regular patterned spacing for ATRX and 82-kDa ChAT, and for SATB1 after A β 1–42 cell treatment. SATB1 did not show any patterned inter-peak spacing after vehicle treatment.

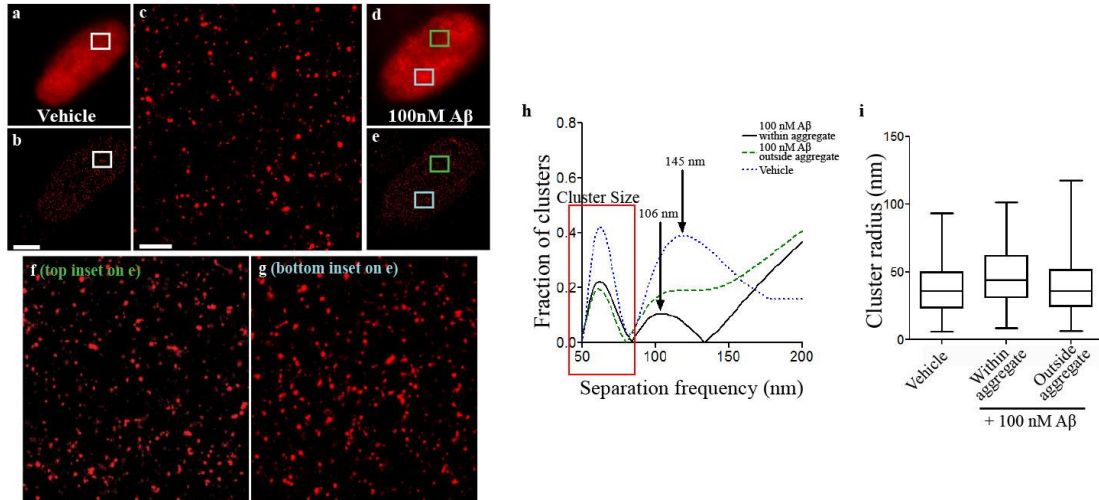


Figure 3-15. 82-kDa ChAT has patterned protein distribution in nuclei of SH-SY5Y cells.

SR-GSDIM imaging for SH-SY5Y cells stably expressing 82-kDa ChAT treated with for 4 h either vehicle or 100 nM A β_{1-42} . Epi-fluorescence images show diffuse staining for vehicle-treated cells (a) and nuclear aggregates after A β treatment (d). SR-GSDIM images show diffuse punctate staining for both vehicle (b) and A β (e) treated cells. Enlarged ROIs for vehicle-treated cell (c), and a region either outside (f) or within (g) an A β -induced 82-kDa ChAT aggregate. Scale bars on (b) 3 μ m and on (c) 500 nm; n = 6 with at least 4 cells per treatment. For each ROI, clusters were identified and the average inter-cluster distance was quantified (h). Vehicle-treated ROIs or A β -induced aggregates showed even spacing between clusters (arrows on h), while clusters from ROIs outside an aggregate did not show even spacing. Cluster size did not vary significantly for any of the conditions (red box on h,i). n = 3 with 2 cells used for each ROI in each condition.

respectively], with an enlarged region of interest (ROI, **Fig. 3-15[c]**). For A β -treated cells, we observed nuclear aggregates of 82-kDa ChAT when cells were imaged in both epi-fluorescence mode (**Fig. 3-15[d]**) and in SR-GSDIM [**e**] mode. SR-GSDIM imaging showed 82-kDa ChAT predominantly in multimeric clusters in vehicle-treated (**Fig. 3-15[c]**) and A β -exposed regions not associated with an aggregate (**Fig. 3-15[f]**), or within an aggregate (**Fig. 3-15[g]**). Using a Fourier transform, we quantified the spacing between clusters in these ROIs. Two peaks were apparent in the Fourier analysis (**Fig. 3-15[h]**), the first corresponding to the average cluster size and the second indicating regular spacing between clusters. We found that in 38% of vehicle-treated cells and in 10% of regions containing an A β -induced aggregate the clusters displayed even spacing, while regions in A β -exposed cells not associated with an aggregate did not contain any regular patterning. In vehicle-treated cells, the peak of inter-cluster distance was found to be 145 nm, while in regions containing an A β -induced aggregate this distance was reduced to 106 nm. We measured the size of the individual clusters and found no significant difference in any of the conditions (box on **Fig. 3-15[h,i]**).

82-kDa ChAT interacts with RNA splicing, nuclear matrix and chromatin organization proteins, shown by mass spectrometry

The 82-kDa ChAT protein interacts with SATB1 to promote the formation of S/MARs. Therefore, we asked what other proteins may be in complex with these proteins and if this impacts the potential roles for 82-kDa ChAT in gene expression changes after cell exposure to A β . We identified putative 82-kDa ChAT-interacting proteins by Co-IP from nuclear extracts followed by identification of proteins by MALDI-TOF mass spectrometry (**Fig. 3-16**). First, we compared SH-SY5Y cells expressing an empty vector to cells having stable heterologous expression of 82-kDa ChAT (**Fig. 3-16A**). SDS-PAGE gels resulting from separation of proteins in these samples showed multiple bands for 82-kDa ChAT-expressing cells after either vehicle or 100 nM A β ₁₋₄₂ treatment, but not for vector-expressing cells. As a control, total nuclear lysate samples, each containing 5 μ g of protein, were run in parallel for each treatment to ensure that the original samples

had similar concentrations of protein per volume. Next, we identified unique bands in 82-kDa ChAT-expressing samples that were present in vehicle and/or A β ₁₋₄₂ treated samples and not seen in vector-expressing cells, and sent several of these for protein identification by MALDI-TOF (**Fig. 3-16B**). For this gel, the IP prepared from the vector-expressing cells treated with vehicle did not work properly, but the A β ₁₋₄₂ treatment did. Since we have observed previously that A β treatment did not affect the distribution of bands present in vector-expressing cells (**Fig. 3-16A**), we were confident that unique bands seen in 82-kDa ChAT expressing samples were specific to those samples.

Using this approach, we identified 12 unique proteins and the 82-kDa ChAT protein itself (**Fig. 3-16B, table; Fig. 3-17**). Many of the proteins identified were related to mRNA splicing and transport, including: DNA helicase II, which is involved in transcription and replication, but can also bind to naturally occurring double-stranded pre-mRNAs (Tuteja *et al.* 1994; Zhang and Grosse 1997; Portal *et al.* 2015); heterogeneous nuclear ribonucleoprotein C (C1/C2), isoform CRA_c (HNRNPC) and Heterogeneous nuclear ribonucleoproteins A1 and A2/B1 (HNRNPA1/A2B1) are involved in pre-mRNA splicing and transport (He and Smith 2009; McCloskey *et al.* 2012); M-phase phosphoprotein 4/ interleukin enhancer binding factor 3 (ILF3), which in neurons is involved in *Tau* mRNA transport from the nucleus to the axon (Larcher *et al.* 2004); and splicing factor proline- and glutamine-rich (SFPQ), involved in pre-mRNA splicing and the formation of the spliceosome complex (Cristobo *et al.* 2011; Cosker *et al.* 2016; Knott *et al.* 2016). In the A β ₁₋₄₂-treated samples, we also identified pre-RNA splicing factor 8 (PRP8), which functions as a nuclear scaffolding for the spliceosome complex to form (reviewed in Grainger and Beggs 2005). Though this band was present in the vehicle-treated sample, when we tested the sample there were no identifiable proteins. In a second repeat of the vehicle-treated samples, we identified Matrin3, a nuclear scaffolding protein previously found to interact with 82-kDa ChAT by co-immunoprecipitation (unpublished data from our lab). Though it is part of the nuclear scaffold, Matrin3 has also been demonstrated to play a role in post-transcriptional pre-mRNA stabilization and the regulation of alternative splicing events (Zeitz *et al.* 2009; Salton *et al.* 2011; Coelho *et al.* 2015). Vimentin, a cytosolic scaffolding protein present

in developing neurites in cultured hippocampal cells and in hippocampal dendrites of AD patients, was also identified (Boyne *et al.* 1996; Levin *et al.* 2009).

Additional proteins identified included heat-shock protein 90 (HSP90), which is integral for the stabilization and folding of other proteins (reviewed in Wegele *et al.* 2004); and in A β_{1-42} -treated samples we identified heat-shock protein 70 or heat shock cognate 71 (HSP70/HSC70; MASCOT identification could not distinguish between these two proteins) which are both involved in identifying proteins that are incorrectly folded and either facilitates their refolding or directs them to the proteasome for degradation (Lüders *et al.* 2000; Wegele *et al.* 2004). Finally, we found structural maintenance of chromosomes protein 1A isoform 1 (SMC1A) in the A β_{1-42} -treated sample. SMC proteins are involved in chromatin condensation, looping, DNA repair and recombination, and cell division in mitotic cells (reviewed in Hirano 2002; and Jessberger 2002).

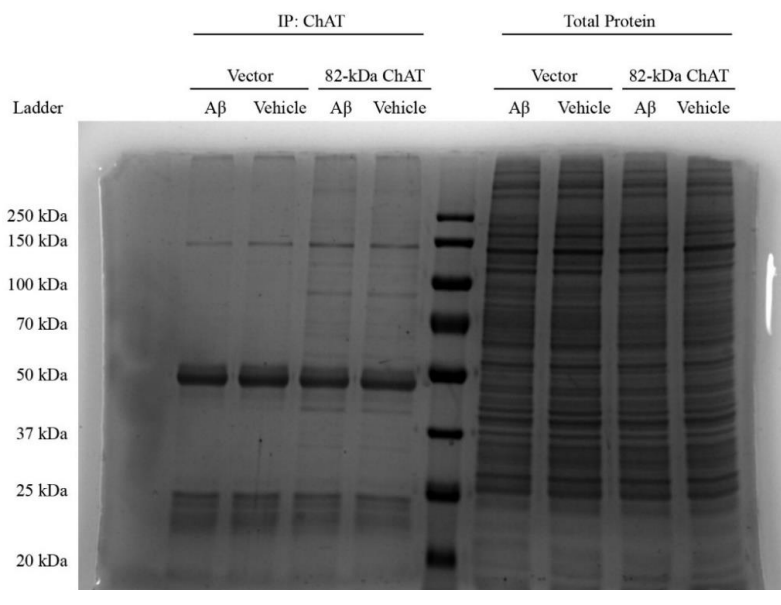
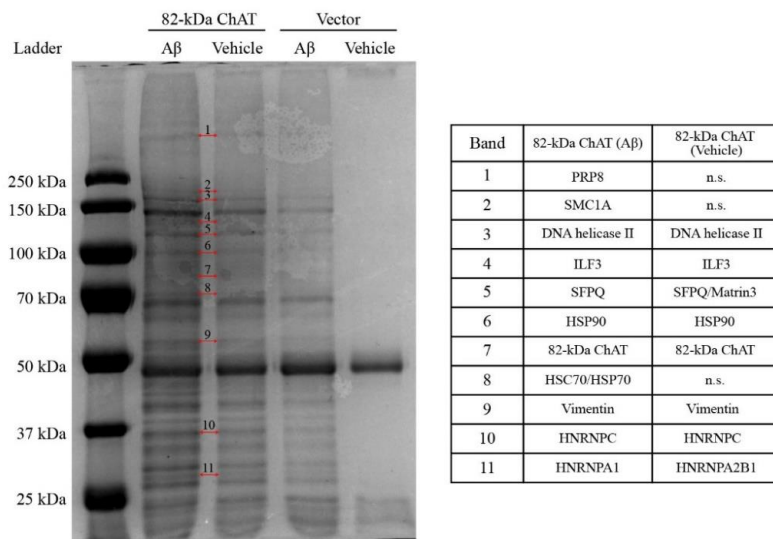
A**B**

Figure 3-16. 82-kDa ChAT co-immunoprecipitation and identification of interacting proteins.

(A) SH-SY5Y cells were treated for 4 h with either vehicle or 100 nM A β ₁₋₄₂ prior to nuclear isolation and immunoprecipitation for 82-kDa ChAT. Immunoprecipitated proteins were separated by SDS-PAGE and stained with Imperial Protein Stain. Sample aliquots containing 5 μ g of total nuclear lysate protein were run in parallel ensure that the original samples had similar concentrations of protein per volume. Vector-expressing cells had a few non-specific bands, while 82-kDa ChAT expressing cells had multiple unique bands. (B) Representative gel used for spot picking and mass spectrometry

analysis. Bands that were picked and successfully analyzed are numbered. The corresponding identified protein is shown in the accompanying table. n.s. = no statistically significant protein identified.

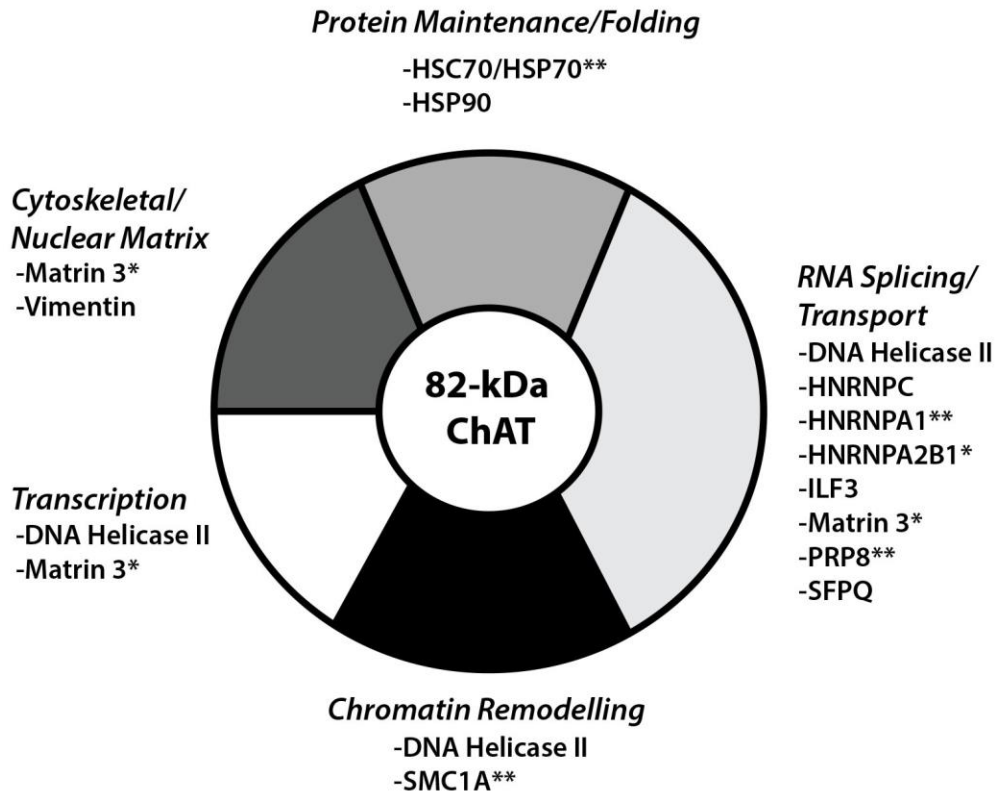


Figure 3-17. 82-kDa ChAT protein interactions as revealed by mass spectrometry analysis.

Potential interacting proteins as revealed by immunoprecipitation for 82-kDa ChAT in SH-SY5Y cells treated for 4 h with either vehicle or 100 nM A β ₁₋₄₂. Mass spectrometry analysis found several proteins related to RNA splicing and transport. Other proteins included chromatin remodelling, transcription, scaffolding, and protein maintenance related proteins. * protein was identified in vehicle-treated samples only; ** protein was found in A β ₁₋₄₂-treated samples only

3.4 Discussion

In this chapter, we demonstrated that both 82-kDa ChAT and SATB1 facilitate and participate in an epigenetic response at S/MARs in human neural cells. Specifically, we found that (1) 82-kDa ChAT and SATB1 co-localize in cell nuclei after A β ₁₋₄₂ treatment of cells; (2) the presence of A β -induced aggregates of 82-kDa ChAT and SATB1 in cell nuclei are dependent on the presence of both proteins; (3) SATB1 had a similar genomic distribution as 82-kDa ChAT, and increased its association with gene introns and promoters at synapse and membrane associated genes after cells were exposed to A β ₁₋₄₂; (3) 82-kDa ChAT and SATB1 are both necessary to prevent an increase in an isoform of *APP* after treatment of cells with A β ₁₋₄₂; (4) 82-kDa ChAT and SATB1 are associated with S/MARs and have features of chromatin organizers; and (5) 82-kDa ChAT associates with RNA splicing/transport and chromatin organization-related proteins, identified by mass spectrometry.

When we observed the subcellular localization of 82-kDa ChAT and SATB1 after exposure of cells to oligomeric A β ₁₋₄₂, we determined that SATB1 formed aggregates in nuclei that were co-localized with the ChAT aggregates. We were unable to determine whether 82-kDa ChAT and SATB1 were directly interacting by Co-IP due to technical difficulties with this approach in this situation. Further investigation by both Co-IP and other methods (i.e. Förster or bioluminescence resonance energy transfer) could help clarify whether these proteins can interact directly. It is an interesting observation that these A β ₁₋₄₂-induced aggregates are dependent on the presence of both 82-kDa ChAT and SATB1 in nuclei and that both SIRT1 activation and exposure of cells to A β result in SATB1 entry into the nuclear interior, but that 82-kDa ChAT aggregates can be produced independently by resveratrol treatment. Resveratrol is known to increase SIRT1 activity (Ye *et al.* 2013), but also increases mitochondrial activity through PGC-1 α activity (Lagouge *et al.* 2006), promotes the oxidative stress response via induction of manganese superoxide dismutase (Tanno *et al.* 2010), and may have both anti- and pro-oxidant properties (Roemer and Mahyar-Roemer 2002; Ahmad *et al.* 2003). Though Xue *et al.* (2012) showed that SIRT1 deacetylates SATB1 to promote the formation of S/MARs at

the β -globulin locus, SIRT1 is a histone and protein deacetylase which has several other non-SATB1 targets (Brunet *et al.* 2004; Stünkel *et al.* 2007; Liu *et al.* 2009). A further possible explanation for the resveratrol-induced aggregates after SATB1 siRNA knockdown is that we were only able to reduce SATB1 levels by 29%. While this was sufficient to reduce AB-induced 82-kDa ChAT aggregation, it may not be a large enough SATB1 reduction to affect the resveratrol-induced aggregates. Whether the 82-kDa ChAT aggregates are related to an anti-oxidant response, what other SIRT1 targets could be contributing to 82-kDa ChAT nuclear aggregation, or whether further reductions in SATB1 could alter the resveratrol-induced 82-kDa ChAT aggregation requires further investigation.

When we analyzed ChIP-seq datasets for 82-kDa ChAT and SATB1, we saw several similarities including increases in promoter and intragenic targets. We observed that both proteins had smaller peak lengths after exposure to $A\beta_{1-42}$ (~130 nt after AB compared to ~190 nt after vehicle treatment for 82-kDa ChAT; ~145 nt after AB compared to ~175 nt after vehicle treatment for SATB1), which suggests targeted genomic associations as small peak lengths (~50-150 nt) are associated with sequence-specific DNA targets and is a signature of transcription-factor binding (Pepke *et al.* 2009). We observed that 82-kDa ChAT and SATB1 have associations with sequences that are enriched with S/MAR binding motifs, in particular SATB1 binding motifs and an origin of replication sequence. In addition, we also observed the same partial NFAT TC₂-₃AT motif after both vehicle and $A\beta_{1-42}$ -treatment of cells for SATB1 as observed for 82-kDa ChAT, further supporting the hypothesis that these proteins may form a complex. However, there were also important differences between the datasets. For 82-kDa ChAT there were a similar number of peaks after vehicle or $A\beta$ -exposure, but for SATB1 there were more than double the number of associations found after $A\beta$ -exposure. In addition, we found no significant GO terms for genes associated with 82-kDa ChAT after cells were treated with vehicle or $A\beta$ alone, but for SATB1 after $A\beta$ -exposure we found GO enrichment for several terms including nucleotide, ATP-binding, zinc and cell adhesion. Interestingly, however, when we considered genes that were found associated with either multiple treatments or multiple proteins, we found significant GO terms related to the synapse and membrane. This observation, combined with the DREME motif analysis

showing that both SATB1 and 82-kDa ChAT are enriched for multiple shared motifs, supports the hypothesis that 82-kDa ChAT and SATB1 may be forming a complex together with other proteins.

It is important to note that this is the first report of whole genome ChIP-sequencing in any cell type for either SATB1 or 82-kDa ChAT. Previously, only locus specific ChIP or chromatin conformation capture (3C) studies have been published for SATB1 (Kumar *et al.* 2007; Li *et al.* 2007; Gong *et al.* 2010; Fessing *et al.* 2011; Gong *et al.* 2011; Xue *et al.* 2012; Yang *et al.* 2015), and to the author's knowledge no other studies have reported that 82-kDa ChAT associates with DNA. There are a number of novel genome-wide patterns that have been observed from these datasets that provide valuable information on the nature of these protein-DNA interactions. For example, we observed that a subset of the genome associations for 82-kDa ChAT had regular patterned spacing and, at the nano-resolution level, that 82-kDa ChAT forms patterned clusters with the distance between clusters decreasing after A β -exposure. We found a subset of SATB1 genome associations with regular patterned spacing after cells were exposed to A β ₁₋₄₂, but not for vehicle-treated cells. Patterned spacing on the genome has been previously reported for chromatin organizers, and is a feature of S/MARs on the *D. melanogaster* genome (Pathak *et al.* 2014). These data are especially interesting in light of the centromeric associations seen for both 82-kDa ChAT and SATB1.

When we analyzed ChIP-seq patterns for 82-kDa ChAT and SATB1, it was evident that both proteins were highly-enriched in regions flanking the centromere, and in some cases within the centromere as well. Further, we found 82-kDa ChAT associated with SMC1A by Co-IP and mass spectrometry; SMC1A is involved in chromatin condensation and looping, as well as cell division (Hirano 2002; Jessberger 2002). Centromeres tend to be largely enriched with heterochromatin, with further condensation occurring during mitosis (Guenatri *et al.* 2004; Nakano *et al.* 2008). In post-mitotic cells, the centromere must remain heterochromatic for the entire lifespan of the cell, but cell cycle re-entry has been observed in neurons in brain of Alzheimer's disease (AD) patients (McShea *et al.* 1997; Nagy *et al.* 1997). Further, neurons can undergo a senescence-like phenotype where they have been observed to re-enter the cell cycle

(Spremo-Potporević *et al.* 2008). In these cells, the centromere of the X-inactivated chromosome also becomes activated (Spremo-Potporević *et al.* 2008), though our data did not test the X-inactivated chromosome as SH-SY5Y cells were derived from a male.

Several studies have demonstrated that ChIP-seq data can falsely identify centromere enrichment due to the presence of multiple tandem non-specific A/T-rich repeats (Nix *et al.* 2008; Teytelman *et al.* 2013). This is unlikely the case in our ChIP-seq dataset, as DNA input levels were subtracted from the data, enrichment was not found equally across all the centromeres, and on most chromosomes the enrichment was found in non-repeat rich centromere flanking regions. Further, a common theme found for both 82-kDa ChAT and SATB1 was association with A/T-rich motifs (including multiple A/T-rich S/MAR motifs), both in genic and non-genic regions. Enrichment of 82-kDa ChAT and SATB1 near these regions may be significant for the cessation of cell division, and thus further investigation should assess the contributions of 82-kDa ChAT and SATB1 to centromere organization.

The present study found that 82-kDa ChAT and SATB1 are both enriched at an *in silico* predicted S/MAR on the APP gene after exposure of cells to A β ₁₋₄₂. While APP mRNA expression is altered in AD patients (Rockenstein *et al.* 1995; Karim *et al.* 2014), and increased after MAPK activation by anisomycin in SH-SY5Y cells (Guo *et al.* 2011), other studies suggest that there may be an increase in the isoforms that contain KPI in AD patients (Moir *et al.* 1998; Preece *et al.* 2004). These studies show that total APP mRNA steady-state levels are unchanged, but this alternative expression pattern correlates to an increase in soluble A β ₁₋₄₂ and to severity of cognitive impairment (Moir *et al.* 1998; Preece *et al.* 2004). We found previously that total APP mRNA steady-state levels were not changed when 82-kDa ChAT was expressed in primary neurons from APP/PS1 mice (Albers *et al.* 2014). Our current findings complement these studies, as we demonstrate that cells expressing 82-kDa ChAT have lower steady-state levels of KPI-containing isoforms of APP compared to vector-expressing cells, with no change in total APP mRNA levels. The change in APP-KPI was prevented when we used siRNA targeted to SATB1, demonstrating that SATB1 is also necessary for this change in gene expression. We postulate that expression of 82-kDa ChAT protein may contribute to preventing the

increased production of these KPI-containing isoforms in neurons after exposure to environmental stress, with this potentially disrupted when the subcellular localization of 82-kDa ChAT is altered in aging, MCI or AD (Gill *et al.* 2007). It is important to note that the KPI-containing APP mRNA isoform is alternatively spliced to include exon 7 (Sandbrink *et al.* 1994), while 82-kDa ChAT and SATB1 bind to a region in intron 13. While a linear genomic relationship between these two regions is unlikely, it is possible that SATB1/82-kDa ChAT-mediated loops could bring these regions close together. It will be important for future studies to understand how chromatin may be organized in these regions, in order to elucidate how the interaction of SATB1 and 82-kDa ChAT may influence the steady-state mRNA levels of APP-KPI.

Though preliminary, the mass spectrometry results exploring proteins that may interact with 82-kDa ChAT provide valuable insight into the potential roles for the protein at chromatin. For example, an interaction with SMC1A may further support the hypothesis that 82-kDa ChAT associates with centromere and peri-centromere regions, as discussed above. It is interesting that 82-kDa ChAT could associate with many RNA splicing, spliceosome, and RNA transport proteins. RNA splicing occurs both temporally and spatially with transcription, and is regulated with RNA and spliceosome-binding proteins (Reviewed by Braunschweig *et al.* 2013). If 82-kDa ChAT associates with chromatin near spliceosomes, it could alter how pre-mRNAs are processed. Alternatively, changes to chromatin looping could alter how the transcript is produced. This could provide one potential explanation for the reduction in the APP-KPI isoform in 82-kDa ChAT-expressing cells after cells are exposure to A β . The 82-kDa ChAT protein and SATB1 protein are only associated with the APP gene after A β -exposure, and the resulting chromatin structural changes could restrict long-range access to the KPI-specific exon 7. Further, the nuclear spliceosome complex is anchored to the nuclear matrix (Bisotto *et al.* 1995; Coelho *et al.* 2015), and thus the 82-kDa ChAT association with RNA splicing proteins may be a result of an interaction with the nuclear matrix protein Matrin3 found in our mass spectrometry screen. Matrin3 has is involved in the regulation of alternative splicing (Coelho *et al.* 2015), and was found by co-immunoprecipitation with 82-kDa ChAT by our laboratory (unpublished data). If 82-kDa ChAT is constitutively associated with Matrin3 it may not only explain interactions with the

spliceosome, but also possibly the interaction of 82-kDa ChAT with S/MARs. Finally, 82-kDa ChAT and/or SATB1-mediated looping changes could alter mRNA movement through the nuclear pore. Genes associated with the lamina-associated domains (LADs) that are localized near nuclear pores are often euchromatic to facilitate transcriptional activation and rapid mRNA transport out of the nucleus (Brickner *et al.* 2012). If 82-kDa ChAT is restricting access to the nuclear pore via changes in chromatin looping, this could also explain how APP-KPI mRNA levels are altered in this model.

An interesting finding from the mass spectrometry data was the identification of HSP70/HSC70 after cells were exposed to A β . HSP70 and HSC70 are both important for the identification of incorrectly folded proteins, and either facilitates their refolding or directs them to the proteasome for degradation (Lüders *et al.* 2000; Wegele *et al.* 2004). This is an important observation as both 69-kDa and 82-kDa ChAT have abnormally high cysteine residue contents (3.2% compared to the 2.26% present in most mammalian proteins [Miseta and Csutora 2000]), and cysteines are sensitive to oxidation by reactive oxygen species (Davies 2016; Fujii *et al.* 2016). Cell exposure to A β can lead to oxidation of proteins (reviewed in Butterfield 2002), oxidative stress can result in protein misfolding, dysfunction, and the induction of the heat-shock response (Kalmar and Greensmith 2009; reviewed in Pisoschi and Pop 2015), and our lab has previously demonstrated that 69-kDa ChAT can be ubiquitinated and targeted for proteosomal degradation (Morey *et al.* 2016). Combined with the finding that 82-kDa ChAT can be found in an insoluble protein fraction following cell exposure to A β , these observations lead to an interesting hypothesis that a portion of 82-kDa ChAT could be oxidized and misfolded following A β -exposure of cells, and then directed to the proteasome via the heat-shock family of chaperones.

The data presented in this chapter demonstrates that 82-kDa ChAT participates in, and is required for, the binding of S/MARs to the nuclear matrix in human neural cells after acute exposure to oligomeric A β ₁₋₄₂. Together with the findings from the first objective, we suggest a model whereby 82-kDa ChAT is constitutively associated with chromatin, but is brought to SATB1 anchored S/MARs after cells are treated with A β (**Fig. 3-18**). These data support two separate hypotheses for the role of 82-kDa ChAT at

chromatin, whether at SATB1 anchored S/MARs or on other regions. First, 82-kDa ChAT may be altering pre-mRNA processing by interacting with the spliceosome. Evidence for this hypothesis includes 82-kDa ChAT mass spectrometry associations with RNA splicing, transport and spliceosome proteins and changes to the APP-KPI mRNA isoform due to A β -induced 82-kDa ChAT/SATB1 *APP* gene association. Given that 82-kDa ChAT has features of chromatin organizers, one possibility is that 82-kDa ChAT associations with chromatin either restrict or allow access to specific exons for transcription. An interaction with the nuclear matrix protein Matrin3 could also help facilitate the interaction with the spliceosome. Both the potential interaction with Matrin3 and possible involvement with the spliceosome require further investigation. Alternatively, or perhaps in addition to alternative RNA splicing, 82-kDa ChAT could be part of a complex with transcription factors (TFs), likely resulting in locus-dependent transcriptional activation and/or repression. DREME motif analysis suggests that 82-kDa ChAT and SATB1 are part of a multi-protein complex, with NFAT one possible TF involved. Overall, our data suggest that cholinergic neurons can have an epigenetic response to A β -exposure, and given that the nuclear levels of 82-kDa ChAT decline with increasing age and the onset of cognitive impairment (Gill *et al.* 2007), the loss of this epigenetic response may have implications for the onset or progression of MCI and AD.

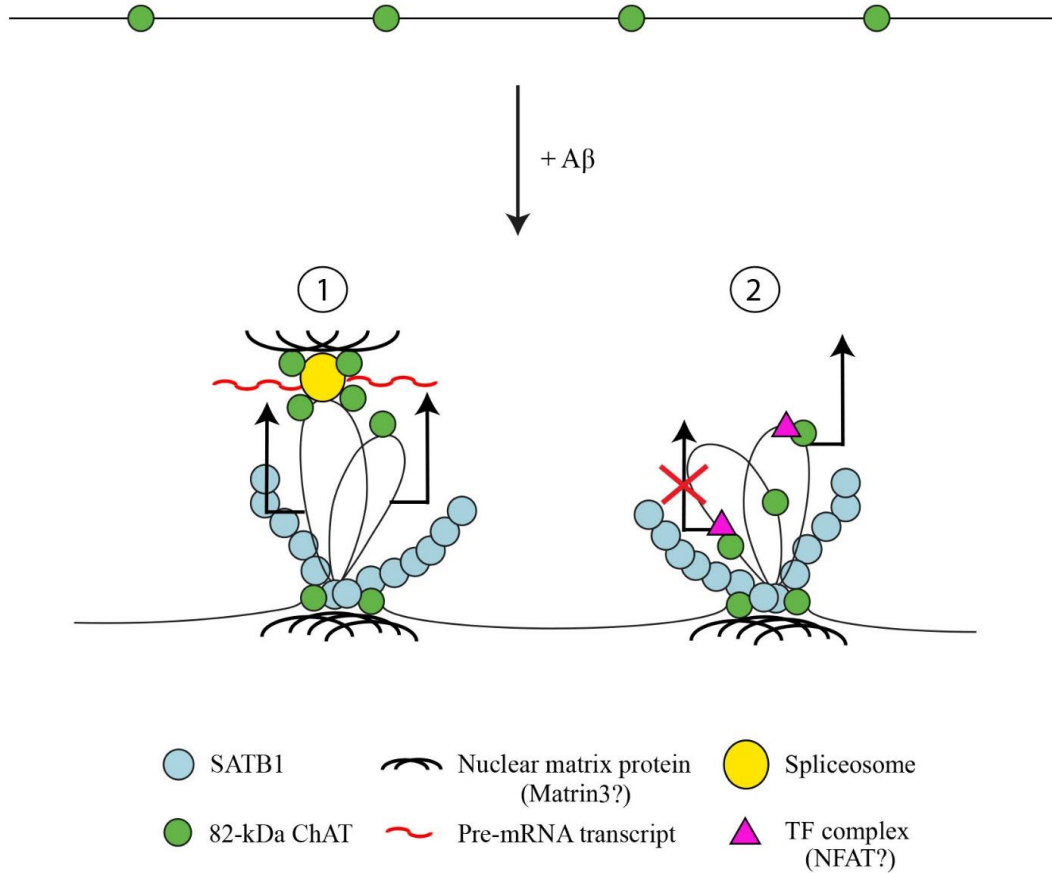


Figure 3-18. Model for 82-kDa ChAT and SATB1 chromatin association in SH-SY5Y cells.

82-kDa ChAT is constitutively associated with DNA, but is brought to SATB1 anchored S/MARs after exposure to oligomeric AB1-42. 82-kDa ChAT interacts with chromatin and the nuclear matrix, possibly through Matrin3. Through these interactions, 82-kDa ChAT may alter pre-mRNA processing/splicing via an interaction with the spliceosome, and/or alter transcriptional activation as part of a multi-protein TF complex. DREME motif analysis suggests that NFAT may be one of these TFs. See discussion for more detail.

3.5 References

- Ahmad KA, Clement MV, Pervaiz S (2003) Pro-oxidant activity of low doses of resveratrol inhibits hydrogen peroxide-induced apoptosis. *Ann N Y Acad Sci*, 1010: 365-373.
- Albers S, Inthathirath F, Gill SK, Winick-Ng W, Jaworski E, Wong DY, Gros R, Rylett RJ (2014) Nuclear 82-kDa choline acetyltransferase decreases amyloidogenic APP metabolism in neurons from APP/PS1 transgenic mice. *Neurobiol Dis*, 69: 32-42.
- Ankerst M, Breunig MM, Kriegel H, Sander J (1999) OPTICS: ordering points to identify the clustering structure in *Proceedings of the 1999 ACM SIGMOD international conference on Management of data- SIGMOD '99* (eds. Delis A. *et al.*) 49–60 (ACM Press).
- Bisotto S, Lauriault P, Duval M, Vincent M (1995) Colocalization of a high molecular mass phosphoprotein of the nuclear matrix (p255) with spliceosomes. *J Cell Sci*, 108: 1873-1882.
- Boyne LJ, Fischer I, Shea TB (1996) Role of vimentin in early stages of neuritogenesis in cultured hippocampal neurons. *Int J Dev Neurosci*, 14: 739-748.
- Bradford MM (1976) A rapid and sensitive method for the quantitation of microgram quantities of protein utilizing the principle of protein-dye binding. *Anal Biochem*, 72: 248-254.
- Braunschweig U, Gueroussov S, Plocik AM, Graveley BR, Blencowe BJ (2013) Dynamic integration of splicing within gene regulatory pathways. *Cell*, 152: 1252-1269.
- Brickner DG, Ahmed S, Meldi L, Thompson A, Light W, Young M, Hickman TL, Chu F, Fabre E, Brickner JH (2012) Transcription factor binding to a DNA zip code

controls interchromosomal clustering at the nuclear periphery. *Dev Cell*, 22: 1234-1246.

Brunet A, Sweeney LB, Sturgill JF, Chua KF, Greer PL, Lin Y, Tran H, Ross SE, Mostoslavsky R, Cohen HY, Hu LS, Cheng HL, Jedrychowski MP, Gygi SP, Sinclair DA, Alt FW, Greenberg ME (2004) Stress-dependent regulation of FOXO transcription factors by the SIRT1 deacetylase. *Science*, 303: 2011-2015.

Butterfield DA (2002) Amyloid beta-peptide (1-42)-induced oxidative stress and neurotoxicity: implications for neurodegeneration in Alzheimer's disease brain. A review. *Free Radic Res*, 36: 1307-1313.

Cai S, Han HJ, Kohwi-Shigematsu T (2003) Tissue-specific nuclear architecture and gene expression regulated by SATB1. *Nat Genet*, 34: 42-51.

Caetano FA, Dirk BS, Tam JH, Cavanagh PC, Goiko M, Ferguson SS, Pasternak SH, Dikeakos JD, de Bruyn JR, Heit B (2015) MIiSR: Molecular Interactions in Super-Resolution Imaging Enables the Analysis of Protein Interactions, Dynamics and Formation of Multi-protein Structures. *PLoS Comput Biol*, 11: e1004634.

Chong ZZ, Maiese K (2008) Enhanced tolerance against early and late apoptotic oxidative stress in mammalian neurons through nicotinamidase and sirtuin mediated pathways. *Curr Neurovasc Res*, 5: 159-170.

Coelho MB, Attig J, Bellora N, König J, Hallegger M, Kayikci M, Eyraş E, Ule J, Smith CW (2015) Nuclear matrix protein Matrin3 regulates alternative splicing and forms overlapping regulatory networks with PTB. *EMBO J*, 34: 653-658.

Cosker KE, Fenstermacher SJ, Pazyra-Murphy MF, Elliott HL, Segal RA (2016) The RNA-binding protein SFPQ orchestrates an RNA regulon to promote axon viability. *Nat Neurosci*, 19: 690-696.

- Cristobo I, Larriba MJ, de los Ríos V, García F, Muñoz A, Casal JI (2011) Proteomic analysis of $1\alpha,25$ -dihydroxyvitamin D₃ action on human colon cancer cells reveals a link to splicing regulation. *J Proteomics*, 75: 384-397.
- Davenport AM, Huber FM, Hoelz A (2014) Structural and functional analysis of human SIRT1. *J Mol Biol*, 426: 526-541.
- Davies MJ (2016) Protein oxidation and peroxidation. *Biochem J*, 463: 805-825.
- Fessing MY, Mardaryev AN, Gdula MR, Sharov AA, Sharova TY, Rapisarda V, Gordon KB, Smorodchenko AD, Poterlowicz K, Ferone G, Kohwi Y, Missero C, Kohwi-Shigematsu T, Botchkarev VA (2011) p63 regulates Satb1 to control tissue-specific chromatin remodeling during development of the epidermis. *J Cell Biol*, 194: 825-839.
- Fölling J, Bossi M, Bock H, Medda R, Wurm CA, Hein B, Jakobs S, Eggeling C, Hell SW (2008) Fluorescence nanoscopy by ground-state depletion and single-molecule return. *Nat Methods*, 5: 943-945.
- Fujii S, Sawa T, Nishida M, Ihara H, Ida T, Motohashi H, Akaike T (2016) Redox signaling regulated by an electrophilic cyclic nucleotide and reactive cysteine persulfides. *Arch Biochem Biophys*, 595: 140-146.
- Galante S, Purbey PK, Notani D, Kumar PP (2007) The third dimension of gene regulation: organization of dynamic chromatin loopscape by SATB1. *Curr Opin Genet Dev*, 17: 408-414.
- Gill SK, Ishak M, Dobransky T, Haroutunian V, Davis KL, Rylett RJ. 82-kDa choline acetyltransferase is in nuclei of cholinergic neurons in human CNS and altered in aging and Alzheimer disease. *Neurobiol Aging*, 28: 1028-1040.
- Gong F, Sun L, Sun Y (2010) A novel SATB1 binding site in the BCL2 promoter region possesses transcriptional regulatory function. *J Biomed Res*, 24: 452-459.

- Gong F, Sun L, Wang Z, Shi J, Li W, Wang S, Han X, Sun Y (2011) The BCL2 gene is regulated by a special AT-rich sequence binding protein 1-mediated long range chromosomal interaction between the promoter and the distal element located within the 3'-UTR. *Nucleic Acids Res*, 39: 4640-4652.
- Grainger RJ, Beggs JD (2005) Prp8 protein: at the heart of the spliceosome. *RNA*, 11: 533-557.
- Guenatri M, Bailly D, Maison C, Almouzni G (2004) Mouse centric and pericentric satellite repeats form distinct functional heterochromatin. *J Cell Biol*, 166: 493-505.
- Guo X, Wu X, Ren L, Liu G, Li L (2011) Epigenetic mechanisms of amyloid- β production in anisomycin-treated SH-SY5Y cells. *Neuroscience*, 194: 272-281.
- Hashemi SH, Li JY, Ahlman H, Dahlström A (2003) SSR2(a) receptor expression and adrenergic/cholinergic characteristics in differentiated SH-SY5Y cells. *Neurochem Res*, 28: 449-460.
- He Y, Smith R (2009) Nuclear functions of heterogeneous nuclear ribonucleoproteins A/B. *Cell Mol Life Sci*, 66: 1239-1256.
- Heintzmann R, Jovin TM, Cremer C (2002) Saturated patterned excitation microscopy - a concept for optical resolution improvement. *J Opt Soc Am A Opt Image Sci Vis*, 19: 1599-1609.
- Hirano T (2002) The ABCs of SMC proteins: two-armed ATPases for chromosome condensation, cohesion, and repair. *Genes Dev*, 16: 399-414.
- Jessberger R (2002) The many functions of SMC proteins in chromosome dynamics. *Nat Rev Mol Cell Biol*, 3: 767-778.
- Junier I, Dale RK, Hou C, Képès F, Dean A (2012) CTCF-mediated transcriptional regulation through cell type-specific chromosome organization in the β -globin locus. *Nucleic Acids Res*, 40: 7718-7727.

- Kalmar B, Greensmith L (2009) Induction of heat shock proteins for protection against oxidative stress. *Adv Drug Deliv Rev*, 61: 310-318.
- Karim S, Mirza Z, Ansari SA, Rasool M, Iqbal Z, Sohrab SS, Kamal MA, Abuzenadah AM, Al-Qahtani MH (2014) Transcriptomics study of neurodegenerative disease: emphasis on synaptic dysfunction mechanism in Alzheimer's disease. *CNS Neurol Disord Drug Targets*, 13: 1202-1212. Abstract available only.
- Kernohan KD, Vernimmen D, Gloor GB, Bérubé NG (2014) Analysis of neonatal brain lacking ATRX or MeCP2 reveals changes in nucleosome density, CTCF binding and chromatin looping. *Nucleic Acids Res*, 42: 8356-8368.
- Knott GJ, Bond CS, Fox AH (2016) The DBHS proteins SFPQ, NONO and PSPC1: a multipurpose molecular scaffold. *Nucleic Acids Res*, 44: 3989-4004.
- Kumar PP, Bischof O, Purbey PK, Notani D, Urlaub H, Dejean A, Galande S (2007) Functional interaction between PML and SATB1 regulates chromatin-loop architecture and transcription of the MHC class I locus. *Nat Cell Biol*, 9: 45-56.
- Lagouge M, Argmann C, Gerhart-Hines Z, Meziane H, Lerin C, Daussin F, Messadeq N, Milne J, Lambert P, Elliott P, Geny B, Laakso M, Puigserver P, Auwerx J (2006) Resveratrol improves mitochondrial function and protects against metabolic disease by activating SIRT1 and PGC-1 α . *Cell*, 127: 1109-1122.
- Larcher JC, Gasmi L, Viranaïcken W, Eddé B, Bernard R, Ginzburg I, Denoulet P (2004) Ilf3 and NF90 associate with the axonal targeting element of Tau mRNA. *FASEB J*, 18: 1761-1763.
- Law MJ, Lower KM, Voon HP, Hughes JR, Garrick D, Viprakasit V, Mitson M, De Gobbi M, Marra M, Morris A, Abbott A, Wilder SP, Taylor S, Santos GM, Cross J, Ayyub H, Jones S, Ragoussis J, Rhodes D, Dunham I, Higgs DR, Gibbons RJ (2010) ATR-X syndrome protein targets tandem repeats and influences allele-specific expression in a size-dependent manner. *Cell*, 143: 367-378.

- Levin EC, Acharya NK, Sedeyn JC, Venkataraman V, D'Andrea MR, Wang HY, Nagele RG (2009) Neuronal expression of vimentin in the Alzheimer's disease brain may be part of a generalized dendritic damage-response mechanism. *Brain Res*, 1298: 194-207.
- Levy MA, Kernohan KD, Jiang Y, Bérubé NG (2015) ATRX promotes gene expression by facilitating transcriptional elongation through guanine-rich coding regions. *Hum Mol Genet*, 24: 1824-1835.
- Li K, Cai R, Dai BB, Zhang XQ, Wang HJ, Ge SF, Xu WR, Lu J (2007) SATB1 regulates SPARC expression in K562 cell line through binding to a specific sequence in the third intron. *Biochem Biophys Res Commun*, 356: 6-12.
- Liu T, Liu PY, Marshall GM (2009) The critical role of the class III histone deacetylase SIRT1 in cancer. *Cancer Res*, 69: 1702-1705.
- Lüders J, Demand J, Höhfeld J (2000) The ubiquitin-related BAG-1 provides a link between the molecular chaperones Hsc70/Hsp70 and the proteasome. *J Biol Chem*, 275: 4613-4617.
- McCloskey A, Taniguchi I, Shinmyozu K, Ohno M (2012) hnRNP C tetramer measures RNA length to classify RNA polymerase II transcripts for export. *Science*, 335: 1643-1646.
- McShea A, Harris PL, Webster KR, Wahl AF, Smith MA (1997) Abnormal expression of the cell cycle regulators P16 and CDK4 in Alzheimer's disease. *Am J Pathol*, 150: 1933-1939.
- Miseta A, Csutora P (2000) Relationship Between the Occurrence of Cysteine in Proteins and the Complexity of Organisms. *Mol Biol Evol*, 17: 1232-1239.
- Moir RD, Lynch T, Bush AI, Whyte S, Henry A, Portbury S, Multhaup G, Small DH, Tanzi RE, Beyreuther K, Masters CL (1998) Relative increase in Alzheimer's disease of soluble forms of cerebral Abeta amyloid protein precursor containing the Kunitz protease inhibitory domain. *J Biol Chem*, 273: 5013-5019.

- Morey TM, Albers S, Shilton BH, Rylett RJ (2016) Enhanced ubiquitination and proteasomal degradation of catalytically deficient human choline acetyltransferase mutants. *J Neurochem*, 137: 630-646.
- Nagy Z, Esiri MM, Smith AD (1997) Expression of cell division markers in the hippocampus in Alzheimer's disease and other neurodegenerative conditions. *Acta Neuropathol*, 93: 294-300.
- Nakano M, Cardinale S, Noskov VN, Gassmann R, Vagnarelli P, Kandels-Lewis S, Larionov V, Earnshaw WC, Masumoto H (2008) Inactivation of a human kinetochore by specific targeting of chromatin modifiers. *Dev Cell*, 14: 507-522.
- Nix DA, Courdy SJ, Boucher KM (2008) Empirical methods for controlling false positives and estimating confidence in ChIP-Seq peaks. *BMC Bioinformatics*, 9: 523.
- Pathak RU, Srinivasan A, Mishra RK (2014) Genome-wide mapping of matrix attachment regions in *Drosophila melanogaster*. *BMC Genomics*, 15: 1022.
- Peck B, Chen CY, Ho KK, Di Fruscia P, Myatt SS, Coombes RC, Fuchter MJ, Hsiao CD, Lam EW (2010) SIRT inhibitors induce cell death and p53 acetylation through targeting both SIRT1 and SIRT2. *Mol Cancer Ther*, 9: 844-855.
- Pepke S, Wold B, Mortazavi A (2009) Computation for ChIP-seq and RNA-seq studies. *Nat Methods*, 6: S22-32.
- Pisoschi AM, Pop A (2015) The role of antioxidants in the chemistry of oxidative stress: A review. *Eur J Med Chem*, 97: 55-74.
- Portal MM, Pavet V, Erb C, Gronemeyer H (2015) Human cells contain natural double-stranded RNAs with potential regulatory functions. *Nat Struct Mol Biol*, 22: 89-97.

- Preece P, Virley DJ, Costandi M, Coombes R, Moss SJ, Mudge AW, Jazin E, Cairns NJ (2004) Amyloid precursor protein mRNA levels in Alzheimer's disease brain. *Brain Res Mol Brain Res*, 122: 1-9.
- Rockenstein EM, McConlogue L, Tan H, Power M, Masliah E, Mucke L (1995) Levels and alternative splicing of amyloid beta protein precursor (APP) transcripts in brains of APP transgenic mice and humans with Alzheimer's disease. *J Biol Chem*, 270: 28257-28267.
- Roemer K, Mahyar-Roemer M (2007) The basis for the chemopreventive action of resveratrol. *Drugs Today*, 38: 571-580.
- Sandbrink R, Masters CL, Beyreuther K (1994) APP gene family: unique age-associated changes in splicing of Alzheimer's betaA4-amyloid protein precursor. *Neurobiol Dis*, 1: 13-24.
- Salton M, Elkon R, Borodina T, Davydov A, Yaspo ML, Halperin E, Shiloh Y (2011) Matrin 3 binds and stabilizes mRNA. *PLoS One*, 6: e23882.
- Singh GB, Kramer JA, Krawetz SA (1997) Mathematical model to predict regions of chromatin attachment to the nuclear matrix. *Nucleic Acids Res*, 25: 1419-1425.
- Spremo-Potparević B, Zivković L, Djelić N, Plečas-Solarović B, Smith MA, Bajić V (2008) Premature centromere division of the X chromosome in neurons in Alzheimer's disease. *J Neurochem*, 106: 2218-2223.
- Stümel W, Peh BK, Tan YC, Nayagam VM, Wang X, Salto-Tellez M, Ni B, Entzeroth M, Wood J (2007) Function of the SIRT1 protein deacetylase in cancer. *Biotechnol J*, 2: 1360-1368.
- Tanno M, Kuno A, Yano T, Miura T, Hisahara S, Ishikawa S, Shimamoto K, Horio Y (2010) Induction of manganese superoxide dismutase by nuclear translocation and activation of SIRT1 promotes cell survival in chronic heart failure. *J Biol Chem*, 285: 8375-8382.

- Teytelman L, Thurtle DM, Rine J, van Oudenaarden A (2013) Highly expressed loci are vulnerable to misleading ChIP localization of multiple unrelated proteins. *Proc Natl Acad Sci U S A*, 110: 18602-18607.
- Tuteja N, Tuteja R, Ochem A, Taneja P, Huang NW, Simoncsits A, Susic S, Rahman K, Marusic L, Chen J, *et al.* (1994) Human DNA helicase II: a novel DNA unwinding enzyme identified as the Ku autoantigen. *EMBO J*, 13: 4991-5001.
- Wegele H, Müller L, Buchner J (2004) Hsp70 and Hsp90--a relay team for protein folding. *Rev Physiol Biochem Pharmacol*, 151: 1-44.
- Wu Y, Li X, Zhu JX, Xie W, Le W, Fan Z, Jankovic J, Pan T (2011) Resveratrol-activated AMPK/SIRT1/autophagy in cellular models of Parkinson's disease. *Neurosignals*, 19: 163-174.
- Xue Z, Lv X, Song W, Wang X, Zhao GN, Wang WT, Xiong J, Mao BB, Yu W, Yang B, Wu J, Zhou LQ, Hao DL, Dong WJ, Liu DP, Liang CC (2012) SIRT1 deacetylates SATB1 to facilitate MAR HS2-MAR ϵ interaction and promote ϵ -globin expression. *Nucleic Acids Res*, 40: 4804-4815.
- Yang Y, Wang Z, Sun L, Shao L, Yang N, Yu D, Zhang X, Han X, Sun Y (2015) SATB1 Mediates Long-Range Chromatin Interactions: A Dual Regulator of Anti-Apoptotic BCL2 and Pro-Apoptotic NOXA Genes. *PLoS One*, 10: e0139170.
- Yasui D, Miyano M, Cai S, Varga-Weisz P, Kohwi-Shigematsu T (2002) SATB1 targets chromatin remodelling to regulate genes over long distances. *Nature*, 419: 641-645.
- Ye J, Liu Z, Wei J, Lu L, Huang Y, Luo L, Xie H (2013) Protective effect of SIRT1 on toxicity of microglial-derived factors induced by LPS to PC12 cells via the p53-caspase-3-dependent apoptotic pathway. *Neurosci Lett*, 553: 72-77.
- Zeitz M, Malyavantham K, Seifert B, Berezney R (2009) Matrin 3: Chromosomal Distribution and Protein Interactions. *J Cell Biochem*, 108: 125-133.

Zhang S, Grosse F (1997) Domain structure of human nuclear DNA helicase II (RNA helicase A). *J Biol Chem*, 272: 11487-11494.

Zhao H, Zhu X, Wang K, Gent JI, Zhang W, Dawe RK, Jiang J (2015) Gene Expression and Chromatin Modifications Associated with Maize Centromeres. *G3*, 6: 183-192.

Chapter 4

4 Objective III- A role for nuclear 82-kDa ChAT in cholinergic synapse development

Figure 4-1 was produced in collaboration with Mrs. Jennifer Winick-Ng, using the statistical programming software SAS.

Figure 4-11 - data collection was produced in collaboration with Ms. Heather Rotz.

4.1 Introduction and Rationale

We previously demonstrated that 82-kDa choline acetyltransferase (82-kDa ChAT) protein and special AT-rich sequence binding protein 1 (SATB1) are associated with scaffolding/matrix attachment regions after neuronal cells were exposed to A β (Winick-Ng *et al.* 2016). Among other outcomes, using DREME motif analysis of chromatin immunoprecipitation sequencing (ChIP-seq) peaks associated with both 82-kDa ChAT and SATB1 in SH-SY5Y human neuroblastoma cells, we screened hundreds of known transcription factors (TF) for motifs that may be enriched in this dataset (Kheradpour and Kellis 2014). This results from this screen revealed motifs that had homology to nuclear factor of activated T cells (NFAT) DNA-binding motifs (**see Fig 2-14 in Chapter 2; Fig 2-4 and Fig 3-8 in Chapters 2 and 3, respectively**). NFAT is a ubiquitously expressed TF that has been well characterized for the regulation of cytokine genes during T-cell activation (reviewed by Macian 2005). NFAT has also been shown to regulate T-cell development (Macian 2005; Benita *et al.* 2010), oncogenic growth in pancreatic cancer (König *et al.* 2010), and the development and growth of many cell types, including cardiac muscle cells (Chen and Cao 2009), skeletal muscle cells (Delling *et al.* 2000), pancreatic islet cells (Heit *et al.* 2006), and epidermal cells during embryonic development (Mammucari *et al.* 2005).

In neurons, NFAT has an important role in synapse development and maintenance. NFAT null mice have impairments in axonal guidance and pathfinding (Graef *et al.* 2003; Nguyen and Di Giovanni 2008), as well as *in vitro* brain-derived neurotrophic factor (BDNF)-dependent neurite outgrowth (Groth and Mermelstein 2003). NFAT has also been shown to reduce pre-synaptic synaptic boutons and neurotransmitter release in *Drosophila* motor neurons (Freeman *et al.* 2011). Further, NFAT TFs are involved in cellular responses to neurotrophins as it binds to the inositol 1,4,5-triphosphate receptor type 1 (*IP3R1*) promoter upon BDNF stimulation of cells, and is thus important for release of intracellular stores of Ca²⁺ and neuron signaling following stimulation (Groth and Mermelstein 2003). NFAT was also demonstrated to increase *COX2* expression in cultured spinal neurons (Groth *et al.* 2007). This is noteworthy

considering elevated Cyclooxygenase-2 (COX-2) can lead to enhanced neurotransmission and long-term potentiation (Reviewed in Yang and Chen 2008).

Importantly, elevated NFAT levels may also have a role in the synapse degeneration seen early in Alzheimer's disease (AD) pathology. Soluble oligomeric A β -induced Ca²⁺ entry has been shown to hyper-activate the Ca²⁺/calmodulin dependent protein phosphatase calcineurin, which dephosphorylates NFAT thereby revealing its nuclear import sequence (Wu *et al.* 2010). NFAT then enters the nucleus and, in combination with other TFs (e.g. activator protein 1 [AP-1], nuclear factor kappa-light-chain-enhancer of activated B cells [Nf- κ B], BDNF), alters transcription (Macián *et al.* 2001; Groth and Mermelstein 2003; Fisher *et al.* 2006; Liu *et al.* 2012). A β -induced constitutive NFAT activation results in dendritic spine density reductions, simplification and degeneration, eventually leading to activation of the apoptotic pathway (Agostinho *et al.* 2008; Wu *et al.* 2010). There are also isoform specific changes to NFAT nuclear levels in both mild cognitive impairment (MCI) and AD patients; NFAT1 is increased in MCI but decreased in AD, NFAT3 is decreased in MCI and increased in AD, while NFAT2 levels have no observed changes in either MCI or AD (reviewed in Abdul *et al.* 2010). Interestingly, the partial NFAT ChIP-seq motifs found for 82-kDa ChAT and SATB1 have homology with NFAT1 and NFAT2.

The NFAT TFs have a role in synapse formation but may also be dysregulated during AD. Therefore, in this chapter we explore the hypothesis that 82-kDa ChAT has a role in changes to the expression of synapse and membrane related genes that have high NFAT DNA binding site enrichment. We test whether there are changes in expression for genes with 82-kDa ChAT peaks that have high NFAT DNA binding compared to empty vector when treated with either vehicle or oligomeric A β ₁₋₄₂. We further investigate whether this correlates to differences in protein expression, and test downstream phenotypic and morphological consequences associated with these changes.

4.2 Methods

Cell culture and conditioned media experiments

SH-SY5Y cells from American Type Culture Collection (Manassus, VA) that stably express either 82-kDa ChAT or empty vector (Albers *et al.* 2014) were grown in Dulbecco's modified Eagle medium (DMEM) containing 8% fetal bovine serum (FBS) and differentiated using 10 μ M all-trans-retinoic acid for 3 days, which produces substantial morphological and biochemical cholinergic differentiation of cells (Hashemi *et al.* 2003). A β oligomers were prepared as described (Chapter 2; Stine *et al.* 2003) from lyophilized A β ₁₋₄₂ or the reverse peptide purchased from rPeptide (Bogart, GA, USA). Cells were treated with either 100 nM oligomeric A β ₁₋₄₂, F12 media (vehicle) or recombinant human neuregulin 1 (NRG1) extracellular peptide (R&D Systems, Minneapolis, MN, USA) in PBS containing 0.02% bovine serum albumin (BSA) at the times and concentrations indicated.

In some experiments, cells expressing 82-kDa ChAT or empty vector were cultured on 100 mm dishes for at least 4 days in retinoic acid at a density of 1.5×10^6 cells/plate, with culture medium changed every 48 h. At 96, 144 and 192 h following plating, the culture media was removed from these cells and was used as "conditioned medium". To test the effects of feeding cells with conditioned medium, SH-SY5Y cells that were expressing either 82-kDa ChAT or empty vector were divided into groups, then culture media was removed from the cells and cells were fed with either fresh DMEM containing 8% fetal bovine serum (FBS) and 10 μ M all-trans-retinoic acid, or conditioned media from vector-expressing cells or conditioned media from 82-kDa ChAT-expressing cells to which 10 μ M all-trans-retinoic acid was added. For protein phosphorylation experiments, 4 mL of either fresh or conditioned media was added to the receiving cells for the times indicated. For neurite outgrowth experiments, 3 mL of fresh or conditioned media was added to the receiving cells for the times indicated. To test the role of NRG1 released from cells on outcome measures, 5 μ g/mL anti-NRG1 antibody was added to

fresh media for 1 h with rotation at room temperature (RT) prior to these media being added to cells. As a control, some media was treated with 5 µg/mL anti-FLAG antibody.

Antibodies

Anti-NRG1 (sc-33269), anti-neurologin 1 (NLGN1; sc-50393), anti-β-actin (sc-1616-R) and anti-receptor tyrosine-protein kinase erbB-4 (ERBB4; sc-8050) antibodies were from Santa Cruz Biotechnology (Dallas, TX, USA); Anti-metabotropic glutamate receptor 5 (mGlu5; ab76316) and anti-phospho(Y1284) ERBB4 (p-ERBB4) antibodies were from Abcam Inc. (Toronto, ON, Canada). Anti-FLAG (F7425) antibody was from Sigma-Aldrich (Oakville, ON, Canada).

Reverse transcription (RT) real-time PCR (qPCR)

For reverse transcription-qPCR (RT-qPCR), RNA was isolated from cells expressing either 82-kDa ChAT or empty vector as described in Chapter 3 and previously (Albers *et al.* 2014). PCR amplification primers (**Table 4-1**) and subsequent quantification was also carried out as described in Chapter 3 and previously (Albers *et al.* 2014).

Cell lysis and immunoblotting

Total cellular protein was obtained by lysing cells in radioimmunoprecipitation (RIPA) buffer as described in Chapter 3. Thirty to fifty µg of protein were separated on SDS-polyacrylamide gel electrophoresis (SDS-PAGE) gels, followed by transfer of proteins onto polyvinylidene difluoride (PVDF) membranes. Non-specific proteins were blocked in an appropriate buffer, then membranes were incubated in primary and secondary antibodies as shown in **Table 4-2**. Immunoreactive bands were visualized

using Image Lab (Version 5.0, BioRad), and band density was then determined and normalized to β -actin immunoreactivity for each sample.

For experiments testing effects of condition media, media conditioned by 82-kDa ChAT or vector-expressing SH-SY5Y cells was concentrated from 4 mL to 500 μ L by centrifugation at 4000 \times g for 60-75 min using a 3 kDa Amicon® Ultra centrifugal filter (EMD Millipore Ltd.). Concentrated media was then heated in 2x Laemmli sample buffer (126 mM Tris-HCl; pH 6.8, 20% (v/v) glycerol, 4% (w/v) SDS, 0.01% (w/v) bromophenol blue, and 5% (v/v) 2-mercaptoethanol) for 15 min at 95°C, with intermittent vortex mixing. In parallel, cells were lysed in RIPA buffer and total cellular protein isolated as above. Twenty μ L of total lysate was heated in 1x Laemmli's buffer at 95°C for 5 min. Media and cell lysate samples were separated on 16% SDS-PAGE gels, followed by immunoblotting as above.

Confocal imaging

For confocal imaging, cells were harvested as described previously, permeabilized and stained with 2.5 μ g/mL Hoechst for 5 min. Images were acquired and processed as described in Chapter 2. Following processing in ImageJ, differential contrast images were subjected to the “invert LUT” function to better visualize neurites.

Table 4-1. RT-qPCR primers used in this chapter.

Gene	Direction	Primer, 5'-3'
Human <i>NRG1</i> , variant HRG- β 1	Forward	AACTTGTTGGA ACTCCGGGC
	Reverse	AGGTTATCACCGTCCTGCTC
Human <i>ERBB4</i> , variant JM-a/CVT- 1	Forward	CACCCAAGGGTGTAACGGTC
	Reverse	GCTGCAATCAGGGGAGTTCT
Human <i>NLGN1</i>	Forward	CTTACCTGTGAAGCTTGAGGC
	Reverse	TGGGCATTGACTGCAGATTT
Human <i>NRXN1</i> , variant α 2	Forward	GGCCACATAACCCTACCCTT
	Reverse	CTTAAGCACGAAATGGTGCCG
Human <i>SHANK1</i>	Forward	CCATGACTCGGATTCGGGAG
	Reverse	CTTATGCAGTGCGGTCATGC
Human <i>DLGAP1</i> , variant 1	Forward	TCTCTCGAGTCCTTCCCGTC
	Reverse	ATGTTCAACTGCTCTGGCCG
Human <i>GRM5</i> , variant a/b	Forward	GAGCTCCTCGTCGTTGTGAA
	Reverse	CGTAACCAGGCGACTATGCT
Human <i>PLCB1</i> , variant 1	Forward	AGGATGTGCTGAATGGTGCG
	Reverse	AAGGCGAAGAGAAGCCGAG
Human <i>DLG2</i> , variant 1	Forward	ACTCCTGTGGCAGTGAAAG
	Reverse	GCTCGGTCAGTATCTTATGGC
Human <i>GAPDH</i>	Forward	TGTTGCCATCAATGACCCCTT
	Reverse	CTCCACGACGTA CTACGCG

Table 4-2. Antibody conditions for western immunoblotting.

Antibody		Buffer	Concentration
β -Actin	Block	5% Milk	--
	Primary	5% Milk	1:1000
	Secondary (rabbit)	5% Milk	1:10000
NRG1	Block	5% Horse Serum	--
	Primary	5% Horse Serum	1:200
	Secondary (goat)	5% Horse Serum	1:5000
NLGN1	Block	3% BSA	--
	Primary	3% BSA	1:1000
	Secondary (rabbit)	3% BSA	1:10000
mGlu5	Block	5% Milk	--
	Primary	5% Milk	1:2000
	Secondary (mouse)	5% Milk	1:10000
ERBB4	Block	5% BSA	--
	Primary	3% BSA	1:200
	Secondary (mouse)	3% BSA	1:10000
p-ERBB4	Block	4% BSA	--
	Primary	3% BSA	1:750
	Secondary (rabbit)	3% BSA	1:10000

NRG1 enzyme-linked immunosorbent assay (ELISA)

To detect and quantify NRG1 extracellular peptide in conditioned media collected from cells expressing either 82-kDa ChAT or empty vector, we used a DuoSet solid phase sandwich ELISA (R&D Systems) specific for human NRG1- β 1 extracellular peptide (range 125 - 4000 pg/mL), according to the manufacturer's specifications. Briefly, NRG1 capture antibody (4 μ g/mL) was added to 96-well plates and incubated overnight at RT. Blocking solution (1% BSA in PBS) was added to wells of the plate for 1 h at RT. Media samples were prepared from DMEM without FBS added, DMEM containing 8% FBS, media conditioned by cells expressing either empty vector or 82-kDa ChAT, or media samples concentrated as described above. To construct standard curves for the ELISA, recombinant NRG1 peptide was reconstituted in either PBS containing 1% BSA or the non-concentrated conditioned media samples above over the concentration range of 0.125 to 4 ng/mL. Samples were incubated on the ELISA plate for 2 h at RT, followed by the addition of NRG1 detection antibody (150 ng/mL in TBS-T containing 2% normal goat serum and 1% BSA) for 2 h at RT. Following the addition of streptavidin-HRP for 20 min at RT, NRG1 was detected using a substrate solution (1:1 mixture of H₂O₂ and tetramethylbenzidine) for 20 min. The reaction was halted using 2 N H₂SO₄, and the absorbance read at 450 nm using a Spectra Max M5 microplate reader (San Francisco, CA, USA). An additional reading was taken at 540 nm to account for background optical readings on the plate, and subtracted from the 450 nm readings. Concentrations in the media were determined by comparing optical densities (ODs) to a standard curve generated using the standards as described above.

Data Analysis

The data are presented as mean \pm SEM and analyzed as described in Chapters 2 and 3. Statistical significance was determined by one or two-way ANOVA, followed by Bonferroni's post hoc multiple comparison test. Statistically significant changes in gene expression were determined by a one-sample t-test, as indicated. For all one-sample t-

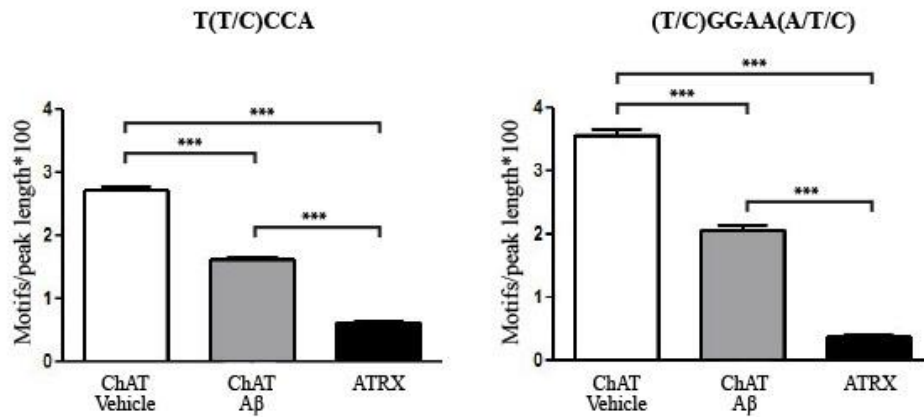
tests performed, the population mean was assumed to be equal to 1. For all measures, statistical significance was defined as $p \leq 0.05$.

4.3 Results

82-kDa ChAT associates with synapse-related genes, leading to changes in gene and protein expression

The 82-kDa ChAT protein associates with chromatin at sequences with sequence homology to NFAT binding motifs, therefore we first assessed whether there was significant enrichment for NFAT binding motifs in 82-kDa ChAT chromatin immunoprecipitation-next generation sequencing (ChIP-seq) peaks from SH-SY5Y cells that were previously treated for 4 h with either vehicle or 100 nM A β ₁₋₄₂ (NCBI GEO accession: GSE73576; Winick-Ng *et al.* 2016). As a control, we compared enrichment from 82-kDa ChAT ChIP-seq peaks to a dataset for human Alpha Thalassemia/Mental Retardation Syndrome X-Linked (ATRX) (NCBI GEO database accession number: GSE22162; Law *et al.* 2010), a protein involved in chromatin looping and enriched at tandem G-quadruplex repeats (Law *et al.* 2010; Kernohan *et al.* 2014; Levy *et al.* 2015). We first tested the NFAT binding motif T(T/C)CCA as identified by Kheradpour and Kellis (2014), and the NFAT-specific sequence (T/C)GGAA(A/T/C) (Boise *et al.* 1993; Chen *et al.* 1998; Badran *et al.* 2002) for 82-kDa ChAT or ATRX enrichment (**Fig. 4-1A**). As we determined previously, 82-kDa ChAT had average peak lengths of 192 ± 3.2 nucleotides (nt) and 132.6 ± 2.2 nt for vehicle and A β ₁₋₄₂ treatments, respectively, while ATRX had an average peak length of 483.4 ± 2.4 (Chapters 2 and 3). Therefore, we determined the number of motifs in each peak weighted by the inverse of the peak length and divided by a scaling factor of 100. For the T(T/C)CCA motif, we found that there were significantly higher motifs/peak for 82-kDa ChAT treated with either vehicle (2.7 ± 0.06) or A β ₁₋₄₂ (1.6 ± 0.04) when compared to ATRX (0.6 ± 0.004). The number of motifs/peak was also significantly higher after vehicle treatment compared to A β ₁₋₄₂. We saw a similar pattern for the (T/C)GGAA(A/T/C) motif, with 82-kDa ChAT peaks after vehicle treatment (3.6 ± 0.1) significantly higher than after A β ₁₋₄₂ treatment (2.1 ± 0.08). Again, both treatments were significantly increased compared to ATRX (0.4 ± 0.004).

A



B

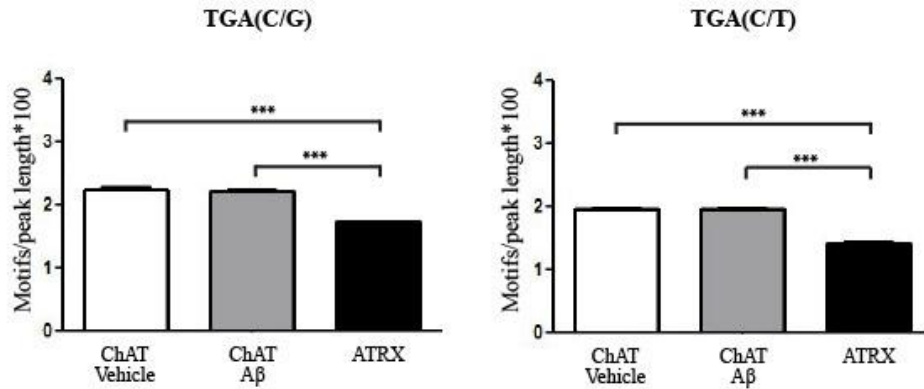


Figure 4-1. 82-kDa ChAT has significant enrichment for NFAT and c-Fos motifs.

Mean weighted NFAT (A) and c-Fos (B) DNA binding motifs/ChIP-seq peak, computed as the number of motifs/peak length*100. For NFAT motifs, SH-SY5Y cells expressing 82-kDa ChAT and treated with vehicle had significantly higher motifs/peak than 82-kDa ChAT peaks after 4 h 100 nM A β ₁₋₄₂-exposure. For both NFAT and c-Fos motifs, the number of motifs/peaks for 82-kDa ChAT after vehicle and A β ₁₋₄₂ treatment were significantly higher than for peaks for human ATRX. *** p < 0.001.

NFAT has been previously shown to associate with and bind adjacent to AP-1 TF binding sites (Macián *et al.* 2001). AP-1 is produced by the dimerization of c-Fos and c-Jun subunits (Nakabeppu *et al.* 1988; Kouzarides and Ziff 1988; Gustems *et al.* 2014), therefore we also assessed the number of motifs/peak for the c-Fos binding motifs TGA(C/G) and TGA(C/T) (Gustems *et al.* 2014; **Fig. 4-1B**). For both the TGA(C/G) and TGA(C/T) motifs, we found no significant differences in the number of motifs/peak for 82-kDa ChAT after exposure of cells to either vehicle (2.3 ± 0.03 and 2.0 ± 0.02 , respectively) or A β_{1-42} (2.2 ± 0.02 and 2.0 ± 0.02 , respectively). However, the number of motifs/peak for 82-kDa ChAT in either treatment was significantly higher than ATRX (1.7 ± 0.01 for TGA(C/G) and 1.4 ± 0.01 for TGA(C/T)). Together, these data demonstrate that 82-kDa ChAT ChIP-seq peaks are enriched for both NFAT and c-Fos motifs, with A β_{1-42} -exposure reducing the number of NFAT motifs/peak. NFAT was shown previously to be involved in axon growth and guidance, as well as synapse maturation during synapse development (Graef *et al.* 2003; Groth and Mermelstein 2003; Nguyen and Di Giovanni 2008). NFAT is also activated after neuron stimulation, and following acute exposure to A β (Groth and Mermelstein 2003; Wu *et al.* 2010). Interestingly, by gene ontology (GO), we showed that the ChIP-seq peaks for both 82-kDa ChAT and SATB1 were significantly associated with synapse and membrane related genes regardless of vehicle or A β treatment (Chapters 2 and 3). Additionally, we found significant GO enrichment for calcium-related genes ($p = 1.4E-06$, $-\log(\text{FDR}) = 2.8$) in genes that had peaks associated with both 82-kDa ChAT and special AT-rich sequence binding protein 1 (SATB1). Therefore, we determined the percentage of peaks that had the NFAT binding motif T(T/C)CCA for 82-kDa ChAT and SATB1 for all peaks, or for peaks found in genes related to synapse, membrane, or calcium regulation GO groups (**Fig. 4-2**).

For 82-kDa ChAT associated peaks, we found that 42% of all peaks had at least one motif after vehicle treatment, and 41% after A β treatment. Though there were no overall differences, we did find some interesting changes in individual GO groups. For example, for genes in the ‘calcium’ GO group, we found 32% of peaks with at least 1 motif after vehicle treatment, with this increasing to 56% after A β -exposure of cells. For the ‘synapse’ and ‘tyrosine kinase’ groups in the vehicle treated cells group, we found

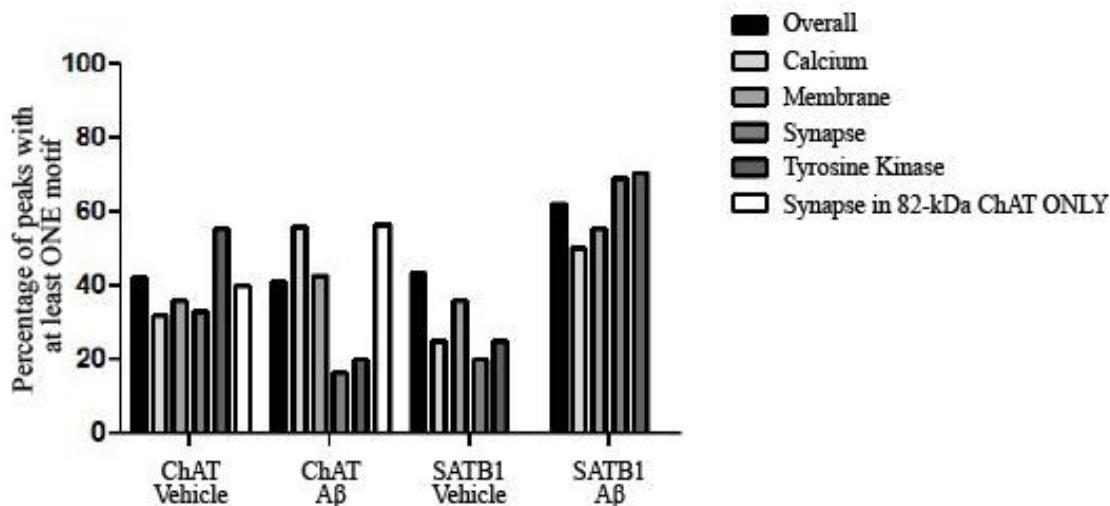


Figure 4-2. NFAT binding motifs in gene ontology groups for 82-kDa ChAT and SATB1.

Percentage of peaks with at least one NFAT motif T(T/C)CCA from different gene ontology (GO) groupings for 82-kDa ChAT and SATB1 after SH-SY5Y cells were exposed to either 4 h vehicle or 100 nM A β ₁₋₄₂. There were no differences for 82-kDa ChAT associated peaks overall, however the percentage of peaks with motifs increased after A β -exposure for peaks from calcium-related genes and synapse related genes (for genes that had 82-kDa ChAT peaks but no SATB1 peaks). For synapse related genes (that had peaks for both 82-kDa ChAT and SATB1) and tyrosine kinase related genes, the percentage of 82-kDa ChAT peaks with motifs was reduced. For SATB1 related peaks, there was an overall increase in the percentage of peaks that had motifs after cells were exposed to A β , with similar increases for each GO group.

33% and 56% of peaks with at least one motif, respectively. In contrast, following cell exposure to A β , this was reduced to 17% for synapse and 20% for tyrosine kinase, respectively. However, when we considered synapse related genes that only had peaks for 82-kDa ChAT, 40% of peaks had at least one motif after vehicle treatment with this increasing to 57% after cells were exposed to A β . For SATB1, we found that 44% of peaks had at least one T(T/C)CCA NFAT binding motif after vehicle treatment, with this increasing to 62% after treatment with A β . All of the individual GO groups tested had similar increases after A β -exposure.

Based on these observations, we decided to target synapse and calcium-related genes that had ChIP-seq peaks for 82-kDa ChAT after cells were exposed to either vehicle or A β . From this analysis, we chose 9 genes related to synapse formation and maintenance for further analysis (**Table 4-3**). *NRG1* encodes the protein neuregulin 1 (NRG1), a membrane bound protein involved in synapse development and response to neuronal stimulation of NMDA and AMPA receptors (Gerecke *et al.* 2004; Bjarnadottir *et al.* 2007; Chen *et al.* 2010; Ting *et al.* 2011). *ERBB4* encodes receptor tyrosine-protein kinase erbB-4 (ERBB4; also known as HER4), a membrane bound protein involved in signal transduction and cholinergic synapse formation (Zhu *et al.* 1995; Neddens and Buonanno 2011; Woo *et al.* 2011; Reviewed in Iwakura and Nawa 2013). *NRXN1* encodes neuroligin 1 (NRXN1), which forms a complex with neuroligin 1 (NLGN1; encoded by *NLGN1*). NRXN1 and NLGN1 anchor the pre- and post- synaptic membranes together, respectively (Craig and Kang 2007; Choi *et al.* 2011). *SHANK1* and *DLGAP1* encode SHANK and GKAP that together are part of the post-synaptic scaffolding (Tao-Cheng *et al.* 2015). Typically, this scaffolding complex is also composed of post-synaptic density protein 95 (PSD-95) (Hayashi *et al.* 2009), but PSD-93 (encoded by *DLG2*) is highly expressed in cholinergic post-synaptic scaffolding and has also been shown to complex with both SHANK and GKAP (Parker *et al.* 2004). *GRM5* encodes the metabotropic glutamate receptor 5 (mGlu5), which has been shown to promote cholinergic synapse formation during neuron development in rat neural progenitor cells (Zhao *et al.* 2014). Finally, *PLCB1* encodes phospholipase C- β 1 (PLCB1) which is involved in intracellular signaling of extracellular ligands for mGlu5

Table 4-3. Locations for 82-kDa ChAT ChIP-seq peaks for synapse-related genes.

Gene	82-kDa ChAT (Vehicle)	Number of Peaks	82-kDa ChAT (100 nM Aβ)	Number of Peaks
<i>NRG1</i>	50 kb downstream	1	Promoter, Exon 2	2
<i>ERBB4</i>	100 kb downstream	1	100 kb upstream, Intron 1	2
<i>NLGN1</i>	Intron 1 (near promoter), Intron 2	2	Intron 2, 40 kb downstream	3
<i>NRXN1</i>	Intron 3	2	Intron 5	1
<i>SHANK1</i>	--	--	15 kb downstream, 40 kb upstream	2
<i>DLGAP1</i>	Intron 5	1	Intron 4	1
<i>GRM5</i>	Intron 3	1	--	--
<i>PLCB1</i>	Intron 4	1	Intron 4	1
<i>DLG2</i>	Intron 7, Intron 8, Intron 9, 4 kb downstream	6	Intron 7	1

(Hannan *et al.* 2001; Domenici *et al.* 2003). PLC- β 1 phosphorylation results in inositol 1,4,5-trisphosphate (IP3) formation (Nash *et al.* 2002; Kammermeier and Worley 2007). IP3-mediated Ca^{2+} release has been shown to activate multiple cell signaling pathways in cholinergic neurons, including Ca^{2+} /calmodulin-dependent protein kinase (CAMK) and protein kinase C (PKC) (Shindo *et al.* 1996; Slonimsky *et al.* 2006; Nakamuta *et al.* 2011).

Based on the observed ChIP-seq interactions for 82-kDa ChAT at synapse and membrane related genes, we next tested whether there were changes in expression of genes in **Table 4-3** in SH-SY5Y cells expressing 82-kDa ChAT compared to empty vector. For each gene, we compared the expression level in cells expressing 82-kDa ChAT to cells expressing empty vector using a one-sample t-test, with an expected theoretical mean of 1 for the vector expressing cells (**Fig. 4-3**). Using this approach, we determined that *NRG1* (1.7 ± 0.2 fold), *NLGNI* (1.4 ± 0.2), *NRXNI* (1.5 ± 0.1), *SHANK1* (1.4 ± 0.1), and *GRM5* (1.9 ± 0.2) all were significantly increased in 82-kDa ChAT expressing cells compared to cells expressing an empty vector. We found no significant differences for *ERBB4* (1.1 ± 0.2), *DLGAP1* (1.2 ± 0.1), *PLCB1* (1.2 ± 0.2), or *DLG2* (1.6 ± 0.4).

We also observed ChIP-seq peak changes for 82-kDa ChAT after 4 h exposure of cells to 100 nM $\text{A}\beta_{1-42}$, therefore tested whether there were also $\text{A}\beta_{1-42}$ -induced changes in expression for the genes in **Table 4-3** in cells expressing 82-kDa ChAT compared to empty vector (**Fig. 4-4**). Compared to vehicle treatment, there were no changes in expression of any of the genes tested in either vector or 82-kDa ChAT expressing cells after 1 h exposure to 100 nM $\text{A}\beta_{1-42}$. In cells expressing 82-kDa ChAT and treated for 2 h with $\text{A}\beta_{1-42}$, we observed significant increases in gene expression for *NLGNI* (1.7 ± 0.1 fold), *NRXNI* (1.9 ± 0.1) and *PLCB1* (2.8 ± 0.3) compared to vector expressing cells (0.8 ± 0.1 , 1.0 ± 0.04 and 0.9 ± 0.1 , respectively). These changes were no longer significant after 4 h treatment with $\text{A}\beta_{1-42}$, but after 8 h of treatment, *GRM5* (1.3 ± 0.1) and *DLG2* (1.5 ± 0.2) were significantly increased in 82-kDa ChAT expressing cells compared to vector cells (0.9 ± 0.05 , 0.7 ± 0.1 , respectively). Finally, we determined that in 82-kDa

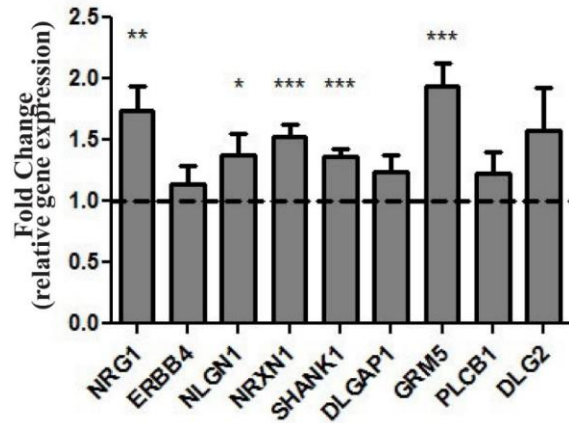


Figure 4-3. 82-kDa ChAT expression in SH-SY5Y cells alters gene expression of synapse related genes.

Steady-state mRNA expression of synapse related genes in 82-kDa ChAT expressing cells compared to vector expressing cells. Data are presented as fold-enrichment compared to reference (*GAPDH*) mRNA levels and vector expressing cells (dashed-line). 82-kDa ChAT expressing cells have higher steady-state mRNA levels for *NRG1*, *NLGN1*, *NRXN1*, *SHANK1*, and *GRM5*. * $p < 0.05$, ** $p < 0.01$, *** $p < 0.001$ (one-sample t-test with theoretical mean = 1), $n = 8$.

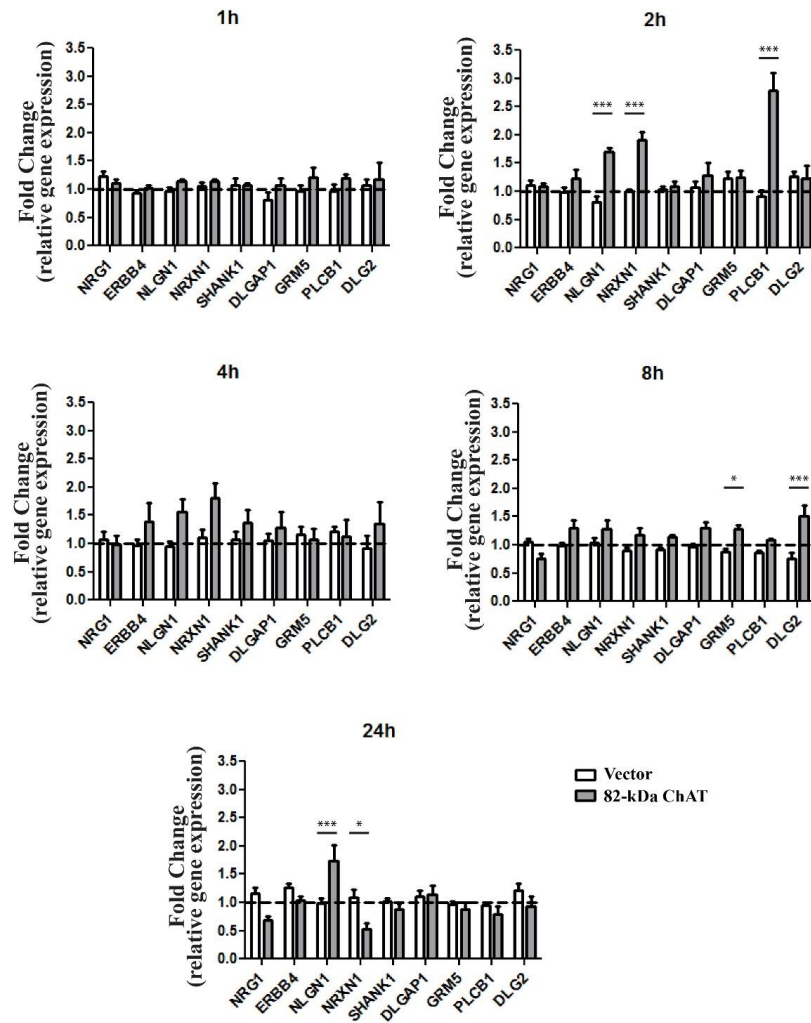


Figure 4-4. 82-kDa ChAT expression in SH-SY5Y cells alters gene expression of synapse related genes after exposure to oligomeric $A\beta_{1-42}$.

Steady-state mRNA expression of synapse related genes in 82-kDa ChAT or vector-expressing SH-SY5Y cells after exposure to 100 nM oligomeric $A\beta_{1-42}$ for various time points. Data are presented as fold change compared to *GAPDH* and vehicle-treated cells (represented by the dashed-line). There were no changes in mRNA levels after 1 h, however *NLGN1*, *NRXN1*, and *PLCB1* were significantly increased in 82-kDa ChAT expressing cells after 2 h exposure to $A\beta_{1-42}$ (n = 4). Gene expression changes were no longer significant after 4 h of $A\beta_{1-42}$ -exposure. *GRM5* and *DLG2* were significantly increased in 82-kDa ChAT expressing cells after 8 h of $A\beta_{1-42}$ -exposure. After 24 h of $A\beta_{1-42}$ treatment, *NLGN1* was significantly increased and *NRXN1* was significantly decreased in 82-kDa ChAT expressing cells. n = 5 *p < 0.05, **p < 0.01, ***p < 0.001 (two-way ANOVA with Bonferroni's post-hoc test).

ChAT expressing cells treated with A β ₁₋₄₂ for 24 h *NLGN1* is significantly increased compared to that measured in vector expressing cells treated for 24 h with A β ₁₋₄₂ (1.7 ± 0.3 compared to 1.0 ± 0.1), while *NRXN1* is significantly reduced (0.5 ± 0.1 compared to 1.1 ± 0.1). Though not significant, *NRG1* was also reduced in 82-kDa ChAT expressing cells (0.7 ± 0.1) compared to vector expressing cells (1.2 ± 0.1 ; $\alpha = 0.006$, $p = 0.009$, ns) after 24 h treatment with A β ₁₋₄₂.

SH-SY5Y cells expressing 82-kDa ChAT had altered expression for synapse and membrane related genes compared to cells expressing an empty vector. Therefore, we evaluated whether there were also differences in steady-state protein levels for NRG1, mGlu5 or NLGN1 in 82-kDa ChAT compared to vector expressing cells that had been treated with either vehicle or 100 nM A β ₁₋₄₂ for 24 h (**Fig. 4.5**). For all three proteins, we did not observe any differences in steady-state levels after 24 h of A β ₁₋₄₂-exposure compared to vehicle treatment. Though there were no differences due to treatment, we observed a significant increases in steady-state protein levels when we compared protein levels in 82-kDa ChAT-expressing cells to empty vector for NRG1 (1.4 ± 0.1 , 0.5 ± 0.1 respectively for vehicle treatment; 1.4 ± 0.2 , 0.5 ± 0.1 respectively for A β ₁₋₄₂), mGlu5 (1.5 ± 0.2 , 0.3 ± 0.1 respectively for vehicle treatment; 1.8 ± 0.2 , 0.3 ± 0.2 respectively for A β ₁₋₄₂) and NLGN1 (1.2 ± 0.1 , 0.8 ± 0.05 respectively for vehicle treatment; 1.2 ± 0.1 , 0.9 ± 0.1 respectively for A β ₁₋₄₂).

82-kDa ChAT expression in SH-SY5Y cells results in NRG1-dependent neurite outgrowth

SH-SY5Y cells that stably express heterologous 82-kDa ChAT have higher steady-state levels of synapse formation and maintenance related genes and proteins compared to cells expressing an empty vector. Therefore, we tested whether there were related morphologic and phenotypic changes in these cells after cholinergic differentiation with retinoic acid. In **Figure 4.6**, we assessed the morphology of SH-SY5Y cells differentiated for 7 days with retinoic acid. In particular, we focused on processes extending from the cell body, greater than 2 cell bodies in length. Since we

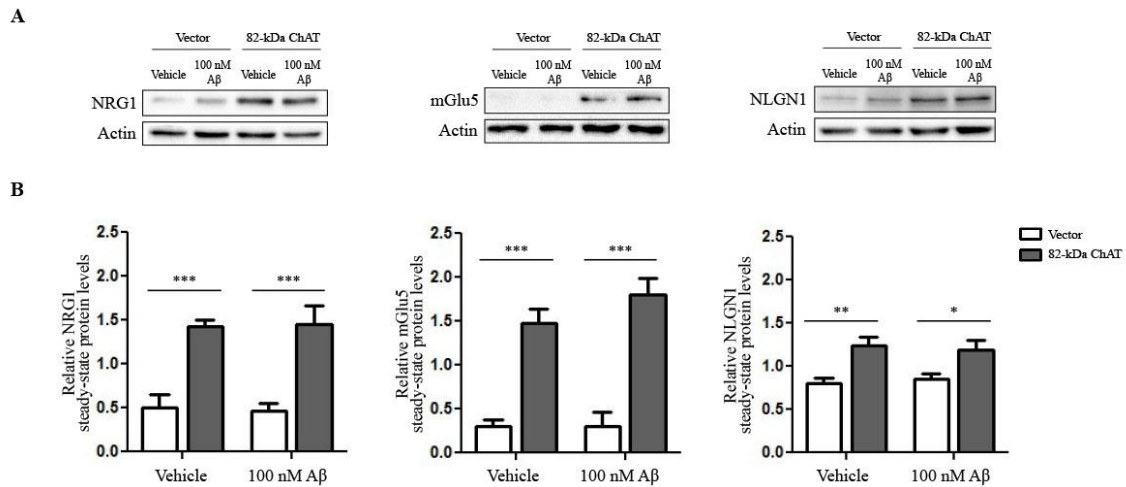


Figure 4-5. 82-kDa ChAT expression in SH-SY5Y cells alters steady-state protein levels of neuregulin 1, neuroligin 1 and the metabotropic glutamate receptor 5.

(A) Representative western immunoblots showing NRG1, mGlu5 and NLGN1 steady-state protein levels in SH-SY5Y cells stably expressing 82-kDa ChAT or empty vector and treated with either vehicle or 100 nM A β_{1-42} for 24 h. β -actin is shown as a loading control. All 3 proteins had higher band density in 82-kDa ChAT expressing cells. (B) Quantification of band density relative to β -actin confirmed significantly increased steady-state protein levels for NRG1, mGlu5 and NLGN1 in 82-kDa ChAT expressing cells. For all 3 proteins there was no effect of treatment with either vehicle or A β_{1-42} . n = 5, *p < 0.05, **p < 0.01, ***p < 0.001 (two-way ANOVA with Bonferroni's post hoc test).

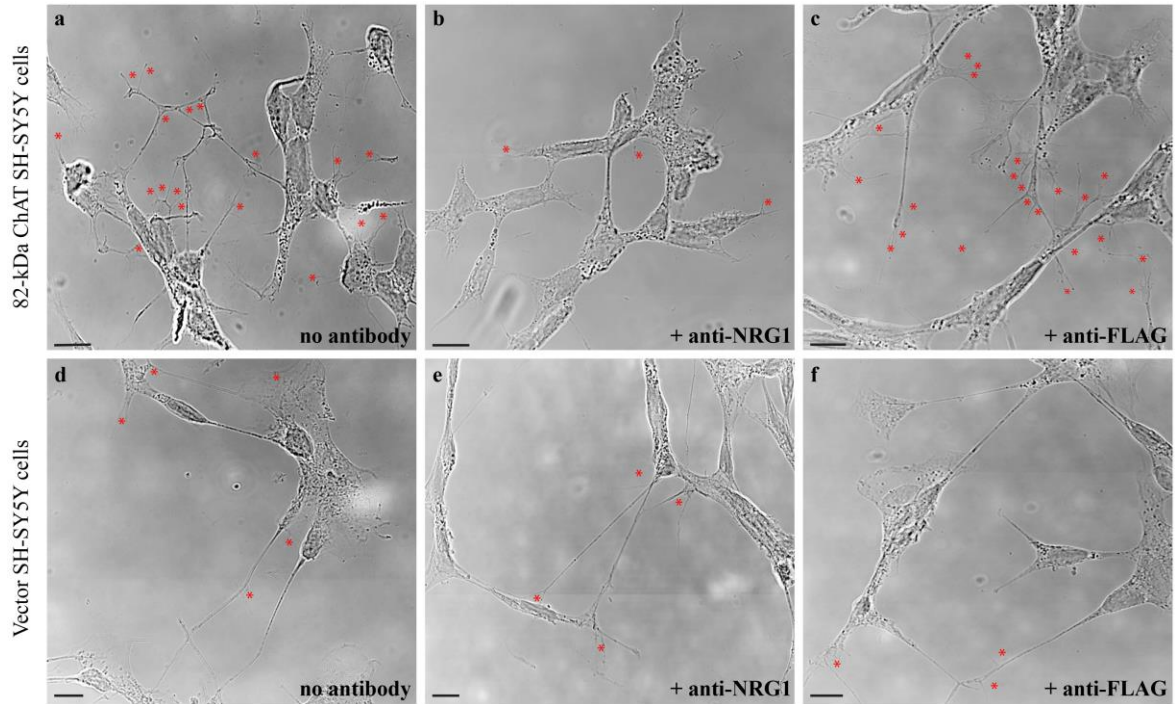


Figure 4-6. 82-kDa ChAT expressing SH-SY5Y cells grow highly branched NRG1-dependent neurites.

Representative images for 82-kDa ChAT or vector expressing SH-SY5Y cells differentiated for 7 d with retinoic acid. Cells expressing 82-kDa ChAT (**a**) have short, branched (indicated by *) cell processes (neurites) that interconnect, while cells expressing empty vector (**d**) have longer neurites with few branches. When cells are grown for 7 d in the presence of retinoic acid and anti-NRG1 antibody, 82-kDa ChAT expressing cells (**b**) grow fewer neurites that do not have branches. Vector-expressing cells (**e**) grown with anti-NRG1 produce neurites that appear similar to cells grown in the absence of antibody. Cells expressing either 82-kDa ChAT (**c**) or empty vector (**f**) that were grown in the presence of anti-FLAG antibody had neurites that look similar to cells grown in the absence of antibody. Three independent experiments were performed with at least 5 images (10-30 cells/image) captured per replicate. Scale bar = 10 μ m.

cannot determine whether these processes are axonal or dendritic, we refer to them as ‘neurites’. Cells expressing 82-kDa ChAT have neurites extending from the cell body that are highly branched and interconnected with adjacent cell processes (**Fig. 4.6[a]**). In contrast, cells expressing an empty vector have longer neurites than 82-kDa ChAT expressing cells, but these neurites have fewer branches (**Fig. 4.6[d]**).

NRG1 is cleaved within the cell membrane to produce a 6-8 kDa extracellular epidermal growth factor (EGF) domain peptide that promotes synapse development (Gerecke *et al.* 2004; Luo *et al.* 2011; Ting *et al.* 2011; Merballi *et al.* 2012). Therefore we assessed whether depletion of NRG1 peptide from the culture media using an antibody directed to the peptide would alter the neurite growth in either vector or 82-kDa ChAT expressing cells. We incubated fresh culture media with anti-NRG1 antibody for 1 h prior to using this to feed either vector or 82-kDa ChAT expressing cells; fresh media containing antibody was added to cells every 48 h. Importantly, cells expressing 82-kDa ChAT fed with media containing anti-NRG1 antibody produced few neurites with almost no branching (**Fig. 4.6[b]**), whereas media containing the anti-NRG1 antibody had no effect on neurites produced in cells expressing an empty vector (**Fig. 4.6[e]**). As a control, we added an antibody against the FLAG polypeptide protein tag to fresh culture medium as SH-SY5Y cells do not express the peptide and the antibody should have no effect on cell morphology. Cells expressing either 82-kDa ChAT (**Fig. 4.6[c]**) or empty vector (**Fig. 4.6[f]**) grown in medium containing anti-FLAG antibody showed no changes to neurite morphology when compared to cells grown in medium containing no antibody. These results demonstrate that 82-kDa ChAT expressing cells have more complex neurites compared to vector expressing cells. In addition, the 82-kDa ChAT cells produce neurites that are dependent on extracellular NRG1, whereas neurites from vector expressing cells are not.

Next, based on the assumption that 82-kDa ChAT expressing cells may be producing elevated levels of the extracellular NRG1 EGF domain peptide, we grew either vector or 82-kDa ChAT expressing SH-SY5Y cells for 7 d in either fresh media or media that was conditioned on 82-kDa ChAT or vector expressing cells for 48 h. All

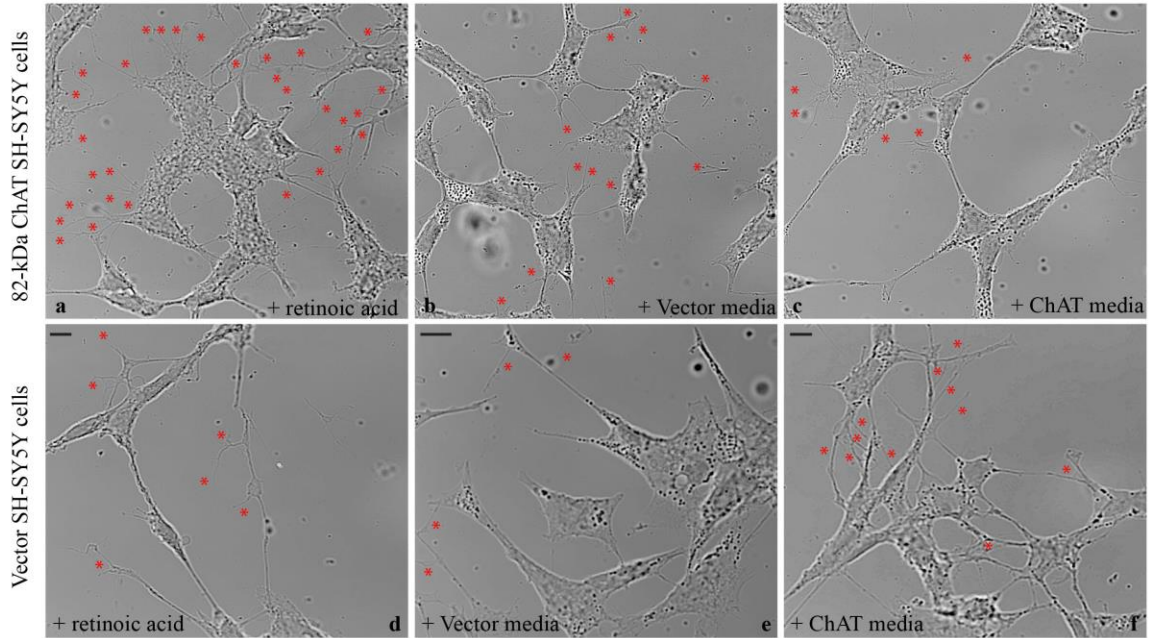


Figure 4-7. Media conditioned on 82-kDa ChAT expressing SH-SY5Y cells alters neurite outgrowth of vector expressing cells.

Representative images for 82-kDa ChAT or vector expressing SH-SY5Y cells differentiated for 7 d with retinoic acid. Cells expressing 82-kDa ChAT (**a**) have short, branched (indicated by *) cell processes (neurites) that interconnected, while cells expressing empty vector (**d**) had longer neurites with few branches. When cells were grown for 7 d in the presence of media conditioned on vector expressing cells for 48 h, 82-kDa ChAT (**b**) and vector (**e**) expressing cells grew neurites that had few branches. 82-kDa ChAT expressing cells (**c**) grown for 7 d in the presence of media conditioned for 48 h on cells expressing 82-kDa ChAT also grew neurites with few branches. Vector expressing cells (**f**) grown in the presence of 82-kDa ChAT conditioned media grew neurites that had many more branches than cells grown (**d**). $n = 3$ with at least 5 images (10-30 cells/image) per replicate, scale bar = 10 μm .

experiments were done in the presence of retinoic acid, and we assessed the morphological and phenotypic changes in these cells. **Figure 4.7** shows that, in agreement with the previous experiment, 82-kDa ChAT expressing cells grown in fresh media produce neurites that are complex and highly branched (**Fig. 4.7[a]**). Vector expressing cells again had neurites with few branches (**Fig. 4.7[d]**). When we treated cells with media conditioned on vector expressing cells, both 82-kDa ChAT (**Fig. 4.7[b]**) and vector (**Fig. 4.7[e]**) expressing cells grew neurites with few branches. Surprisingly, 82-kDa ChAT expressing cells grown in 82-kDa ChAT conditioned media also grew neurites with few branches (**Fig. 4.7[c]**). Interestingly, when we grew vector expressing cells in 82-kDa ChAT conditioned media the cells grew neurites with extensive branching (**Fig. 4.7[f]**).

Cells that express 82-kDa ChAT have a more robust ERBB4 phosphorylation response following agonist stimulation

82-kDa ChAT expression in SH-SY5Y cells increases the steady-state NRG1 protein levels, resulting in extracellular NRG1 dependent neurite outgrowth. One possible mechanism to explain this interaction may be long-term NRG1 EGF domain stimulation of ERBB4, a membrane bound epidermal growth factor receptor. Long-term, low level release of NRG1 can promote the recruitment of ERBB2 to ERBB4, forming a heterodimer (Graus-Porta *et al.* 1997; Sweeney *et al.* 2000; Gerecke *et al.* 2004; Iwakura and Nawa 2013) (**Fig. 4.8**). ERBB4 can recruit and form dimers with ERBB1-4, but NRG1 can only bind ERBB3 and ERBB4 (Graus-Porta *et al.* 1997; Sweeney *et al.* 2000). In the heterodimer state, NRG1 binding promotes tyrosine phosphorylation of ERBB4 and the maintenance of the receptors at the cell surface (Sweeney *et al.* 2000; Iwakura and Nawa 2013). NRG1 dependent signaling to ERBB4 and recruitment of the ERBB2:ERBB4 heterodimer has been shown previously to induce neurite extension and branching in cultured E18 hippocampal cells (Gerecke *et al.* 2004). Gerecke *et al.* (2004) showed that the NRG1 dependent neurite branching involved the p42/44 extracellular signal-regulated kinase (ERK) and PKC signaling pathways via mGlu5 activation, but not

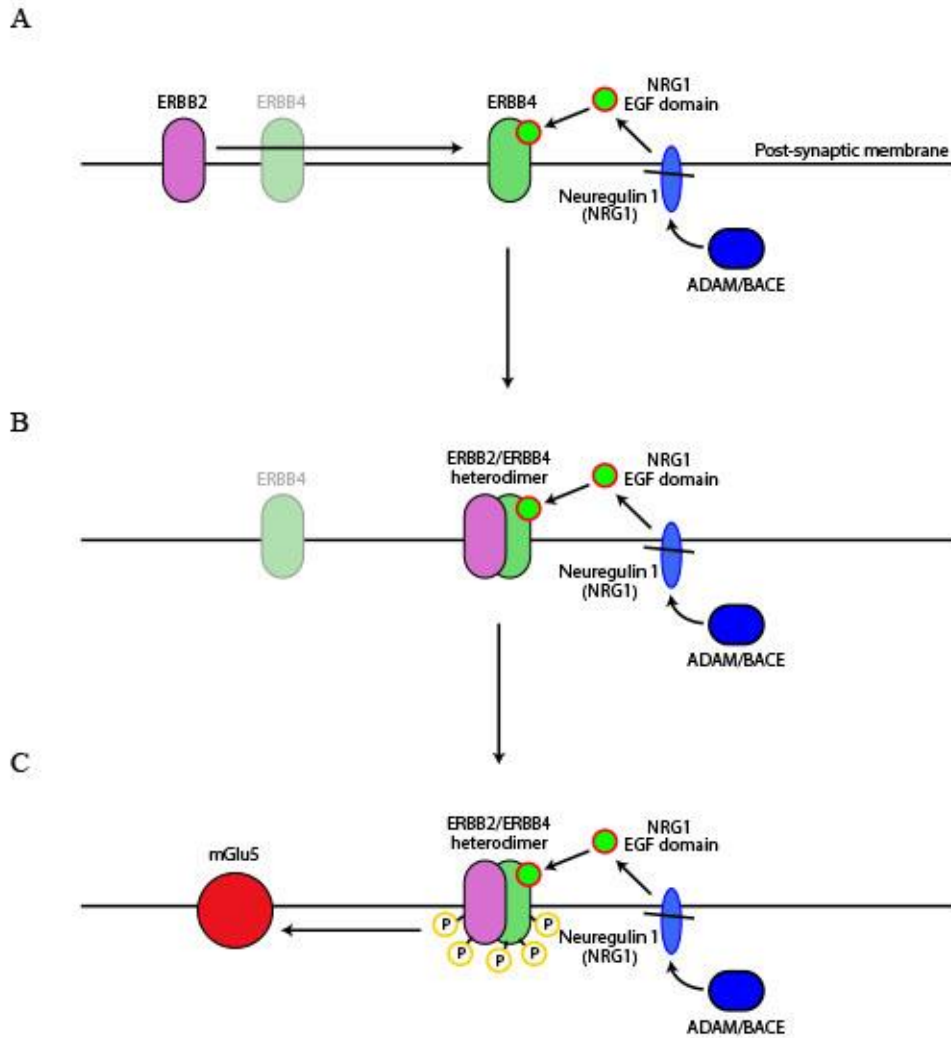


Figure 4-8. Long-term NRG1 signaling promotes ERBB4 phosphorylation.

(A) NRG1 is cleaved in the membrane by ADAM or BACE enzymes to produce a 6-8 kDa extracellular NRG1 EGF domain peptide. Long-term, low levels of NRG1 EGF domain peptide binds to ERBB4 and promotes the recruitment of ERBB2 and (B) the formation of an ERBB2:ERBB4 heterodimer. (C) ERBB2:ERBB4 heterodimers are tyrosine phosphorylated via autophosphorylation, leading to enhanced signaling to mGlu5 receptors. Downstream signaling promotes synapse formation and maintenance. See results for more detail.

PI3K or p38 mitogen activated protein kinase (MAPK) pathways. In BACE null mice with impaired NRG1 processing, binding of ERBB4 to post-synaptic density (PSD) proteins is also impaired which correlates to reduced dendritic spine density (Savonenko *et al.* 2008).

Exposure to acute NRG1 results in low levels of ERBB4 tyrosine phosphorylation and internalization of the ERBB4 receptor (**Fig. 4.9**) (Kwon *et al.* 2005; Li *et al.* 2007; Syed *et al.* 2010; Seshadi *et al.* 2015). Previous research has suggested that this is likely due to preferential ERBB4:ERBB4 homodimerization, which has a lower phosphorylation state than the higher affinity ERBB2:ERBB4 heterodimer (Sweeney *et al.* 2000; Mei and Xiong 2008). Further, ERBB4 phosphorylation is impaired when ERBB2 is not available for heterodimer formation (Graus-Porta *et al.* 1997). This is further supported by the observations that high levels of exogenous NRG1 peptide exposure reverses long-term potentiation (LTP) in the *cornu ammonis* area 1 (CA1) region of the mouse hippocampus (Kwon *et al.* 2005), and blocks LTP induction at CA1 synapses in hippocampal slices (Huang *et al.* 2000). Importantly, Bjarnadottir *et al.* (2007) showed that low doses of NRG1 increases tetanus and theta-burst induced LTP in the CA1, but higher doses suppress LTP.

Based on our results above, expression of 82-kDa ChAT in SH-SY5Y cells promotes NRG1-dependent neurite outgrowth, but that neurite outgrowth in vector-expressing cells is NRG1-independent. Since NRG1 can stimulate the phosphorylation of the EGF receptor ERBB4 (Sweeney *et al.* 2000; Iwakura and Nawa 2013), we assessed whether there were differences in ERBB4 phosphorylation (p-ERBB4) levels after differentiated SH-SY5Y cells were exposed to fresh media or media that was conditioned on either 82-kDa ChAT or vector expressing cells for 48 h (**Fig. 4.10**). Prior to the addition of the test media, cells were incubated in serum-free media for 1 h to remove ERBB4-bound serum proteins and allow the receptors to traffic to the cell surface. After 1 min of exposure to fresh media containing FBS, both vector and 82-kDa ChAT expressing cells had increased p-ERBB4 levels (**Fig. 4.10A**). The levels of p-ERBB4 were higher in 82-kDa ChAT expressing cells compared to cells expressing empty vector, with no detectable differences in total ERBB4 levels (n = 2).

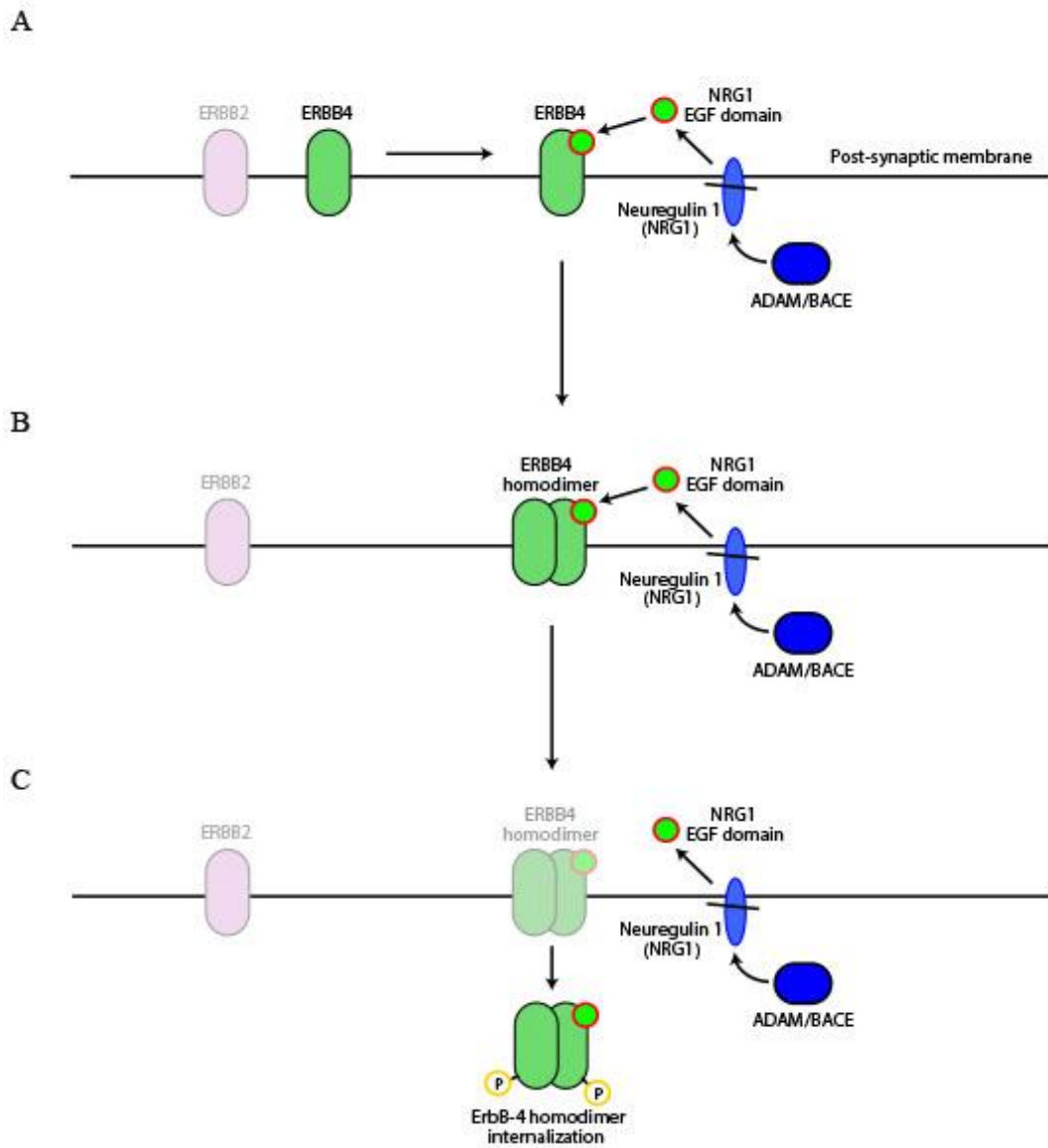


Figure 4-9. Acute NRG1 signaling reduces ERBB4 phosphorylation.

(A) Acute release or over-expression of NRG1 EGF domain peptide binds ERBB4 and promotes the recruitment of ERBB4 and (B) the formation of an ERBB4:ERBB4 homodimer. (C) ERBB4:ERBB4 heterodimers have low levels of tyrosine phosphorylation and are more rapidly internalized compared to heterodimers. This results in loss of signaling, leading to reductions in synapse formation and the inhibition of long-term potentiation. See results for more detail.

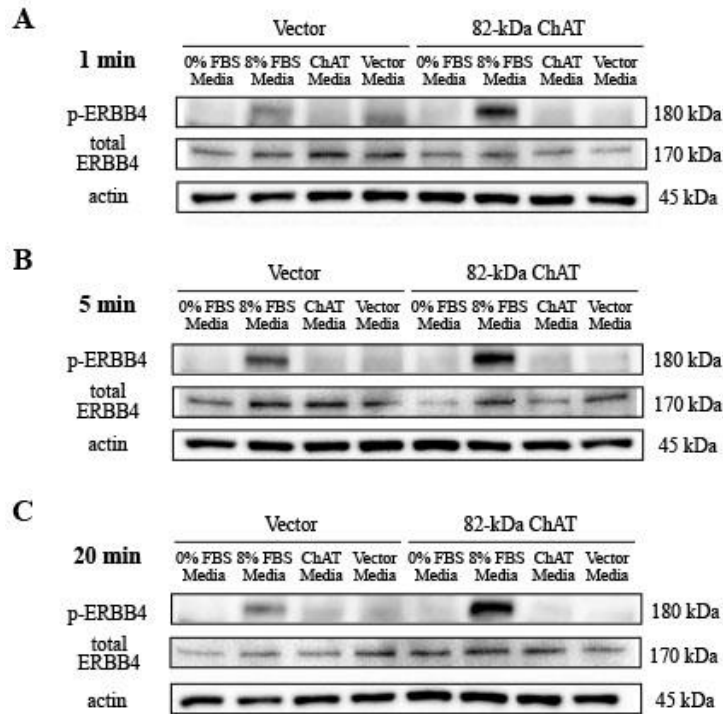


Figure 4-10. 82-kDa ChAT expressing cells have enhanced ERBB4 phosphorylation in response to growth factors.

(A) Representative immunoblot showing phosphorylated ERBB4 (p-ERBB4), total ERBB4 and β -actin steady-state levels in vector or 82-kDa ChAT expressing SH-SY5Y cells treated for 1 min with cell media containing no fetal bovine serum (FBS), 8% FBS or media containing FBS conditioned for 48 h on either 82-kDa ChAT or vector expressing cells. In each case, cells were grown in media containing no FBS for 1 h prior to the addition of test media. Both vector and 82-kDa ChAT expressing cells showed little or no p-ERBB4 following treatment with serum-free media or media conditioned on vector or 82-kDa ChAT expressing cells. Vector expressing cells treated with fresh FBS containing media had a low level of p-ERBB4, while 82-kDa ChAT expressing cells had a stronger immunoreactive band for p-ERBB4. There were no differences in total ERBB4 levels. $n = 2$. (B) Vector or 82-kDa ChAT expressing cells were treated in the same conditions above for 5 min. Both vector and 82-kDa ChAT expressing cells had no p-ERBB4 band for serum-free or conditioned media, as in (A). Both 82-kDa ChAT and vector expressing cells had a stronger band for the FBS-containing media treatment as compared to (A), with ChAT expressing cells again showing an increased response compared to vector cells. $n = 4$. (C) Cells treated for 20 min in the same condition as (A) again had no p-ERBB4 bands for serum-free media or conditioned media treatments. Vector expressing cells treated with media containing FBS had a lower level p-ERBB4 band compared to the 5 min treatment, and compared to 82-kDa ChAT expressing cells. 82-kDa ChAT cells treated with media containing FBS had no change in p-ERBB4 levels compared to 5 min. $n = 2$.

After 5 min, p-ERBB4 levels were increased in both cell lines after fresh media treatment, with 82-kDa ChAT expressing cells again having higher p-ERBB4 levels compared to cells expressing the empty vector (**Fig. 4.10B**, n = 4). After 20 min, p-ERBB4 levels were reduced in vector expressing cells exposed to fresh media containing FBS compared to 5 min, but were similar to 5 min levels in cells expressing 82-kDa ChAT (**Fig. 4.10C**, n = 2). We did not detect phosphorylation changes for any time points for cells treated with serum-free media or media conditioned on either 82-kDa ChAT or vector expressing cells. In some cases, we observed an immunoreactive band with lower molecular mass in vector expressing cells that were treated with medium that was conditioned on vector expressing cells (visible in **Fig. 4.10A**), but this result was not consistent across replicate experiments and time points.

Based on the observed increase in ERBB4 phosphorylation in 82-kDa ChAT expressing cells following exposure to fresh culture medium containing FBS, we hypothesized that these cells may also be more responsive to exogenous NRG1 EGF domain peptide treatment. Therefore, we treated SH-SY5Y cells expressing either vector or 82-kDa ChAT with recombinant NRG1 EGF domain peptide for 5 min and measured the resulting levels of p-ERBB4 (**Fig. 4.11**, n = 2). In vector expressing cells, we observed a low level of phosphorylation in untreated cells and cells treated with 1.25 ng NRG1 peptide. Following the addition of 2.5 ng NRG1 peptide, there was an observable increase in p-ERBB4, with this enhanced further following exposure to 5 ng NRG1. Increasing the dose to 10 ng NRG1 resulted in p-ERBB4 levels that were similar to untreated cells. In comparison, with 82-kDa ChAT expressing cells we observed higher levels of p-ERBB4, including in untreated cells, compared to vector expressing cells. Peak p-ERBB4 levels were observed with 1.25 ng NRG1 treatment, and p-ERBB4 levels in 82-kDa ChAT expressing cells treated with 2.5, 5 or 10 ng NRG1 being similar to untreated cells.

Together with the observed increases in p-ERBB4 levels and duration following treatment with media containing FBS, these data suggest that ERBB4 receptors are activated at lower agonist concentrations in 82-kDa ChAT expressing SH-SY5Y cells compared to cells expressing an empty vector. To determine whether these observations

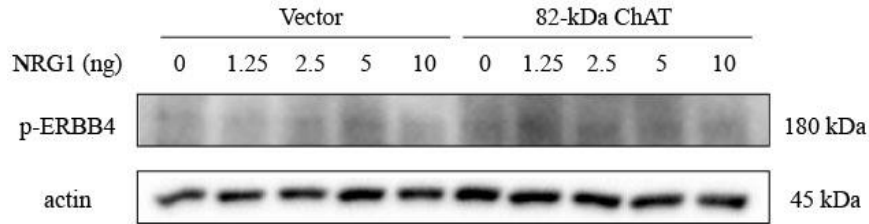


Figure 4-11. 82-kDa ChAT expression increases the response to NRG1 stimulation of p-ERBB4.

Representative immunoblots showing phosphorylated ERBB4 (p-ERBB4) and β -actin steady-state levels in vector or 82-kDa ChAT expressing SH-SY5Y cells treated for 5 min with recombinant NRG1 EGF domain peptide. Vector expressing cells showed increased p-ERBB4 levels after treatment with 2.5 and 5 ng of NRG1 peptide, with a peak at 5 ng. Treatment with 10 ng NRG1 resulted in p-ERBB4 levels close to untreated cells. 82-kDa ChAT expressing cells showed peak p-ERBB4 levels following 1.25 ng NRG1 peptide treatment, with 2.5, 5 and 10 ng NRG1 treatment resulting in p-ERBB4 levels similar to untreated cells. The total levels of ERBB4 still need to be determined for this experiment $n = 2$.

may be due to increased levels of extracellular NRG1 EGF domain peptide released by 82-kDa ChAT expressing cells, we endeavored to detect and quantify the levels of NRG1 EGF domain peptide produced by cells expressing either empty vector or 82-kDa ChAT. First, we tried to detect NRG1 EGF peptide levels in media conditioned for 48 h on either 82-kDa ChAT or vector expressing cells by immunoblotting, but were unsuccessful (data not shown). Interestingly, when we concentrated samples of these conditioned media by 8-fold we were able to detect an immunoreactive band at 6 kDa for NRG1 in media collected from 82-kDa ChAT expressing cells, but not from the vector expressing cells (**Fig. 4.12**, n = 3). Actin from cell lysate was used as a loading control, with equal volumes loaded for vector and 82-kDa ChAT expressing cells.

Next, we performed sandwich ELISAs with antibody directed to the NRG1 EGF domain peptide using media that was conditioned for 48 h on 82-kDa ChAT or vector expressing SH-SY5Y cells (**Table 4.4**). Optical density values were compared to a standard curve generated with recombinant NRG1 EGF domain peptide to determine a NRG1 concentration. We were not able to detect NRG1 peptide levels in media conditioned on 82-kDa ChAT or vector expressing cells over the concentration range tested (n = 8), and concentrating media 8-fold produced values that were also below the limit of detection (n = 2). Concentrating media could also concentrate any serum proteins present in the media. Therefore, to address whether the presence of FBS in the medium could alter the NRG1 concentrations measured by ELISA, we added recombinant NRG1 peptide to either serum-free medium or medium containing 8% FBS (n = 1). When NRG1 peptide was added to serum-free medium, the concentration of the peptide measured was within $\pm 15\%$ of the amount of peptide added. However, adding NRG1 peptide to FBS-containing media resulted in detected NRG1 concentrations that were nearly 50% below the expected values, suggesting that serum proteins can reduce the detection of NRG1. Finally, we added exogenous NRG1 peptide to media conditioned on either vector or 82-kDa ChAT expressing cells, mainly observing that the measured NRG1 levels were $\pm 15\%$ of expected values (**Table 4.4**, n = 1). Interestingly, one notable exception was in media conditioned on 82-kDa ChAT expressing cells and treated with the lowest detectable concentration of NRG1 for the ELISA (125 pg/mL),

where we detected an NRG1 concentration that was 52% higher than expected. More experiments are needed to confirm these ELISA results.

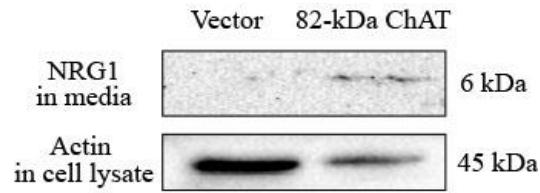


Figure 4-12. 82-kDa ChAT expression increases NRG1 extracellular peptide release in SH-SY5Y media.

Representative immunoblot showing extracellular NRG1 EGF domain peptide detected in media samples conditioned on either vector or 82-kDa ChAT expressing SH-SY5Y cells for 48 h. Media was concentrated 8-fold following collection. Total protein was also isolated from cells in each condition and an equal volume of cell lysate was separated by electrophoresis to show β -actin as a loading control. An immunoreactive band was detected for NRG1 in 82-kDa ChAT expressing cells, but not for vector expressing cells. $n = 3$.

Table 4-4. NRG1 concentrations as measured by ELISA.

n = 8 for conditioned media with 0 ng NRG1 added, n = 2 for concentrated media, n = 1 for all other samples.

Treatment (NRG1 peptide concentration)	Measured Concentration	Percentage Difference
Serum-free media		
0 ng	0.034 ng	--
0.125 ng	0.106 ng	-15.3%
1 ng	1.087 ng	+8.6%
4 ng	4.463 ng	+11.6%
8% FBS media		
0 ng	0.022 ng	--
0.125 ng	0.095 ng	-24.0%
1 ng	0.505 ng	-49.6%
4 ng	2.221 ng	-44.5%
Vector cell conditioned media		
0 ng	0.008 ng	--
0.125 ng	0.145 ng	+15.7%
1 ng	1.062 ng	+6.2%
4 ng	3.349 ng	-16.3%
82-kDa ChAT conditioned media		
0 ng	0.000 ng	--
0.125 ng	0.190 ng	+51.9%
1 ng	0.958 ng	-4.2%
4 ng	3.100 ng	-22.51%
Concentrated media		
Vector	-0.017 ± 0.004 ng	--
ChAT	-0.027 ± 0.002 ng	--

4.4 Discussion

In this chapter, we explored the novel finding that 82-kDa ChAT associated with chromatin enriched with NFAT DNA-binding motifs at synapse development and maintenance related genes. This observation led us to find that (1) 82-kDa ChAT expression alters the expression of a group of related synapse and membrane genes; (2) These gene expression changes led to increased protein levels of mGlu5, NRG1 and NLGN1 which are all involved in synapse development; (3) 82-kDa ChAT expressing neural cells have increased neurite outgrowth and neuritic branching, dependent on extracellular NRG1; and (4) 82-kDa ChAT expression increased the response to agonist-induced ERBB4 phosphorylation by growth factors and NRG1. Overall, these findings show how bioinformatics data can be used to inform a hypothesis related to gene expression and chromatin organization, which can be followed from gene and protein expression changes to morphologic and phenotypic outcomes.

Using ChIP-seq data, we showed that 82-kDa ChAT had significant enrichment for NFAT DNA-binding motifs. It was important that we also found GO groups related to synapse, membrane and calcium, as NFAT has been shown previously to play an important role in axon/dendrite outgrowth and synapse formation during development (Graef *et al.* 2003; Groth and Mermelstein 2003). When we assessed gene expression changes for several synapse related genes that exhibited 82-kDa ChAT peaks containing NFAT motifs, we found that many of these genes had increased mRNA levels in SH-SY5Y cells expressing 82-kDa ChAT compared to cells expressing an empty vector. Given their role in synapse formation during development we chose 3 of these genes to further investigate. We found large increases in protein expression for NRG1, mGlu5 and NLGN1 in cells expressing 82-kDa ChAT compared to empty vector. NFAT is activated after A β -exposure (Wu *et al.* 2010), 82-kDa ChAT peaks were present in altered genomic positions following 4 h of A β ₁₋₄₂-exposure and NFAT levels are altered in AD (Abdul *et al.* 2010). Therefore, we also chose to assess changes after exposure to oligomeric A β ₁₋₄₂. For varying times after A β ₁₋₄₂-exposure, we observed gene expression changes for many of the genes explored, but this did not result in 82-kDa ChAT-mediated protein

expression alterations for NRG1, mGlu5 or NLGN1 after 24 h of A β ₁₋₄₂-exposure. Given that we saw gene expression changes for *NLGN1* at 2 h and *GRM5* at 8 h we expected to see protein expression changes by 24 h, however there are several reasons that could account for this discrepancy. First, the A β ₁₋₄₂-induced effects on gene expression may be transient; by 4 h *NLGN1* was no longer increased, and so there may not be a large effect on translation. Another possible explanation could be differences in protein expression that are not yet apparent, depending on the protein's half-life. Finally, we saw a non-significant decrease in *NRG1* mRNA levels only after 24 h of A β ₁₋₄₂-exposure, and therefore did not expect to see protein expression changes for NRG1 after 24 h.

Though we did not detect any protein related differences after exposure of cells to A β ₁₋₄₂, there was increased expression of NRG1, mGlu5 and NLGN1 in 82-kDa ChAT expressing cells when compared to empty vector. This was a significant finding, as all three of these proteins are important for cholinergic synapse development and the response to neurotransmission. All of the genes that we tested for differences in SH-SY5Y cells expressing either empty vector or 82-kDa ChAT work together to regulate synapse development (**Fig. 4-13**). NRG1 is cleaved within the synaptic membrane by a disintegrin and metalloproteinase (ADAM) or β -secretase (BACE) enzymes to produce the NRG1 EGF domain peptide (Luo *et al.* 2011; Merballi *et al.* 2012). NRG1 binds preferentially to ERBB4, where moderate long-term binding promotes heterodimerization with ERBB2 and tyrosine phosphorylation (Tzahar *et al.* 1996; Graus-Porta *et al.* 1997; Sweeney *et al.* 2000; Gerecke *et al.* 2004; Savonenko *et al.* 2008). This phosphorylation leads to signaling events that, through the PSD-93/GKAP/Shank/Homer complex results to PLC- β 1 phosphorylation and downstream inositol 1,4,5-trisphosphate (IP3) formation via activation of mGlu5 (Tu *et al.* 1999; Alagarsamy *et al.* 2005; Dai *et al.* 2014). At the same time, ERBB4 (via PSD-95) can signal to NLGN1 which promotes new complex formation with NRXN1 and the stabilization of existing synaptic connections (Reviewed in Craig and Kim 2007; Mei and Xiong 2008). The result of these signaling events is the promotion of new synapse formation and maintenance of existing connections (Gerecke *et al.* 2004; Craig and Kim 2007; Mei and Xiong 2008; Ting *et al.* 2011). Importantly, synapse formation via mGlu5-mediated signaling has been shown to

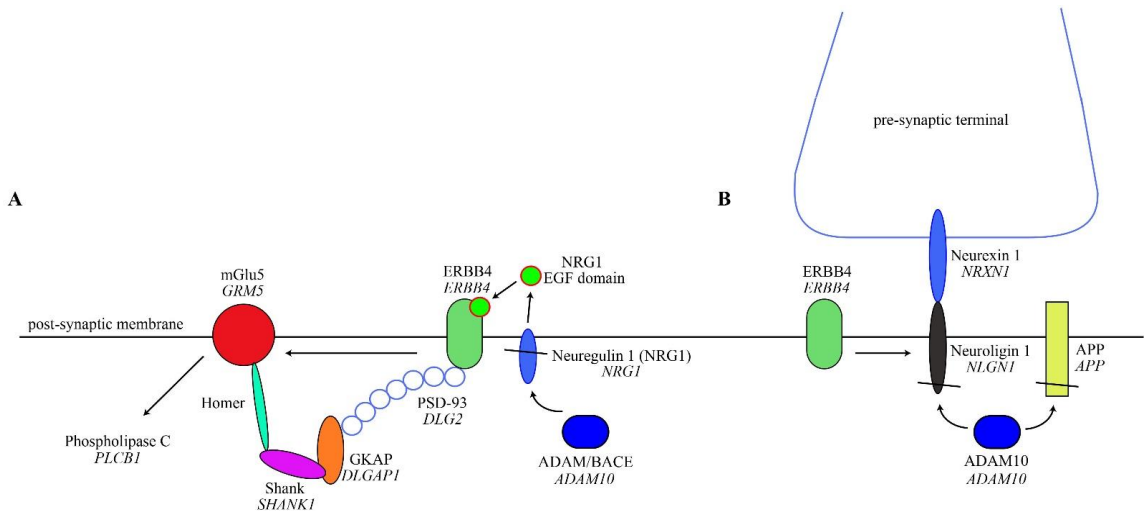


Figure 4-13. ERBB4 signaling promotes cholinergic synapse maintenance and new synapse formation.

(A) In cholinergic neurons, neuregulin 1 (NRG1) is cleaved within the post-synaptic membrane by either ADAM or BACE family members to produce a short extracellular EGF domain peptide. NRG1 binds to ERBB4 and promotes tyrosine phosphorylation which signals to mGlu5 through the PSD-93/GKAP/Shank/Homer complex. mGlu5 activation leads to phosphorylation of phospholipase c, promoting synapse formation. (B) ERBB4 can also signal to neuroligin, which binds to neurexin on the pre-synaptic membrane to stabilize synaptic connections. ERBB4-neuroligin signaling promotes new synapse formation and maintenance of existing synapses. Neuroligin is cleaved within the membrane by ADAM10, which is also responsible for α -secretase cleavage of APP. *Italics* = Encoded genes with 82-kDa ChAT peak associations found by ChIP-seq (GSE73576). See results for more detail.

promote cholinergic synapse development in rat neural progenitor cells (Zhao *et al.* 2014). NLGN1 is also cleaved by ADAM10, an ADAM family member that cleaves membrane-bound APP and NRG1 (Kuhn *et al.* 2010; Luo *et al.* 2011). *ADAM10* also had ChIP-seq peaks for 82-kDa ChAT, but this was not explored in the current study. Based on these relationships, we assessed the morphological features of 82-kDa ChAT expressing cells, finding that they had more complex neurite formation than cells expressing empty vector, depending upon the extracellular NRG1 EGF domain peptide.

It is well established that high levels of p-ERBB4 lead to increased mGlu5 activation through an interaction with the PSD93 or 95/GKAP/Shank/Homer complex (Gerecke *et al.* 2004; Savonenko *et al.* 2008). Low-moderate levels of NRG1 stimulation have been demonstrated to stabilize a PSD95 interaction (Huang *et al.* 2000). Hippocampal brain regions of schizophrenic patients with enhanced NRG1-induced activation of ERBB4 receptors show an increased interaction between ERBB4 and PSD95 (Hahn *et al.* 2006), indicating that the NRG1 stimulated ERBB4-PSD interaction is an important mechanism for downstream signaling. In our data, we observed that 82-kDa ChAT expressing cells have increased and sustained p-ERBB4 in response to cell culture media containing FBS, and increased the response to recombinant NRG1 EGF domain stimulation of p-ERBB4. One conceivable explanation for these observations could be an increase in available surface receptors and resistance to desensitization, a possibility only if ERBB4 is recruiting ERBB2 for heterodimerization (**Fig 4.8**). NRG1 binding to ERBB4 could also increase the likelihood of ERBB4 phosphorylation, in a manner that produces increased responses to stimulation. Though we are not aware of any studies supporting this possibility, 82-kDa ChAT expressing cells have peak p-ERBB4 levels after lower recombinant NRG1 peptide treatment than vector expressing cells suggesting that they may be more sensitive to stimulation. Finally, it is possible that either ERBB4 or other surface receptor stimulation by either growth factors or NRG1 results in NRG1 cleavage by ADAM/BACE and EGF domain peptide release into the extracellular space. This could account for both the enhanced/sustained p-ERBB4 levels following FBS stimulation and the lower NRG1 peptide concentration need to elicit p-ERBB4 in 82-kDa ChAT expressing cells. Further studies will be needed to elucidate the

mechanisms related to the phosphorylation state of ERBB4 in 82-kDa ChAT expressing cells.

In the data presented in this chapter, low levels of NRG1 stimulated p-ERBB4 whereas higher levels inhibited this induction. Though the total levels of ERBB4 still need to be determined for this experiment, the initial data shows that ERBB4 phosphorylation was stimulated by a lower NRG1 dose in 82-kDa ChAT expressing cells compared to cells expressing empty vector, but was also inhibited by lower doses. An important implication from these data may be related to the function of NRG1 in LTP. Exogenous NRG1 treatment has been described as an inverted U curve for LTP induction, very low and very high levels either do not support or suppress LTP; however low-moderate levels can facilitate LTP (Bjarnadottir *et al.* 2007; Li *et al.* 2007; Syed *et al.* 2010). This may be due to moderate levels of NRG1 increasing ERBB4-PSD interactions (Hahn *et al.* 2006; Li *et al.* 2007), and at high levels disrupting this interaction (Li *et al.* 2007). p-ERBB4 signals to mGlu5 via the PSD/GKAP/Shank/Homer complex (Tu *et al.* 1999; Alagarsamy *et al.* 2005; Dai *et al.* 2014), and mGlu5 is critical for LTP induction (Rodrigues *et al.* 2002; Sourdet *et al.* 2003). Collectively, these data suggest that 82-kDa ChAT expressing cells could be more likely to have LTP induction, but also to LTP suppression. In support of this hypothesis, when we added 82-kDa ChAT conditioned media to vector expressing cells, we saw neurite branching similar to 82-kDa ChAT cells grown in new media. However, when we added 82-kDa ChAT conditioned media to cells expressing 82-kDa ChAT, it inhibited neurite outgrowth. If extracellular NRG1 is produced in higher levels by 82-kDa ChAT expressing cells it would explain both of these observations. Therefore further experiments are needed to confirm whether these changes are NRG1 and/or ERBB4-dependent.

Based on the NRG1 dependent neurite outgrowth in 82-kDa ChAT expressing cells, increased response to p-ERBB4 stimulation by FBS and recombinant NRG1, and effects of 82-kDa ChAT conditioned media on vector expressing cells, we tested whether we could measure NRG1 in the media of 82-kDa ChAT or vector expressing cells. We were able to detect an ~6 kDa NRG1 immunoreactive band in concentrated media samples conditioned on 82-kDa ChAT expressing cells, but not in vector expressing cells.

However, when we attempted to measure NRG1 levels by ELISA we were unable to detect NRG1 in conditioned media, whether or not it was concentrated. In fact, when we tested concentrated media NRG1 values fell below values for blank samples, which indicated that a factor present in the media maybe blocking antibody binding. We therefore also explored whether adding FBS to media could alter NRG1 detection. Though only the first replicate, when we added 0.125 ng/mL recombinant NRG1 peptide to media containing FBS we detected NRG1 levels ~25% below expected values, and >50% below expected values for when we added 1 or 4 ng/mL NRG1 to the media. We also observed that high levels (4 ng/mL) of NRG1 peptide, but not low NRG1 treatment (0.125 ng/mL), added to vector or 82-kDa ChAT conditioned media also produced lower than expected (16-20%) values of NRG1. Given that media conditioned on cells for 48 h would have some FBS content, these data support the assumption that FBS may be partially blocking the NRG1 capture antibody, and could explain why low levels of NRG1 could be more easily detected. Interestingly, when we added 0.125 ng/mL NRG1 to conditioned media from vector expressing cells we measured a NRG1 concentration 16% higher than expected, and when we added the same amount to 82-kDa ChAT expressing cells we measured a NRG1 concentration 52% higher than expected. Therefore, it may be possible that the NRG1 concentration in unconcentrated 82-kDa ChAT conditioned media is ~50-60 pg/mL, which is below the 125 pg/mL detection limit of the ELISA assay. More testing is needed to verify this, including producing a NRG1 standard curve in the 100-250 pg/mL range in conditioned media, and comparing it to standard curves generated in serum-free, low serum and high serum cell culture media.

The data presented in this chapter supports a model whereby 82-kDa ChAT association with chromatin at synapse related genes results in increased neurite outgrowth and complexity (**Fig. 4.14**). We show that 82-kDa ChAT associates with synapse related genes at NFAT enriched sequences (possibly in complex with NFAT and AP-1), leading to increased steady-state protein levels of NRG1, mGlu5 and NLGN1. NRG1 is cleaved in the membrane to produce the NRG1 EGF domain, which binds to ERBB4 and promotes p-ERBB4. These changes coincide with increased p-ERBB4 responses, possibly due to increased extracellular NRG1 release and ERBB4 binding, increased surface receptors, or a combination of some or all of these factors. Previous research

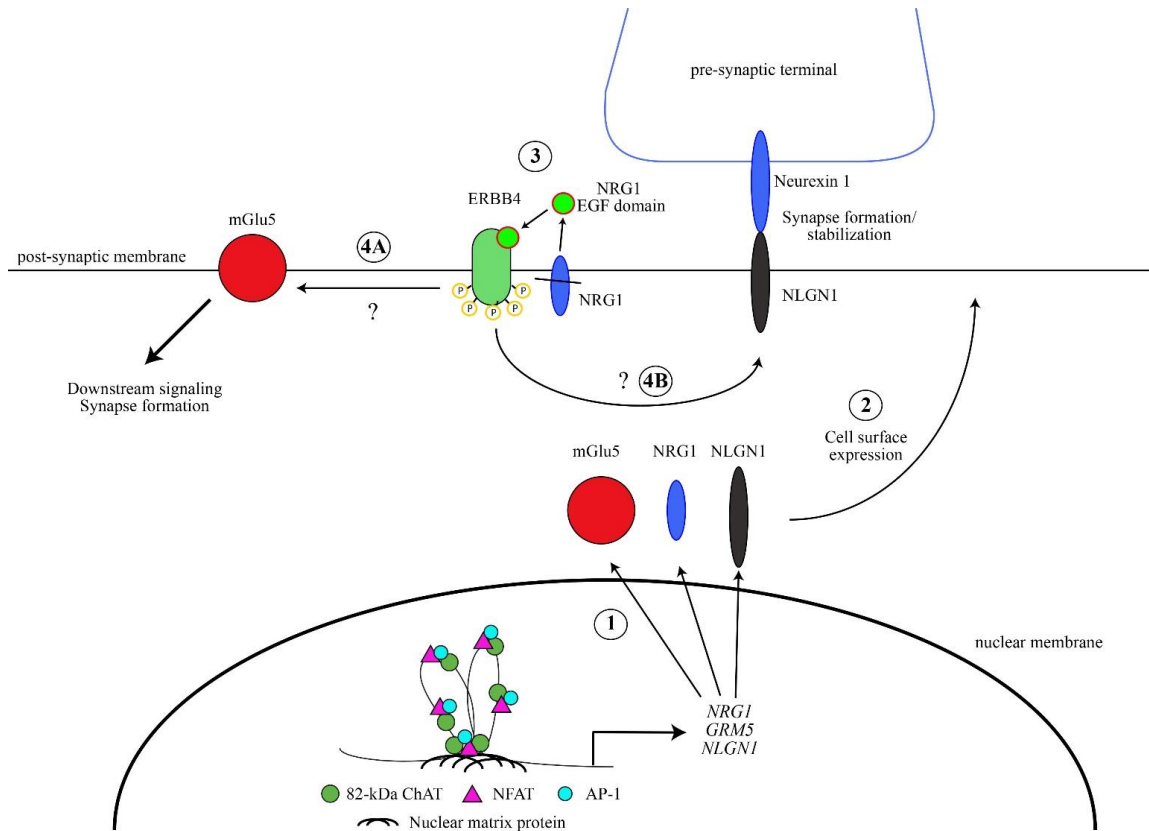


Figure 4-14. Proposed model for the role of 82-kDa ChAT in neurite outgrowth and complexity.

(1) 82-kDa ChAT, possibly in complex with NFAT and AP-1, increases gene expression of *NRG1*, *GRM5* and *NLGN1*, leading to increased protein expression of NRG1, mGlu5 and NLGN1, respectively. (2) This results in increased cell-surface expression of all three proteins. (3) NRG1 is cleaved within the membrane to produce the extracellular NRG1 EGF domain, which binds ERBB4 and increases its phosphorylation. (4) Through unknown mechanisms, phosphorylated ERBB4 may signal to (A) mGlu5, causing downstream signaling leading to increased synapse formation; and/or (B) NLGN1 to promote complex formation with neurexin 1, leading to increased synapse formation and stabilization. See discussion for more detail.

suggests that signaling from p-ERBB4 to mGlu5 and NLGN1 may then result in the observed increases in neurite complexity seen in 82-kDa ChAT expressing cells, though this remains to be investigated in this model system.

We have demonstrated that NRG1, mGlu5 and NLGN1 are increased in 82-kDa ChAT expressing cells, that the cells are more responsive to p-ERBB4 by NRG1 and growth factors, and that the cells produce complex neuritic branching. However, there are still a few additional experiments that are needed to support the data presented in this chapter. For example, additional experiments will help determine how 82-kDa ChAT expressing cells have an increased and sustained p-ERBB4 response to growth factors and exogenous NRG1. We can differentiate 82-kDa ChAT or vector expressing cells in the presence of NRG1 antibody to see if that reverses the increased p-ERBB4 response to agonist stimulation. Cell-surface biotinylation in both reducing and non-reducing conditions can be used to determine how many surface receptors are present, whether they are in a complex with ERBB2 or other EGF receptors, and to test an interaction with PSD93. Another key experiment will be to co-culture 82-kDa ChAT and vector expressing cells, separated by a permeable transwell insert, in the presence or absence of NRG1 antibody. By measuring p-ERBB4 levels following agonist stimulation in vector expressing cells, we can clarify whether NRG1 or another factor released by the 82-kDa ChAT expressing cells could alter the response to ERBB4 phosphorylation in other cells. In other experiments we can repeat neurite outgrowth experiments with low dose EGFR inhibitors, in order to explore whether EGF receptors such as ERBB4 are the main signal transduction pathway involved. It will also be important to culture vector expressing cells in the presence of exogenous NRG1 to show whether this produces similar neurite branching to 82-kDa ChAT expressing cells. We can assess downstream signaling pathways by measuring PLCB1 phosphorylation, IP3 formation, or looking at downstream PKC and/or ERK activation of NF- κ B or AP-1. For example, atypical PKC- ι overexpression has been shown to be involved in NF- κ B-mediated neuronal differentiation of PC12 cells (Wooten *et al.* 1999). Finally, we can determine whether NFAT is required for the observed protein expression changes using siRNA knockdown, and can assess how 82-kDa ChAT could be altering gene expression using CHIP for RNA

Polymerase II and histone acetylation/methylation markers at gene promoters or near peak binding sites.

If 82-kDa ChAT expression in human cholinergic neurons results in increased synaptic complexity during development and synapse maintenance in adulthood, the potential importance of these findings should not be understated. Increased synaptic connections to cholinergic projection areas have implications for normal processing in these regions and for the response to stimulation. For example, synapse complexity and level of dendritic arborization in the hippocampus correlate with the magnitude of LTP response (Toni *et al.* 1999; Alonso *et al.* 2004; Chen *et al.* 2010). Increasing dendritic arborization in the CA3 of mice leads to improvements in spatial memory tasks (Vollala *et al.* 2011), and stress-induced reductions in hippocampal dendritic spine density correlates to LTP attenuation and long-term depression induction (Chen *et al.* 2010). Disruptions in normal synapse development can lead to neurological diseases, such as schizophrenia (Reviewed in Faludi and Mirnics 2011; Yin *et al.* 2012). *NRG1* has been identified as a schizophrenia susceptibility gene (Stefansson *et al.* 2002; Stefansson *et al.* 2003; Norton *et al.* 2006), and *NRG1* levels are abnormally increased in schizophrenia patients (Chong *et al.* 2008; Pitcher *et al.* 2011). Importantly, the same *NRG1* schizophrenia susceptibility haplotype on 8p12 was found significantly associated with late-onset Alzheimer's disease (AD) patients; correlated to increased cognitive deficits and rapid decline (Go *et al.* 2005). In the same study, Go *et al.* (2005) reported a significant *NRG1* single-nucleotide polymorphism (rs392499) also associated with these late-onset patients. In AD, initial gain-of-function LTP induction is followed quickly by synapse dysfunction and degeneration in the hippocampus and frontal cortex, and is one of the earliest markers of the toxic effects of A β (Reviewed in Selkoe 2002; Lacor *et al.* 2007; Reviewed in Arendt 2009). It is noteworthy that synapse dysfunction is also correlated with memory impairments seen early in AD (DeKosky and Scheff 1990). Further, mGlu5 has been shown to bind to oligomeric A β -cellular prion protein (PrP(C)) complexes, leading to dendritic spine loss and learning and memory impairments (Um *et al.* 2013), which may mean that increases in mGlu5 not only promote synapse maintenance but also increase sensitivity to A β toxicity. Finally, NFAT isoform nuclear levels are altered in both MCI and AD (Abdul *et al.* 2010). The data presented in this

chapter supports the hypothesis that NFAT and 82-kDa ChAT work together to alter the gene and protein expression of mGlu5, NLGN1 and NRG1, leading to increased complexity of neurite branching. Therefore, 82-kDa ChAT expression during development may have important implications for cognition, learning and memory. In addition, altered localization of 82-kDa ChAT during MCI or AD (Gill *et al.* 2007) may have implications for the etiology and progression of AD or other neurodegenerative diseases.

4.5 References

- Abdul HM, Furman JL, Sama MA, Mathis DM, Norris CM (2010) NFATs and Alzheimer's Disease. *Mol Cell Pharmacol*, 2: 7-14.
- Agostinho P, Lopes JP, Velez Z, Oliveira CR (2008) Overactivation of calcineurin induced by amyloid-beta and prion proteins. *Neurochem Int*, 52: 1226-1233.
- Alagarsamy S, Saugstad J, Warren L, Mansuy IM, Gereau RW 4th, Conn PJ (2005) NMDA-induced potentiation of mGluR5 is mediated by activation of protein phosphatase 2B/calcineurin. *Neuropharmacology*, 49 Suppl 1: 135-145.
- Albers S, Inthathirath F, Gill SK, Winick-Ng W, Jaworski E, Wong DY, Gros R, Rylett RJ (2014) Nuclear 82-kDa choline acetyltransferase decreases amyloidogenic APP metabolism in neurons from APP/PS1 transgenic mice. *Neurobiol Dis*, 69: 32-42.
- Arendt T (2009) Synaptic degeneration in Alzheimer's disease. *Acta Neuropathol*, 118: 167-179.
- Aznavour N, Mechawar N, Descarries L (2002) Comparative analysis of cholinergic innervation in the dorsal hippocampus of adult mouse and rat: a quantitative immunocytochemical study. *Hippocampus*, 12: 206-217.
- Badran BM, Wolinsky SM, Burny A, Willard-Gallo KE (2002) Identification of three NFAT binding motifs in the 5'-upstream region of the human CD3gamma gene that differentially bind NFATc1, NFATc2, and NF-kappa B p50. *J Biol Chem*, 277: 47136-47148.
- Benita Y, Cao Z, Giallourakis C, Li C, Gardet A, Xavier RJ (2010) Gene enrichment profiles reveal T-cell development, differentiation, and lineage-specific transcription factors including ZBTB25 as a novel NF-AT repressor. *Blood*, 115: 5376-5384.

- Bloem B, Schoppink L, Rotaru DC, Faiz A, Hendriks P, Mansvelder HD, van de Berg WD, Wouterlood FG (2014) Topographic mapping between basal forebrain cholinergic neurons and the medial prefrontal cortex in mice. *J Neurosci*, 34: 16234-16246.
- Bjarnadottir M, Misner DL, Haverfield-Gross S, Bruun S, Helgason VG, Stefansson H, Sigmundsson A, Firth DR, Nielsen B, Stefansdottir R, Novak TJ, Stefansson K, Gurney ME, Andresson T (2007) Neuregulin1 (NRG1) signaling through Fyn modulates NMDA receptor phosphorylation: differential synaptic function in NRG1^{+/-} knock-outs compared with wild-type mice. *J Neurosci*, 27: 4519-4529.
- Boise LH, Petryniak B, Mao X, June CH, Wang CY, Lindsten T, Bravo R, Kovary K, Leiden JM, Thompson CB (1993) The NFAT-1 DNA binding complex in activated T cells contains Fra-1 and JunB. *Mol Cell Biol*, 13: 1911-1919.
- Chen L, Glover JN, Hogan PG, Rao A, Harrison SC (1998) Structure of the DNA-binding domains from NFAT, Fos and Jun bound specifically to DNA. *Nature*, 392: 42-48.
- Chen Y, Cao X (2009) NFAT directly regulates Nkx2-5 transcription during cardiac cell differentiation. *Biol Cell*, 101: 335-349.
- Chen Y, Rex CS, Rice CJ, Dubé CM, Gall CM, Lynch G, Baram TZ (2010) Correlated memory defects and hippocampal dendritic spine loss after acute stress involve corticotropin-releasing hormone signaling. *Proc Natl Acad Sci U S A*, 107: 13123-13128.
- Chen YJ, Zhang M, Yin DM, Wen L, Ting A, Wang P, Lu YS, Zhu XH, Li SJ, Wu CY, Wang XM, Lai C, Xiong WC, Mei L, Gao TM (2010) ErbB4 in parvalbumin-positive interneurons is critical for neuregulin 1 regulation of long-term potentiation. *Proc Natl Acad Sci U S A*, 107: 21818-21823.
- Choi YB, Li HL, Kassabov SR, Jin I, Puthanveetil SV, Karl KA, Lu Y, Kim JH, Bailey CH, Kandel ER (2011) Neurexin-neuroigin transsynaptic interaction mediates

learning-related synaptic remodeling and long-term facilitation in aplysia. *Neuron*, 70: 468-481.

Chong VZ, Thompson M, Beltaifa S, Webster MJ, Law AJ, Weickert CS (2008) Elevated neuregulin-1 and ErbB4 protein in the prefrontal cortex of schizophrenic patients. *Schizophr Res*, 100: 270-280.

Craig AM, Kang Y (2007) Neurexin-neuroligin signaling in synapse development. *Curr Opin Neurobiol*, 17: 43-52.

Dai SH, Qin N, Chen T, Luo P, Zhang L, Rao W, Yang YF, Jiang XF, Fei Z (2014) Activation of mGluR5 attenuates NMDA-induced neurotoxicity through disruption of the NMDAR-PSD-95 complex and preservation of mitochondrial function in differentiated PC12 cells. *Int J Mol Sci*, 15: 10892-10907.

DeKosky ST, Scheff SW (1990) Synapse loss in frontal cortex biopsies in Alzheimer's disease: correlation with cognitive severity. *Ann Neurol*, 27: 457-464.

Delling U, Tureckova J, Lim HW, De Windt LJ, Rotwein P, Molkentin JD (2000) A calcineurin-NFATc3-dependent pathway regulates skeletal muscle differentiation and slow myosin heavy-chain expression. *Mol Cell Biol*, 20: 6600-6611.

Domenici MR, Pintor A, Potenza RL, Gaudi S, Grò MC, Passarelli F, Reggio R, Galluzzo M, Massotti M, Popoli P (2003) Metabotropic glutamate receptor 5 (mGluR5)-mediated phosphoinositide hydrolysis and NMDA-potentiating effects are blunted in the striatum of aged rats: a possible additional mechanism in striatal senescence. *Eur J Neurosci*, 17: 2047-2055.

Eckenstein FP, Baughman RW, Quinn J (1988) An anatomical study of cholinergic innervation in rat cerebral cortex. *Neuroscience*, 25: 457-474.

Faludi G, Mirnics K (2011) Synaptic changes in the brain of subjects with schizophrenia. *Int J Dev Neurosci*, 29: 305-309.

- Ferguson SM, Savchenko V, Apparsundaram S, Zwick M, Wright J, Heilman CJ, Yi H, Levey AI, Blakely RD (2003) Vesicular localization and activity-dependent trafficking of presynaptic choline transporters. *J Neurosci*, 23: 9697-9709.
- Fisher WG, Yang PC, Medikonduri RK, Jafri MS (2006) NFAT and NFkappaB activation in T lymphocytes: a model of differential activation of gene expression. *Ann Biomed Eng*, 34: 1712-1728.
- Freeman A, Franciscovich A, Bowers M, Sandstrom DJ, Sanyal S (2011) NFAT regulates pre-synaptic development and activity-dependent plasticity in *Drosophila*. *Mol Cell Neurosci*, 46: 535-547.
- Gerecke KM, Wyss JM, Carroll SL (2004) Neuregulin-1beta induces neurite extension and arborization in cultured hippocampal neurons. *Mol Cell Neurosci*, 27: 379-393.
- Gill SK, Ishak M, Dobransky T, Haroutunian V, Davis KL, Rylett RJ (2007) 82-kDa choline acetyltransferase is in nuclei of cholinergic neurons in human CNS and altered in aging and Alzheimer disease. *Neurobiol Aging*, 28: 1028-1040.
- Go RC, Perry RT, Wiener H, Bassett SS, Blacker D, Devlin B, Sweet RA (2005) Neuregulin-1 polymorphism in late onset Alzheimer's disease families with psychoses. *Am J Med Genet B Neuropsychiatr Genet*, 139B: 28-32.
- Graef IA, Wang F, Charron F, Chen L, Neilson J, Tessier-Lavigne M, Crabtree GR (2003) Neurotrophins and netrins require calcineurin/NFAT signaling to stimulate outgrowth of embryonic axons. *Cell*, 113: 657-670.
- Graus-Porta D, Beerli RR, Daly JM, Hynes NE (1997) ErbB-2, the preferred heterodimerization partner of all ErbB receptors, is a mediator of lateral signaling. *EMBO J*, 16: 1647-1655.
- Groth RD, Mermelstein PG (2003) Brain-derived neurotrophic factor activation of NFAT (nuclear factor of activated T-cells)-dependent transcription: a role for the

transcription factor NFATc4 in neurotrophin-mediated gene expression. *J Neurosci*, 23: 8125-8134.

Groth RD, Coicou LG, Mermelstein PG, Seybold VS (2007) Neurotrophin activation of NFAT-dependent transcription contributes to the regulation of pro-nociceptive genes. *J Neurochem*, 102: 1162-1174.

Gustems M, Woellmer A, Rothbauer U, Eck SH, Wieland T, Lutter D, Hammerschmidt W (2014) c-Jun/c-Fos heterodimers regulate cellular genes via a newly identified class of methylated DNA sequence motifs. *Nucleic Acids Res*, 42: 3059-3072.

Hahn CG, Wang HY, Cho DS, Talbot K, Gur RE, Berrettini WH, Bakshi K, Kamins J, Borgmann-Winter KE, Siegel SJ, Gallop RJ, Arnold SE (2006) Altered neuregulin 1-erbB4 signaling contributes to NMDA receptor hypofunction in schizophrenia. *Nat Med*, 12: 824-828.

Hannan AJ, Blakemore C, Katsnelson A, Vitalis T, Huber KM, Bear M, Roder J, Kim D, Shin HS, Kind PC (2001) PLC-beta1, activated via mGluRs, mediates activity-dependent differentiation in cerebral cortex. *Nat Neurosci*, 4: 282-288.

Hashemi SH, Li JY, Ahlman H, Dahlström A (2003) SSR2(a) receptor expression and adrenergic/cholinergic characteristics in differentiated SH-SY5Y cells. *Neurochem Res*, 28: 449-460.

Hayashi MK, Tang C, Verpelli C, Narayanan R, Stearns MH, Xu RM, Li H, Sala C, Hayashi Y (2009) The postsynaptic density proteins Homer and Shank form a polymeric network structure. *Cell*, 137: 159-171.

Heit JJ, Apelqvist AA, Gu X, Winslow MM, Neilson JR, Crabtree GR, Kim SK (2006) Calcineurin/NFAT signalling regulates pancreatic beta-cell growth and function. *Nature*, 443: 345-349.

Huang YZ, Won S, Ali DW, Wang Q, Tanowitz M, Du QS, Pelkey KA, Yang DJ, Xiong WC, Salter MW, Mei L (2000) Regulation of neuregulin signaling by PSD-95 interacting with ErbB4 at CNS synapses. *Neuron*, 26: 443-455.

- Iwakura Y, Nawa H (2013) ErbB1-4-dependent EGF/neuregulin signals and their cross talk in the central nervous system: pathological implications in schizophrenia and Parkinson's disease. *Front Cell Neurosci*, 7: 4.
- Kammermeier PJ, Worley PF (2007) Homer 1a uncouples metabotropic glutamate receptor 5 from postsynaptic effectors. *Proc Natl Acad Sci U S A*, 104: 6055-6060.
- Kernohan KD, Vernimmen D, Gloor GB, Bérubé NG (2014) Analysis of neonatal brain lacking ATRX or MeCP2 reveals changes in nucleosome density, CTCF binding and chromatin looping. *Nucleic Acids Res*, 42: 8356-8368.
- Kheradpour P, Kellis M (2014) Systematic discovery and characterization of regulatory motifs in ENCODE TF binding experiments. *Nucleic Acids Res*, 42: 2976-2987.
- König A, Fernandez-Zapico ME, Ellenrieder V (2010) Primers on molecular pathways-the NFAT transcription pathway in pancreatic cancer. *Pancreatology*, 10: 416-422.
- Kouzarides T, Ziff E (1988) The role of the leucine zipper in the fos-jun interaction. *Nature*, 336: 646-651.
- Kuhn PH, Wang H, Dislich B, Colombo A, Zeitschel U, Ellwart JW, Kremmer E, Rossner S, Lichtenthaler SF (2010) ADAM10 is the physiologically relevant, constitutive alpha-secretase of the amyloid precursor protein in primary neurons. *EMBO J*, 29: 3020-3032.
- Kwon OB, Longart M, Vullhorst D, Hoffman DA, Buonanno A (2005) Neuregulin-1 reverses long-term potentiation at CA1 hippocampal synapses. *J Neurosci*, 25: 9378-9383.
- Lacor PN, Buniel MC, Furlow PW, Clemente AS, Velasco PT, Wood M, Viola KL, Klein WL (2007) Abeta oligomer-induced aberrations in synapse composition, shape, and density provide a molecular basis for loss of connectivity in Alzheimer's disease. *J Neurosci*, 27: 796-807.

- Law MJ, Lower KM, Voon HP, Hughes JR, Garrick D, Viprakasit V, Mitson M, De Gobbi M, Marra M, Morris A, Abbott A, Wilder SP, Taylor S, Santos GM, Cross J, Ayyub H, Jones S, Ragoussis J, Rhodes D, Dunham I, Higgs DR, Gibbons RJ (2010) ATR-X syndrome protein targets tandem repeats and influences allele-specific expression in a size-dependent manner. *Cell*, 143: 367-378.
- Levy MA, Kernohan KD, Jiang Y, Bérubé NG (2015) ATRX promotes gene expression by facilitating transcriptional elongation through guanine-rich coding regions. *Hum Mol Genet*, 24: 1824-1835.
- Li B, Woo RS, Mei L, Malinow R (2007) The neuregulin-1 receptor erbB4 controls glutamatergic synapse maturation and plasticity. *Neuron*, 54: 583-597.
- Liu Q, Chen Y, Auger-Messier M, Molkentin JD (2012) Interaction between NFκB and NFAT coordinates cardiac hypertrophy and pathological remodeling. *Circ Res*, 110: 1077-1086.
- Luo X, Prior M, He W, Hu X, Tang X, Shen W, Yadav S, Kiryu-Seo S, Miller R, Trapp BD, Yan R (2011) Cleavage of neuregulin-1 by BACE1 or ADAM10 protein produces differential effects on myelination. *J Biol Chem*, 286: 23967-23974.
- Macian F (2005) NFAT proteins: key regulators of T-cell development and function. *Nat Rev Immunol*, 5: 472-484.
- Macián F, López-Rodríguez C, Rao A (2001) Partners in transcription: NFAT and AP-1. *Oncogene*, 20: 2476-2489.
- Magno L, Kretz O, Bert B, Ersözülü S, Vogt J, Fink H, Kimura S, Vogt A, Monyer H, Nitsch R, Naumann T (2011) The integrity of cholinergic basal forebrain neurons depends on expression of Nkx2-1. *Eur J Neurosci*, 34: 1767-1782.
- Mammucari C, Tommasi di Vignano A, Sharov AA, Neilson J, Havrda MC, Roop DR, Botchkarev VA, Crabtree GR, Dotto GP (2005) Integration of Notch 1 and calcineurin/NFAT signaling pathways in keratinocyte growth and differentiation control. *Dev Cell*, 8: 665-676.

- Marballi K, Cruz D, Thompson P, Walss-Bass C (2012) Differential neuregulin 1 cleavage in the prefrontal cortex and hippocampus in schizophrenia and bipolar disorder: preliminary findings. *PLoS One*, 7: e36431.
- Mei L, Xiong WC (2008) Neuregulin 1 in neural development, synaptic plasticity and schizophrenia. *Nat Review Neurosci*, 9: 437-452.
- Nakabeppu Y, Ryder K, Nathans D (1988) DNA binding activities of three murine Jun proteins: stimulation by Fos. *Cell*, 55: 907-915.
- Nakamuta S, Funahashi Y, Namba T, Arimura N, Picciotto MR, Tokumitsu H, Soderling TR, Sakakibara A, Miyata T, Kamiguchi H, Kaibuchi K (2011) Local application of neurotrophins specifies axons through inositol 1,4,5-trisphosphate, calcium, and Ca²⁺/calmodulin-dependent protein kinases. *Sci Signal*, 4: ra76.
- Nash MS, Schell MJ, Atkinson PJ, Johnston NR, Nahorski SR, Challiss RA (2002) Determinants of metabotropic glutamate receptor-5-mediated Ca²⁺ and inositol 1,4,5-trisphosphate oscillation frequency. Receptor density versus agonist concentration. *J Biol Chem*, 277: 35947-35960.
- Neddens J, Buonanno A (2011) Expression of the neuregulin receptor ErbB4 in the brain of the rhesus monkey (*Macaca mulatta*). *PLoS One*, 6: e27337.
- Nguyen T, Di Giovanni S (2008) NFAT signaling in neural development and axon growth. *Int J Dev Neurosci* 26: 141-145.
- Norton N, Moskvina V, Morris DW, Bray NJ, Zammit S, Williams NM, Williams HJ, Preece AC, Dwyer S, Wilkinson JC, Spurlock G, Kirov G, Buckland P, Waddington JL, Gill M, Corvin AP, Owen MJ, O'Donovan MC (2006) Evidence that interaction between neuregulin 1 and its receptor erbB4 increases susceptibility to schizophrenia. *Am J Med Genet B Neuropsychiatr Genet*, 141B: 96-101.
- Parker MJ, Zhao S, Brecht DS, Sanes JR, Feng G (2004) PSD93 regulates synaptic stability at neuronal cholinergic synapses. *J Neurosci*, 24: 378-388.

- Pitcher GM, Kalia LV, Ng D, Goodfellow NM, Yee KT, Lambe EK, Salter MW (2011) Schizophrenia susceptibility pathway neuregulin 1-ErbB4 suppresses Src upregulation of NMDA receptors. *Nat Med*, 17: 470-478.
- Rodrigues SM, Bauer EP, Farb CR, Schafe GE, LeDoux JE (2002) The group I metabotropic glutamate receptor mGluR5 is required for fear memory formation and long-term potentiation in the lateral amygdala. *J Neurosci*, 22: 5219-5229.
- Savonenko AV, Melnikova T, Laird FM, Stewart KA, Price DL, Wong PC (2008) Alteration of BACE1-dependent NRG1/ErbB4 signaling and schizophrenia-like phenotypes in BACE1-null mice. *Proc Natl Acad Sci U S A*, 105: 5585-5590.
- Selkoe DJ (2002) Alzheimer's disease is a synaptic failure. *Science*, 298: 789-791.
- Seshadri S, Faust T, Ishizuka K, Delevich K, Chung Y, Kim SH, Cowles M, Niwa M, Jaaro-Peled H, Tomoda T, Lai C, Anton ES, Li B, Sawa A (2015) Interneuronal DISC1 regulates NRG1-ErbB4 signalling and excitatory-inhibitory synapse formation in the mature cortex. *Nat Commun*, 6: 10118.
- Shindo H, Thomas TP, Larkin DD, Karihaloo AK, Inada H, Onaya T, Stevens MJ, Greene DA (1996) Modulation of basal nitric oxide-dependent cyclic-GMP production by ambient glucose, myo-inositol, and protein kinase C in SH-SY5Y human neuroblastoma cells. *J Clin Invest*, 97: 736-745.
- Slonimsky JD, Mattaliano MD, Moon JI, Griffith LC, Birren SJ (2006) Role for calcium/calmodulin-dependent protein kinase II in the p75-mediated regulation of sympathetic cholinergic transmission. *Proc Natl Acad Sci U S A*, 103: 2915-2919.
- Sourdret V, Russier M, Daoudal G, Ankri N, Debanne D (2003) Long-term enhancement of neuronal excitability and temporal fidelity mediated by metabotropic glutamate receptor subtype 5. *J Neurosci*, 23: 10238-10248.

- Stine WB Jr, Dahlgren KN, Krafft GA, LaDu MJ (2003) In vitro characterization of conditions for amyloid-beta peptide oligomerization and fibrillogenesis. *J Biol Chem*, 278: 11612-11622.
- Sweeney C, Lai C, Riese DJ 2nd, Diamonti AJ, Cantley LC, Carraway KL 3rd (2000) Ligand discrimination in signaling through an ErbB4 receptor homodimer. *J Biol Chem*, 275: 19803-19807.
- Stefansson H, Sigurdsson E, Steinthorsdottir V, Bjornsdottir S, Sigmundsson T, Ghosh S, Brynjolfsson J, Gunnarsdottir S, Ivarsson O, Chou TT, Hjaltason O, Birgisdottir B, Jonsson H, Gudnadottir VG, Gudmundsdottir E, Bjornsson A, Ingvarsson B, Ingason A, Sigfusson S, Hardardottir H, Harvey RP, Lai D, Zhou M, Brunner D, Mutel V, Gonzalo A, Lemke G, Sainz J, Johannesson G, Andresson T, Gudbjartsson D, Manolescu A, Frigge ML, Gurney ME, Kong A, Gulcher JR, Petursson H, Stefansson K (2002) Neuregulin 1 and susceptibility to schizophrenia. *Am J Hum Genet*, 71: 877-892.
- Stefansson H, Sarginson J, Kong A, Yates P, Steinthorsdottir V, Gudfinnsson E, Gunnarsdottir S, Walker N, Petursson H, Crombie C, Ingason A, Gulcher JR, Stefansson K, St Clair D (2003) Association of neuregulin 1 with schizophrenia confirmed in a Scottish population. *Am J Hum Genet*, 72: 83-87.
- Syed N, Reddy K, Yang DP, Taveggia C, Salzer JL, Maurel P, Kim HA (2010) Soluble neuregulin-1 has bifunctional, concentration-dependent effects on Schwann cell myelination. *J Neurosci*, 30: 6122-6131.
- Szabó GG, Holderith N, Gulyás AI, Freund TF, Hájos N (2010) Distinct synaptic properties of perisomatic inhibitory cell types and their different modulation by cholinergic receptor activation in the CA3 region of the mouse hippocampus. *Eur J Neurosci*, 31: 2234-2246.
- Tao-Cheng JH, Yang Y, Reese TS, Dosemeci A (2015) Differential distribution of Shank and GKAP at the postsynaptic density. *PLoS One*, 10: e0118750.

- Ting AK, Chen Y, Wen L, Yin DM, Shen C, Tao Y, Liu X, Xiong WC, Mei L (2011) Neuregulin 1 promotes excitatory synapse development and function in GABAergic interneurons. *J Neurosci*, 31: 15-25.
- Toni N, Buchs PA, Nikonenko I, Bron CR, Muller D (1999) LTP promotes formation of multiple spine synapses between a single axon terminal and a dendrite. *Nature*, 402: 421-425.
- Tu JC, Xiao B, Naisbitt S, Yuan JP, Petralia RS, Brakeman P, Doan A, Aakalu VK, Lanahan AA, Sheng M, Worley PF (1999) Coupling of mGluR/Homer and PSD-95 complexes by the Shank family of postsynaptic density proteins. *Neuron*, 583-592.
- Tzahar E, Waterman H, Chen X, Levkowitz G, Karunakaran D, Lavi S, Ratzkin BJ, Yarden Y (1996) A hierarchical network of interreceptor interactions determines signal transduction by Neu differentiation factor/neuregulin and epidermal growth factor. *Mol Cell Biol*, 16: 5276-5287.
- Um JW, Kaufman AC, Kostylev M, Heiss JK, Stagi M, Takahashi H, Kerrisk ME, Vortmeyer A, Wisniewski T, Koleske AJ, Gunther EC, Nygaard HB, Strittmatter SM (2013) Metabotropic glutamate receptor 5 is a coreceptor for Alzheimer $\alpha\beta$ oligomer bound to cellular prion protein. *Neuron*, 79: 887-902.
- Vollala VR, Upadhy S, Nayak S (2011) Enhanced dendritic arborization of hippocampal CA3 neurons by Bacopa monniera extract treatment in adult rats. *Rom J Morphol Embryol*, 52: 879-886.
- Winick-Ng W, Caetano FA, Winick-Ng J, Morey TM, Heit B, Rylett RJ (2016) 82-kDa choline acetyltransferase and SATB1 localize to β -amyloid induced matrix attachment regions. *Sci Rep*, 6: 23914.
- Woo RS, Lee JH, Yu HN, Song DY, Baik TK (2011) Expression of ErbB4 in the neurons of Alzheimer's disease brain and APP/PS1 mice, a model of Alzheimer's disease. *Anat Cell Biol*, 44: 116-127.

- Wooten MW, Seibenhener ML, Zhou G, Vandenplas ML, Tan TH (1999)
Overexpression of atypical PKC in PC12 cells enhances NGF-responsiveness and survival through an NF-kappaB dependent pathway. *Cell Death Differ*, 6: 753-764.
- Wu HY, Hudry E, Hashimoto T, Kuchibhotla K, Rozkalne A, Fan Z, Spires-Jones T, Xie H, Arbel-Ornath M, Grosskreutz CL, Bacskai BJ, Hyman BT (2010)
Amyloid beta induces the morphological neurodegenerative triad of spine loss, dendritic simplification, and neuritic dystrophies through calcineurin activation. *J Neurosci*, 30: 2636-2649.
- Yang H, Chen C (2008) Cyclooxygenase-2 in synaptic signaling. *Curr Pharm Des*, 14: 1443-1451.
- Yin DM, Chen YJ, Sathyamurthy A, Xiong WC, Mei L (2012) Synaptic dysfunction in schizophrenia. *Adv Exp Med Biol*, 970: 493-516.
- Zhao L, Jiao Q, Huang C, Hou N, Chen X, Zhang J, Yang P, Xu X, Song T, Liu Y (2014) mGluR5 promotes the differentiation of rat neural progenitor cells into cholinergic neurons and activation of extracellular signal-related protein kinases. *Neuroreport*, 25: 427-434.
- Zhu X, Lai C, Thomas S, Burden SJ (1995) Neuregulin receptors, erbB3 and erbB4, are localized at neuromuscular synapses. *EMBO J*, 14: 5842-5848.

Chapter 5

5 Discussion

The studies presented in this thesis describe a novel role for nuclear localized 82-kDa choline acetyltransferase in chromatin organization, gene expression, neurite outgrowth and in an epigenetic response to cellular perturbations. Broadly, by performing the first full genome sequencing chromatin immunoprecipitation study for both 82-kDa ChAT and special-AT rich binding protein 1 (SATB1), we found that 82-kDa ChAT associates with chromatin at gene promoters and introns in cholinergic cells. Following exposure of cultured neural cells to oligomeric A β ₁₋₄₂, 82-kDa ChAT was co-localized with SATB1, with both proteins increasing these genic associations. Both 82-kDa ChAT and SATB1 were localized to scaffolding/matrix attachment regions (S/MARs) and had features of chromatin organizers. 82-kDa ChAT and SATB1 associations with the *APP* gene resulted in A β -induced gene expression reductions of an amyloid precursor protein (*APP*) mRNA transcript variant that is increased in AD patients and which correlates to increases in A β ₁₋₄₂. The 82-kDa ChAT protein exhibited features of chromatin organizers in vehicle-treated cells, and associated at DNA binding motifs for transcription factors involved in synapse formation (**Fig 3-18**). This led us to find that 82-kDa ChAT is involved in neurite outgrowth and complexity during cholinergic differentiation (**Fig 4-14**).

5.1 Limitations of the current studies

There were a number of important limitations to consider from the presented data. First, most of the results presented in this thesis are from *in vitro* cell models of cholinergic expression in differentiated SH-SY5Y cell neuroblastoma cells. It will be important for future studies to verify the results in this thesis using other cholinergic cell

types, including human IMR32 and LA-N-2 neuroblastoma cells to address whether the results are cell-line specific. Additionally, though these cells have morphological and phenotypic characteristics of cholinergic neurons following differentiation (Hashemi *et al.* 2003), cells derived from neuroblastoma lines likely have gene and protein expression characteristics that would not reflect neurons in brain (Reviewed in Gordon *et al.* 2013). Further, cell culture conditions do not fully reflect the environment in the brain without supporting glial cells. Future studies using *in vivo* models to address these limitations are discussed below.

An additional consideration for the presented data is that, though the depth of the data obtained from studies involving ChIP-seq is extensive and can inform a number of novel hypotheses, the data must be verified by further molecular analyses. A good example of this was the ChIP-seq peak identified for SATB1 on *APP*. The ChIP-seq data showed a peak at the region for SATB1 following cell exposure to A β , but no peak in vehicle treated cells. However, when we verified this pattern using ChIP-qPCR we found that there was no statistical difference in the genic association with this region. The apparent inconsistency could be due to stringency on the peak calling. We used $p < 0.00001$ for the peak calling, which is the default peak calling p-value for Galaxy.org, and necessary to produce data that has low false positives and confidence in the data. However, this high level of stringency also has the potential for false negatives. When we reduce the stringency to $p < 0.001$, we now see a peak in the vehicle sample for SATB1, but also ~2000 more peaks for that sample. As this was the first whole genome sequencing study for SATB1 and baseline binding occupancy is unknown, decreasing the stringency of peak calling could introduce a higher false positive rate. Therefore, we decided to use the $p < 0.00001$ value, even though it did not show a peak for SATB1 in the vehicle treatment. An additional limitation was that we were only able to perform the ChIP-seq from stably transfected cells that were derived from a single clone, and with only one repeat for each treatment. Thus, it will be important for future studies to verify ChIP associations for both 82-kDa ChAT and SATB1 on other genomic regions by ChIP-qPCR, and to establish baseline values in regions where 82-kDa CHAT and SATB1 are not predicted to bind.

5.2 Future studies that expand the presented data

The data presented in this thesis point to an important role for 82-kDa ChAT in chromatin organization, leading to an epigenetic response to A β -exposure and changes to neurite development. We found that 82-kDa ChAT alters gene expression of synapse related genes, as well as the *APP* mRNA isoforms containing the Kunitz-type serine protease inhibitor domain (Moir et al. 1998; APP-KPI) in response to exposure of cells to A β . There are some clues in the data presented as to the reasons for these changes, including interactions of 82-kDa ChAT with spliceosome machinery and the nuclear matrix protein Matrin3 identified by mass spectrometry, and the observed changes to the alternatively spliced APP-KPI mRNA isoform. Additionally, 82-kDa ChAT may be in complex with the NFAT transcription factor, involved in synapse formation and maintenance. However, there are a number of interesting hypotheses and questions that have still yet to be explored, as discussed below.

The data obtained to date provide an intriguing hypothesis that 82-kDa ChAT is involved in mRNA splicing of transcripts from synapse formation-related genes. However, we have not yet determined the mechanisms of how the 82-kDa ChAT-chromatin interaction leads to these changes in gene expression; whether this is through mRNA splicing changes, promoter activation or other mechanisms. Additionally, we did not explore whether alterations in chromatin organization could be responsible for the observed changes in synapse-related gene expression. It is possible that these findings are linked, and chromatin looping changes lead to altered gene utilization or mRNA stability. Since we found gene ontology (GO) terms related to synapse and membrane for both 82-kDa ChAT and SATB1 after both vehicle and A β -treatment of cells, we can also hypothesize that these genes may be part of an inter-Topologically Associated Domain (TAD) locus since *NRG1* (chromosome 8 [Chr8]), *GRM5* (Chr11), and *NLGN1* (Chr3) are all on different chromosomes and thus unlikely to be within the same TAD. 82-kDa ChAT could also be involved in transcription elongation, as the chromatin organizer

Alpha Thalassemia/Mental Retardation Syndrome X-Linked (ATRX) prevents the stalling of RNA polymerase II (RNA Pol II) at intragenic regions by interfering with G-quadruplex structure (Levy et al. 2015). It will therefore be important for future studies to use chromatin conformation capture techniques to identify gene and locus specific chromatin looping changes and global chromatin organization. Moreover, ChIP for RNA Pol II and histone markers should also be employed to assess promoter-specific activation and intragenic transcription elongation.

Another interesting finding is the exciting possibility that 82-kDa ChAT could bind directly to DNA. We demonstrated that 82-kDa ChAT has tandem DNA-binding motifs at AT-rich regions and associates with chromatin at regions enriched with AT-rich S/MAR binding motifs. However, these data were indirect and did not prove a direct 82-kDa ChAT-DNA interaction. Thus, we used electrophoretic mobility shift assays (EMSAs) with purified recombinant 82-kDa ChAT with the goal of determining if there is a direct DNA oligomer interaction. When we incubated 82-kDa ChAT with ATC-rich DNA oligomers we were able to observe a shifted band that was stronger than a non-specific band at the same height. This indicated that there may be direct DNA-binding, but the biotinylated-DNA EMSA requires further optimization (i.e. less DNA input, different oligomers, different electrophoresis conditions, comparisons to recombinant 69-kDa ChAT). As an alternative approach, we could perform the EMSA using ³²P-labelled DNA, or other techniques such as microplate ELISA-based assays, or *in vivo* methods such as proximity ligation assays, fluorescence resonance energy transfer (FRET) or atomic force microscopy. Understanding whether 82-kDa ChAT binds directly to DNA, and how this interaction occurs will be important for further elucidating how the protein can alter chromatin organization or gene expression.

As outlined in Chapter 4, there are a number of experiments that are still required to address how 82-kDa ChAT expression alters chromatin organization and gene expression resulting in altered neurite outgrowth and complexity. We showed that the 82-kDa ChAT increases neurite complexity, dependent on extracellular neuregulin 1 (NRG1) peptide. NRG1 also has increased protein levels in cells expressing 82-kDa ChAT. Interestingly, receptor tyrosine-protein kinase erbB-4 (ERBB4), which has a

binding site for NRG1 (Tzahar *et al.* 1996; Sweeney *et al.* 2000; Savonenko *et al.* 2008), had increased phosphorylation in response to agonist activation in 82-kDa ChAT-expressing cells. In addition, ERBB4 phosphorylation has been shown previously to result in downstream signaling that promotes synapse formation and maintenance (Zhu *et al.* 1995; Gerecke *et al.* 2004; Reviewed in Iwakura and Nawa 2013). However to date, we have not yet tested whether there is a direct link between NRG1, ERBB4 and these downstream signals, or how 82-kDa ChAT leads to the observed gene expression changes. Some of the essential experiments include: cell surface biotinylation to assess ERBB4 receptor density and complex formation; measuring downstream signal transduction pathways; and ChIP/chromatin conformation capture techniques to address the mechanisms for gene expression changes (see Chapter 4 for more detail). These experiments will help elucidate the pathway from gene expression changes to phenotype changes observed in these cells, with implications for neurodevelopmental changes in human cholinergic cells. As these proteins are also involved in synapse maintenance and the response to stimulation, we can also consider the implications for aging individuals with lower 82-kDa ChAT expression and individuals with mild cognitive impairment (MCI) and AD where the nuclear localization is lost (Gill *et al.* 2007).

5.3 New studies and hypotheses generated from the presented data

There were a number of experiments that yielded novel data that were not part of the main hypothesis of this thesis, which could be extended to future studies. As discussed in Chapter 3, one significant finding from the ChIP-sequencing data was the discovery that both 82-kDa ChAT and SATB1 are associated with regions within and flanking the centromeres. Centromere organization is required for cell cycle regulation, and essential in neural cells to maintain a post-mitotic state (DeBeauchamp *et al.* 2008; Spremo-Potparević *et al.* 2008; Fernius *et al.* 2013). We also found, by mass spectrometry, an association with structural maintenance of chromosomes protein 1A isoform 1 (SMC1A), a protein involved in chromatin condensation and looping, as well

as cell division (Hirano 2002; Jessberger 2002). Further, we have observed that SH-SY5Y cells expressing 82-kDa ChAT have slower growth *in vitro* both prior to and following differentiation (unpublished observations). Moreover, microarray revealed that IMR32 cells transiently expressing 82-kDa ChAT have gene expression changes for cell cycle related genes (NCBI GEO database accession number: GSE3506; Albers *et al.* 2014). Combined with the findings that 82-kDa ChAT is involved in chromatin organization, and promotes neurite complexity during differentiation, these data collectively suggest that 82-kDa ChAT could play an important role in cholinergic differentiation by promoting neuronal phenotype changes. The cessation of cell division is an important part of neuronal development and cell maintenance in adulthood (reviewed in Herrup and Yang 2007; Frade and Ovejero-Benito 2015). This importance is exemplified in AD where neurons can re-enter the cell cycle accompanied with abnormal centromere division (Spremo-Potparević *et al.* 2008). Therefore, future studies should be designed to explore the role of 82-kDa ChAT in cell cycle regulation.

The CHIP-seq data also revealed a significant gene ontology (GO) term ‘programmed cell death’ for peaks associated with both 82-kDa ChAT and SATB1 after cells were treated with A β . This GO term included 46 genes, many of which with interesting functions related to cell survival or apoptosis. Some of these included *DLC1*, which encodes deleted in liver cancer 1 (DLC1), is involved in caspase-3 and Bcl-2 mediated apoptosis (Zhang *et al.* 2009) and was 2.9 fold increased in our 82-kDa ChAT gene expression microarray (Albers *et al.* 2014); *DCC*, encoding DCC (deleted in colorectal cancer), which prevents apoptosis when bound by its ligand netrin-1, but initiates apoptosis in the absence of ligand (Mehlen *et al.* 1998); and *XRCC2*, which encodes X-ray repair cross complementing 2 (XRCC2) and is involved in DNA double-stranded break repair (Johnson *et al.* 1999). One additional interesting gene was *PRUNE2*, which encodes Prune homolog 2 (PRUNE2). PRUNE2 is involved in many cellular pathways, including apoptosis, synapse function and neuronal differentiation (Machida *et al.* 2006; Valencia *et al.* 2007; Li *et al.* 2012; Tatsumi *et al.* 2015), and was identified as an AD susceptibility gene by genome wide association studies (GWAS) (Potkin *et al.* 2009; Bertram 2011). Therefore, it will be important for future studies to

address how 82-kDa ChAT may help respond to the environmental stress or DNA damage.

In addition to the GO term ‘programmed cell death’, there were a number of additional significant GO terms for 82-kDa ChAT and SATB1 that would be of interest for future studies (**Appendix 10**). Some of these included ‘nucleotide binding’ (114 genes), ‘protein kinase activity’ (55 genes) and ‘GTP-ase binding’ (18 genes), all of which could have interesting implications for transcriptional processing, cell signaling and cell organization. It may be important to understand these additional pathways, as it could explain how we have previously observed gene expression changes without ChIP-association. For example, we previously found that transient 82-kDa ChAT expression in primary neurons altered *GGA3* gene expression, leading to increased lysosomal degradation of β -secretase (Albers *et al.* 2014), but we did not find that 82-kDa ChAT was associated with *GGA3* in our ChIP-seq dataset. Though it is possible our ChIP-seq parameters were too stringent to pick up this interaction, it is more likely that *GGA3* expression was altered through another, as yet unknown, mechanism. Though the regulation of *GGA3* transcription is largely unknown, Kametaka *et al.* (2005) showed that epidermal growth factor receptor (EGFR) activation results in transient phosphorylation of *GGA3* and increased association of *GGA3* with membranes. We found the GO term ‘protein kinase activity’ for 82-kDa ChAT and SATB1 in our ChIP-seq data, and observed increases in the magnitude and duration of receptor tyrosine-protein kinase ERBB4 phosphorylation in 82-kDa ChAT expressing cells. Therefore an intriguing hypothesis is that 82-kDa ChAT alters EGFR responses through ERBB4 or other protein kinases, which results in transient *GGA3* phosphorylation and increased lysosomal degradation of the β -secretase BACE1. Thus, the link between *GGA3*-mediated trafficking of BACE1 and ERBB4 phosphorylation would be an intriguing target for future study. As another example, the aforementioned microarray changes in cell cycle genes (such as *CCND1* [encoding Cyclin D1] which was increased 4.1 fold) did not correspond to any ChIP-seq findings, again implying that other mechanisms or gene expression changes may be related to the observed gene expression changes. Exploring other possible pathways that could affect the expression of these genes will be important for future studies.

One finding from the ChIP-seq dataset that is of particular interest for AD is that 82-kDa ChAT has associations with many genes identified as AD susceptibility genes by genome-wide association studies (GWAS) meta-analysis (Bertram 2011). These included the aforementioned *PRUNE2*, but also several others including: *BINI*, which encodes BIN1 (bridging integrator 1, also known as amphiphysin) and is involved in synaptic vesicle endocytosis and recycling (David *et al.* 1996; Hayashida *et al.* 2015); *CRI*, which encodes CR1 (complement receptor 1), involved in immune responses and A β -clearance (Crehan *et al.* 2012; Hazrati *et al.* 2012); and *EFNA5*, which encodes Ephrin A5 and is involved in motor neuron growth and axon guidance (Eberhart *et al.* 2000; Eberhart *et al.* 2004). *EFNA5*, along with *DLGAP1* (also found by ChIP-seq in this study) has also been shown to have single-nucleotide polymorphisms (SNPs) associated with obsessive-compulsive disorder (OCD; Li *et al.* 2015). We also found the GWAS-identified gene *GAB2*, which encodes GAB2 (GRB2-associated-binding protein 2) that interacts with many receptor tyrosine kinases and membrane proteins such as APP (Reviewed in Pan *et al.* 2010). *GAB2* has 10 SNPs associated with AD in apolipoprotein E ϵ 4 carriers (Reiman *et al.* 2007). Finally, we found ChIP-associations with the GWAS-identified genes *MAGI2* (a synaptic scaffolding molecule; Danielson *et al.* 2012) and *MTHFDIL* (important for folate metabolism; Momb *et al.* 2013), whose potential contributions to AD have not yet been explored. Whether 82-kDa ChAT alters the expression of these genes, and whether this has implications for AD susceptibility would be of interest for future studies.

In addition to the GWAS-identified genes, we also observed ChIP-seq peaks for many genes that either interacted with APP, or were involved in APP processing (**Table 3.3**). Several of the genes identified also had microarray changes (Albers *et al.* 2014), but we have currently only verified *APP* itself. APP processing is important for synapse maintenance and regulation of neural activity (Furukawa *et al.* 1996; Furukawa *et al.* 1996b; Kojro *et al.* 2001; Stein *et al.* 2004), and β -secretase mediated cleavage results in A β ₁₋₄₂ production (Chow *et al.* 2010). Importantly, 82-kDa ChAT expression in primary neurons from APP/presenilin 1 (PS1) double transgenic mice reduces A β ₁₋₄₂ secretion and BACE1 expression levels (Albers *et al.* 2014). Together with the observed reductions in APP-KPI mRNA levels found in the present study, these data suggest that 82-kDa ChAT-

mediated gene expression changes result in altered APP processing. Therefore it is of great interest whether 82-kDa ChAT expression in neural cells alters the expression of other genes that alter APP processing, and what contribution these changes have to the observed reductions in A β ₁₋₄₂ production.

Another interesting piece of data was the finding that 82-kDa ChAT may associate with Matrin3. Though the present study showed the Matrin3 interaction by mass spectrometry, the interaction was also previously found by mass spectrometry and confirmed by co-immunoprecipitations performed in our lab (unpublished data). An interaction with Matrin3 could explain the finding that 82-kDa ChAT associates with S/MARs as well as the mass spectrometry associations with nuclear spliceosome-related proteins. Matrin3 has been shown to play a role in post-transcriptional pre-mRNA stabilization and the regulation of alternative splicing events (Zeitz *et al.* 2009; Salton *et al.* 2011; Coelho *et al.* 2015), which fits well with the data showing that the APP-KPI mRNA isoform has altered expression in 82-kDa ChAT expressing cells following A β -exposure. There are many unanswered questions that are important for future research including: Are 82-kDa ChAT and Matrin3 directly binding to one another? What is the relationship between 82-kDa ChAT, Matrin3 and the spliceosome complex? Does 82-kDa ChAT have a role in exon availability for transcription and/or pre-mRNA splicing or stability?

5.4 Future studies for 82-kDa ChAT that have not yet been explored

There are a number of interesting and important questions about 82-kDa ChAT expression and function that were not addressed in the current studies. For example, in **Figure 1.5**, we hypothesize that 82-kDa ChAT could alter gene expression through multiple mechanisms, including transcription factor (TF) and/or histone modifier recruitment, direct histone acetylation, or changes to acetylcholine availability. The data presented in this thesis shows that 82-kDa ChAT is associated with chromatin, has a role in chromatin organization with SATB1, and may be in complex with the NFAT TF.

However, we did not address the other hypotheses regarding changes to histone acetylation. Since SATB1 recruits histone modifying proteins to S/MARs (Yasui *et al.* 2002; Cai *et al.* 2003; Galande *et al.* 2007), it is possible that STAB1 is recruiting 82-kDa ChAT in this model to modify histone acetylation. Though 82-kDa ChAT is unlikely able to mediate the N-acetylation required for histone acetylation (Grant and Berger 1999) based on the structural features of its catalytic domain (Kim *et al.* 2005), Britton *et al.* (2013) showed that histone H3 can be acetylated by O-acetylation at several serine and threonine residues. If 82-kDa ChAT is acting as a histone acetyltransferase and thus altering access to DNA for TFs or RNA Pol II, it could partially explain differences in exon availability for transcription, especially if there are SATB1-mediated chromatin looping changes following A β -exposure.

As a result of the observed changes to neurite outgrowth and neurite complexity, there are a number of new questions related to 82-kDa ChAT's involvement in cholinergic neurodevelopment. When is 82-kDa ChAT expressed in development? Can 82-kDa ChAT influence the development or synaptic properties of other neural cells (i.e. glutamatergic, GABAergic, etc.) or glial cells? These are important considerations given that chromatin organization is critical for neurodevelopment (Williams *et al.* 2006; reviewed in Alexander and Lomvardas 2014). Dysregulation of chromatin organizers has been linked to intellectual disability, schizophrenia and autism spectrum disorder (Grayson *et al.* 2006; Gong *et al.* 2008; LaSalle and Yasui 2009; Gregor *et al.* 2013; McCarthy *et al.* 2014; Cotney *et al.* 2015), and all of these developmental disorders display hippocampal related changes correlated to memory and learning impairments (DeLong 1992; Heckers and Konradi 2002; Weiss *et al.* 2003; Dager *et al.* 2007; Zhang *et al.* 2015; Zhang *et al.* 2016). Since cholinergic neurons project to the hippocampus (Aznavour *et al.* 2002; Bloem *et al.* 2014), changes in synapse formation in these cells could influence hippocampal function. Epilepsy has also been linked to developmental changes in the hippocampus (Reviewed in Huang 2014), and more recently there has been evidence of developmental hippocampal structural alterations in patients with OCD (Hong *et al.* 2007). Given that 82-kDa ChAT is specifically expressed in humans and other primates, understanding how 82-kDa ChAT contributes to neural circuitry in the

hippocampus may also be important for understanding learning and memory differences between humans and other mammals.

An important extension of the data presented will be to determine if we can recapitulate our findings in an *in vivo* model. As discussed above, cells derived from neuroblastoma lines likely have gene and protein expression characteristics that would not reflect neurons in brain, and are grown in conditions that may not fully reflect the environment in brain (Gordon *et al.* 2013). Thus, it will be important to also consider these factors and try to determine whether these changes can occur in an animal model of human 82-kDa ChAT expression in cholinergic neurons. Recently, our lab has developed a transgenic mouse model of basal forebrain specific expression of 82-kDa human ChAT. Though this mouse is still undergoing characterization, we can use this mouse model to address whether findings from these studies are supported in an *in vivo* model. Is 82-kDa ChAT associated with chromatin in cholinergic neurons in this mouse model and does this lead to altered gene expression of *NLGN1*, *NRG1*, *GRM5*, *SATB1* and others? Does 82-kDa ChAT expression in this model lead to increased synapse formation in cholinergic projection regions, such as the hippocampus or prefrontal cortex? These mice can also be crossed with a mouse model of AD, for example transgenic mice expressing an APP/PS1 double mutation that rapidly produces A β_{1-42} , to test if there is an impact on APP metabolism (Albers *et al.* 2014). The 82-kDa ChAT/APP/PS1 triple transgenic mice are also invaluable to ask whether 82-kDa ChAT has a role in responses of neurons to A β_{1-42} -induced stress. Using these mice, we can determine if 82-kDa ChAT forms nuclear aggregates in response to A β *in vivo*, whether it associates with SATB1, and whether these proteins lead to gene expression changes of APP-KPI or other genes. Finally, we can determine whether 82-kDa ChAT expression leads to phenotype changes in APP/PS1 mice; if changes in synapse formation and maintenance result in neuroprotection from the toxic effects of A β_{1-42} and/or protect from the memory and learning impairments observed in this mouse model.

Finally, it is still unknown how 82-kDa ChAT nuclear localization is established. We have previously shown that 82-kDa ChAT has a unique NLS that results in stable nuclear localization (Resendes *et al.* 1999; Gill *et al.* 2003). However, we do not know

what molecular chaperone(s) may be responsible for nuclear import, and whether nuclear export is different between 82-kDa and 69-kDa ChAT. These questions are particularly relevant, given the observed mislocalization of 82-kDa ChAT in the cytoplasm of cholinergic cells from patients with mild cognitive impairment (MCI) and AD (Gill *et al.* 2007). Other epigenetic and transcription mediators are also mislocalized following long-term A β -exposure and in MCI and AD, including DNA methyltransferase (DNMT), RNA Pol II, repressor element 1-silencing transcription (REST), and H3K4me3 (Mastroeni *et al.* 2013; Lu *et al.* 2014; Mastroeni *et al.* 2015). These changes may be due to importin- α and/or Ran-GTP mediated changes in cholinergic cells (Lee *et al.* 2006; Mastroeni *et al.* 2013), and thus would be good targets for initial experiments addressing 82-kDa ChAT nuclear import. In addition, preliminary confocal imaging experiments performed in our laboratory suggests that long-term A β -exposure may reduce nuclear levels of 82-kDa ChAT (unpublished data). Determining the mechanisms of nuclear import and export are key for understanding the changes that human cholinergic cells may undergo when nuclear localization is lost, and for identifying potential interventions for preventing or reversing the nuclear localization changes observed in MCI and AD.

5.5 Overall conclusions and significance

The data presented in this thesis represent a significant advancement in understanding the role of nuclear-localized 82-kDa ChAT in cholinergic nuclei. We showed that 82-kDa ChAT is involved in chromatin organization and gene expression changes at S/MARs in cholinergic nuclei, leading to an epigenetic response following A β -exposure. Many chromatin organizers are also involved in neurodevelopment, a feature that may also be true for 82-kDa ChAT. Neural cells expressing 82-kDa ChAT had gene expression changes leading to increased neurite complexity during cholinergic differentiation, supporting the hypothesis that 82-kDa ChAT may also be involved in neurodevelopmental synapse formation. It will be important for future studies to determine how 82-kDa ChAT alters gene expression, and whether there are resulting

changes to chromatin looping or access to promoters and exons. It will also be important to verify these results in 82-kDa ChAT and AD transgenic mouse models, and to further understand the phenotypic changes resulting from 82-kDa ChAT nuclear expression using these models. The nuclear levels of 82-kDa ChAT decline in aging and are mislocalized in individuals with MCI or AD (Gill *et al.* 2007), and synapse degeneration occurs early in the progression of AD (Reviewed in Selkoe 2002; Lacor *et al.* 2007; Reviewed in Arendt 2009). Therefore the loss of both the epigenetic response to A β and gene expression changes related to synapse formation and maintenance may have implications for the etiology or progression of MCI and AD.

5.6 References

- Alexander JM, Lomvardas S (2014) Nuclear architecture as an epigenetic regulator of neural development and function. *Neuroscience*, 264: 39-50.
- Albers S, Inthathirath F, Gill SK, Winick-Ng W, Jaworski E, Wong DY, Gros R, Rylett RJ (2014) Nuclear 82-kDa choline acetyltransferase decreases amyloidogenic APP metabolism in neurons from APP/PS1 transgenic mice. *Neurobiol Dis*, 69: 32-42.
- Arendt T (2009) Synaptic degeneration in Alzheimer's disease. *Acta Neuropathol*, 118: 167-179.
- Aznavour N, Mechawar N, Descarries L (2002) Comparative analysis of cholinergic innervation in the dorsal hippocampus of adult mouse and rat: a quantitative immunocytochemical study. *Hippocampus*, 12: 206-217.
- Bertram L (2011) Alzheimer's genetics in the GWAS era: a continuing story of 'replications and refutations'. *Curr Neurol Neurosci Rep*, 11: 246-253.
- Britton LM, Newhart A, Bhanu NV, Sridharan R, Gonzales-Cope M, Plath K, Janicki SM, Garcia BA (2013) Initial characterization of histone H3 serine 10 O-acetylation. *Epigenetics*, 8: 1101-1113.
- Cai S, Han HJ, Kohwi-Shigematsu T (2003) Tissue-specific nuclear architecture and gene expression regulated by SATB1. *Nat Genet*, 34: 42-51.
- Chow VW, Mattson MP, Wong PC, Gleichmann M (2010) An overview of APP processing enzymes and products. *Neuromolecular Med*, 12: 1-12.
- Coelho MB, Attig J, Bellora N, König J, Hallegger M, Kayikci M, Eyraş E, Ule J, Smith CW (2015) Nuclear matrix protein Matrin3 regulates alternative splicing and forms overlapping regulatory networks with PTB. *EMBO J*, 34: 653-658.

- Cotney J, Muhle RA, Sanders SJ, Liu L, Willsey AJ, Niu W, Liu W, Klei L, Lei J, Yin J, Reilly SK, Tebbenkamp AT, Bichsel C, Pletikos M, Sestan N, Roeder K, State MW, Devlin B, Noonan JP (2015) The autism-associated chromatin modifier CHD8 regulates other autism risk genes during human neurodevelopment. *Nat Commun*, 6: 6404.
- Crehan H, Holton P, Wray S, Pocock J, Guerreiro R, Hardy J (2012) Complement receptor 1 (CR1) and Alzheimer's disease. *Immunobiology*, 217: 244-250.
- Dager SR, Wang L, Friedman SD, Shaw DW, Constantino JN, Artru AA, Dawson G, Csernansky JG (2007) Shape mapping of the hippocampus in young children with autism spectrum disorder. *AJNR Am J Neuroradiol*, 28: 672-677.
- Danielson E, Zhang N, Metallo J, Kaleka K, Shin SM, Gerges N, Lee SH (2012) S-SCAM/MAGI-2 is an essential synaptic scaffolding molecule for the GluA2-containing maintenance pool of AMPA receptors. *J Neurosci*, 32: 6867-6980.
- David C, McPherson PS, Mundigl O, de Camilli P (1996) A role of amphiphysin in synaptic vesicle endocytosis suggested by its binding to dynamin in nerve terminals. *Proc Natl Acad Sci U S A*, 93: 331-335.
- Debeauchamp JL, Moses A, Noffsinger VJ, Ulrich DL, Job G, Kosinski AM, Partridge JF (2008) Chp1-Tas3 interaction is required to recruit RITS to fission yeast centromeres and for maintenance of centromeric heterochromatin. *Mol Cell Biol*, 28: 2154-2166.
- DeLong GR (1992) Autism, amnesia, hippocampus, and learning. *Neurosci Biobehav Rev*, 16: 63-70.
- Eberhart J, Barr J, O'Connell S, Flagg A, Swartz ME, Cramer KS, Tosney KW, Pasquale EB, Krull CE (2004) Ephrin-A5 exerts positive or inhibitory effects on distinct subsets of EphA4-positive motor neurons. *J Neurosci*, 24: 1070-1078.

- Eberhart J, Swartz M, Koblar SA, Pasquale EB, Tanaka H, Krull CE (2000) Expression of EphA4, ephrin-A2 and ephrin-A5 during axon outgrowth to the hindlimb indicates potential roles in pathfinding. *Dev Neurosci*, 22: 237-250.
- Fernius J, Nerusheva OO, Galander S, Alves Fde L, Rappsilber J, Marston AL (2013) Cohesin-dependent association of scc2/4 with the centromere initiates pericentromeric cohesion establishment. *Curr Biol*, 23: 599-606.
- Frade JM, Ovejero-Benito MC (2015) Neuronal cell cycle: the neuron itself and its circumstances. *Cell Cycle*, 14: 712-720.
- Galante S, Purbey PK, Notani D, Kumar PP (2007) The third dimension of gene regulation: organization of dynamic chromatin loopscape by SATB1. *Curr Opin Genet Dev*, 17: 408-414.
- Gerecke KM, Wyss JM, Carroll SL (2004) Neuregulin-1beta induces neurite extension and arborization in cultured hippocampal neurons. *Mol Cell Neurosci*, 27: 379-393.
- Gill SK, Bhattacharya M, Ferguson SS, Rylett RJ (2003) Identification of a novel nuclear localization signal common to 69- and 82-kDa human choline acetyltransferase. *J Biol Chem*, 278: 20217-20224.
- Gill SK, Ishak M, Dobransky T, Haroutunian V, Davis KL, Rylett RJ (2007) 82-kDa choline acetyltransferase is in nuclei of cholinergic neurons in human CNS and altered in aging and Alzheimer disease. *Neurobiol Aging*, 28: 1028-1040.
- Gong X, Bacchelli E, Blasi F, Toma C, Betancur C, Chaste P, Delorme R, Durand CM, Fauchereau F, Botros HG, *et al.* (2008) Analysis of X chromosome inactivation in autism spectrum disorders. *Am J Med Genet B Neuropsychiatr Genet*, 147B: 830-835.
- Furukawa K, Barger SW, Blalock EM, Mattson MP (1996) Activation of K⁺ channels and suppression of neuronal activity by secreted beta-amyloid-precursor protein. *Nature*, 379: 74-78.

- Furukawa K, Sopher BL, Rydel RE, Begley JG, Pham DG, Martin GM, Fox M, Mattson MP (1996b) Increased activity-regulating and neuroprotective efficacy of alpha-secretase-derived secreted amyloid precursor protein conferred by a C-terminal heparin-binding domain. *J Neurochem*, 67: 1882-1896.
- Gordon J, Amini S, White MK (2013) General overview of neuronal cell culture. *Methods Mol Biol*, 1078: 1-8.
- Grant PA, Berger SL (1999) Histone acetyltransferase complexes. *Semin Cell Dev Biol*, 10: 167-177.
- Grayson DR, Chen Y, Costa E, Dong E, Guidotti A, Kundakovic M, Sharma RP (2006) The human reelin gene: transcription factors (+), repressors (-) and the methylation switch (+/-) in schizophrenia. *Pharmacol Ther*, 272-286.
- Gregor A, Oti M, Kouwenhoven EN, Hoyer J, Sticht H, Ekici AB, Kjaergaard S, Rauch A, Stunnenberg HG, Uebe S, Vasileiou G, Reis A, Zhou H, Zweier C (2013) De novo mutations in the genome organizer CTCF cause intellectual disability. *Am J Hum Genet*, 93: 124-131.
- Hashemi SH, Li JY, Ahlman H, Dahlström A (2003) SSR2(a) receptor expression and adrenergic/cholinergic characteristics in differentiated SH-SY5Y cells. *Neurochem Res*, 28: 449-460.
- Hayashida M, Tanifuji S, Ma H, Murakami N, Mochida S (2015) Neural activity selects myosin IIB and VI with a specific time window in distinct dynamin isoform-mediated synaptic vesicle reuse pathways. *J Neurosci*, 35: 8901-8913.
- Hazrati LN, Van Cauwenberghe C, Brooks PL, Brouwers N, Ghani M, Sato C, Cruts M, Sleegers K, St George-Hyslop P, Van Broeckhoven C, Rogaeva E (2012) Genetic association of CR1 with Alzheimer's disease: a tentative disease mechanism. *Neurobiol Aging*, 33: 2949.e5-2949.e12.
- Heckers S, Konradi C (2002) Hippocampal neurons in schizophrenia. *J Neural Transm (Vienna)*, 109:891-905.

- Herrup K, Yang Y (2007) Cell cycle regulation in the postmitotic neuron: oxymoron or new biology? *Nat Rev Neurosci*, 8: 368-378.
- Hirano T (2002) The ABCs of SMC proteins: two-armed ATPases for chromosome condensation, cohesion, and repair. *Genes Dev*, 16: 399-414.
- Hong SB, Shin YW, Kim SH, Yoo SY, Lee JM, Kim IY, Kim SI, Kwon JS (2007) Hippocampal shape deformity analysis in obsessive-compulsive disorder. *Eur Arch Psychiatry Clin Neurosci*, 257: 185-190.
- Huang T (2014) Early-life stress impacts the developing hippocampus and primes seizure occurrence: cellular, molecular, and epigenetic mechanisms. *Front Mol Neurosci*, 7: 8.
- Iwakura Y, Nawa H (2013) ErbB1-4-dependent EGF/neuregulin signals and their cross talk in the central nervous system: pathological implications in schizophrenia and Parkinson's disease. *Front Cell Neurosci*, 7: 4.
- Jessberger R (2002) The many functions of SMC proteins in chromosome dynamics. *Nat Rev Mol Cell Biol*, 3: 767-778.
- Johnson RD, Liu N, Jasin M (1999) Mammalian XRCC2 promotes the repair of DNA double-strand breaks by homologous recombination. *Nature*, 401: 397-399.
- Kim AR, Dobransky T, Rylett RJ, Shilton BH (2005) Surface-entropy reduction used in the crystallization of human choline acetyltransferase. *Acta Crystallogr D Biol Crystallogr*, 61: 1306-1310.
- Kojro E, Gimpl G, Lammich S, Marz W, Fahrenholz F (2001) Low cholesterol stimulates the nonamyloidogenic pathway by its effect on the alpha -secretase ADAM 10. *Proc Natl Acad Sci U S A*, 98: 5815-5820.
- Lacor PN, Buniel MC, Furlow PW, Clemente AS, Velasco PT, Wood M, Viola KL, Klein WL (2007) Abeta oligomer-induced aberrations in synapse composition,

shape, and density provide a molecular basis for loss of connectivity in Alzheimer's disease. *J Neurosci*, 27: 796-807.

LaSalle JM, Yasui DH (2009) Evolving role of MeCP2 in Rett syndrome and autism. *Epigenomics*, 1: 119-130.

Lee HG, Ueda M, Miyamoto Y, Yoneda Y, Perry G, Smith MA, Zhu X (2006) Aberrant localization of importin alpha1 in hippocampal neurons in Alzheimer disease. *Brain Res*, 1124: 1-4.

Levy MA, Kernohan KD, Jiang Y, Bérubé NG (2015) ATRX promotes gene expression by facilitating transcriptional elongation through guanine-rich coding regions. *Hum Mol Genet*, 24: 1824-1835.

Li J, Cui J, Wang X, Ma J, Niu H, Ma X, Zhang X, Liu S (2015) An association study between DLGAP1 rs11081062 and EFNA5 rs26728 polymorphisms with obsessive-compulsive disorder in a Chinese Han population. *Neuropsychiatr Dis Treat*, 11: 897-905.

Li S, Hayakawa-Yano Y, Itoh M, Ueda M, Ohta K, Suzuki Y, Mizuno A, Ohta E, Hida Y, Wang MX, Nakagawa T (2012) Olfaxin as a novel Prune2 isoform predominantly expressed in olfactory system. *Brain Res*, 1488: 1-13.

Lu T, Aron L, Zullo J, Pan Y, Kim H, Chen Y, Yang TH, Kim HM, Drake D, Liu XS, Bennett DA, Colaiácovo MP, Yankner BA (2014) REST and stress resistance in ageing and Alzheimer's disease. *Nature*, 507: 448-454.

Machida T, Fujita T, Ooo ML, Ohira M, Isogai E, Mihara M, Hirato J, Tomotsune D, Hirata T, Fujimori M, Adachi W, Nakagawara A (2006) Increased expression of proapoptotic BMCC1, a novel gene with the BNIP2 and Cdc42GAP homology (BCH) domain, is associated with favorable prognosis in human neuroblastomas. *Oncogene*, 25: 1931-1942.

Mastroeni D, Chouliaras L, Grover A, Liang WS, Hauns K, Rogers J, Coleman PD (2013) Reduced RAN expression and disrupted transport between cytoplasm and

nucleus; a key event in Alzheimer's disease pathophysiology. *PLoS One*, 8: e53349.

- Mastroeni D, Delvaux E, Nolz J, Tan Y, Grover A, Oddo S, Coleman PD (2015) Aberrant intracellular localization of H3k4me3 demonstrates an early epigenetic phenomenon in Alzheimer's disease. *Neurobiol Aging*, 36: 3121-3129.
- McCarthy SE, Gillis J, Kramer M, Lihm J, Yoon S, Berstein Y, Mistry M, Pavlidis P, Solomon R, Ghiban E, *et al.* (2014) De novo mutations in schizophrenia implicate chromatin remodeling and support a genetic overlap with autism and intellectual disability. *Mol Psychiatry*, 19: 652-658.
- Mehlen P, Rabizadeh S, Snipas SJ, Assa-Munt N, Salvesen GS, Bredesen DE (1998) The DCC gene product induces apoptosis by a mechanism requiring receptor proteolysis. *Nature*, 395: 801-804.
- Moir RD, Lynch T, Bush AI, Whyte S, Henry A, Portbury S, Multhaup G, Small DH, Tanzi RE, Beyreuther K, Masters CL (1998) Relative increase in Alzheimer's disease of soluble forms of cerebral Abeta amyloid protein precursor containing the Kunitz protease inhibitory domain. *J Biol Chem*, 273: 5013-5019.
- Momb J, Lewandowski JP, Bryant JD, Fitch R, Surman DR, Vokes SA, Appling DR (2013) Deletion of *Mthfd11* causes embryonic lethality and neural tube and craniofacial defects in mice. *Proc Natl Acad Sci U S A*, 110: 549-554.
- Pan XL, Ren RJ, Wang G, Tang HD, Chen SD (2010) The Gab2 in signal transduction and its potential role in the pathogenesis of Alzheimer's disease. *Neurosci Bull*, 26: 241-246.
- Potkin SG, Guffanti G, Lakatos A, Turner JA, Kruggel F, Fallon JH, Saykin AJ, Orro A, Lupoli S, Salvi E, Weiner M, Macciardi F; Alzheimer's Disease Neuroimaging Initiative (2009) Hippocampal atrophy as a quantitative trait in a genome-wide association study identifying novel susceptibility genes for Alzheimer's disease. *PLoS One*, 4: e6501.

- Reiman EM1, Webster JA, Myers AJ, Hardy J, Dunckley T, Zismann VL, Joshipura KD, Pearson JV, Hu-Lince D, Huentelman MJ, Craig DW, Coon KD, Liang WS, Herbert RH, Beach T, Rohrer KC, Zhao AS, Leung D, Bryden L, Marlowe L, Kaleem M, Mastroeni D, Grover A, Heward CB, Ravid R, Rogers J, Hutton ML, Melquist S, Petersen RC, Alexander GE, Caselli RJ, Kukull W, Papassotiropoulos A, Stephan DA (2007) GAB2 alleles modify Alzheimer's risk in APOE epsilon4 carriers. *Neuron*, 54: 713-720.
- Resendes MC, Dobransky T, Ferguson SS, Rylett RJ (1999) Nuclear localization of the 82-kDa form of human choline acetyltransferase. *J Biol Chem*, 274: 19417-19421.
- Salton M, Elkon R, Borodina T, Davydov A, Yaspo ML, Halperin E, Shiloh Y (2011) Matrin 3 binds and stabilizes mRNA. *PLoS One*, 6: e23882.
- Savonenko AV, Melnikova T, Laird FM, Stewart KA, Price DL, Wong PC (2008) Alteration of BACE1-dependent NRG1/ErbB4 signaling and schizophrenia-like phenotypes in BACE1-null mice. *Proc Natl Acad Sci U S A*, 105: 5585-5590.
- Selkoe DJ (2002) Alzheimer's disease is a synaptic failure. *Science*, 298: 789-791.
- Spremo-Potparević B, Zivković L, Djelić N, Plečas-Solarović B, Smith MA, Bajić V (2008) Premature centromere division of the X chromosome in neurons in Alzheimer's disease. *J Neurochem*, 106: 2218-2223.
- Stein TD, Anders NJ, DeCarli C, Chan SL, Mattson MP, Johnson JA (2004) Neutralization of transthyretin reverses the neuroprotective effects of secreted amyloid precursor protein (APP) in APPSW mice resulting in tau phosphorylation and loss of hippocampal neurons: support for the amyloid hypothesis. *J Neurosci*, 24: 7707-7717.
- Sweeney C, Lai C, Riese DJ 2nd, Diamonti AJ, Cantley LC, Carraway KL 3rd (2000) Ligand discrimination in signaling through an ErbB4 receptor homodimer. *J Biol Chem*, 275: 19803-19807.

- Szabó GG, Holderith N, Gulyás AI, Freund TF, Hájos N (2010) Distinct synaptic properties of perisomatic inhibitory cell types and their different modulation by cholinergic receptor activation in the CA3 region of the mouse hippocampus. *Eur J Neurosci*, 31: 2234-2246.
- Tatsumi Y, Takano R, Islam MS, Yokochi T, Itami M, Nakamura Y, Nakagawara A (2015) BMCC1, which is an interacting partner of BCL2, attenuates AKT activity, accompanied by apoptosis. *Cell Death Dis*, 6: e1607.
- Tzahar E, Waterman H, Chen X, Levkowitz G, Karunagaran D, Lavi S, Ratzkin BJ, Yarden Y (1996) A hierarchical network of interreceptor interactions determines signal transduction by Neu differentiation factor/neuregulin and epidermal growth factor. *Mol Cell Biol*, 16: 5276-5287.
- Valencia CA, Cotten SW, Liu R (2007) Cleavage of BNIP-2 and BNIP-XL by caspases. *Biochem Biophys Res Commun*, 364: 495-501.
- Weiss AP, Schacter DL, Goff DC, Rauch SL, Alpert NM, Fischman AJ, Heckers S (2003) Impaired hippocampal recruitment during normal modulation of memory performance in schizophrenia. *Biol Psychiatry*, 53: 48-55.
- Williams RR, Azuara V, Perry P, Sauer S, Dvorkina M, Jørgensen H, Roix J, McQueen P, Misteli T, Merckenschlager M, Fisher AG (2006) Neural induction promotes large-scale chromatin reorganisation of the Mash1 locus. *J Cell Sci*, 119: 132-140.
- Yasui D, Miyano M, Cai S, Varga-Weisz P, Kohwi-Shigematsu T (2002) SATB1 targets chromatin remodelling to regulate genes over long distances. *Nature*, 419: 641-645.
- Zhang CL, Houbaert X, Lepleux M, Deshors M, Normand E, Gambino F, Herzog E, Humeau Y (2015) The hippocampo-amygdala control of contextual fear expression is affected in a model of intellectual disability. *Brain Struct Funct*, 220: 3673-3682.

Zhang Q, Gao X, Li C, Feliciano C, Wang D, Zhou D, Mei Y, Monteiro P, Anand M, Itohara S, Dong X, Fu Z, Feng G (2016) Impaired Dendritic Development and Memory in Sorbs2 Knock-Out Mice. *J Neurosci*, 36: 2247-2260.

Zhang T, Zheng J, Jiang N, Wang G, Shi Q, Liu C, Lu Y (2009) Overexpression of DLC-1 induces cell apoptosis and proliferation inhibition in the renal cell carcinoma. *Cancer Lett*, 283: 59-67.

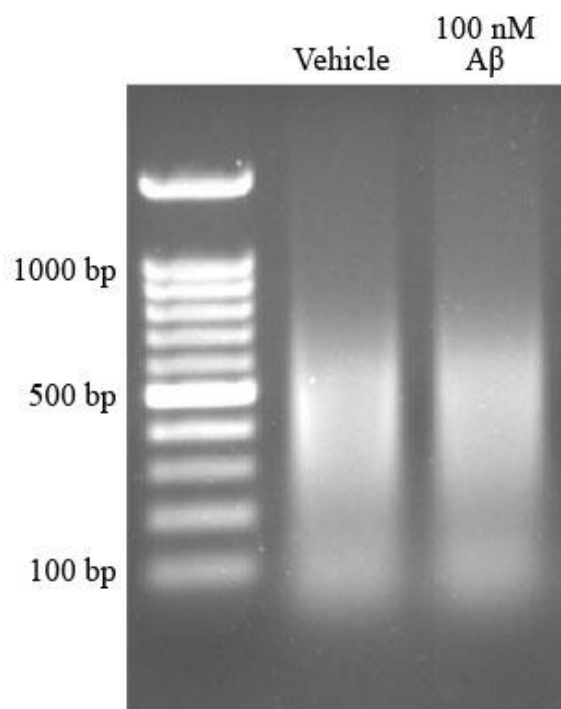
Zhu X, Lai C, Thomas S, Burden SJ (1995) Neuregulin receptors, erbB3 and erbB4, are localized at neuromuscular synapses. *EMBO J*, 14: 5842-5848.

Zeitz M, Malyavantham K, Seifert B, Berezney R (2009) Matrin 3: Chromosomal Distribution and Protein Interactions. *J Cell Biochem*, 108: 125-133.

Appendices

Appendix 1- DNA fragment optimization for ChIP.

5 μ L of sonicated input DNA was run on a 1% agarose gel. DNA fragments ranged mainly from 300-500 bp.



Appendix 2- 82-kDa ChAT vehicle gene ontology.

Appendix 2 can be found in online supplemental information.

Appendix 3- 82-kDa ChAT A β gene ontology.

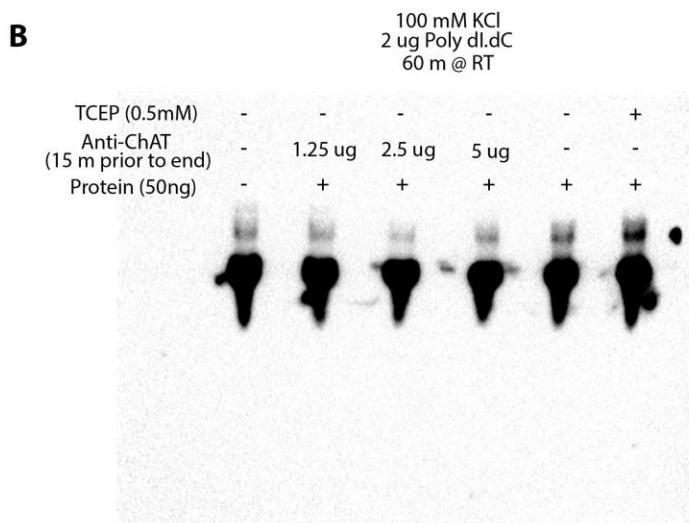
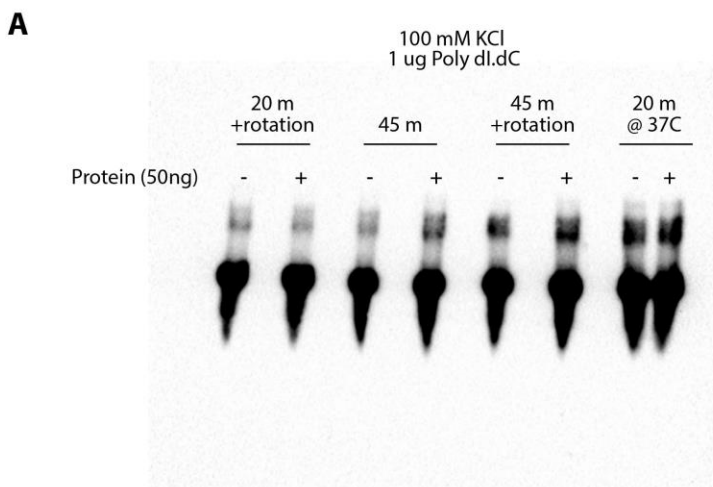
Appendix 3 can be found in online supplemental information.

Appendix 4- 82-kDa ChAT vehicle and A β gene ontology.

Appendix 4 can be found in online supplemental information.

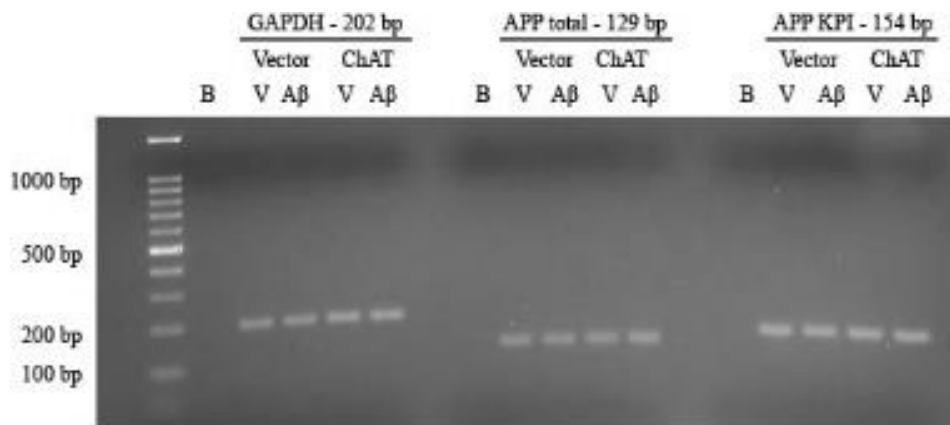
Appendix 5- EMSA optimization experiments

Purified recombinant 82-kDa ChAT was incubated with annealed biotinylated DNA oligomers from Table 2.1 (only the ATC-Rich 1 motif was used for these experiments at 125 fmol) and then separated on TBE electrophoresis gels. DNA and proteins were transferred to nylon membranes and exposed to stabilized streptavidin-horseradish peroxidase conjugate. **(A)** Increasing the incubation time from 20 min to 45 min increased the presence of a shifted immunoreactive DNA bands, but did not affect the background observed from samples incubated without added 82-kDa ChAT. Mixing the samples by rotation during incubation or increasing the incubation temperature to 37°C also increased the intensity of the non-specific band observed in samples that did not contain ChAT protein. **(B)** The addition of increasing amounts of an anti-ChAT antibody at 15 min prior to the end of the reaction period attenuated the intensity of the shifted band, with 2.5 µg appearing to have the greatest effect. The addition of the reducing agent TCEP resulted in an increase in the intensity of shifted immunoreactive band. DNA concentration was decreased to 100 fmol in these samples. N = 2.



Appendix 6- Representative PCR gel for primers used in RT-qPCR experiments.

SH-SY5Y cells stably expressing either an empty vector or 82-kDa ChAT were treated with either vehicle or 100 nM oligomeric A β ₁₋₄₂. Total RNA was extracted and reverse transcribed prior to PCR amplification with primers specific to GAPDH, total APP or APP-KPI mRNA. For all primer sets, there was a single PCR product at the predicted size.



Appendix 7- SATB1 vehicle gene ontology.

Appendix 7 can be found in online supplemental information.

Appendix 8- SATB1 A β gene ontology.

Appendix 8 can be found in online supplemental information.

Appendix 9- SATB1 vehicle and A β gene ontology.

Appendix 9 can be found in online supplemental information.

Appendix 10- 82-kDa ChAT and SATB1 A β gene ontology.

Appendix 10 can be found in online supplemental information.

Appendix 11- 82-kDa ChAT and SATB1 vehicle and A β gene ontology.

Appendix 11 can be found in online supplemental information.

Curriculum Vitae

Name: Warren Winick-Ng

Citizenship: Canadian

Postsecondary Education

2012 - 2016	Ph.D. Physiology and Pharmacology, Supervisor: Dr. R. Jane Rylett University of Western Ontario
2011 - 2012	Masters of Biomedical Science-Neuroscience, Supervisors: Dr. Bettina Kalisch and Dr. Francesco Leri University of Guelph
2010 - 2011	Continuing Education Certificate- Anatomy and Physiology for Health Care Professionals Michener Institute, Toronto, Ontario
2003 - 2007	B.Sc. (Honours) Bio-Medical Science

Honours and Awards

Western Graduate Research Scholarship, \$4500/year	2015 - 16
George W. Stavrakys Scholarship for Teaching, \$1000	2014
Dean's PhD Scholarship for Graduate Research, \$25,000/year	2012 - 16
University of Guelph Dean's List (Undergraduate)	2003 - 07

Publications

Winick-Ng W, Caetano F, Winick-Ng J, Morey TM, Heit B, Rylett J (2016) *82-kDa choline acetyltransferase and SATB1 facilitate β -amyloid induced matrix attachment region formation*. Scientific Reports 6:23914.

Albers S, Inthathirath F, Gill SK, **Winick-Ng W**, Jaworski E, Wong DY, Gros R, Rylett RJ (2014) *Nuclear 82-kDa choline acetyltransferase decreases amyloidogenic APP metabolism in neurons from APP/PS1 transgenic mice*. Neurobiology of Disease 69: 32-42.

Cuddy LK, **Winick-Ng W**, Rylett RJ (2014) *Regulation of the high-affinity choline transporter activity and trafficking by its association with cholesterol-rich lipid rafts*. Journal of Neurochemistry 128: 725-740.

Winick-Ng W, Leri F, Kalisch BE (2012) *Nitric oxide and histone deacetylases modulate cocaine-induced mu-opioid receptor levels in PC12 cells*. BMC Pharmacology and Toxicology 13: 11.

Teaching and mentoring

Undergraduate Student Lectures and Tutorials

November 2015	Lecturer - Cell Signaling (2 lectures) Physiology 3140 – Cell Physiology Department of Physiology and Pharmacology University of Western Ontario
2014 - 2016	Lead Teaching Assistant Physiology 2130 - Human Physiology Department of Physiology and Pharmacology University of Western Ontario
November 2014	Lecturer - Cardiology (3 lectures) Physiology 2130 - Human Physiology Department of Physiology and Pharmacology University of Western Ontario
2013 - 2014	Teaching Assistant Physiology 2130 - Human Physiology Department of Physiology and Pharmacology University of Western Ontario
2012 - 2013	Teaching Assistant Physiology 3120 - Mammalian Physiology Department of Physiology and Pharmacology University of Western Ontario

Student Supervision

05/2016 – present	Heather Rotz, Honours thesis and accelerated Masters of Science student
-------------------	---

Thesis title: *Assessing the protective effects of 82-kDa ChAT in cholinergic neurons in response to A β -induced oxidative or nitrosative stress.*

2015 – 2016

Jeeae Choi, Honours thesis student

Thesis title: *The effect of 82-kDa choline acetyltransferase expression on amyloid precursor protein processing in response to β -amyloid exposure.*

2014 – 2015

Marshall Kurniawan, Honours thesis student

Thesis title: *Amyloid-beta treatment alters the subcellular localization of 82-kDa choline acetyltransferase.*

2013 – 2014

Alan Wu, Honours thesis student

Thesis title: *Investigating the DNA binding properties of 82-kDa choline acetyltransferase using multiple DNA binding compounds.*

Abstracts and Presentations at Conferences

Rylett RJ, Winick-Ng J, Winick-Ng W. 82-kDa choline acetyltransferase alters APP processing and expression of synapse formation related genes. XVth International Symposium on Cholinergic Mechanisms; 2016 Oct 16-20; Marseille, France (Poster presented by Rylett RJ)

Winick-Ng W, Caetano F, Winick-Ng J, Heit B, Rylett J. 82-kDa choline acetyltransferase and SATB1 co-locate at synapse and cell-stress related genes after amyloid beta exposure. London Health Research Day; 2016 March 29; London, ON (Poster)

Winick-Ng W, Caetano F, Winick-Ng J, Heit B, Rylett J. 82-kDa choline acetyltransferase and SATB1 co-locate at synapse and cell-stress related genes after amyloid beta exposure. 10th annual Physiology and Pharmacology Research Day; 2015 Nov 1; London, ON (Poster)

Winick-Ng W, Caetano F, Winick-Ng J, Heit B, Rylett J. 82-kDa choline acetyltransferase and SATB1 co-locate at synapse and cell-stress related genes after amyloid beta exposure. Society for Neuroscience Annual Meeting; 2015 Oct 17-21; Chicago IL (Selected talk)

Winick-Ng W, Caetano F, Rylett RJ. 82-kDa choline acetyltransferase interacts with chromatin after exposure to β -amyloid. London Health Research Day; 2015 April 1; London, ON (Poster)

Winick-Ng W. Three-minute thesis oral presentation competition. 2015 March 20; London, ON (Presentation)

Winick-Ng W, Caetano F, Rylett RJ. Nuclear Localized 82-kDa Choline Acetyltransferase Drives an Epigenetic Response to Amyloid Beta Exposure. 9th annual Physiology and Pharmacology Research Day; 2014 Nov 4; London, ON (Poster)

Winick-Ng W, Caetano F, Rylett RJ. Nuclear Localized 82-kDa Choline Acetyltransferase Drives an Epigenetic Response to Amyloid Beta Stress. Poster session presented at: 2nd Canadian Conference on Epigenetics: Epigenetics, Eh!; 2014 June 24-27; London, ON (Poster)

Winick-Ng W, Albers S, Rylett RJ. Nuclear Localized 82-kDa Choline Acetyltransferase Drives an Epigenetic Response to Amyloid Beta Stress. 34th Annual Meeting for the Southern Ontario Neuroscience Association; 2014 May 5; London, ON (Poster)

Winick-Ng W, Albers S, Rylett RJ. Nuclear Localized 82-kDa Choline Acetyltransferase Drives an Epigenetic Response to Amyloid Beta Stress. London Health Research Day; 2014 March 18; London, ON (Poster)

Winick-Ng W, Rylett RJ. The role of an 82-kDa Nuclear Choline Acetyltransferase in Cellular Stress and the Epigenome. Society for Neuroscience Annual Meeting; 2013 Nov 9-13; San Diego, CA (Poster)

Winick-Ng W, Rylett RJ. The role of an 82-kDa Nuclear Choline Acetyltransferase in Cellular Stress and the Epigenome. 8th annual Physiology and Pharmacology Research Day; 2013 Nov 5; London, ON (Poster)

Winick-Ng W, Leri F and Kalisch B. The effects of histone modifications on PC12 cell protein expression. University of Guelph Neuroscience Day, 2012 April 3; Guelph, ON (Presentation)

Winick-Ng W, Leri F and Kalisch B. Cocaine and nerve growth factor modulate mu opioid receptor expression in PC12 cells. University of Guelph Neuroscience Day; 2009 March 31; Guelph, ON (Poster)

Winick-Ng W, Leri F and Kalisch B. Cocaine modulates the in vitro expression of MOR and NO production in PC12 cells. CAN-ACN Canadian Neuroscience Meeting; 2008 May 25-28; Toronto, ON (Poster)

Governance and Committees

Robarts Strategic Planning Committee	2015-present
Robarts Research Institute Scientific Director Search Committee	2014-2015